MECHANICAL AND RHEOLOGICAL PROPERTIES OF STEEL FIBRE REINFORCED SELF-COMPACTING CONCRETE

by

Anil Nis

B.S., Civil Engineering, Pamukkale University, 2008

M.S., Civil Engineering, Boğaziçi University, 2011

Submitted to the Institute for Graduate Studies in
Science and Engineering in partial fulfillment of
the requirements for the degree of
Doctor of Philosophy

Graduate Program in Civil Engineering

Boğaziçi University

2017

ACKNOWLEDGEMENTS

I would like to express my gratitude to all the people who in one way or another contributed to the development of this PhD research. I would like to express my sincere appreciation to my thesis supervisor Prof. Turan Ozturan for their invaluable help in instructing, guiding and supporting me throughout the duration of the thesis. I would like to express my special thanks to Assoc. Prof. Nilufer Ozyurt Zihnioğlu for her kindness, cheerful face, support, assistance, encouragement throughout the duration of the thesis.

I would like to manifest my special thanks to Assoc. Prof. Hakan Nuri Atahan and Assoc. Prof. Kutay Orakçal for their knowledgeable and advisory guidance.

I want to emphasize my special thanks to Boğaziçi University assistants and my close friends, Ahmet Onur Pehlivan, Abdullah Huzeyfe Akca, and Hasan Yıldırım, and our Construction Material Laboratory fellow, Ümit Melep for his help during my experiments.

I want to acknowledge the support of Boğaziçi University Research Fund (Project Codes: 14A04D2, 15A04D1) and also Akcansa, Boğaziçi Beton and BASF - YKS for the material contribution. I would like to thank Hasan Nuri Türkmenoğlu for his support on the rheology tests and equipment. I would like to state my special thanks to Ayşe Aydın for her help during the thesis. I am also thankful to my friends, especially, İbrahim Çinar, Adem Afsin Ulu, Faruk Bozkaya, Süleyman Konukız, Mustafa Aktaşoğlu, Murat Mustafa Ayhan, Gökhan Kip, Baran Şenkaya, Adem Konya and Fadıl Fatih Kavarnalı who support and encourage me during the thesis.

I dedicate this thesis to my family. I would like to express my sincere and very special thanks to my wife, Beril Çiler Niş, for her love, encouragement and support throughout every phase of the PhD thesis and without her this thesis could not be written. I would like to express my very special thanks to my father, Metin Niş, my

mother Zinet Niş, my brother Onur Niş my younger brother Okan Niş for their endless support, encouragement and love they have given me throughout my life.

ABSTRACT

MECHANICAL AND RHEOLOGICAL PROPERTIES OF STEEL FIBRE REINFORCED SELF-COMPACTING CONCRETE

Main objective of the research was to further understand the different parameters affecting performance of SFR-SCC with different steel fiber volumes and types. Fresh and hardened state properties of these materials were investigated by using several experimental methods. For this purpose 5 mixes; plain and reinforced with 2 different fiber volumes (0.5 and 1.0%) and two different fiber lengths; were produced. Flowability and rheology as well as static and dynamic segregation resistance of the above mentioned mixes were studied in the fresh state. Specimens with varying sizes were produced with these 5 mixes. Six different width and depth (30 mm to 100 mm), four different length (200 mm to 425 mm) were used to investigate the effect of shear span to depth ratio (a/d) and specimen thickness to fiber length (t/f_L) on the mechanical performance of small size beams. As a result 35 different specimen groups were obtained. Compressive strength, splitting tensile strength and 4-point bending tests were carried out on these specimens for thoroughly evaluating mechanical performance and cracking mechanisms. Detailed fiber orientation tests were carried out on the selected specimens in the hardened state, to understand the fiber orientation states of the specimens and their effects on the resulting performance. The results showed that fiber orientation in the casting direction can be made possible by using a casting flow methodology. Both of the investigated parameters (a/d and t/f_L ratios) and varying fiber parameters were found to highly affect resulting mechanical performance and cracking patterns under bending. 3 point bending tests on notched specimens were done for modeling bending behavior by using an existing model and the model was further developed by introducing new parameters for short FRC.

ÖZET

KENDİLİĞİNDEN YERLEŞEN ÇELİK LİFLİ BETONLARIN MEKANİK VE REOLOJİ ÖZELLİKLERİ

Bu araştırmanın temel amacı farklı çelik lif hacim ve tipleri (kısa ve uzun) içeren kendiliğinden yerleşen çelik lifli betonların performansı etkileyen değişik parametrelerin daha da anlaşılmasıdır. Bu malzemelerin taze ve sertleşmiş haldeki özellikleri çeşitli deney yöntemleri kullanılarak araştırılmıştır. Bu amaçla lifsiz ve 2 faklı çelik lif hacmi (0.5% ve 1%) ve iki farklı lif uzunluğu içeren 5 karışım üretilmiştir. Akışkanlık ve reolojinin yanı sıra yukarıda belirtilen karışımların statik ve dinamik ayrışma direnci taze halde incelenmiş ve rapor edilmiştir. Bu 5 karışım ile değişik boyutlarda numuneler üretildi. 6 farklı genişlik ve derinlik (30 mm - 100 mm), 4 değişik uzunluk (200 mm - 425 mm) kullanılarak, kesme açıklığının kiriş derinliğine oranı (a/d) ve numune kalınlığının lif uzunluğuna oranı (t/f_L) parametrelerinin küçük boyutlu kirişlerin mekanik performansı üzerine olan etkileri incelendi. Sonuç olarak 35 farklı numune grubu üretildi. Mekanik performansı kapsamlı şekilde değerlendirmek ve değişik parametrelerden kaynaklanan çatlak mekanizmasını incelemek için bu numuneler üzerinde basınç dayanımı, yarmada çekme dayanımı ve 4 noktalı eğilme deneyleri yapılmıştır. Numunelerin lif yönlendirme durumlarını ve elde edilen performans üzerindeki etkilerini anlamak için seçilen numuneler üzerinde sertleşmiş halde ayrıntılı çelik lif oryantasyon testleri gerçekleştirildi. Sonuçlar, bir döküm akış metodolojisi kullanılarak döküm yönünde lif yönlendirmesinin yapılabileceğini gösterdi. Incelenen parametrelerden her ikisi de (a/d ve t/f_L oranı) ve değişen lif parametreleri, elde edilen mekanik performansı ve eğilme atındaki çatlak biçimlerini büyük ölçüde etkilemiştir. Çentikli numuneler üzerinde gerçekleştirilen 3 noktalı eğilme deneyleri mevcut bir model kullanılarak lifli numunelerin eğilme davranışını modellemek için yapılmıştır ve bu model kısa lifli numuneler için yeni parametreler kullanılarak daha da geliştirilmiştir.

TABLE OF CONTENTS

LIST OF FIGURES

LIST OF TABLES

LIST OF SYMBOLS

E	Elastic Modulus
T/F_L	Specimen thickness to fiber length ratio
f_c	Concrete compressive strength
$f_{fctm,ax}$	Uniaxial elastic tensile strength
$f_{fctm,eq,bil}$	Equivalent post cracking tensile strength
$f_{fctm,splt}$	Splitting tensile strength
w_0	Critical crack width
w_c	Characteristic crack width
ε_{c0}	Linear elastic strain limit
ε_{cmax}	Ultimate strain limit
ε_{ct}	Uniaxial elastic tensile strain

LIST OF ACRONYMS/ABBREVIATIONS

C	Control or plain specimens
L5	0.5% long fiber reinforced specimens
S5	0.5% short fiber reinforced specimens
L10	1% long fiber reinforced specimens
H10	1% hybrid (0.5% short and 0.5% long) fiber reinforced specimens
FTF	Flexural Toughness Factor
a/d	Shear span to depth ratio
EBS	Equivalent bending strength
CMOD	Crack mouth opening displacement
COD	Crack opening displacement

1. INTRODUCTION

Self-compacting concrete (SCC) is widely used for construction of civil engineering structures in order to eliminate compaction and vibration, which result in reduced construction time and energy consumption. It has to be placed under its own weight with superior flow characteristics without segregation and bleeding. High cement content and chemical admixtures are required to obtain high flowability, which cause increased cost, high thermal stresses and shrinkage. Mineral admixtures such as fly ash, silica fume and slag are added to the concrete so as to decrease cement amount, thermal stresses and shrinkage of the concrete [82].

The use of steel fibers in concretes has many advantages in terms of durability, serviceability and ultimate limit state behavior. Steel fibers have superior tensile strength capacity compared to conventional concrete and support concrete in the shear and tension zones. Steel fibers have crack bridging capacity so that crack distribution can be controlled and further growth of the cracks can be hindered. Crack control or reduced crack width on concrete decreases permeability of aggressive ions/agents into the concrete, contributes to structural integrity and durability of the structure. In addition, steel fiber usage decreases the thickness of concrete cover so that specimen sizes and weight of the structural elements decrease; therefore, structures experience lesser earthquake forces resulting increased structural safety. The amount of shear and tensile reinforcement can be reduced by adding high percentage of steel fibers in structural elements [83].

Steel fiber reinforced concrete (SFRC) has been used in both columns and beams where shear stresses are of critical and steel fibers have been partially used instead of stirrups as shear reinforcement. In high seismic zones, design codes impose the use of transverse reinforcements in order to obtain ductile behavior and large amounts of transverse reinforcements are required especially in heavier structural elements. However, such congested reinforcements may cause concrete placement problem in narrower structural elements. The use of steel fiber can reduce the amount of transverse rein-

forcements and can be a solution for the concrete placement. In most situations, high amount of steel fiber reinforcement ($\geq 1\%$) is required to obtain better structural performance. However, such amount of steel fiber may also cause workability problem in concrete. A combination of steel fiber reinforced concrete with a self compacting concrete is used and defined as steel fiber reinforced self-compacting concrete (SFR-SCC) in order to obtain high flowability to solve workability and concrete placement problem [84].

SFR-SCC usage has many advantages in concrete industry. SFR-SCC has contributed to noise pollution, construction time and labor cost due to lack of external vibration. In nowadays, electric energy and labor costs become a significant part in the overall cost of the structure. SFR-SCC can flow under its self-weight without segregation and bleeding, and can fill the moulds without a need of vibration and man-power. SFR-SCC has used in semi-structural applications where steel fibers used as secondary reinforcement. Structural applications of the SFR-SCC are; slabs and pavements, water tanks, channels, pipes, precast piles, precast walls, and blast resistance structures. SFR-SCC will be used more when steel fibers totally take place of the conventional steel reinforcement with further investigation [6].

Use of steel fibers in SCC is still limited due to lack of required codes & standards in this field. More research is required to understand the effects of steel fibers on mechanical strength and durability properties of concrete. Steel fiber type (smooth, hooked-end), fiber fractions (amounts), fiber geometry (lengths, aspect ratios) and fiber dispersion characteristics should be investigated thoroughly and steel fibers should be involved in the design phase of SCC [85].

In this research, main parameters; steel fiber types and amounts, specimen thickness to fiber length ratio (t/f_L) and shear span to depth ratio (a/d) were investigated on different specimen sizes for better understanding of the material behavior of the SFR-SCC. Crack pattern / monitoring was also investigated based on the main parameters. In conventional concrete beams, a/d determines the types of failure; bending types of failure is realized when a/d is high, whereas shear types of failure is observed when a/d

ratio is low, depending on the amount of shear and flexural reinforcement. In SFR-SCC concrete (without rebar), a/d may be found an effective parameter by contribution of higher amounts of steel fibers. In addition, previous studies showed that specimen thickness to fiber length ratio (t/f_L) was also found an important parameter influencing the flexural strength and toughness characteristics of the material. In literature, there is no or very limited study about the effects of varying a/d and t/f_L ratios on the mechanical performance of small size beams (when no conventional reinforcement was used). Small size beam specimens are commonly used for material characterization. Therefore, possible effects of varying a/d and t/f_L ratio on mechanical performance of only fiber reinforced concretes are not known. Therefore, it is important to understand different mechanism which may affect the material behavior and characterization when no conventional reinforcement was used. Material characterization is needed for design of fiber reinforced composite materials. Bending tests are commonly used for material characterization and therefore, it is important to understand different mechanisms which may affect the material behavior for fiber reinforced materials. Due to lack of tensile stress-strain diagrams and lack of material characterization, FRC has not been standardized yet. Therefore, an inverse model (multi-layer model) was adopted from previous studies and modified for different steel fiber types and amounts in order to predict tensile stress-strain behavior of SFR-SCC. In this research, further understanding of the SFR-SCC behavior and a contribution of the modelling of the tensile stress-strain diagram for standardization is aimed.

2. LITERATURE REVIEW

2.1. Steel Fiber Reinforced Self-Compacting Concrete (SFR-SCC)

Self-compacting concrete (SCC) is widely used for construction of civil engineering structures, especially in pre-cast industries, high rise buildings and structures that need congested reinforcement. SCC technology achieved a significant breakthrough in construction industry with the three main advantages which are workability, flowability and passing ability. Thanks to these properties, concrete can be placed to complex shape moulds under its own weight without segregation and/or bleeding. During casting, energy consumption, labor works and construction time are reduced since external vibration is not required. SCC can flow between narrower openings easily; thus reducing structural element sizes, formwork and material costs.

Plain concrete is a brittle heterogeneous material that is strong in compression conversely weak in tension and flexure. Due to this weakness, concrete cracks under relatively small tensile stresses and with limited energy absorption capacity resulting in sudden failure. With the advent of technology, this deficiency has been solved placing steel reinforcement on tensile region in structural members, which resulted in improved tensile strength and toughness of the reinforced concrete.

From the light of the structural steel reinforcement contribution to the tensile strength of concrete, steel fiber usage in concrete industry has also been developed recently. Steel fiber reinforced concrete has superior tensile and flexural performance with respect to plain concrete depending on the type and amount of the steel fibers. In addition to this, the role of crack bridging ability and crack width control increases interest in using steel fibers in concrete, especially in the post-cracking phase. Most important contributions of the steel fibers into the concrete are increased toughness (area under the load-deflection curve) especially under flexural loading, increased tensile and shear strength capacity and modified crack formation mechanism. These important properties made fiber reinforced concrete popular in the research.

Steel fiber inclusion into self-compacted concrete affects mainly workability of the mixes. Flowability and passing ability of the self-compacted concrete generally decreases with an increase in steel fiber amount in the concrete. The amount of the steel fibers should be carefully selected so that steel fiber reinforced self-compacted concrete (SFR-SCC) can go through between congested reinforcements without blocking. At the same time, fiber driving ability of the concretes should be so high that discontinuous steel fibers can be dispersed randomly in a specimen volume without static and dynamic segregation. The load transfer between discontinuous fibers should be possible provided that steel fibers are randomly dispersed around the concrete.

Use of steel fibers in SCC is still limited due to lack of required codes & standards in this field. More research is required to understand the effects of steel fibers on mechanical strength and durability properties of concrete. Steel fiber type (smooth, hooked-end), usable fiber percentage (amount), fiber geometry (lengths, aspect ratios) and fiber dispersion characteristics should be investigated thoroughly and steel fibers should be involved in the design phase of SCC [29]. For this purpose, two types of steel fibers with various fiber fractions were used in the research in order to find out the effect of steel fibers on flowability, passing ability, rheological & mechanical properties of SCC. Based on these properties, high dynamic and static segregation resistance of the SCC mixes are required in order to obtain random dispersion of steel fibers along the specimen volume, which result in high quality concrete [73].

2.1.1. Introduction to SFR-SCC

2.1.1.1. Definition of the steel fiber reinforced self-compacted concrete. Steel fiber reinforced self-compacted concrete is a heterogeneous composite type concrete that includes different types of discontinues steel fibers. Characteristic features of SCC comes from its ingredients such as cement, supplementary cementitious materials (fly ash, slag and silica fume, etc.), coarse and fine aggregates, water and superplasticizers. Steel fibers are proved to enhance both mechanic and durability properties of concrete. The combination of the two distinct material makes SFR-SCC more flexible, durable and strong than the other cement based materials.

2.1.1.2. Main benefits of steel fibers in concretes. Fibers were originally used in ancient times in order to strengthen the matrix without considering the effect of toughness. With further developments and research, steel fibers started to use and the main benefit of the steel fibers was understood as the improvements in energy absorption capacity (toughness) by carrying tensile stresses after crack formation. Ductility of structural members can be improved by using fibers. In addition, first cracking and ultimate tensile strength, flexural strength, shear strength and impact resistance are also increased with an increase in steel fiber usage. Other main benefits of using steel fibers in SCCs apart from the mechanical improvements are the increased shrinkage crack resistance, delamination and spall resistance, corrosion resistance and fatigue resistance [1].

2.1.1.3. Advantages of using SCC concrete in construction industry. Self compacting concrete has been widely used in construction industry for different purposes. There are many benefits of using SCC in cases that material costs should be minimized. If SCC is preferred instead of normal concrete; construction time and labor costs are reduced, vibration is not required, noise pollution is decreased, since filling ability between congested reinforcements is increased concrete casting and control procedures are easier [2].

2.1.1.4. Current application of steel fibers. In most of the structural applications, steel fibers in the SCC are used as secondary reinforcements due to the lack of national and international standards. Therefore, partially structural applications of the SFR-SCC were given as following [3];

- In the slabs and pavements, used as secondary reinforcement in order to reduce / control cracks caused by the temperature and humidity variation (structural reinforcement is not effective),
- In the tunnel segments, precast piles, precast walls, and blast resistance structures, used to withstand high loads and deformations,
- Thin sheets or elements where structural rebars cannot be used due to either

complex shapes or less concrete cover of structural elements (difficult to protect structural rebar from corrosion).

2.1.2. Parameters affecting Workability of SFR-SCC

The main characteristics of SFR-SCC are flowability, filling and passing ability without segregation and/or bleeding. These properties are mainly affected by mix composition and steel fiber type and amounts. In designing the SCC mix proportions and quantities, typical ranges of materials are listed below. However, further modifications for strength and other performance requirements are as follows [11]:

- Water to powder ratio by volume: 0.8-1.1,
- Total powder amount by weight: 400-600 kg/m^3,
- Coarse aggregate content: 28-35% by volume of the mix,
- Water to cement ratio is selected according to EN 206 requirements. Water content should be less than 200 liters per m3 of concrete.
- Sand amount should balance other material volumes.

The parameters which affect the flow and passing ability properties of SFR-SCC are investigated in details below.

2.1.2.1. Effect of Cement. Different types of cement can be used to obtain SCC properties. The amount of cement is generally determined by required compressive strength and durability characteristics. The minimum cement content is selected for different environmental conditions and exposure classes given in EN 206 standard. For SCC applications, high amount of cement material is needed to increase flowability and facilitate self-compacting. However, too much cement usage increases drying shrinkage and cost of materials. For this purpose, cementitious materials such as fly ash, limestone powder, silica fume, slag are used in SCC in order to increase segregation resistance and reduce the cost of the concrete [12].

2.1.2.2. Effect of Fly Ash. Fly ash is a by-product of coal power plants and it can be used as a partial replacement of Portland cement due to its pozzolanic reactions. The use of fly ash generally enhances durability of concrete and provides resistance to segregation, freeze-thaw, sulphate, abrasion and alkali-silica reactions. Since fly ash is an industrial waste material, its usage decreases environmental pollution and make a positive effect on country's economy [13]. The amount of F- type fly ash in the various studies did not exceed 30% by weight of the total cementitious (cement + fly ash) material [14].

2.1.2.3. Effect of Aggregates. For a given water-to- binder ratio, rounded aggregates have better flowability and less blocking potential with respect to the angular and semi-rounded aggregates. In addition, flaky and elongated aggregates cause blocking in narrower openings. [15] In addition to high deformability of paste and mortar, SCC depends on the segregation resistance between coarse aggregate and mortar when concrete flows between structural reinforcements. Limiting coarse aggregate content decreases the risk of blocking. The amount of fine aggregate in SCC mortar should be 60% so that shear deformations in the concrete is limited in the fresh state [16]. The coarse to fine aggregate ratio in the SCC mixes should be decreased so that coarse aggregates are fully surrounded by a mortar layer. The amount of cementitious paste must be sufficient that total voids of aggregate and fiber-matrix interface should be minimized. In order to obtain mixes with high steel fiber fractions, high binder volume and lower coarse aggregate volume are required [17]. In addition to limitation in coarse aggregate content, maximum grain size of the coarse aggregate is also reduced in order to eliminate the blocking risk. Therefore, maximum grain size of the used coarse aggregates should be reduced to 10 mm [20].

2.1.2.4. Effect of Water. Flowability of a mix depends on the water content in the SCC mix. Water amount should be selected so that concrete can flow without segregation and/or bleeding. In case of low water content, workability of the mixes is compensated by adding superplasticizer or ultrafine powder. However, a change in the superplasticizer amount causes bleeding, which adversely affects cohesiveness. If su-

perplasticizer and ultrafine powder amounts are kept constant, workability of the SCC mixes depends on the water content. The water amount may be increased up to 200 kg/m3 if crushed stone aggregates are used. [18].

2.1.2.5. Effect of Superplasticizer. Superplasticizer (SP) is a chemical admixture which is used as dispersant to prevent segregation and enhance flowability and self-compacting ability of SCC mixes. Different types of superplasticizer exist; however, high range water reducing admixtures are used in the SCC. The amount of superplasticizer is selected based on the water content in the mixes. The addition of an adequate dosage of superplasticizer into a mixture enables reduction of water to binder ratio without influencing workability; therefore, high strength SCC may be obtained [15].

2.1.2.6. Effect of Steel Fiber. Workability of the SFR-SCC mainly depends on steel fiber types and amounts, and the properties of matrix constituents. Uniform distribution of fibers is difficult in concretes with high steel fiber fractions; however, higher steel fiber amounts are required for optimum benefits of steel fibers. Workability of concrete decreases with an increasing amount of steel fibers. For the same steel fiber content, better workability is obtained when lower aspect ratios (steel fiber length to diameter ratio) are used. From structural point of view, better performance of SFR-SCC was obtained at high steel fiber amounts and high aspect ratios [19]. However, it was reported that a higher fiber aspect ratio adversely affected the workability of SCC and caused balling effect during mixing and also defects in hardened state, as a result affects overall mechanical performance of the SFR-SCC. In addition, steel fibers with a small diameter may cause sinking or itching hands of the workers [1].

2.1.3. Fresh State Tests of SFR-SCC

Different test methods have been developed so far in order to evaluate fresh state properties of SCC. However, no single test method has been found to characterize workability aspects such as flowability- filling ability, passing ability and segregation resistance. Therefore, more than one test methods have been used for the each worka-

bility aspects. Test methods for workability properties of SCC and related acceptance criteria are given in Table 2.1 and Table 2.2. [11]. Detailed information about the fresh state test is given below.

Table 2.1. Test methods for workability properties of SCC [11].

	Method	**Property**
1	Slump-Flow by Abrams cone	Filling ability
2	T50cm slump flow	Filling ability
3	J-Ring	Passing ability
4	V-Funnel	Filling ability
5	V-Funnel at T5minutes	Segregation resistance
6	L-Box	Passing ability
7	U-Box	Passing ability
8	Fill-Box	Passing ability
9	GTM screen stability test	Segregation resistance
10	Orimet	Filling ability

Table 2.2. Acceptance criteria for self-compacted concrete [11].

	Method	**Unit**	**Typical Range of values**	
			Minimum	**Maximum**
1	Slump-Flow by Abrams cone	mm	650	800
2	T50cm slump flow	sec	2	5
3	J-Ring	mm	0	10
4	V-Funnel	sec	6	12
5	V-Funnel at T5minutes	sec	0	3
6	L-Box	(h2/h1)	0.8	1
7	U-Box	(h2-h1) mm	0	30
8	Fill-Box	%	90	100
9	GTM screen stability test	%	0	15
10	Orimet	sec	0	5

2.1.3.1. Flowability (Filling Ability). Slump flow test is used to determine the flowability of SCC in the absence of obstacles. Final flow diameter and time to reach 500 mm flow (T50cm) was measured to evaluate the slump flow. This test can be done in laboratory and in-situ with Abram's cone because of its simplicity. Segregation resistance of the mix is inspected visually. Slump flow test apparatus is given in Figure 2.1. In addition to this, typical slump flow classes (SF1, SF2 and SF3) can be adopted for different applications [22]:

- SF1 class (flow diameter ranges from 550-650 mm) is used for unreinforced or slightly reinforced concrete structures (piles, some deep foundations, tunnel linings),
- SF2 class (flow diameter ranges from 660-750 mm) is applicable for structural elements (walls, columns),
- SF3 class (flow diameter ranges from 760-850 mm) is appropriate for very congested reinforcement required structures and structures with complex shapes. In this class, maximum aggregate size (dmax) should be less than 16 mm.

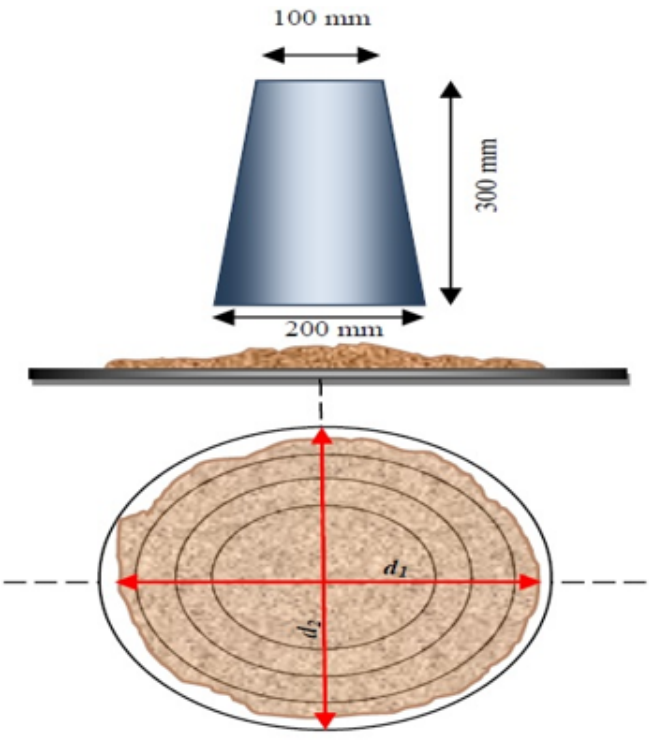

Figure 2.1. Slump flow test apparatus [21].

2.1.3.2. Passing Ability. Passing ability is the ability of a SCC mix to pass between congested reinforcements without blocking, segregation and bleeding. J-ring, L-Box, U-Box and Filling Box tests are used to evaluate passing ability properties of SCC mixes. In the passing ability tests, concrete flows between obstacles and flow height of concrete is measured at inner and outer parts of the ring or box. For considering passing ability, geometry and spacing of structural reinforcement and maximum aggregate size should be taken into account.

Size (d_{max}), shape and amount of the aggregates influence passing ability. With the increasing size and amount, blockage risk increases. Moreover, the steel fiber inclusion into the SFR-SCC, especially hooked-end long fibers, escalate the blocking risk deeply. Passing ability specifications may be divided into 2 classes:

- PA1 class: structures with a gap of 80 mm to 100 mm (housing and vertical structures),
- PA2 class: structures with a gap of 60 mm to 80 mm (civil engineering structures).

Passing ability is not required for structures with a gap greater than 100 mm. For complex structures with a gap lower than 60 mm, specific trials may be required. [22].

For measuring passing ability, J-Ring and L-Box tests are widely used. Both methods use steel rods as obstacles and concrete flow height differences are measured at inner and outer parts of the J-Ring or L-Box test apparatus. In Figure 2.2 and Figure 2.3, J-Ring test apparatus and L-Box test apparatus are given with dimensions, respectively.

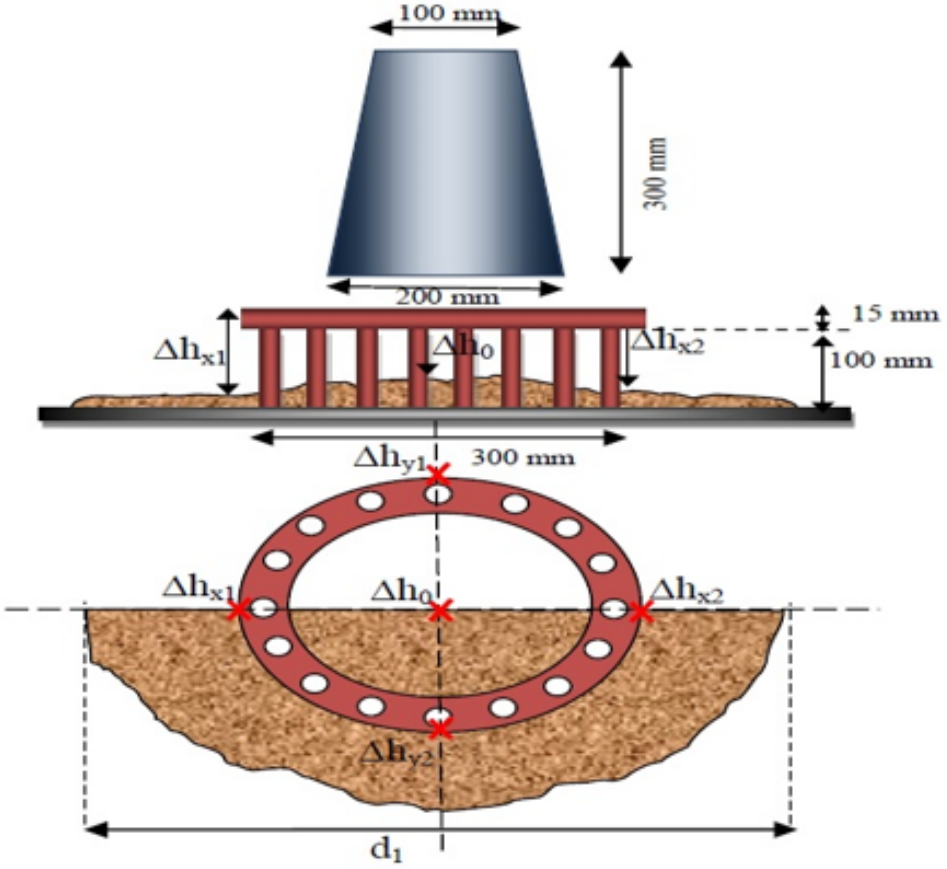

Figure 2.2. J-Ring test apparatus [21].

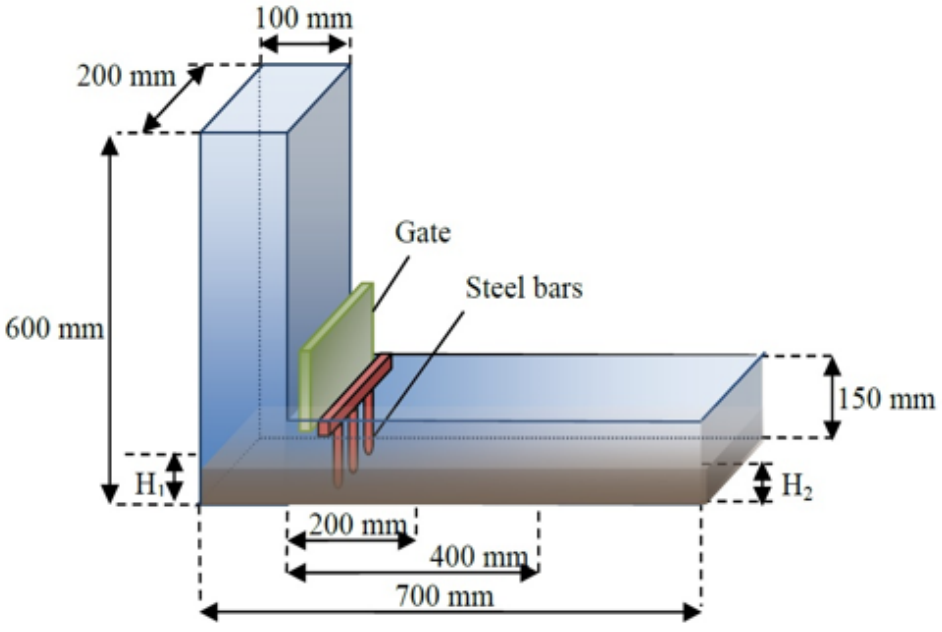

Figure 2.3. L-Box test apparatus [21].

2.1.3.3. Viscosity. Viscosity can be defined as the resistance to flow of concrete after flow has initiated and it can be evaluated with V funnel and T_{500} time of slump-flow test. Concrete with a low viscosity has a quick initial flow that stops in a short period of time. Concrete with a high viscosity may continue to flow for a long period of time. Viscosity is more important for structures with good surface finish and congested reinforcement. Viscosity should not be taken into account in other cases [22].

2.1.3.4. Segregation Resistance. Segregation resistance is an important parameter for SCC in order to obtain homogenous and quality concrete. Segregation may take place during and after casting and also before the setting of concrete. Segregation problem can be hazardous for longer structural elements due to the surface defects (cracks, weak surface) which affect the strength adversely. Segregation resistance becomes important with higher slump and lower viscosity classes. If these applications are not required, there is no need for segregation resistance class. Two segregation resistance classes are available; SR1 is applicable for vertical elements and also thin sections with a flow distance of less than 5 meter. SR^2 is suitable for vertical elements with a flow distance greater than 5 meter [22].

2.1.4. Factors Influencing Mechanical Properties of SFR-SCC

Mechanical properties of SFR-SCC specimens are mainly affected by steel fiber characteristics (steel fiber type, amount, aspect ratio), and concrete material components (binder, aggregate and superplasticizer types and amounts). Properly determined proportions change both fresh and hardened state behavior of SFR-SCCs. Detailed information for each material ingredient and their effects on material behavior are explained herein.

2.1.4.1. Influence of Steel Fiber Type. There is a wide range of fiber types, steel fiber, synthetic fiber, glass fiber, natural organic and inorganic fibers; however, steel fibers are the most used fiber types in construction industry. Steel fiber performance is influenced by 3 different properties: (1) the aspect ratio (L/d) of the steel fiber; (2) steel fiber

shape (straight, hook-end) and surface deformation; (3) surface treatment. Surface deformation is generally conducted in order to increase the anchorage between matrix and fiber. The used steel fibers have a circular cross section with a diameter changing from 0.2 mm to 1 mm, with a length varying from 10 mm to 60 mm and with an aspect ratio less than 100. Types of steel fibers can be seen in Figure 2.4. For better bond between steel fiber and concrete matrix, steel fibers may be modified by surface and mechanical deformations [4].

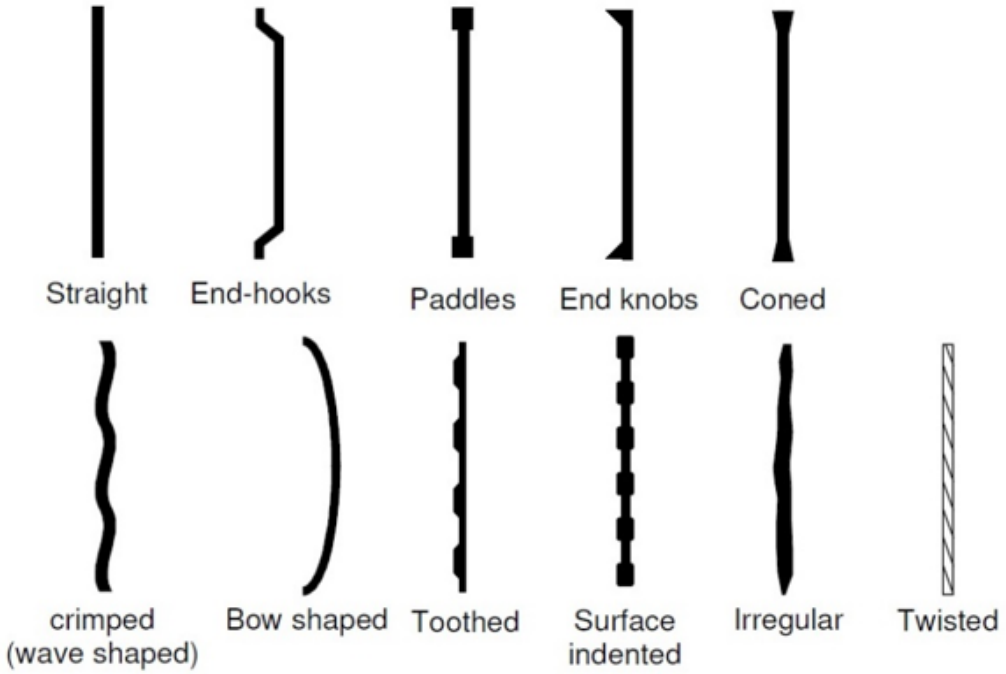

Figure 2.4. Different types of steel fibers [4].

For structural applications, straight and hooked-end type steel fibers have been widely used. Plain concrete goes into failure under tensile or flexural loading by formation of a single crack. However steel fiber reinforced concrete resists additional crack openings and multiple cracks observed before the failure. This is due to two separate mechanisms: (1) when tensile stress on the concrete exceeds its tensile strength, micro-cracks start to emerge. The steel fiber has a capability of arrest the micro cracks and hence prevent the formation of macro-cracks (Micro-crack arrest mechanism); (2) for further stresses, micro-cracks widen and turn into macro cracks. After macro-crack formation, steel fibers bridge the cracks and prevent further widening of the cracks

(Crack bridging mechanism) [5].

Thanks to crack bridging ability of steel fibers, crack distribution can be controlled and further growth of the cracks can be hindered. Reduced crack widths on concrete decreases permeability of aggressive ions/agents into the concrete. In addition, steel fiber use decrease corrosion rate by decreasing crack widths in concretes which have a low water-to-cement ratio. Therefore, steel fibers contribute to structural integrity due to greater bond between aggregates and fiber matrix and so increase life span or durability of the structure [8].

In addition to crack bridging ability of steel fiber in structures, steel fibers increase shear and moment resistance of the structures and also have an influence on stiffness and ductility properties of the composite material. The positive effects of steel fibers on structural behavior are summarized as is seen in Figure 2.5.

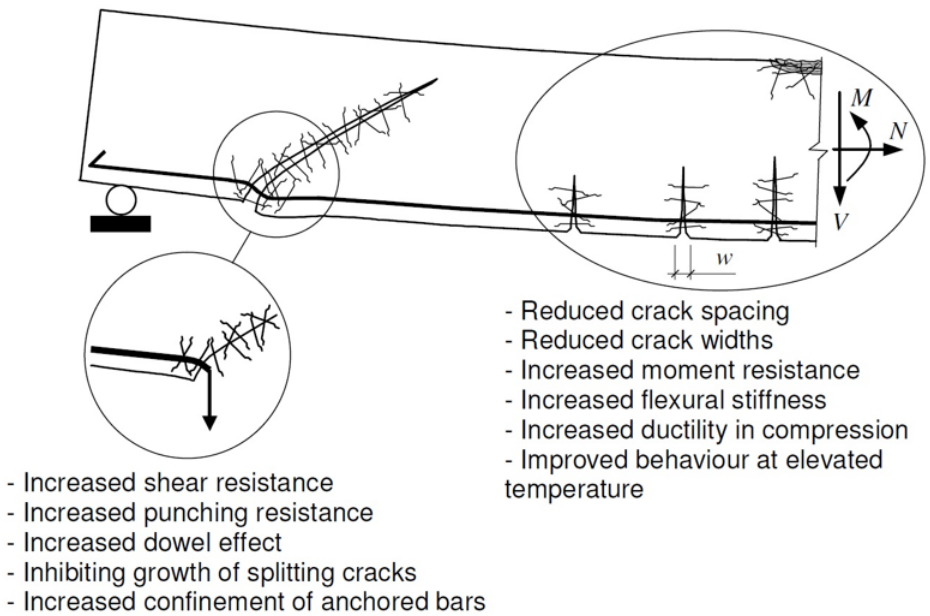

Figure 2.5. Effect of fibers in structural behavior [4].

The overall mechanical behavior of a smooth steel fiber can be identified with two phases: debonding of the matrix and frictional slip of the steel fiber. Steel fiber pullout take place under frictional resistance after the fiber embedment length is fully

debonded. The pullout behavior of smooth steel fibers is identified with load (N) - slip (s) curve as is seen in Figure 2.6. In the first pre-peak curve, the pullout load raises with an increase in slip (0-A). For the A-B region, micro-cracks emerge at the interfacial transition zone (ITZ) referring initiation of debonding process. After the maximum load is reached, for the B-C part (post peak curve), the load declines with an increasing slippage, corresponding unstable crack growth on the post-peak behavior and fully debonding occurs at point C. Fiber pullout takes place between the region of C-D. In this part, frictional area of the fiber decreases with the roughness of the matrix [6].

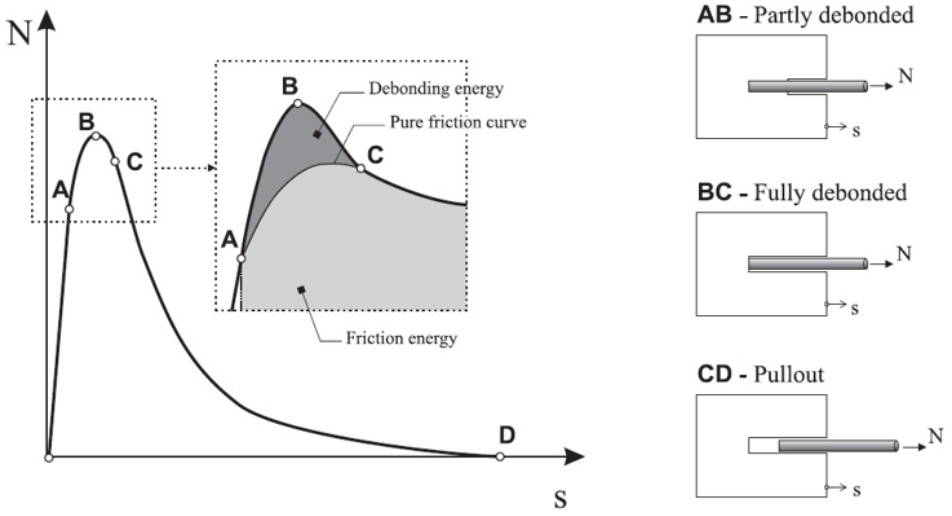

Figure 2.6. Pullout relationships between the load and end slip of a smooth fiber [6].

The pullout relationship of both smooth and hooked-end fibers is given in Figure 2.7. For hook end steel fibers, the pre-peak behavior is identified with 3 phases, 0-A and A-B regions are associated with adhesive bond and debonding process until the point B where full debonding takes place at point B. After full debonding due to mechanical anchorage of fiber hook, additional load increases at points of B-C. At the maximum load at point C, the points 1 and 2 are deformed. Then, mechanical anchorage deforms progressively and pullout force starts to decrease at points of C-D. Later, another peak load is observed during fiber passing the last corner of the fiber projected in the matrix at points of D-E, while hook end fiber has not fully straightened. After the fiber fully straightening at points E-F, pullout process of hook-end fiber becomes similar to

straight fiber's. [6]

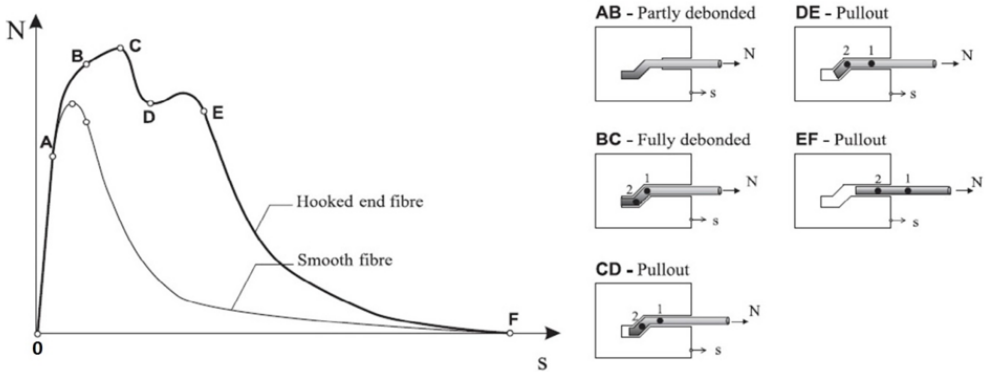

Figure 2.7. Pullout relationships between the load and end slip of a hook end fiber [6].

2.1.4.2. Influence of steel fiber amount (V_f). SFRSCC properties mainly depend on the steel fiber amount or fractions in the mixture. As the amount of steel fibers increases in the mix, flexural strength, shear strength and flexural toughness values are improved due to the enhancement in the ductility of the mix. In addition, tensile strength and crack opening displacement capacity of the concretes improve with an increasing steel fiber fractions (V_f) as is seen in Figure 2.8. Inclusion of the high amount steel fibers especially improved the post crack residual tensile strength and ductility of the concretes [7].

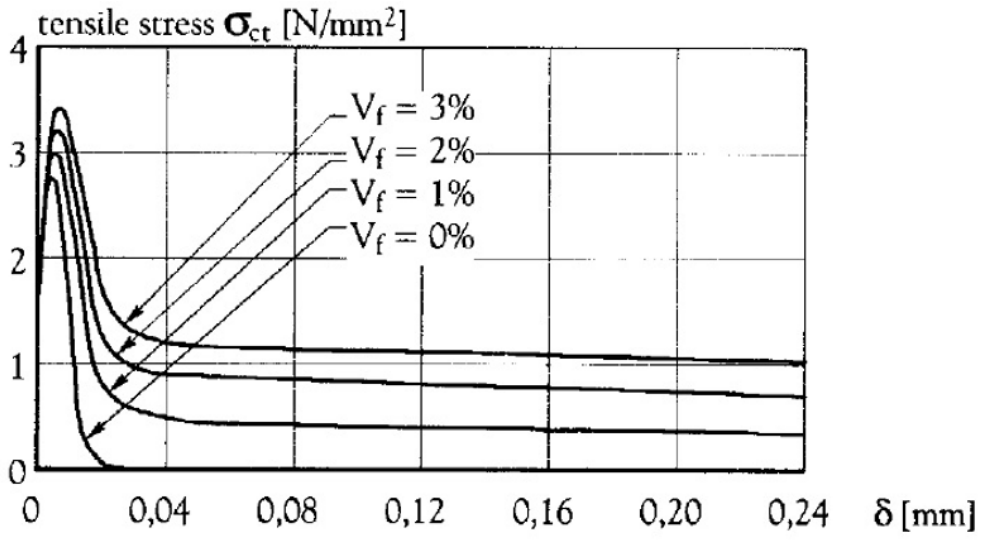

Figure 2.8. Typical stress-crack opening displacement relations for SFRC and plain concrete [7].

Steel fiber content in a mixture generally ranges from 0.3 to 2%. For lower fiber amouns, impact of the fibers on the SCC concrete remains limited. For higher volume fractions than 2%, workability of the SCC reduces and passing ability problems emerge especially in the structures that high percentage structural reinforcement. In addition, steel fibers are expensive materials, usage of higher percentages may become costly. For economic considerations, optimum usage of the steel fibers is considered as 1% for the majority of structures [9].

2.1.4.3. Influence of steel fiber aspect ratio (l/d). Fiber aspect ratio is the ratio of steel fiber length to diameter. In structural applications, l/d ranges from 50 to 100. Large fiber aspect ratio, representing a higher fiber matrix bond area that better bond is available between fiber and matrix and so high energy absorption capacity is obtained in the concretes. The fiber length is also another important factor for structural behavior of the SFR-SCC. Under same fiber aspect ratio, shorter fibers include larger number of fibers than longer fibers; which result in better crack bridging and stress transfer across the cracks [10].

2.2. Fiber Distribution and Orientation Analysis

Fiber distribution is a very important parameter for SFR-SCC. From material selection to hardened state of SCC, different parameters affect the fiber distribution. A uniform fiber distribution enables proper stress transfer between steel fibers throughout SCC so that better durability and mechanical performance of SCC can be obtained. Poor distribution of fibers can cause defects in the matrix fiber interface and failure can be realized. For standardization of SFR-SCC into structural design codes, random fiber distribution along the overall concrete section has to be fulfilled. Therefore, parameters influencing the fiber distribution have to be determined and precautions have to be taken to eliminate possible non-uniform steel fiber distribution.

The main factors influencing the steel fiber distributions are mix composition (steel fiber length and maximum aggregate grain size), sample sizes, direction of con-

crete casting, formwork boundaries, workability and rheological properties of SCC, and presence of obstacles (narrower structural reinforcement). Among them more controlled parameters are the steel fiber length and maximum aggregate grain size. Considering a unit volume of mould, as maximum aggregate grain size (d_{max}) increases, the number of steel fibers in the unit volume decreases as is seen in Figure 2.9, which causes non-uniform distribution of steel fibers. For better fiber distribution, steel fiber length should be at least 2-4 times bigger than the maximum aggregate grain size and steel fiber volume should be maximum 2% (for low aspect ratios) and 1% (for high aspect ratios) [23].

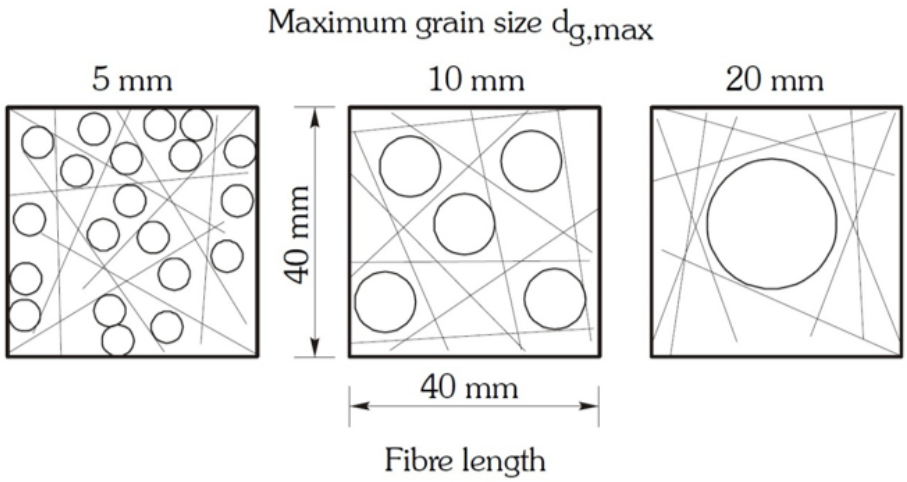

Figure 2.9. Effect of maximum aggregate size on steel fiber distribution [23].

Mechanical performance of steel fibers is related to pullout performance and bond characteristics between fiber and matrix. However, fiber distribution plays a significant role in the first cracking stress and multiple cracking responses. Fiber free areas due to non-uniform distribution of fibers decreases first cracking strength of the composite and sequential bigger cracks occurred depending on the size of the fiber free areas at the cross section. As the size and number of matrix areas that are not supported by fibers rises, crack initiation requires less energy and after the crack formation, cracks further develop in the fiber free matrix easily. If fiber distribution is uniform at first crack localization, an effective crack bridging and toughness of the composite can be obtained [24]. Therefore, homogeneous fiber dispersion is highly significant in order to

obtain better mechanical and durability performance.

There are various methods (non-destructive and destructive) in order to characterize the fiber distribution on fiber reinforced specimens. An electrical characterization method - alternating current-impedance spectroscopy (AC-IS) technique can be used in order to find out fiber dispersion. Fiber dispersion characteristics were evaluated using an intrinsic conductivity approach in which a voltage applied to the concrete specimens and the magnitude and phase of the current is measured [25].

Computer Tomography (CT) scan is another technique for fiber dispersion monitoring and in this method steel fibers can be detected by means of computer tomography with a resolution of 0.4 mm [31].

X-Ray photos of concrete specimens were also used for evaluation of fiber distribution; however, the results obtained were different from actual fiber content and deviation in the results were attributed to the lack of third dimension and higher percentage short fiber amounts [32].

Fiber distribution analysis can be also evaluated by means of statistical point processes. The method examines the fiber intensity, fiber clump tendency and fiber amounts in a cross section. The intensity of fibers in different parts of the specimens gives a general description of the fiber pattern and material properties [33].

Different methods and measurement techniques in order to determine fiber orientation are summarized in Table 2.3 [48].

Table 2.3. Methods to determination of fiber orientation [48].

Method	Measurements	Technique	References
Destructive	Indirect	Manual counting	Soroushian and Lee (1990);
		theoretical expression by Krenchel (1975)	Gettu *et al.*, (2005); Dupont and Vandewalle (2005)
		Mechanical testing	Kooiman (2000); Barragan (2002); Grünewald (2004); Pujadas *et al.*, (2011)
	Direct	Image analysis	Grünewald (2004); Lapp (2007)
		X-Ray method Computarized Tomography	Van Gysel (2004); Robins *et al.*, (2003); Vandewalle *et al.*, (2008) Stahli and van Mier (2007)
Non-destructive	Direct	Alternating current-impedance spectroscopy (AC-IS)	Özyurt *et al.*, (2006); Ferrara *et al.*, (2008)
		Open coaxiay transmission line	Torrents *et al.*, (2009)
		Dielectric waveguid antennas	Requeta *et al.*, (2011)
		Electrical resistivity methods	Lataste *et al.*, (2008)
		Inductive method	Torrents *et al.*, (2012)

In most research, fiber distribution and orientation were destructively monitored by counting the steel fibers one by one on selected specimens in which fracture tests are applied first and then middle portion of the specimens is selected and fiber amounts are monitored. Manual counting is easy when steel fibers having low dosages and average aspect ratios are used. However, manual counting becomes very difficult and time consuming on specimens includes high amount short fiber with higher aspect ratios. Therefore, image analysis techniques are required for these specimens [30].

2.2.1. Image Analysis Method for Fiber Orientation Analysis

Image analysis technique is one of the most used and well-known method for fiber distribution and orientation analysis. It is a basic method for investigating microstructure of cement based materials. In this method, two (2D) or three dimensional (3D) micrographs of a slice taken from a specimen can be obtained by using an optical microscope and evaluation can be done using image analysis program. This method is reliable when used appropriately [28].

Image analysis is a preferred method since it is relatively cheap and it does not require a transparent specimen and with the automated 2D technique it is one of the

efficient and fastest techniques for calculating fiber orientation density (FOD). FOD can be determined by inspection of cross sections taken at predetermined locations. Surface preparation of the cross section is required in order to increase the contrast between steel fiber and concrete matrix. Surface preparation includes grinding and polishing the specimen. When a prepared surface is examined under reflected light microscopy, matrix areas scatter the light and polished fiber cross-sections reflect most of the incident light [34].

When a cylindrical steel fiber cross-section is perpendicular to the section plane, fiber will be visible as a circle, if fiber cross section makes an angle to the section plane, fiber will appear as an ellipse. In the ellipse case, the minor axis of the ellipse corresponds the fiber diameter of b, and the major axis of the ellipse corresponds the fiber length of a, as is seen in Figure 2.11. The out of plane orientation, can be calculated as [34]:

$$\theta = \arccos\left(b/a\right) \tag{2.1}$$

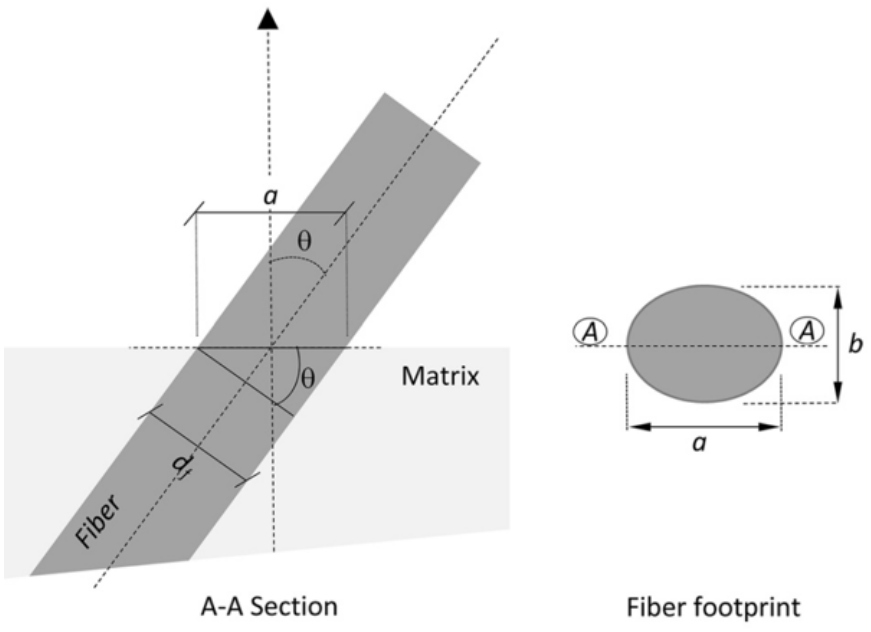

Figure 2.10. Fiber orientation parameters in a section [35].

The in-plane fiber orientation angle ϕ is equal to the ellipse major axis orientation with respect to an arbitrary in plane direction. By using image analysis method, fiber centers (xc, yc) and elliptical parameters (a, b, ϕ) can be determined using local orientation tensors as shown in Figure 2.11 [34].

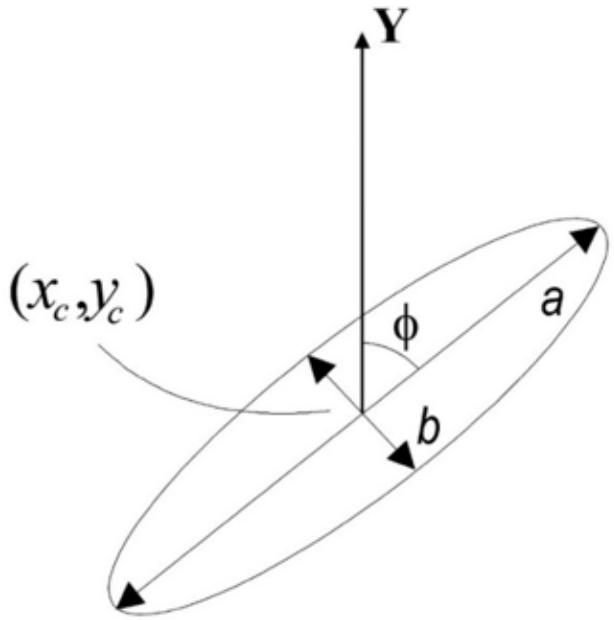

Figure 2.11. The shape and orientation of ellipse fibers [34].

After determining the elliptical parameters, a tensor description method was used in order to calculate fiber orientation densities in the global x, y and z directions. A detailed description of the used tensor method is given in Part 3.4.8.

2.2.2. Fiber Orientation

The mechanical behavior of SFRC is related to the orientation of steel fibers. The new technology of dispersed reinforcements enables direct and random fiber orientations in SFRC. A direct fiber dispersion along the stress direction results in higher mechanical strength rather than the random orientation, while fiber orientation along the transverse direction (perpendicular to flow direction) would not give any contribution to the strength.

Fiber orientation is influenced by a number of parameters, steel fiber type and geometry, interaction effect caused by aggregate, fiber and mould, flow characteristics of SCC, the means of casting and compacting of SCC, and geometry of the formwork and dimensions. Among these effects, rheological parameters of SCC, especially yield stress of the concrete and wall effect caused by the moulds could be considered as the most pronounced effects. A good orientation of fibers also is an indicator of higher ductility of fiber reinforced composites [36].

Steel fibers are oriented due to the flow velocity profile. When concrete flows in a channel, the flow velocity changes from zero at the walls to maximum at the centerline of the channel as are seen in Figure 2.12. Due to the various flow velocities, steel fibers can rotate from flow direction to the perpendicular flow direction as shown inFigure 2.12.a and Figure 2.12.b. During flow, SCC concrete is in fluid state and therefore, the fluidity applies hydrodynamic forces to the steel fibers, causing rotation and translation of steel fibers. The rotated steel fibers are also subjected to both forces and moments by the fluid, causing more disturbances on the orientations of steel fibers [36].

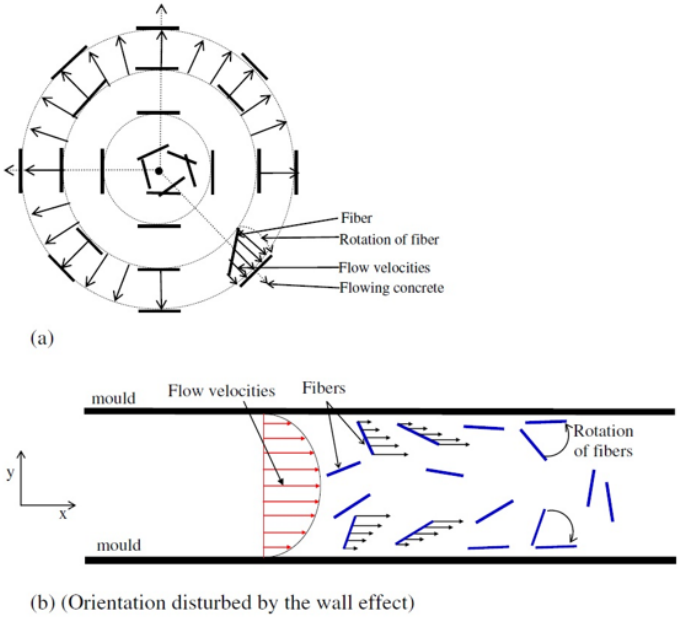

Figure 2.12. Fiber orientation in (a) fountain flowing and (b) canal channel flowing [36].

Fiber orientation depends on the fresh state properties (mainly flow property) of steel fiber reinforced self-compacted concrete (SFR-SCC). As flowability of SCC increases, steel fibers are prone to be aligned in the flow direction. The flexural strength is affected by dispersion and orientation of the steel fibers and this strength enhancement is improved when steel fibers are oriented in the direction of tensile stresses. This preferential orientation can be obtained better by means of good workability [31, 37].

When flexural resistance of a beam is considered, steel fibers should be distributed into the bottom parts of the beam (tension zone) with an orientation parallel in the direction of bending stress; whereas when considering the shear resistance of the beam, steel fibers should disperse uniformly along the beam with an orientation perpendicular with the direction of shear stress [38].

2.2.3. Static and Dynamic Segregation

Segregation resistance can be described as the resistance of SCC to particle separation. SCC components having a high density or a low surface to volume ratio are most susceptible to segregation. Segregation resistance of SCC can be divided to two distinct stages; static (at rest) and dynamic (during flow) segregation. Mixtures showing segregation have very smooth, fault-free surfaces as finer (cement or fly ash) particles segregates at the walls of the moulds [23].

Fresh state properties influence segregation resistance and mechanical performance. If vibration time is increased, the extent of segregation increased. Therefore, SCC has superior segregation resistance with respect to conventional concrete due to lack of vibration. In addition, SCC mixes have high viscosity and low yield stress. This is an important advantage since high viscosity guarantees high segregation resistance and low yield stress provides better place ability of concretes [25].

Dynamic segregation resistance is different from the static segregation resistance. Dynamic segregation resistance is related with flow induced particle migration based on different phenomena, while, static segregation is correlated with aggregate settling

process resulted from the density difference between the components when the concrete sample is at rest [27].

2.2.3.1. Static Segregation. Static segregation is the particle migration when concrete is at rest (static condition). SCC if properly designed may have advantages by means of static segregation resistance since it is more viscous when compared to conventional concrete. However, static segregation may still occur to some extent and affect resulting mechanical performance. Therefore, it is important to control fresh mixes by means of static segregation resistance [28].

2.2.3.2. Dynamic Segregation. Dynamic segregation can be defined as the flow-induced particle migration and may be divided into 3 physical phenomena: (i) shear induced particle migration, (ii) gravity induced particle migration, (iii) granular blocking. Shear induced particle migration and wall effect govern in pumping process and gravity induced particle migration governs all other potential sources of heterogeneity during flow. During casting, gravity induced particle migration dominates, and thus affects coarse particle concentration in concrete [27]. There are internal friction and cohesive forces between particles and also suspending phase decreases with an increase in casting flow length meanwhile after a certain flow length, suspending phase cannot resist gravitational forces. This can be the explanation of segregation of high density particles (coarse aggregate and steel fibers) [26].

Segregation resistance of concrete during flow and rest conditions can be determined by fresh state tests. After determining a stable mix, steel fibers and coarse aggregates do not have a tendency of downward settlement, meaning no static segregation expected. However, this may not be sufficient to guarantee all casting (flow) conditions. A concrete which is stable at rest (no static segregation), may be unstable during flow, (dynamic segregation) causing non-uniform distribution of coarse aggregates and steel fibers. Coarse aggregates showed a tendency of downward settlement as casting distance becomes 3m. (Figure 2.13) [27].

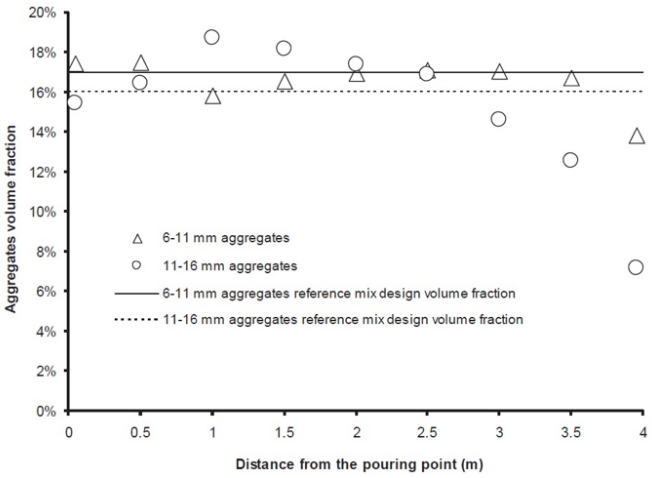

Figure 2.13. Aggregate volume fraction vs. distance from the casting point [27].

Static segregation can be identified with the sedimentation of fibers under gravity load as is seen Figure 2.14.a. However, during flow condition (dynamic segregation state), aggregate and fiber particles push each other with upcoming concrete flow so that aggregate and fiber particles may be distributed randomly in a concrete volume without segregation as shown in Figure 2.14.b [29].

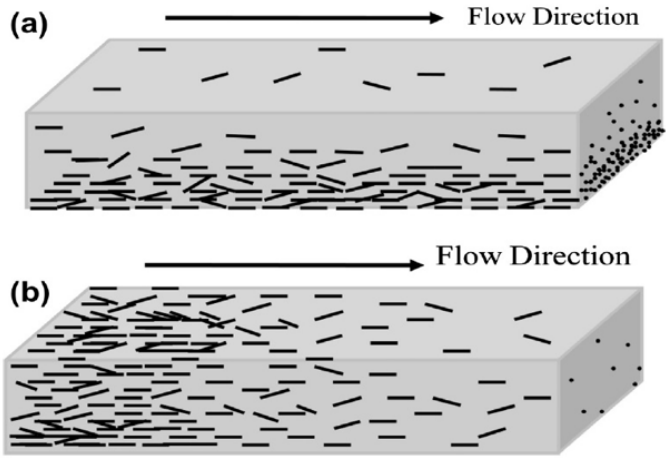

Figure 2.14. Representation of static (a) and dynamic (b) segregation of fibers in a FRC beam [29].

2.3. Compressive Behavior of SFR-SCC

The effect of steel fibers on compressive strength of concrete is much debated in literature. Most researchers found no significant effect of steel fibers on compressive strength, [7], while some researchers found that compressive strength of concrete increases with fiber addition, [4]. In most studies, an increase in steel fiber amount of SCC generally resulted in limited or negligible effect on compressive strength for small fiber fractions.

Compressive strength of concrete decreases due to large amount of pores by addition of steel fibers into concrete matrix, whereas compressive strength of concrete increases due to fiber bridging effects of steel fibers. Therefore, compressive strength depends on the magnitude of both effects. Concrete mix design, steel fiber type, amount and manufacturing process affect compressive strength of concrete [40].

When steel fibers exist in the matrix, concrete becomes more ductile. Main influence of steel fibers on the compressive behavior is the resistance against the longitudinal crack growth. This is highly related with the steel fiber type, amount, sizes and properties of both steel fiber and matrix. In general, it can be concluded that steel fibers with a fiber fraction of smaller than 1% (moderate dosages) do not influence pre-peak properties, while strain at crack localization and failure strain increase. However, for higher steel fiber amounts greater than 1%, compressive strength also increases in the concrete. Stress versus strain diagrams of both plain concrete and FRC are given in Figure 2.15. It can be concluded from below figure that maximum stresses remain approximately same for both concrete; however, strain values are much higher in the case of FRC [4].

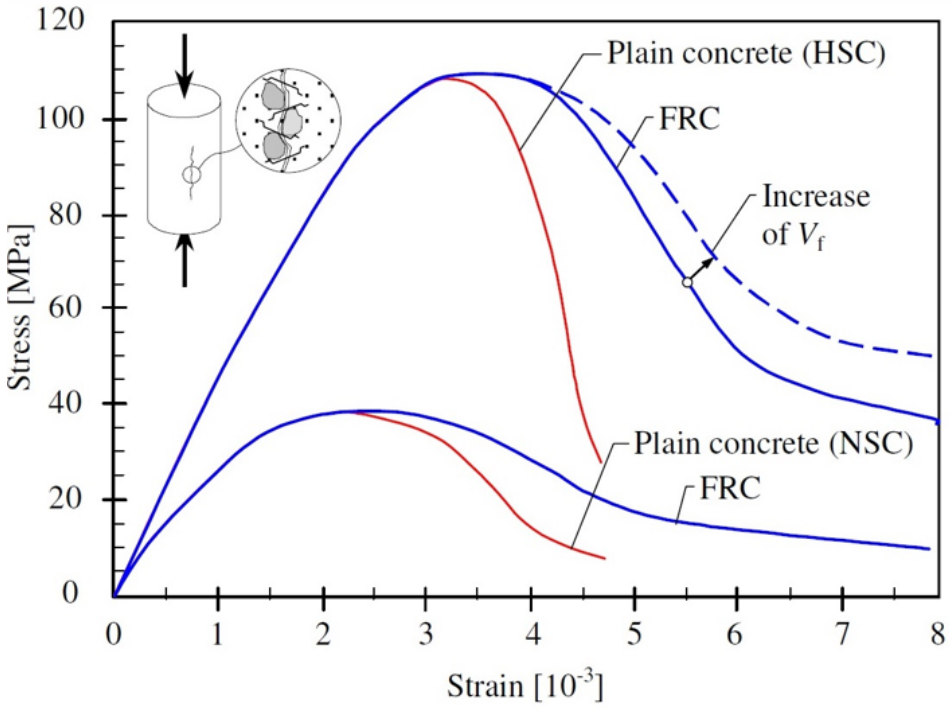

Figure 2.15. Behavior of plain concrete and FRC in compression [4].

Transverse reinforcement is placed into concrete in order to improve the toughness of concrete in compression. Transverse reinforcements, such as stirrups confine the lateral expansion of concrete by creating hoop tension under compression. In the case of steel fiber reinforced concrete, steel fibers bridge longitudinal cracks caused by the lateral expansion of concrete under compression. Toughness of the steel fiber reinforced concrete increases as the number of crack and crack width increases [39].

2.4. Shear Behavior of SFR-SCC

Structural reinforced concrete elements are designed in order to carry structural loads and failure of the element is preferred to be ductile rather than brittle. Shear type of failure is a brittle failure which is very dangerous for structures. High strength concrete is more prone to this type of failures. Addition of steel fibers promotes the ductility of the structural member; thus, eliminating the sudden failure risk, and also controlling the cracks and these features give a chance of using fiber as shear reinforcement instead of using stirrups.

Considering a third point loading on a simply supported plain concrete beam (without longitudinal reinforcement and stirrups), the moment and shear force acting on the beam is given in Figure 2.16. Normal and shear stresses can be calculated for x<a as follows:

$$f(x,y) = -\frac{My}{I} = -\frac{12Vxy}{bh^3} \tag{2.2}$$

$$v(y) = \frac{VQ}{Ib} = \frac{6V}{bh^3}\left(\frac{h^2}{4} - y^2\right) \tag{2.3}$$

The beam is subjected to compression and tensile stresses at top and bottom of the beam respectively. Maximum tensile stress emerges at the bottom of the beam at a distance x from the left of the beam support and equal to:

$$f_{max}(x, y = -h/2) = -\frac{6Vx}{bh^2} \tag{2.4}$$

Maximum shear stress occurs at the mid-span of the beam and calculated as follows:

$$v_{max}(y = 0) = \frac{3V}{2bh} \tag{2.5}$$

In general, a RC beam is subjected to normal and shear forces and failure occurs due to moment and /or shear. Shear force in the RC beams without stirrups can be carried by compression zone, the aggregate interlock mechanism, and dowel action of steel reinforcement. The failure is expected to be under flexural loading if the beam has an adequate slenderness ratio or high shear span to depth ratios. The shear type of failure is expected when a deep beam is considered or shear span to depth ratio is lower [44].

Beam failure types are described by ASCE-ACI Committee 426 (1973) and shear type of failures are the shear tension failures, diagonal tension failure and shear compression failure as is seen in Figure 2.17 [45].

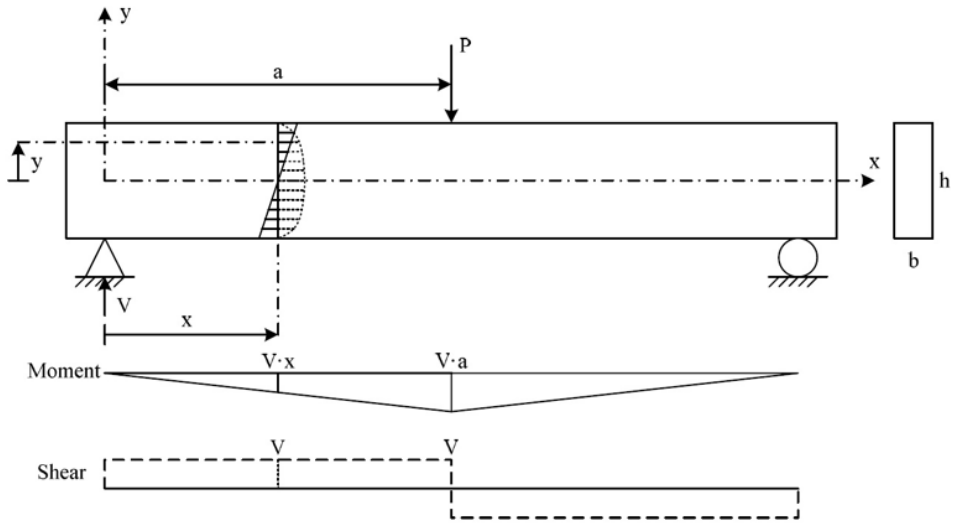

Figure 2.16. Plain concrete beam subjected to three point loading [44].

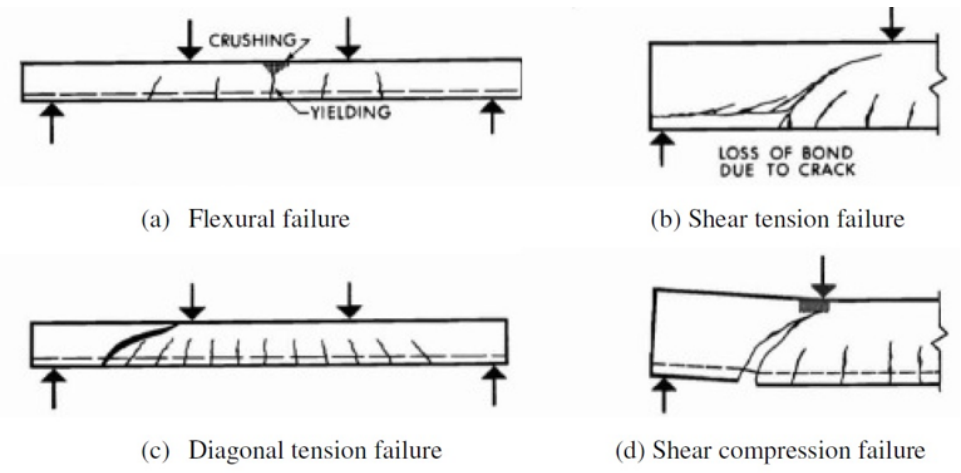

Figure 2.17. Beam failure types [45].

The flexural failure is expected in slender beams with a shear span to depth ratio is greater than 5.5. Flexural cracks emerge in the middle third of the beam span and failure occurs due to yielding of longitudinal rebars or crushing of the concrete. In the diagonal tension failure shear span to depth ratio is ranging from 2.5 to 5.5 and in this failure mode, both flexural and diagonal cracks are formed. In this failure, 2 or 3

cracks forms at a distance of 1.5d to 2d from the support. In the shear compression failure, a/d ratio ranges from 1 to 2.5 and in this type of failure diagonal cracks form out of the middle third section and these cracks propagate up to compression zone and failure occurs when cracks reach the crushed concrete around the applied load [46].

Parameters influencing shear behavior of reinforced concrete are the shear span to depth ratio (a/d) ratio, compressive strength of the concrete, the amount of steel reinforcement, and the volume fraction of steel fiber. Most studies showed that steel fiber amount less than 0.75% by volume will not contribute the shear strength and in order to improve the ductility and shear strength of concrete, the combination of stirrups and steel fibers as shear reinforcement can be used in the structures [41].

Reedy *et al.*, 2015 studied the effect of steel fibers on shear strength of high strength concretes (fc=65 MPa). They used different steel fiber dosages (0.4, 0.8 and 1.2 by volume of concrete) and various shear span-to-depth (a/d) ratios (1, 2, 3 and 4) without shear reinforcement. They used steel fibers both throughout the concrete (termed as FR). Parts of the concrete where shear loads are critical (termed as CFR) and also for both concrete longitudinal reinforcement amounts are kept constant. They concluded that;

- Shear capacity of the beams are found to be similar for specimens including steel fibers throughout the concrete (FR) and part of the concrete where shear loads are critical (CFR). They added that steel fiber use in shear critical regions is highly cost effective than using steel fibers in throughout the concrete.
- Effects of steel fibers on shear strength of concretes decreased at higher a/d ratios.
- Advantage of steel fibers on first and ultimate crack loads is especially significant at lower a/d ratios (especially smaller than 2).
- Toughness of the concretes at all a/d ratios are superior when compared to non-fibrous specimens.
- From both experimental and analytical results, specimens including 0.8 % steel fiber volume fraction exhibited the highest shear strength increase for all shear span to depth ratios. Further increase in steel fiber amount did not contribute to

shear strength capacity as can be seen in Figure 2.18.

- Shear load capacity of the specimens with a/d ratio equals to 1, is twofold of the specimens with a/d ratio equals to 2. It can be concluded that steel fibers have a great influence on specimens with a/d ratio equals to 1, as can be seen in Figure 2.18[42].

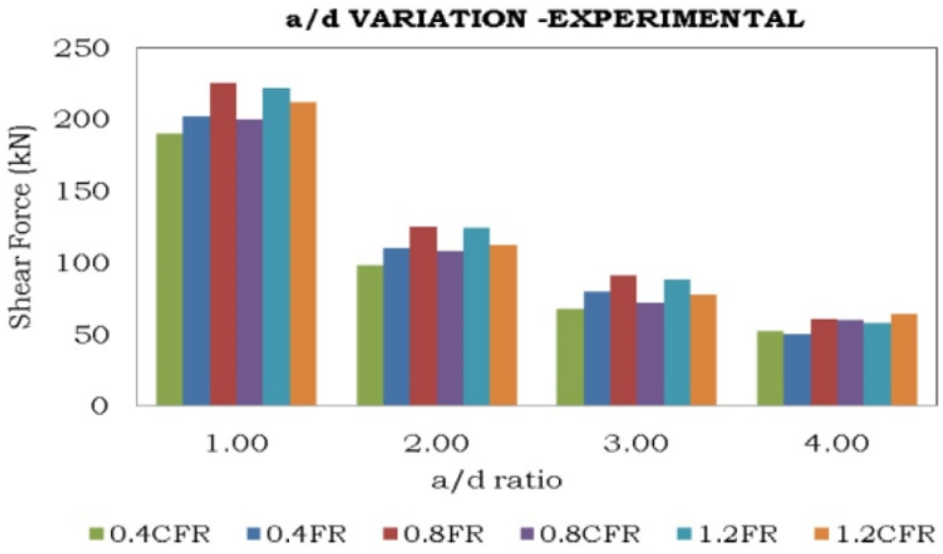

Figure 2.18. Experimental results of FR-CFR at different a/d ratio and steel fiber amount [42].

Naik and Cute (2014) studied the effect of shear span-to depth ratio (a/d) on shear strength of SFRC deep beams using an artificial neural network technique. The investigated parameters were effective beam depths ranging from 300 mm to 500 mm, steel fiber amounts ranging from 0.5% to 2% by volume of concrete, shear span-to-depth ratio changing from 0.5 to 2, and different compressive strengths (30-80 MPa), fiber aspect ratios (20-80) and longitudinal steel amounts (0-2.5%). The findings of the study as follows were summarized;

- In terms of effective depth, shear strength increased as depth of the specimens were increased at low a/d ratio of 0.5. However, for the other a/d ratios, beam widths became another important parameter for shear strength. Researchers found that for high strength concretes, shear strength increased with the increas-

ing a/d ratio for specimens having beam width to depth ratio less than 0.43. For beam width to depth greater than 0.43, shear strength decreased with increasing a/d ratios.

- In terms of steel fiber amounts, all parameters were kept constant and only a/d and steel fiber amount were changed. It was observed that as steel fiber amounts increased, shear strength of concretes also increased for all a/d ratios up to 2. However, this strength increase changed little for steel fiber amounts greater than 1.5% [43].

2.5. Flexural Behavior of SFR-SCC

Tensile behavior of SFR-SCC can be determined by uniaxial tension test, splitting tensile test and flexural tensile tests. Uniaxial tension test is a direct method of determining the stress crack width relationship of concretes. However, uniaxial test requires sophisticated tensile test equipment and it is a time-consuming test to perform. In addition to this, results of the test may be influenced by the specimen-machine interaction. Therefore, flexural test is preferentially used in the standards instead of uniaxial tensile test. Under uniaxial tensile stress, a concrete material can behave as strain hardening or strain softening; however, concrete showing strain softening behavior under uniaxial tensile test can show either deflection softening or hardening under flexural loading (Figure 2.19). This response depends on both toughness and dimensions of the concrete specimens. For instance, a thinner beam can response deflection hardening under flexural load and this response may change to the deflection softening as specimen thickness increases. This behavior may be observed for fiber reinforced concretes depending on fiber distribution and orientations in the specimen geometry [4].

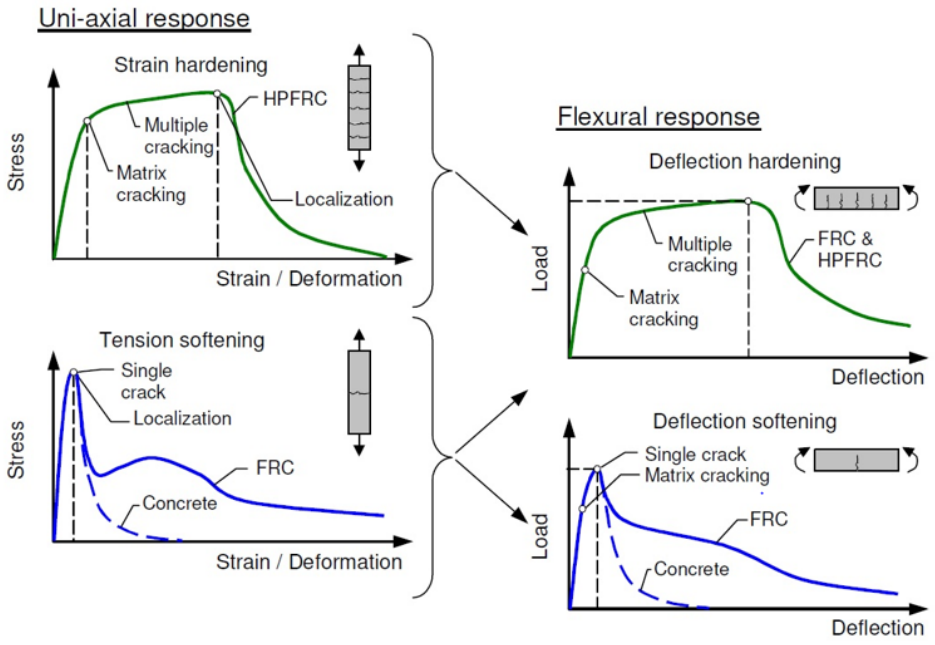

Figure 2.19. Characterization of the tensile and flexural behavior [4].

Flexural performance of SFR-SCC can be determined via three point bending test or four point bending test. International standards and/or guidelines have proposed different configurations (changes in specimen dimensions and test configurations) in determining the flexural performance of fiber reinforced concretes. Area under the load-deflection curve gives toughness value and toughness is calculated up to a defined deflection or displacement value stated in the standards. As compared to the non-fibrous concrete, toughness of steel fiber reinforced concrete improves significantly as steel fiber volume fractions, aspect ratio and interfacial bond strength increases. Typical bending behavior of hooked-end fiber SFRC, straight fiber SFRC and non-fibrous SFRC is given in Figure 2.20 [7].

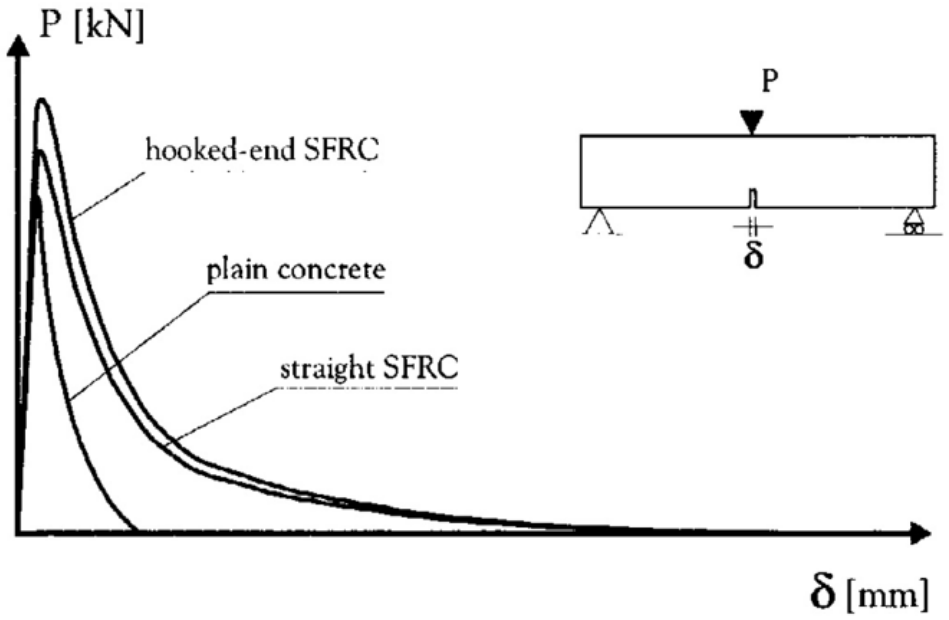

Figure 2.20. Behavior of SFRC in bending [7].

The softening curve of the SFR-SCC is significantly affected by the steel fiber addition. When SFRC structural elements are subjected to bending moments, post-cracking region of the load-displacement curve causes stress redistribution after concrete cracking as is seen in Figure 2.21. The neutral axis of the specimen shifts upward to the compression zone in order to balance force and moment equilibrium. Based on this behavior, steel fiber reinforced concretes can carry the additional loads in a cracked tensile zone. Consequently, maximum moment capacity of steel fiber reinforced concrete surpasses the moment capacity of the plain concrete and this moment increase is related to fiber orientation and pull out behavior of steel fibers [7].

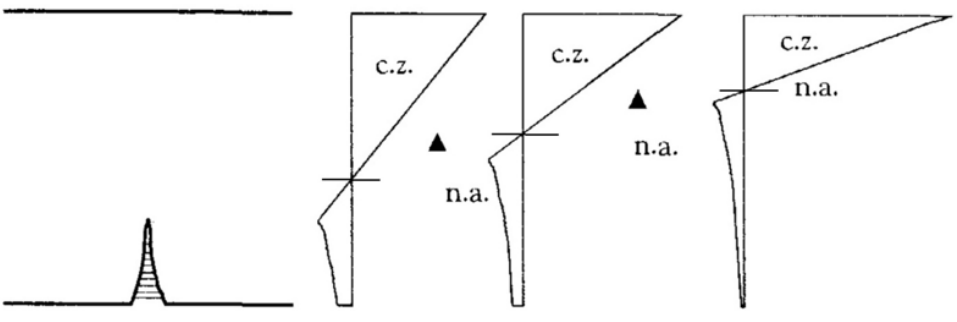

Figure 2.21. Stress redistribution on SFR-SCC specimens under flexural loading [7].

There are methods in order to determine the flexural toughness of concretes such as for point bending tests with standards of ASTM C1018 [63], ASTM C1609/C1609-M12 [64] and JSCE SF4 [49], and three point bending tests on notched specimens with RILEM TC 162-TDF [76] and EN14651 [50] standards. In Japan Society of Civil Engineering standard (JSCE-SF4), toughness value of concretes is calculated according to average flexural strength values. Detailed information about flexural toughness calculation is given in Part 3.4.7, Experimental Methods, Flexural toughness calculations.

In the JSCE method, load - deflection diagram up to L (span)/150 is obtained. Area under the curve gives flexural toughness and flexural toughness factor (FT) is also calculated. FT is considered as an indicator of post crack residual strength of the concretes. In ASTM C1018 method, exact location of the first crack is crucial and it is a very important problem. ASTM C1018 also states that support settlement may cause a concavity at the initial part of the load displacement diagram and it may give misleading deformation measurements. Therefore, standard suggests that first part of the load-deformation curve should be discarded and replaced by the extension of the linear part of the curve. However, in the JSCE-SF4 standard, the location of the crack and instability in the initial portion of the load-displacement curve is not important as end point deflection (L/150) is far away from the initial deflection values. However, this end point is generally criticized as this limit criterion is much greater than the acceptable deflection limit values of structural design codes. In addition, pre-peak and post-peak behaviors are not distinguished by using total area of the curve [47]. Due to the difficulty of first cracking load and instability after peak load, JSCE-SF4 method is preferred for toughness calculations.

Three or 4 point bending test with/without notched set-up and configurations, stress-strain and stress-crack width relationships for different codes and guidelines are given in Figure 2.22. These constitutive model equations are obtained from experimental data of the related standards. In these models, a tendency for residual flexural strength (f_R) instead of equivalent flexural strength (f_{eq}) to was observed. Equivalent flexural strength is the total energy absorption capacity of a concrete up to a certain

deflection value; whereas residual flexural strength is the stress value corresponding to force at a certain deflection [48].

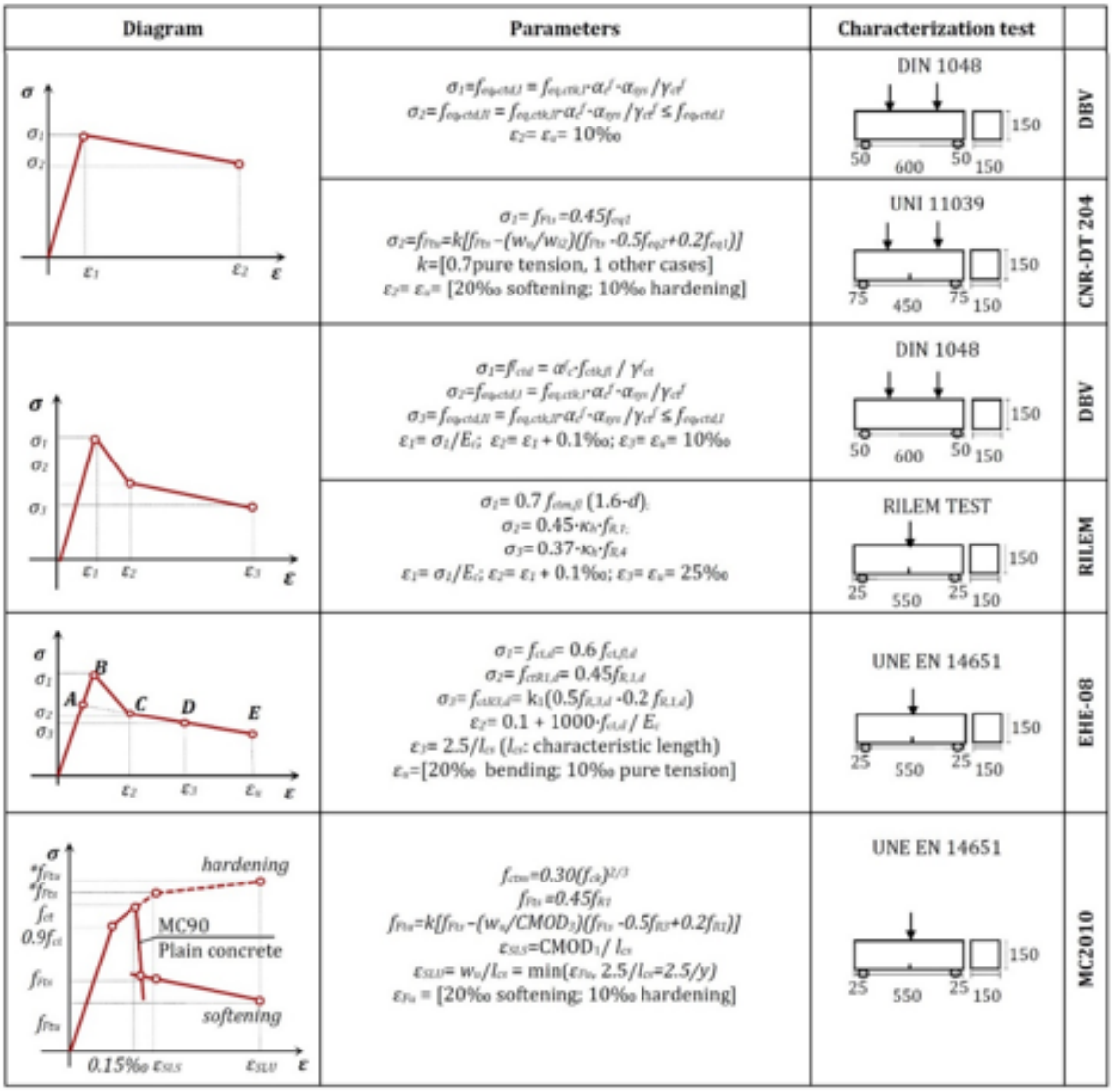

Figure 2.22. Constitutive models and dimensions for different codes and guidelines [48].

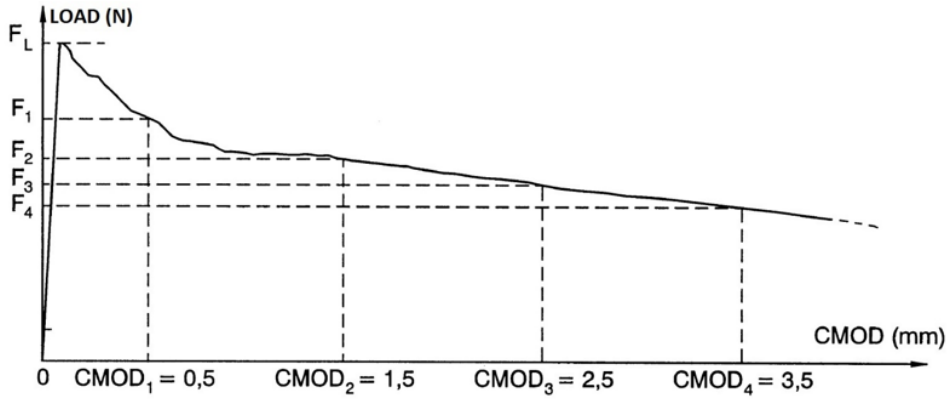

Figure 2.23. Load - CMOD diagram and F_j (j = 1, 2, 3, 4) [50].

In EN 14651, residual flexural strength in the fiber reinforced concretes for different CMOD values (j1=0.5 mm, j2=1.5 mm, j3= 2.5 mm, j4= 3.5 mm), as can be seen in Figure 4.24, can be calculated as following:

$$f_{R,j} = \frac{3F_j l}{2bh_{sp}^2} \tag{2.6}$$

In the formula; $f_{R,j}$ is the residual flexural strength corresponding with CMOD = $CMOD_j$ in N/mm^2, F_j is the load corresponding with CMOD = $CMOD_j$ in N, l is the span length in mm, b is the width of sample in mm, h_{sp} is the distance between top of the specimen and tip of the notch [50].

Amount of steel fibers in the self-compacting concrete specimens significantly effects flexural toughness. Jatale and Mangulkar studied three types of steel fibers; waved steel fibers (WSF), hook ended steel fibers (HESF) and flat steel fibers (FSF), and used various fiber fractions (0.5%, 1%, 1.5%, 2%, 2.5%, 3%, 3.5%, 4% by weight of cementitious material) in order to investigate the effects of different steel fiber types and amounts on flexural strength of SCC specimens. They found that flexural strength increases with an increase in steel fiber amount up to a certain limit of 3.5 %, beyond that percentage flexural strength remains constant or decreases. Specimens including waved steel fibers with 3.5% steel fiber fraction exhibited highest flexural strength as

shown in Figure 2.24 [51].

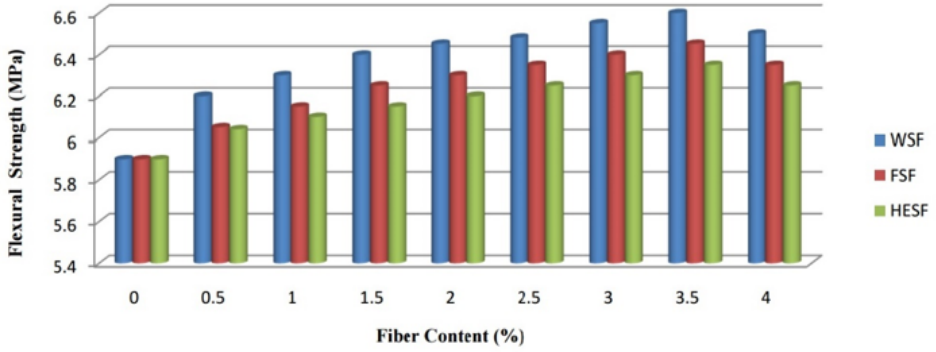

Figure 2.24. Flexure strength of concrete with different steel fibers [51].

Troittier and Banthia (1994) studied the effects of different types of steel fiber and various compressive strengths on flexural strength and flexural toughness using ASTM C1018 and JSCE-SF4 methods. They used four different types of steel fibers; F1 was a circular hooked end fiber with a length of 60 mm and an aspect ratio of 75, F2 was a circular crimped fiber with a length of 60 mm and an aspect ratio of 60, F3 was a crescent crimped fiber with a length of 52 mm and an aspect ratio of 41 and F4 was a circular twin cone fiber with a length of 62 mm and aspect ratio of 62 as shown in Figure 2.25. The amount of steel fiber was kept constant as a 0.5% by volume of concrete. They produced three different concrete strengths of 42 MPa (normal strength), 52 MPa (mid strength) and 85 MPa (high strength). They pointed out that flexural toughness characterizations strongly depended on both steel fiber geometries and matrix strengths [52].

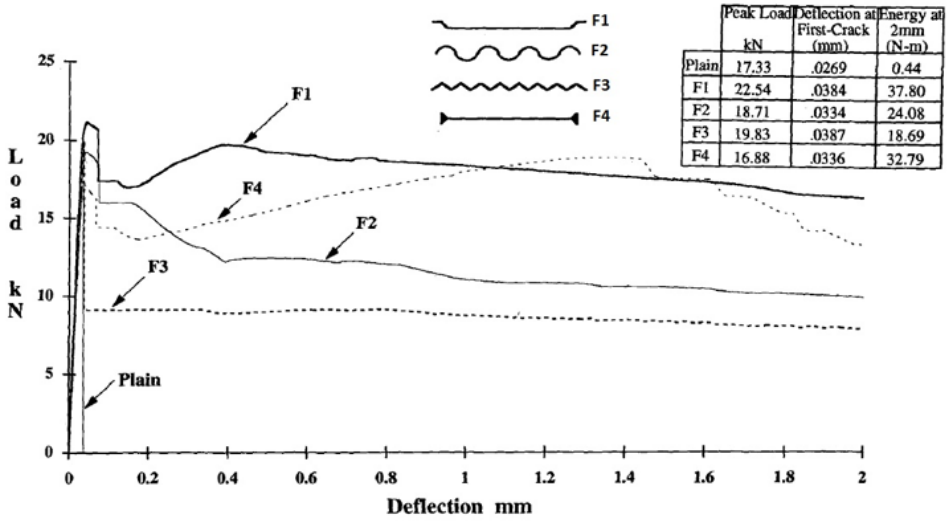

Figure 2.25. Load vs deflection curve of the normal strength concrete (42 MPa) [52].

For normal strength (42MPa) and mid strength (52 MPa) concretes, maximum flexural strength and toughness were observed on specimens including hooked end fibers. It was also pointed out that flexural strength of the crimped fibrous (F3) specimen was the second; whereas flexural toughness of the specimens was observed as last due to sharp decrease after peak load as is seen in Figure 2.25 and Figure 2.26. When maximum flexural strength and toughness values were compared; as concrete strength increased from 42 MPa to 52 MPa, flexural strength also increased; however, toughness values decreased [52].

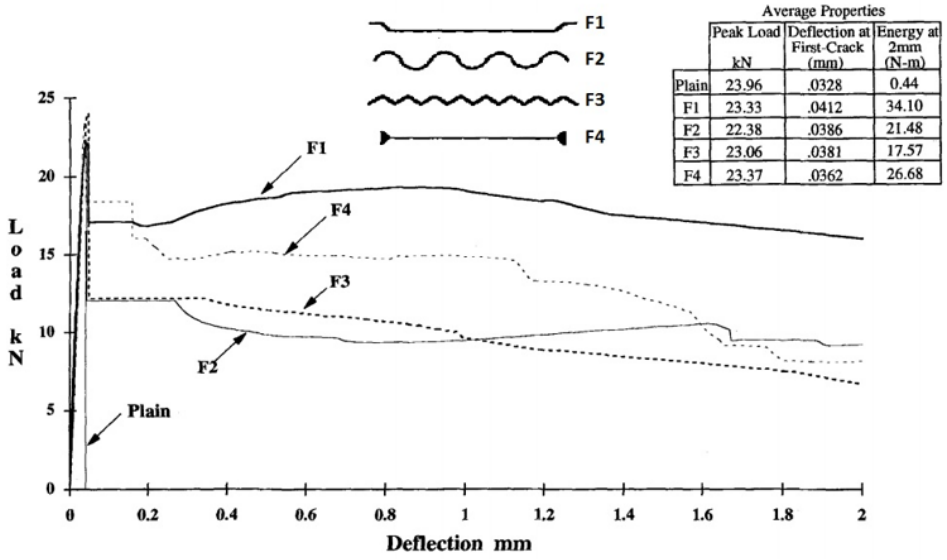

Figure 2.26. Load vs deflection curve of the mid strength concrete (52 MPa) [52].

For high strength (85 MPa) concrete, flexural strength of hooked end fiber specimens showed better performance; whereas circular twin cone fibrous specimens (F4) showed superior flexural toughnesses. When compared to maximum flexural strength and toughness values, as concrete strength increases from normal to high strength, flexural strength also increased; however, toughness values decreased, except for F4 specimens as shown in Figure 2.27.

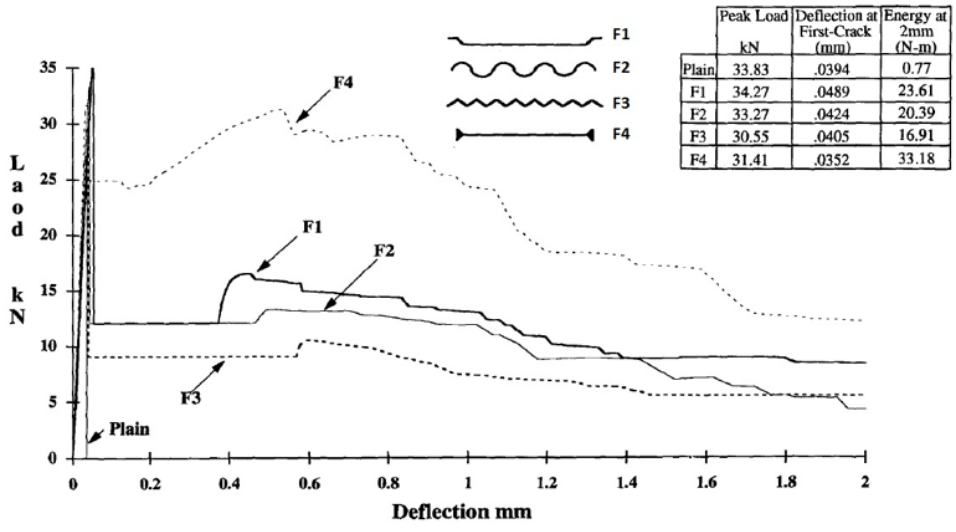

Figure 2.27. Load vs deflection curve of the high strength concrete (85 MPa) [52].

The main significant findings of the study [52] are;

- At low steel fiber fractions, there was no or limited flexural strength improvement observed.
- Steel fibers have a significant influence on flexural toughness or energy absorption capacity of concrete. Based on the different steel fiber geometries, steel fibers with deformations on their ends showed better performance than steel fibers with deformations on entire lengths.
- Strength of concrete strongly affects flexural toughness characteristics. At higher strengths, a steeper and more sudden load drop is observed after first cracking. However, the effect of concrete strength strongly depends on steel fiber geometry.
- As concrete strength increases, concrete becomes more brittle and the amount of steel fiber should be increased in order to obtain further ductility and hence amount of steel fiber may decrease the sudden drop of the loading after first cracking.

Frazao *et al.*, (2015) studied the mechanical and durability properties of steel fiber reinforced self-compacting concrete and they used 60kg/m3 steel fiber in the concretes. They pointed out that;

- Steel fiber content of 60 kg/m3 had no significant impact on compressive strength, elastic modulus of concretes. The addition of steel fibers increased the post-peak behavior and energy absorption capacity of concrete under compression loading.
- Water absorption capacity by capillarity and air penetrability was not affected by the addition of steel fibers.
- The steel fiber introduction reduced electrical resistivity of concrete up to 63%.
- The steel fiber had a significant influence on flexural strength, post cracking flexural resistance or residual flexural strength and toughness. As can be seen in Figure 2.29, after the first cracking corresponding to peak load, a sudden load decrease has emerged in all SCC specimens (red lines) due to brittle character of the concrete. However, for SFR-SCC specimens (blue lines), the increase in the ductility comes from the steel fiber introduction. As the age of the steel

fiber reinforced concrete increases, flexural strength also increases; however, with strength enhancement, more brittle behavior and further decrease of the peak load was observed for further ages of concretes [53].

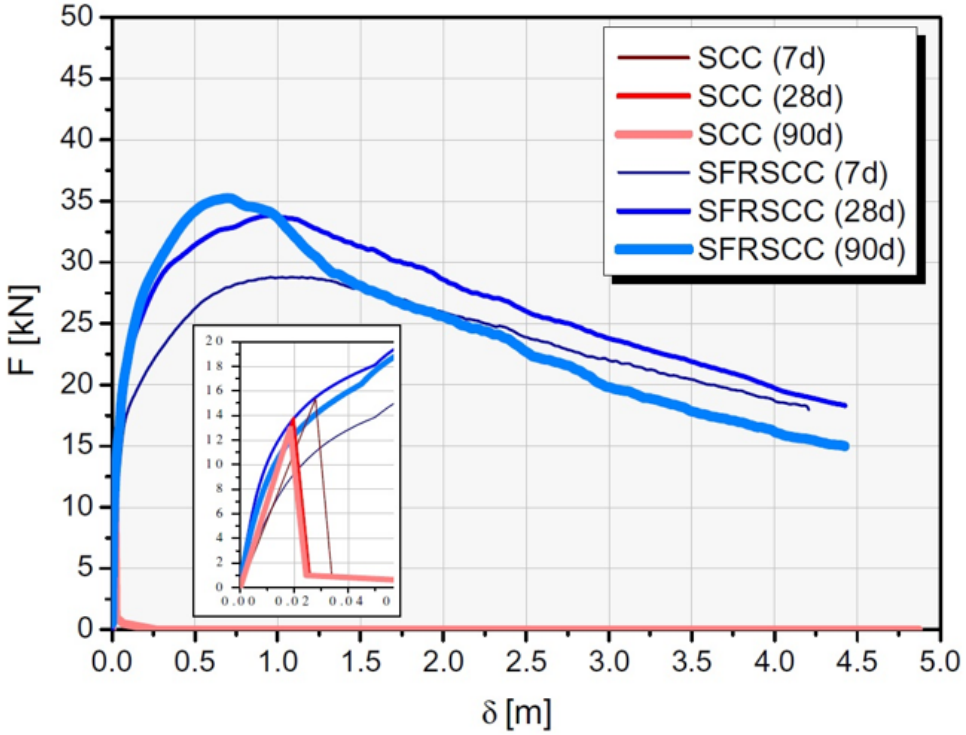

Figure 2.28. Flexural load deflection relationship at different ages [53].

2.6. Tensile Behavior of SFR-SCC

The tensile behavior of concrete is improved when steel fibers are added. Especially, post cracking behavior of concretes enhances significantly since steel fibers have an ability of crack arresting and crack bridging after concrete cracking. For low steel fiber fractions (approximately $< 2\%$), load-displacement curve of a fiber reinforced concrete shows a decreasing branch (tension softening behavior) while it has a residual tensile strength and significant toughness capacity. For high steel fiber amount (greater than > 2 %) post cracking behavior changes form tensile softening to tensile hardening due to multiple cracking as is seen in Figure 2.29. The uniaxial first crack tensile strength of FRC, fFt may be assumed concrete tensile strength. The strength of fiber reinforced concrete showing softening behavior may be equal to maximum ten-

sile strength. The residual tensile strength of FRC depends on the steel fiber volume fraction, aspect ratio of the fibers, bond between concrete and steel fiber, and fiber distribution and orientation that mainly influenced by steel fiber geometry, steel fiber-concrete interface, casting direction, mixing and compaction methods of fresh concrete [52].

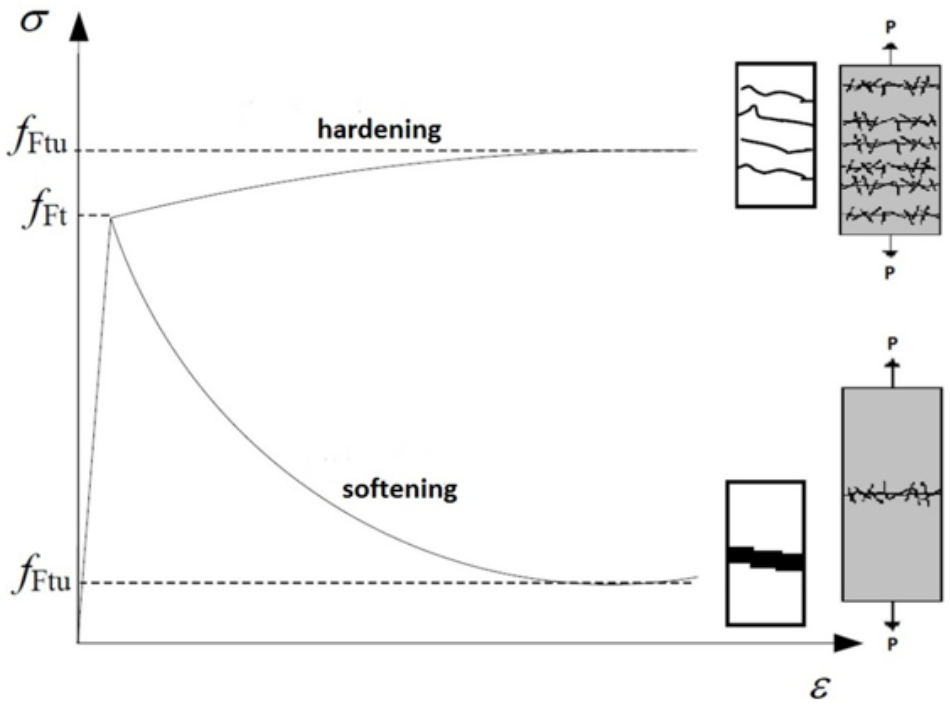

Figure 2.29. Tensile behavior of steel reinforced concrete [55].

In steel fibrous reinforced concrete as compared with non-fibrous concrete, steel fibers act as crack bridging mechanism so that critical crack opening or width increases at least 10 times than that of the plain concrete. A combination of aggregate and fiber bridging contributes to enhancement of crack width; however, aggregate bridging has relatively less contribution than steel fiber as is seen in Figure 2.30. Three different phases can be defined as; [4]

- micro-cracking zones in between the points of A and C, macro crack growth zone in between the points of C and D,
- a bridging zone in between D and E - stress transfer realized by steel fiber pull out and aggregate bridging,

- a traction free zone (after the point of E) - in the relatively larger crack openings.

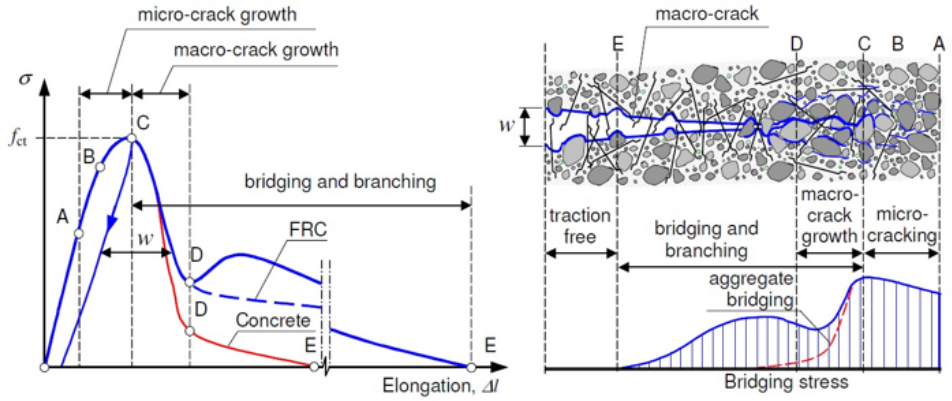

Figure 2.30. Steel fiber effect on fracture process in uniaxial tension [4].

2.7. Modeling the Bending Behavior of SFR-SCC

The limited use of fiber reinforced concrete in structural design mainly stems from the lack of characteristic tensile stress-strain properties of fiber reinforced concretes required for structural design codes. The most important contributions of steel fibers are increase in residual tensile strength and ductility, which depends on the mechanical and geometrical properties of steel fiber used. Tensile behavior of SFR-SCC is stress versus strain relationship before cracking, and after cracking tensile behavior becomes stress versus crack opening displacement. The behavior of stress-crack opening displacement can be obtained directly using uniaxial tensile test which is an expensive method and requires special equipment or indirectly using inverse analysis from a three or four point bending test as is seen in Figure 2.31 [54].

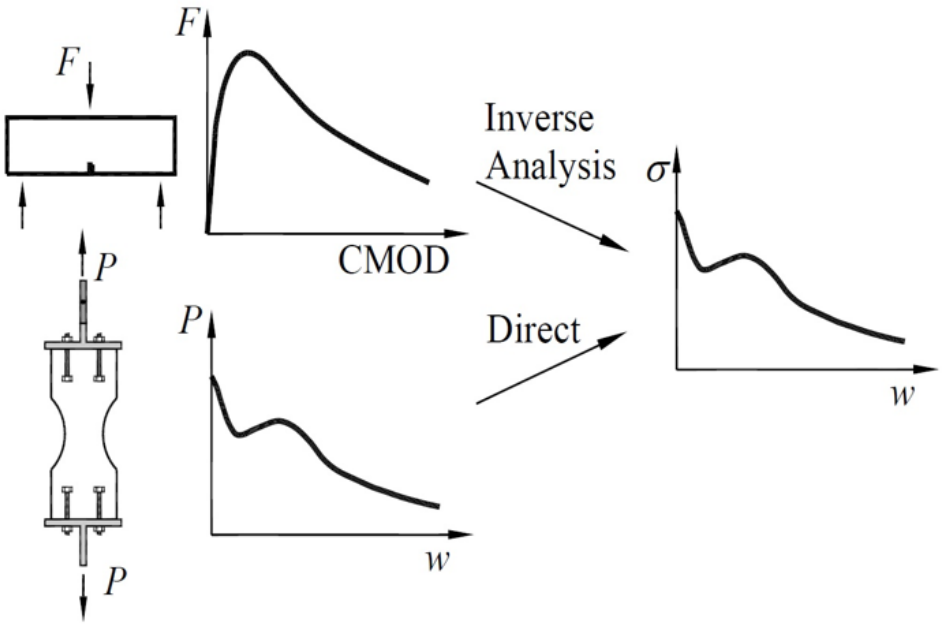

Figure 2.31. Determination of tensile properties of SFRC by directly and indirectly [54].

There are several inverse models (multilayer model) proposed for structural design of fiber reinforced concretes. However, it was shown that the models used are not capable of predicting tensile behavior of wide range of fiber reinforced materials resulting in decreased adaptation of fiber reinforced materials in design. Therefore, further modification of existing models and/or development are required. In the study, an equilibrium based multi-layer model is modified and model results are compared with the experimental results.

Generally a bending test is easier to perform when compared to a direct tensile test. Since most of the design codes are based on a tensile stress-strain relationship, a translation from bending to direct tensile is very important for usage of SFRC in structural applications. Therefore models to predict direct tensile behavior are studied by several researchers. An equilibrium based multi-layer model is developed by Hordijk in 1991 [56]. Hordijk used load-deflection curves for plain concrete in his models. Kooiman (2000) [7] showed that model was also appropriate for modeling the fiber reinforced concrete and he used load-crack opening displacements using three point

bending for fiber reinforced concrete notched beams. Grünewald (2004) [23] used this model for modeling of self-compacted fiber reinforced concretes and Lappa (2007) [57] modified the model in order to model bending behavior of ultra-high strength fiber reinforced concretes.

In the model, a fictive part of the beam referred as fracture zone, is replaced by springs and load-deformation characteristic of these springs is determined by stress - crack opening displacement (COD) and elastic deformation at fracture zone of lf as is seen in Figure 2.33 [56]

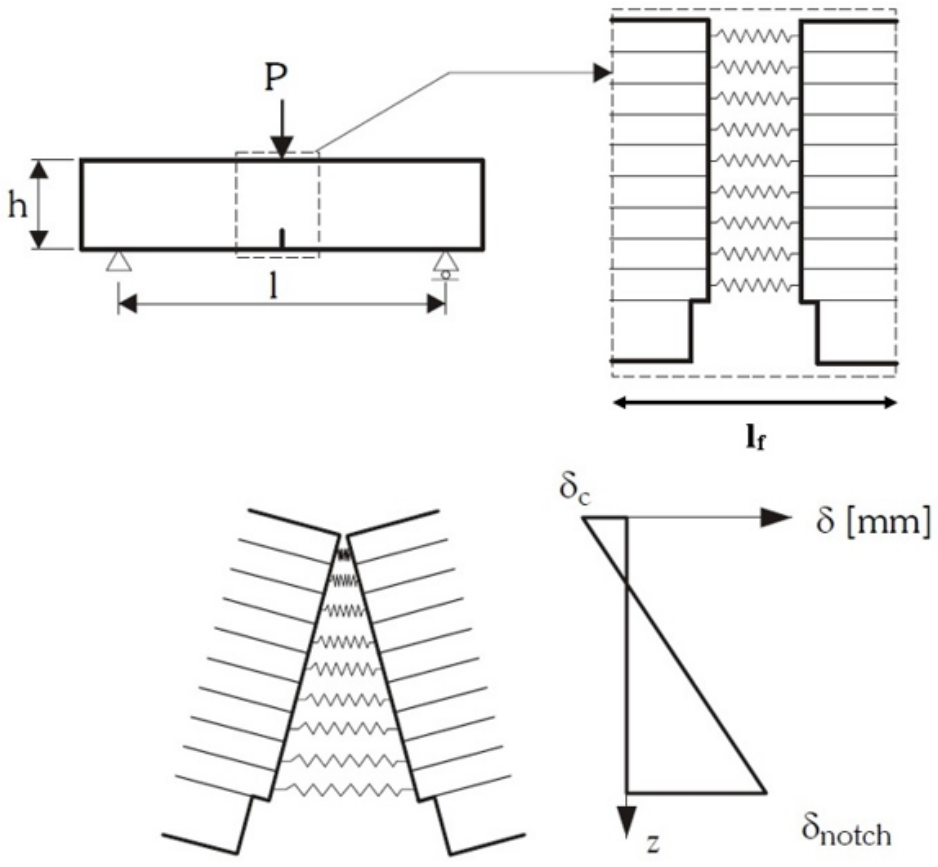

Figure 2.32. First principle of the equilibrium based multi-layer procedure [56].

The equilibrium based multi-layer procedure depends on three basic principles:

In the first principle, the beam is divided into two parts and they are connected by springs over the effective height of the beam (total beam height - notch part height) as

shown in Figure 2.33. This spring region consists of defined number of layers and each spring represents the small layer behavior of the beam. A linear displacement distribution over the effective height is assumed. Fracture zone, lf, also defined as influence length, represents overall beam behavior under bending load and beam assumed to be infinitely stiff apart from the fracture zone [56, 7, 23, 57].

In the second principle of multi-layer procedure;

- the strain in each spring or layer is equal to the average deformation in each layer,
- from strain distribution (average deformation) corresponding stresses calculated for each layer with stress-strain or CMOD relations using input parameters of the model.
- from stresses, bending moment is calculated for each layer and complete cross section up to normal force is equal to zero (N=0). This is the equilibrium condition of the model.
- from bending moments, applied load can be determined using three point bending formula, P = 4* M/L as is seen in Figure 2.34 [56, 7, 23, 57].

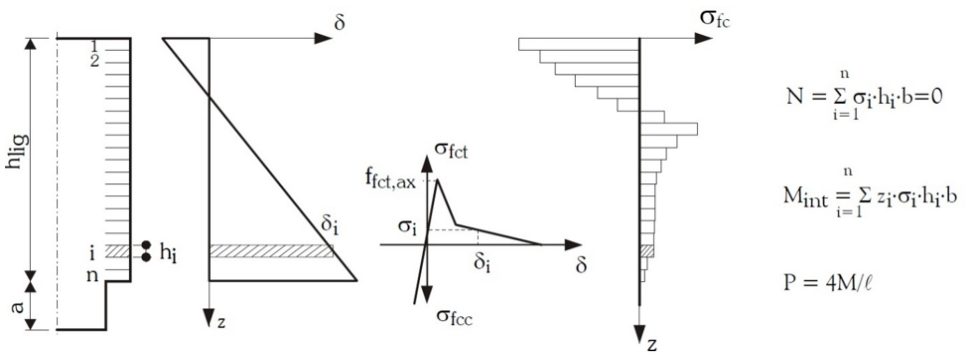

Figure 2.33. Second principle of the equilibrium based multi-layer procedure [56].

In the third principle; an incremental procedure is conducted in order to obtain load displacement curve. At first step, strain at the bottom layer (or above the notch in case of a notched beam) is fixed at a predetermined value and variation of strain as linearly at the upper side of the beam can be found using equilibrium equations up to N is equal to zero. Later, strain values at the bottom layer increased step by step, and

after each step maximum tensile and compressive strains and corresponding moments are calculated. Finally, overall load displacement curve is obtained by combining the applied load as a function of moment and corresponding displacement at each step as is seen in Figure 2.35 and modeling results can be compared with experimental results [56, 7, 23, 57].

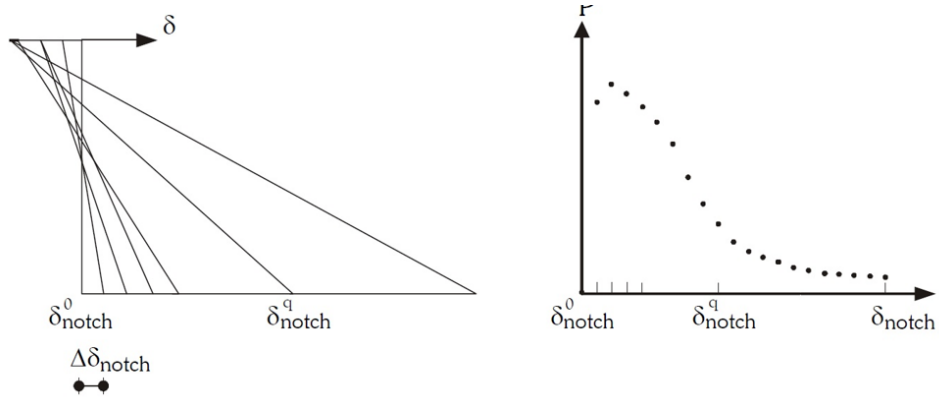

Figure 2.34. Third principle of the equilibrium based multi-layer procedure [56].

2.7.1. Bilinear Stress versus CMOD Relation for SFRC

Kooiman (2000) further developed the Hordijk's multi-layer model and he conducted three point bending tests on notched beam specimens to compare the experimental results to numerical ones. He applied accuracy checks in which he compared toughness and load level and found out that the deviation between numerical analysis and experimental results which was less than 10%. He concluded that the model could be used for structural design of fiber reinforced concrete structures. Therefore, Kooiman's model assumption and proposed input parameters are described in details [7].

2.7.1.1. General Model Parameters. Number of layers and influence length (fracture zone) affected bending simulation results significantly. Number of layers affected the maximum load of the reinforced concrete. Similar with finite element analysis, as number of layer increased the result become more accurate. However, consistency was required between analysis time and simulation accuracy. Kooiman found out that

number of layers greater than 500 hardly affected the peak load as is seen in Figure 2.36 and he used the number of layers in his models as 500.

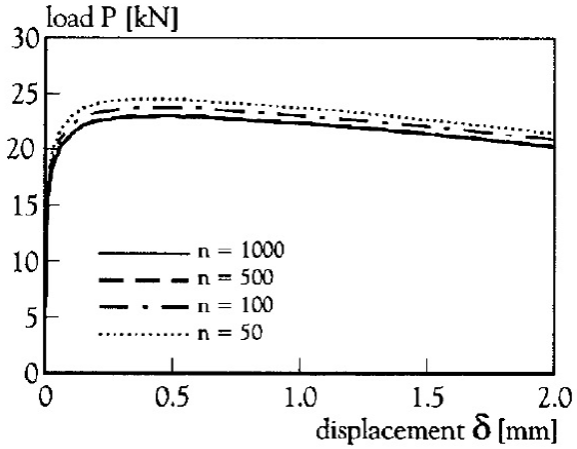

Figure 2.35. Influence of number of layers on multi-layer simulations [7].

The second important parameter was the influence length and it affected ultimate deformation capacity of the model. Influence length (lf) decreased the deformation capacity of the fiber reinforced concrete as is seen in Figure 2.36 and after finite element and simulation calculations, Kooiman [7] determined the influence length as 62.5 mm (0.5*hlig). The same number of layers (500) and influence length (0.5*hlig) were also used by Grünewald and Lappa.

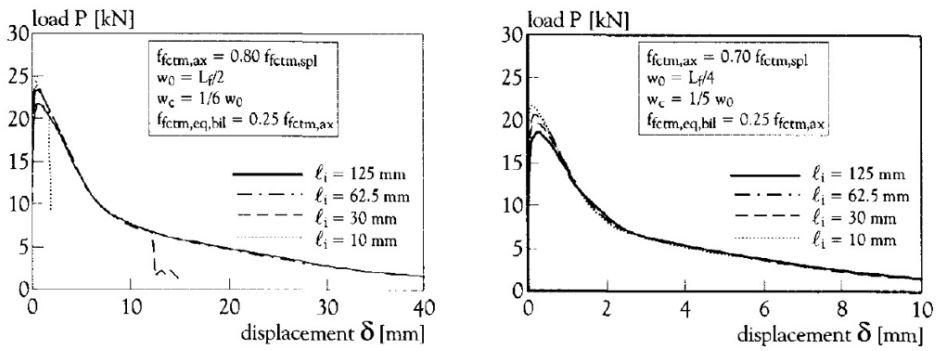

(a) 60 kg/m³ 60/0.75 hooked-end steel fibers (b) 60 kg/m³ 30/0.5 hooked-end steel fibers

Figure 2.36. Effect of influence length on multi-layer simulations [7].

2.7.1.2. Stress-strain diagram for compression. Another important parameter related to accuracy of models is the reliable stress-strain diagrams for compression. Kooiman

(2000) assumed three stress-strain diagram in compression in which post-peak behavior of concrete was changed, as shown in Figure 2.37(a) to observe the effects of compression to bending simulations. He concluded that simulation results depend on the deformation capacity in compression. For low ultimate strain assumptions, compressive failure was observed at simulations as is seen in Figure 2.38.(b). Researcher also stated that the shape of the post-peak behavior had no influence on the bending force-displacement simulation curve as can be shown in Figure 2.37(b) [7]

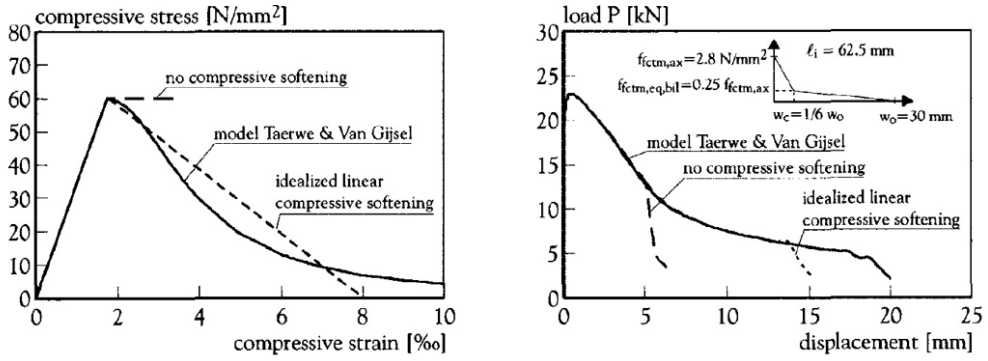

(a) Assumed stress-strain relationships in compression (b) Simulated flexural behavior

Figure 2.37. Effect of assumed stress-strain relationship in compression to simulated flexural behavior [7].

After simulation and finite element analysis results, compressive stress-strain diagram parameters of Kooiman [7]:

- elastic compressive strain ($\varepsilon_{cc,elastic}$) increases linearly up to 1.75‰, this value corresponds to elastic strain in structural design codes,
- compressive strength ranges (f_{ccm}) from 59 MPa to 81 MPa and determined via experimental method using 150x150x150 mm cubes.
- ultimate compressive strain limit ($\varepsilon_{cc,max}$) selected as 8‰ (for 30 mm length of steel fibers) and 10‰ (for 60 mm fibers)

Grunewald (2004) [23] assumed the following parameters of stress-strain relationship for compression as is seen in Figure 2.38:

- elastic compressive strain ($\varepsilon_{cc,elastic}$) is experimentally determined from elastic modulus test on 100x100x400 mm prismatic specimens and strain corresponding to maximum compressive load gives ε_{cc},elastic value.
- compressive strength (f_{ccm}) is the maximum compressive stress obtained experimentally from the elastic modulus test results of 100x100x400 mm prismatic specimens.
- ultimate compressive strain limit ($\varepsilon_{cc,max}$) changes according to steel fiber lengths as 8‰ for 30 mm or shorter steel fiber lengths, 12‰ for 40 mm fiber length and 15‰ for 60 mm length.

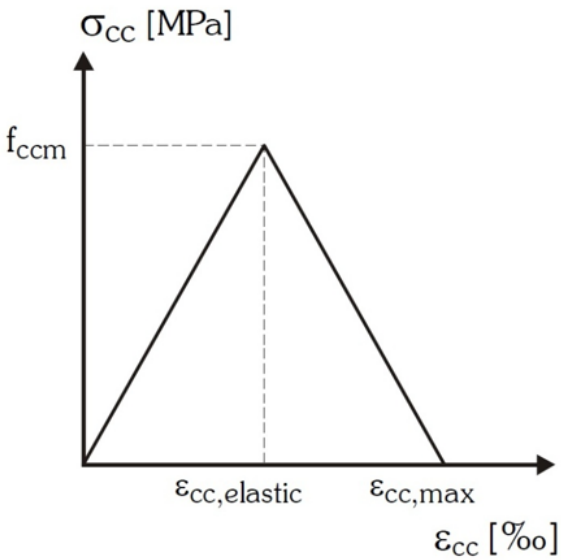

Figure 2.38. Idealized compressive stress - strain behavior SFRC and SCFRC [23].

Lappa (2007) [57] modeled the bending simulation model on ultra-high strength concretes and used a simplified stress strain diagram as shown in Figure 2.38. Researcher found compressive strength of concrete (f_{ccm}) as 120 MPa with an elastic strain limit ($\varepsilon_{cc,elastic}$) of 3‰ experimentally, and assumed the ultimate strain limit ($\varepsilon_{cc,max}$) as 8‰ due to reduced displacement ability caused by higher strength and short fibers of the mix.

2.7.1.3. Stress-strain or crack width relationship for tensile behavior. Stress-strain or crack width relationship can be divided into two parts: linear part up to concrete

cracking and softening part after post-cracking. The elastic behavior in tension is found using uniaxial tensile ($f_{fctm,ax}$) strength and linear elastic strain. The softening behavior is determined using uniaxial tensile strength ($f_{fctm,ax}$), critical crack width (w_0), the equivalent post cracking strength ($f_{fctm,eq,bil}$) and characteristic crack width (w_c) as is seen in Figure 2.39.

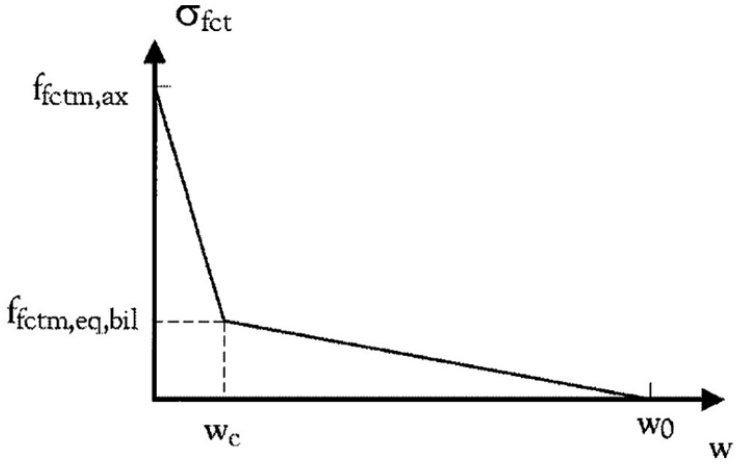

Figure 2.39. Input relation for post cracking behavior of SFRC [7].

The uniaxial tensile strength ($f_{fctm,ax}$) has a great influence on bending simulations on both pre-peak and post-peak regions of stress-strain and stress-crack opening relations. The simulations were performed on the mix including hooked end fiber with a length of 30 mm and found that a lower (0.7) uni-axial tensile strength to splitting tensile strength ratio was more applicable and for higher fiber lengths (60 mm) this ratio increased to 0.8 as is seen in Figure 2.40 [7].

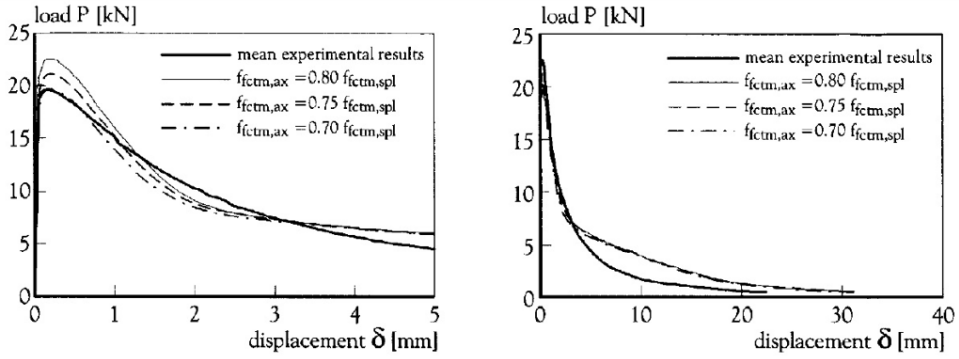

(a) Load- displacement curves up to 5 mm (b) Complete load-displacement curves

Figure 2.40. Influence of $f_{ctm,ax}$ on tension behavior [7].

Critical crack width (w_0) mainly affects the displacement curve of the post-cracking part. Critical crack width changes according to fiber length. For steel fibers having 30 mm length, critical crack width of $L_f/4$ is applicable to represent the experimental load displacement curve. However, for steel fibers having 60 mm length, critical crack width of $L_f/2$ is suitable to represent the experimental load displacement curve as shown in Figure 2.41 [7].

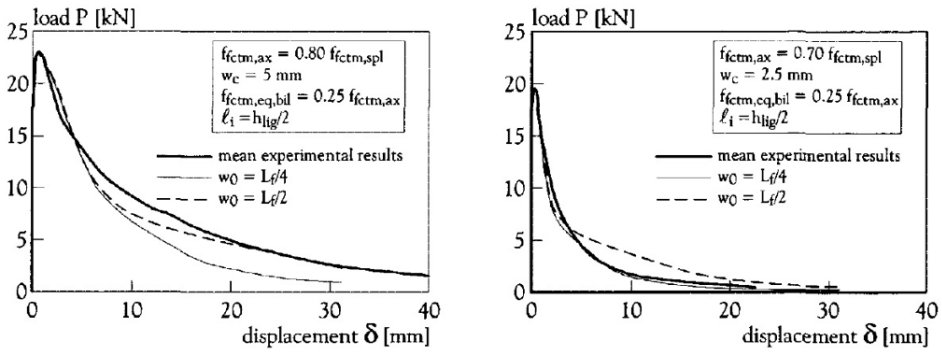

(a) 60 kg/m^3 60/0.75 hooked-end steel fibers (b) 60 kg/m^3 30/0.5 hooked-end steel fibers

Figure 2.41. Influence of critical crack width (w_0) on tension behavior [7].

The effect of w_c and $f_{ct,eq,bil}$ on tension behavior are given in Figure 2.42. Characteristic crack width affects the crack opening part while the stress values are kept constant and equivalent post cracking strength influences the stress value whereas the crack opening values are kept constant as shown in Figure 2.42.

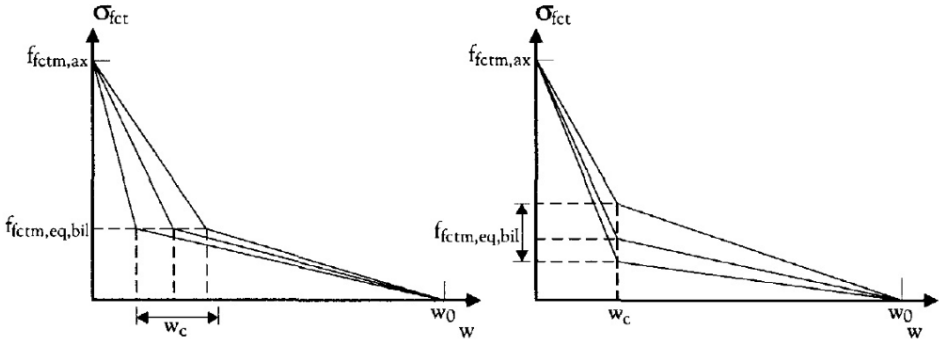

(a) Effect of characteristic crack width (b) Effect of equivalent post cracking strength

Figure 2.42. Influence of w_c and $f_{ct,eq,bil}$ on tension behavior [7].

After simulation and experimental tests, Kooiman (2000) [7] used the following parameters for tensile behavior of SFRC;

- the uniaxial tensile strength ($f_{fctm,ax}$) was 0.7 (30 mm fibers) - 0.8 (60 mm fibers) times the splitting tensile strength.
- critical crack width (w_0) depends on fiber length, type and orientation number. Critical crack width can be used as 0.33 (for 30 mm fibers) and 0.425 (for 60 mm fibers) times the steel fiber length.
- the equivalent post cracking strength ($f_{fctm,eq,bil}$) was accepted to be 30% of the uni-axial tensile strength for 30 mm fibres and 20% for 60 mm fibres.
- characteristic crack width (w_c) depends on the critical crack with (w_0) and change in the (w_c/w_0) (the slope of the bilinear relation) was between 1/5-1/6 of the critical crack width.

Grunewald (2004) [23] used the parameters of stress-strain and stress-crack width relationship for tension behavior of SFRC as following:

- the uniaxial tensile strength ($f_{fctm,ax}$) is in the range of 45-68% of the splitting tensile strength of SFRC and this ratio is independent of steel fiber length.
- critical crack width (w_0) is in the range of 0.26-0.42 of the steel fiber length for SFRC and this crack with affects the stress-crack opening displacement diagram

at larger crack widths (> 5-10 mm) which is not important for most structural applications.

- the equivalent post cracking strength ($f_{fctm,eq,bil}$) changes from 20% to 35% for SFRC.
- characteristic crack width (w_c) varies from 22% - 36% of the critical crack widths (w_0).

Modeling part consists of four stages. In the first stage, input parameters are determined as described above. In the second stage, numerical analysis - multi layer model is composed by using geometry, material and boundary conditions. In the third stage, an accuracy check is performed in order to find out deviation between the simulation results and experimental results. Last stage is the output level in which multi-layer model can be used as tensile behavior of reinforced concrete for structural analysis when the accuracy checks are completed. Model simulations are repeated until the deviation amount (model/experiment) becomes lower than 5%. The following checks are required [7, 23]:
The following checks were realized on steel fiber reinforced specimens;

- Flexural loads were checked up to maximum flexural load (P_{max})and 75% of the maximum experimental flexural load ($0.75P_{max}$ - in the softening region).
- Toughness values were checked up to 75% of the maximum experimental flexural load ($0.75P_{max}$) and up to 4 mm.

3. EXPERIMENTAL STUDY

In the scope of the research, experimental studies were divided into two main categories as fresh and hardened state experimental tests. Fresh state tests were conducted on various steel fiber reinforced self-compacting concretes (SF-SCCs) to obtain required flowability, passing ability and rheological properties. In addition, fiber orientation analysis and static & dynamic segregation resistance analyses were conducted to investigate distribution of fibers throughout concrete. Mechanical performance of the concretes was evaluated by four point flexural bending test, compressive strength test and splitting tensile strength test.

3.1. Mix Design

3.1.1. Materials

Five different types of self-compacting concretes were produced in order to examine the flow characteristics of SF-SCCs. The used materials were coarse and fine aggregates, cement, F-type fly ash, superplasticizer, and steel fibers (hooked-end long and straight short). Sieve analyses were conducted on aggregates so that optimum amounts were determined. Then different trial batches were casted to obtain adequate flowability properties of the control (non-fibrous) concrete without segregation or bleeding. After reaching optimum mix design on control concrete, all other ingredients were kept constant while superplasticizer amounts were changed with inclusions of different steel fiber types and fractions in the other mixes. Several batches were cast and tested and mixes which achieved the best flowability and passing ability characteristics were chosen in the study as is seen in Table 3.1.

Table 3.1. Mix ingredients.

	Batches for SCC (water to binder ratio: 0.37)				
Ingredients, ($1m^3$)	**SCC 1 Control mix**	**SCC 2 0.5 % Long FRC Mix**	**SCC 3 1 % Long FRC Mix**	**SCC 4 0.5 % Short FRC Mix**	**SCC 5 0.5 % S + 0.5 % L Hybrid FRC Mix**
Water (kg)	220	220	220	220	220
Cement (kg)	420	420	420	420	420
Fly Ash (kg)	180	180	180	180	180
Gravel<10 mm (kg)	636	636	636	636	636
Crush Sand (kg)	353	353	353	353	353
Sand (kg)	424	424	424	424	424
Steel Fiber (kg)	0	39	78	39	78
Superplasticizer (kg)	3.4	3.6	4.2	4.2	4.5

The mixtures were produced with a water-to-cement ratio of 0.42 and with a water-to-binder (cement + k_f*fly ash) ratio of 0.37 in which fly ash amount was used with a k_f coefficient of 0.4, which was determined according to TS 13515 standard [67]. The amount of superplasticizer was increased with an increasing steel fiber amounts as shown in Table 3.1.

3.1.1.1. Cement. Ordinary Portland cement (CEM I 42.5R) was used in the study. Physical, chemical and mechanical properties of the cement used are given in Table 3.2, Table 3.3 and Table 3.4.

Table 3.2. Physical Properties of Cement.

Physical Properties of Cement (TS EN 196-3 [68], TS EN 196-6 [69])	
Density	3.14 (g/cm^3)
Initial Setting Time	100 (min.)
Final Setting Time	165 (min.)
Le Chatelier	1 (mm)
Specific Surface	3607 (cm^2/g)
Residue on 45μm sieve	4.5 (%)
Residue on 90μm sieve	0.0 (%)

Table 3.3. Chemical Properties of Cement.

Chemical Properties of Cement (TS EN 196-2) [70]		
SiO_2		19.63 (%)
Insoluble Residue		0.28 (%)
Al_2O_3		5.58 (%)
Fe_2O_3		3.32 (%)
CaO		63.67 (%)
MgO		1.25 (%)
SO_3		3.23 (%)
Loss on Ignition		2.03 (%)
Cl^-		0.0423 (%)
Na_2O / K_2O		0.21 / 0.68 (%)
N/A		0.36 (%)
S.CaO - Free Lime		2.00 (%)
Mineralogical Composition	C_3S	50.36
	C_2S	18.37
	C_3A	9.18
	C_4AF	10.10
LSF		0.96

Table 3.4. Mechanical Properties of Cement.

Mechanical Properties of Cement (TS EN 196-1) [71]		
Compressive Strength (MPa)		
Mechanical Characteristic / day	Standards (MPa)	Test Results (MPa)
Early Strength / 2 day	≥ 20	28.3
Early Strength / 7 day	-	42.1
Standard Strength / 28 day	≥ 42.5 ≤ 62.5	54.8

3.1.1.2. Fly ash. F-type Fly ash was used as a supplementary material, which was supplied from Çatalagzi thermal power plant. Fly ash amount was selected as 30% of the total cementitious material from other studies and laboratory tests. Chemical and physical properties of the F-type fly ash used for SF-SCC specimens were given in Table 3.5 and Table 3.6.

Table 3.5. Chemical Properties of Fly Ash.

Chemical Properties of Fly Ash.	
Loss on Ignition	3.30 (%)
SiO_2	54.76 (%)
Al_2O_3	25.26 (%)
Fe_2O_3	6.28 (%)
CaO	2.10 (%)
MgO	2.08 (%)
SO_3	0.20 (%)
Na_2O	0.38 (%)
K_2O	4.04 (%)
TiO_2	1.16 (%)
Cl^-	0.0043 (%)
Free CaO	0.02 (%)

Table 3.6. Physical Properties of Fly Ash.

Physical Properties of Fly Ash.	
Density	2130 (kg/m^3)
Pozzolanic Activity Index 28 day	83 (%)
Pozzolanic Activity Index 90 day	97 (%)
Residue on $45\mu m$ sieve	29.4 (%)
Soundness	- (mm)

3.1.1.3. Aggregates. Coarse and fine aggregates were used in the study. Coarse aggregate with a maximum grain size (d_{max}) of 10 mm and aggregate density of 2.74 kg/dm^3 was used. Natural sand and crushed sand were used as fine aggregates with densities of 2.60 and 2.68 kg/dm^3, respectively. Sieve analyses were conducted on coarse and fine aggregates; sand, crushed sand and coarse aggregate amounts were determined as 30%, 25% and 45% of the total aggregates, respectively. Grading curves and sieve analysis of aggregates were given in Figure 3.1 and Figure 3.2.

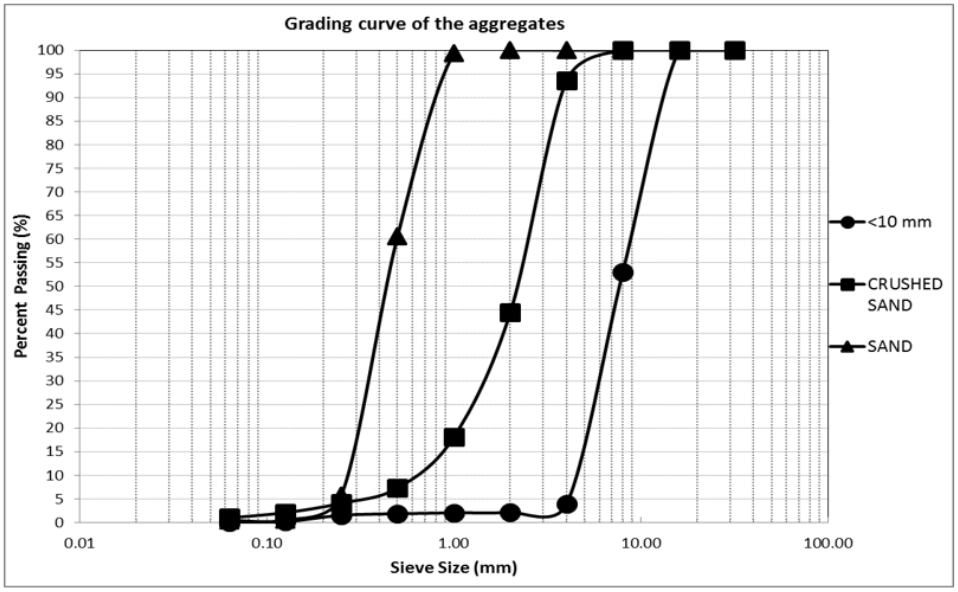

Figure 3.1. Grading curves of the aggregates.

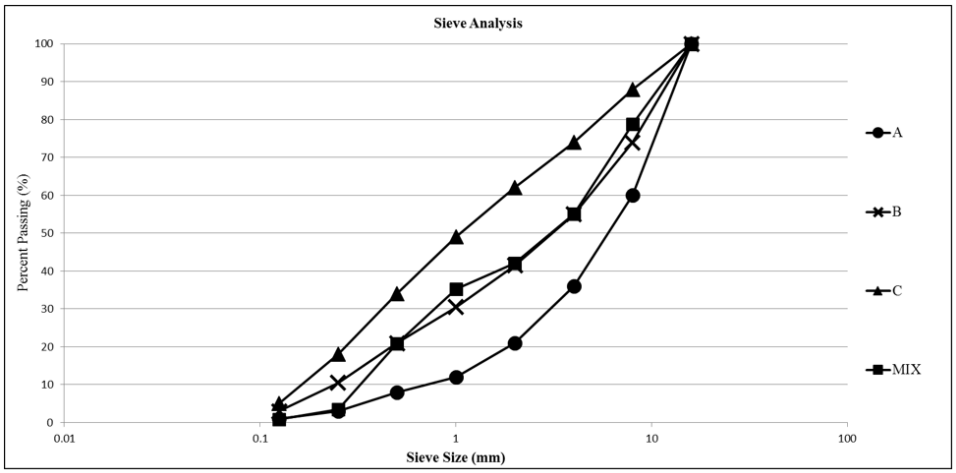

Figure 3.2. Sieve analysis on aggregates.

3.1.1.4. Steel Fibers. Hooked-end long fibers with fractions of 0.5% and 1%, straight short fibers with a fraction of 0.5%, and hybrid fibers (combination of both short and long fibers) with a fraction of 1% (0.5% short fiber + 0.5% long fiber) were used in the research. Steel fibers have a density of 7.8 kg/dm^3. Properties of the steel fibers were given in Table 3.7.

Table 3.7. Properties of steel fibers.

	Straight Short Steel Fibers	**Hooked-end Long Steel Fiber**
Length (mm)	13	35
Diameter (mm)	0.16	0.55
Aspect Ratio	81	64
Tensile Strength (MPa)	1100	1345

3.1.1.5. Superplasticizer. A polycarboxylic ether based high range superplasticizer, which has a density of 1.095 kg/dm^3 was used to obtain high flowability without segregation and/or bleeding.

3.1.2. Mixing Procedure

Concrete materials were prepared in the Construction Material Laboratory. Following mixing procedure was used adopted after several trials;

- In the first step, cementitious material (cement + fly ash) and aggregates were added to the pan mixer and all dry ingredients without fibers were mixed for 2 minutes.
- After that, water and superplasticizer mixed in a container beforehand and were added to the mixer in 1 minute duration and dry + wet ingredients were mixed for 1 more minute.
- In the final step, steel fibers were added (for steel fiber reinforced series) to the mixer in 1 minute and further mixed for 1 minute for homogeneity. For non-fibrous mixes, dry + wet ingredients were mixed for another 2 minute for equal mixing procedure with mixes including steel fibers.

The overall mixing procedure was terminated in 6 minutes and concrete was ready for casting.

3.2. Specimens

Specimens were produced after the required mix designs were obtained for each mixes. Different specimen sizes and mixes were cast and fresh and hardened state tests were conducted, accordingly.

3.2.1. SCC Groups and Specimen Sizes

In the research, two main parameters; specimen thickness-to-depth ratio (a/d) and specimen thickness-to-fiber length ratio (t/f_L) were investigated on bending performance of specimens. For this reason, seven different moulds were designed with various lengths starting from 200 mm to 425 mm. Specimens had equal widths and depths, ranging from 30 mm to 100 mm. All specimen sizes were selected according to flexural loading test machine (MTS) size capability. Five types of SCC mixes were prepared in the study as mentioned before. Control (non-fibrous) mix, 0.5% short fiber reinforced mix, 0.5% long fiber reinforced mix, 1% long and hybrid fiber reinforced mixes. Trials were also made by using 1% short steel fibers; however, after preliminary tests, flowability characteristics of this mix was found inadequate, possibly due to a great number of short fibers in the mix. Therefore, short fiber reinforced mix with 1% fiber fraction was not produced. In conclusion, seven different specimen sizes and five different mixes were used in the scope of the study as is seen in Table 3.8.

Table 3.8. SCC Groups and Specimen Sizes.

SCC Groups	Specimen Sizes (mm)
Control Mix	30x30x275
	40x40x200
0.5 % Long FRC Mix	40x40x350
1 % Long FRC Mix	50x50x425
0.5 % Short FRC Mix	60x60x275
1 % Hybrid FRC Mix	80x80x350
	100x100x425

3.2.2. Nomenclature of Specimens

Specimens were named in accordance with fiber types and fiber amounts, their thicknesses and lengths. For instance, S5T50L425 represents the specimens with short steel fibers with a fiber volume ratio of 0.5%, thickness of 50 mm and length of 425 mm. For the other specimens; the first letters C, L and H point out Control (non-fibrous), Long Fiber and Hybrid Fiber; respectively. In the study, five different SCC groups with seven different sample sizes, 35 series (#) were composed and three specimens were cast for each series as shown in Table 3.9. As a total, 105 specimens were obtained.

Table 3.9. Specimen nomenclature and dimensions.

a/d	#	Specimen	Dimensions (mm)				Fiber Length	Thickness/ Fiber Length
			t	w	a	L	fL	t/f_L
2.5	1	CT50L425	50	50	125	425	-	-
	2	S5T50L425	50	50	125	425	13	3.8
	3	L5T50L425	50	50	125	425	35	1.4
	4	L10T50L425	50	50	125	425	35	1.4
	5	H10T50L425	50	50	125	425	-	-
	6	CT40L350	40	40	100	350	-	-
	7	S5T40L350	40	40	100	350	13	3.1
	8	L5T40L350	40	40	100	350	35	1.1
	9	L10T40L350	40	40	100	350	35	1.1
	10	H10T40L350	40	40	100	350	-	-
	11	CT30L275	30	30	75	275	-	-
	12	S5T30L275	30	30	75	275	13	2.3
	13	L5T30L275	30	30	75	275	35	0.9
	14	L10T30L275	30	30	75	275	35	0.9
	15	H10T30L275	30	30	75	275	-	-
1.25	16	CT100L425	100	100	125	425	-	-
	17	S5T100L425	100	100	125	425	13	7.7
	18	L5T100L425	100	100	125	425	35	2.9
	19	L10T100L425	100	100	125	425	35	2.9
	20	H10T100L425	100	100	125	425	-	-
	21	CT80L350	80	80	100	350	-	-
	22	S5T80L350	80	80	100	350	13	6.2
	23	L5T80L350	80	80	100	350	35	2.3
	24	L10T80L350	80	80	100	350	35	2.3
	25	H10T80L350	80	80	100	350	-	-
	26	CT60L275	60	60	75	275	-	-
	27	S5T60L275	60	60	75	275	13	4.6
	28	L5T60L275	60	60	75	275	35	1.7
	29	L10T60L275	60	60	75	275	35	1.7
	30	H10T60L275	60	60	75	275	-	-
	31	CT40L200	40	40	50	200	-	-
	32	S5T40L200	40	40	50	200	13	3.1
	33	L5T40L200	40	40	50	200	35	1.1
	34	L10T40L200	40	40	50	200	35	1.1
	35	H10T40L200	40	40	50	200	-	-

3.2.3. Casting Procedure

Prepared concrete mixes were cast to the moulds from one end of the specimen and left to flow to the other end. During casting, vibration and/or shaking was not applied to the specimens since concrete was flowing under its self-weight. Concrete surplus was taken by a trowel and surface leveling was applied to all specimens.

3.2.4. Curing of Specimens

The specimens were demolded after 24 hours and kept in a water tank at a temperature of 20 ± 2 °C for 28 day curing period time to obtain required strength for tests.

3.3. Fresh State Tests

3.3.1. Flowability and Passing Ability Tests

The flowability of SCCs were measured via slump flow and V-funnel tests; passing ability was measured using J Ring, L-Box and U-Box tests. Steel fiber reinforced mixes should fulfill the requirements of flowability and passing ability without segregation and/or bleeding. Therefore, flowability and passing ability tests were conducted on SCCs.

3.3.1.1. Slump Flow Test. Slump flow tests were realized on the SCC mixes according to TS EN 12350-8 standard [58]. In the experiment, prepared SCC mixes were poured into the top of the slump cone on a base plate as described in the standard, no striking was applied, waited about 30 second to remove any concrete surplus on the top of the cone and base plate. Then, filled cone was lifted vertically upwards in one movement so that concrete left to the flow on base plate without any obstruction. In Figure 3.3, base plate and slump cone dimensions were given.

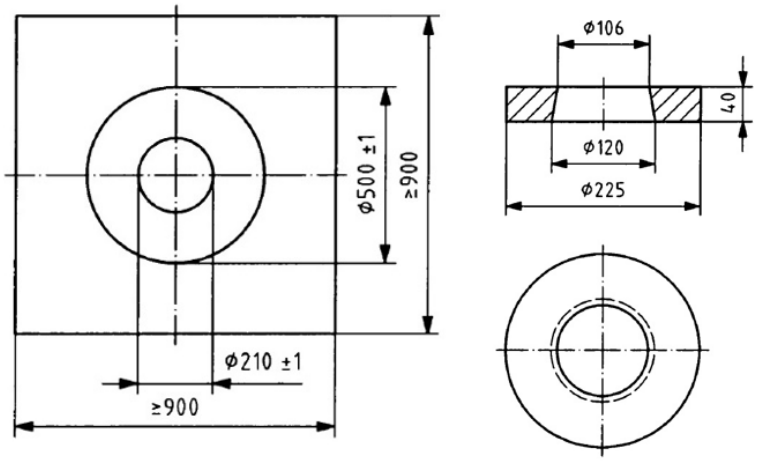

Figure 3.3. Base plate and slump cone dimension (mm) [58].

Slump flow spread in x and y direction was measured, and t_{500} and tfinal durations in which flow diameter reaches up to 500 mm and final flow diameter were recorded.

3.3.1.2. J-Ring Test. J-ring test was performed according to TS EN 12350-12 standard [61]. J-Ring measures passing ability of the SCC mixes between narrower openings (41±1 mm) without segregation and/or blocking. In this test, same procedure with slump flow test was applied; however; this time concrete exposed to J-Ring obstructions, which has a 300±2 mm diameter and 16 steel rods with a diameter of 18±1 mm equally distributed around the J-Ring. After lifting of the cone (indicated as 1 in Figure 3.4), concrete passed the J-ring obstruction (indicated as 2 in Figure 3.4) and spread along the base plate (indicated as 3 in Figure 3.4). Outer concrete heights of $\Delta h_{x1}, \Delta h_{x2}, \Delta h_{y1} and \Delta h_{y2}$ and inner concrete height of Δh_0 (indicated in Figure 3.5) were measured and passing ability of J-Ring (PJ) was calculated as following:

$$\mathrm{PJ} = \frac{\Delta h_{x1} + \Delta h_{x2} + \Delta h_{y1} + \Delta h_{y2}}{4} - \Delta h_0 \tag{3.1}$$

In the test, slump flow and PJ values were measured and t_{500}J and t_{finalJ} durations were recorded.

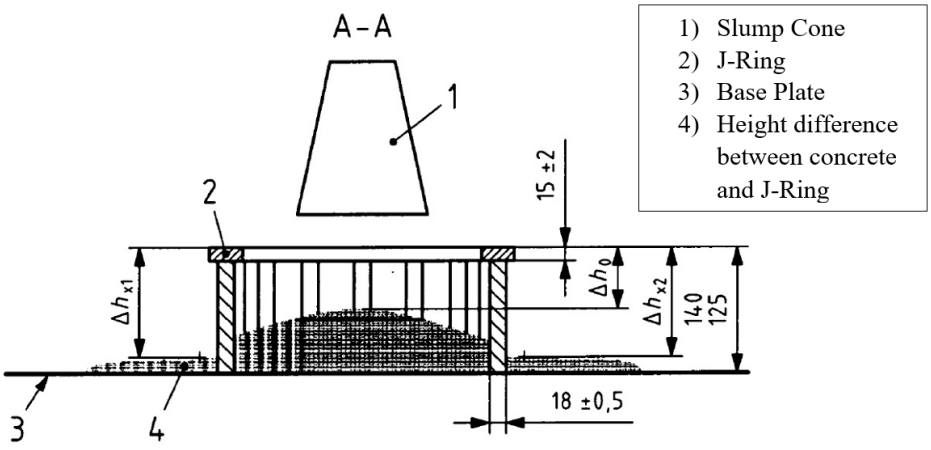

Figure 3.4. A-A section of the J-Ring [61].

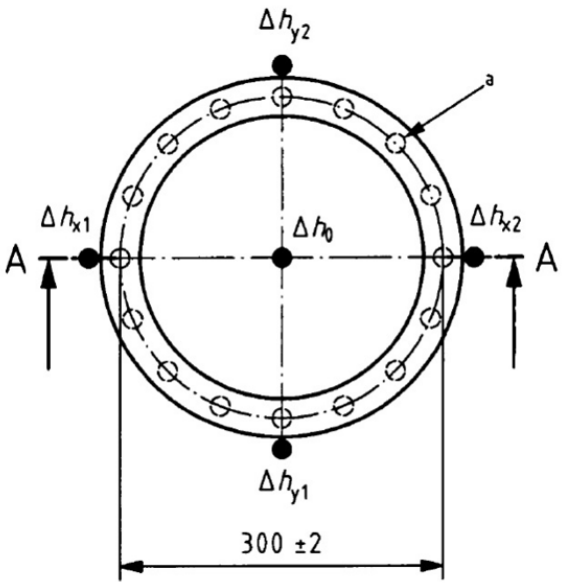

Figure 3.5. J-Ring with narrower openings (41±1 mm) [61].

3.3.1.3. L-Box Test. L-Box test was conducted in accordance with TS EN 12350-10 standard [60]. L-Box test is also an indicator of passing ability of SCC mixes without segregation and/or blocking. L-Box dimensions were given in Figure 3.6. In the test, there is a gate which separates vertical and horizontal sections of the L-Box (indicated as 1 in Figure 3.6). Concrete was filled into the vertical section of the L-Box and waited 60±10 seconds to observe any segregation, if available. Later, closed gate was lifted so that concrete can spread between the steel rods of the horizontal section of the L-Box, which has 200 mm opening with 3 steel rods with diameters of 12 mm, as

shown in Figure 3.7. Concrete heights at the vertical section (ΔH_1) and lateral L-Box sections (ΔH_2) were measured. Passing ability of concrete (PL value) was calculated by dividing the concrete height of the lateral section to the height of the vertical section.

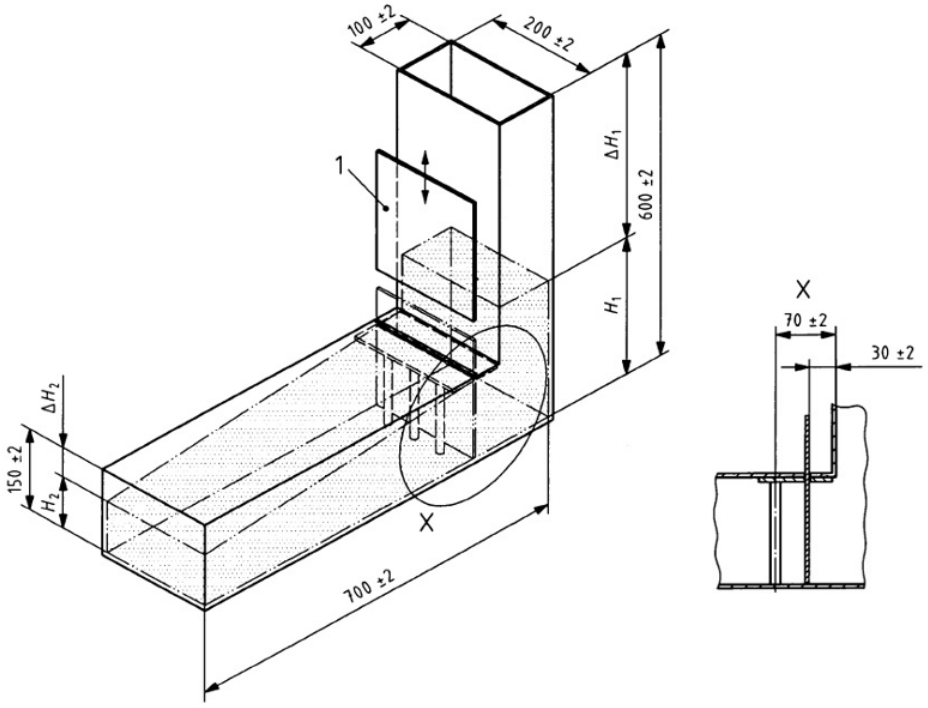

Figure 3.6. L-Box test set-up [60].

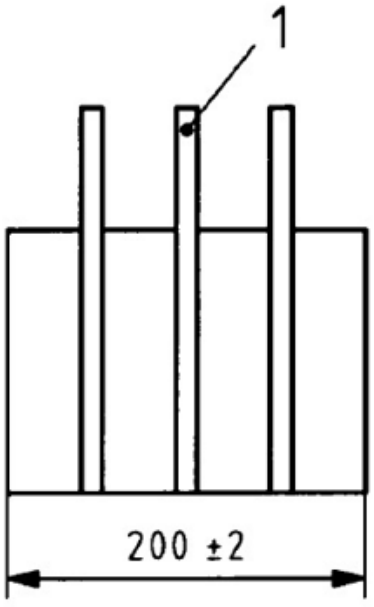

Figure 3.7. L-Box steel rods openings (41±1 mm) [60].

3.3.1.4. U-Box Test. U-Box test was performed in accordance with UNI 11044 standard [62]. Similar to the L-Box test set-up, two vertical sections were divided by a gate, prepared SCC mix was filled into the one vertical section and passed to the other vertical section upon lifting of the gate. In this test, concrete height difference between the two vertical sections was measured.

3.3.1.5. V-Funnel Test. V-Funnel test was realized in conformity with TS EN 12350-9 standard [59]. V Funnel test is an indicator of viscosity / passing ability of the mixes. SCC mix is poured to V-Funnel section and then concrete is let to discharge upon removing a gate (indicated as 1 in Figure 3.8) and discharge time is recorded in the test.

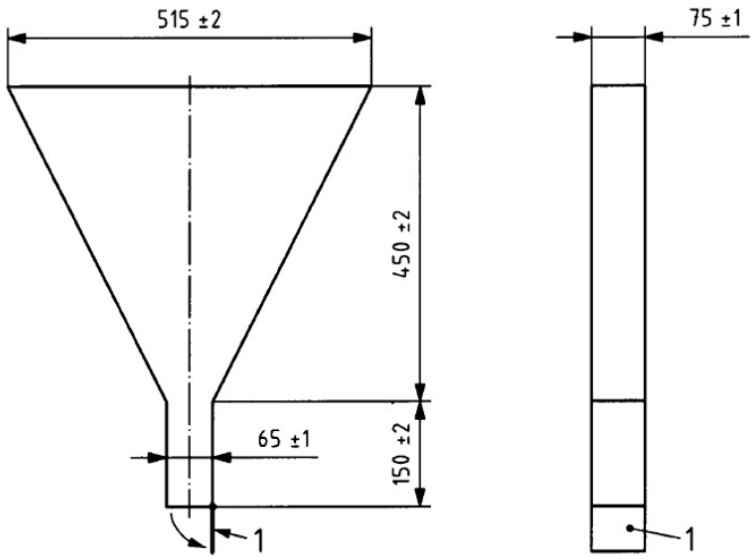

Figure 3.8. V-Funnel test set-up [59].

3.3.2. Dynamic Segregation Resistance Analysis

Dynamic segregation resistance analysis was performed after flowability and passing ability tests on SF-SCC specimens. Dynamic segregation resistance represents the ability of a mixture to drive the fibers with itself in the fresh state. In the research, 4 different types of steel fiber reinforced mixes and 7 different specimen sizes were used and 2 specimens were cast for each mix to use the average value when evaluating segre-

gation resistances of the mixes (56 specimens in total). SCC mix was cast from one end of the specimen and left to flow to the other end during dynamic segregation analyses and specimens were not exposed to vibration or shaking during casting procedure.

In the test procedure, each mould was divided into four equal parts by using steel plates prepared in the laboratory as shown in Figure 3.9. Steel plates were placed just after casting of the concrete.

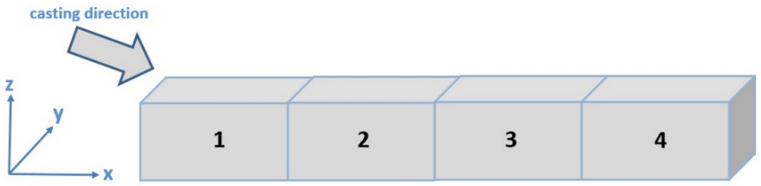

Figure 3.9. Dynamic segregation tests on fresh concrete.

Then, each parts of the fiber reinforced concrete (1^{st}, 2^{nd}, 3^{rd} and 4^{th} region) were collected to plastic containers as is seen in Figure 3.10 and water was added to the container in order to separate fibers from concrete easily. Then, concrete was washed out and fibers were pulled out with a magnet. After cleaning of the container, long fibers were counted one by one easily while short fibers and hybrid (short + long) fibers were left to drying in order to weigh steel fibers accurately, Figure 3.11.

The percentage fiber amount (%) in each volume was found by counting the fibers one by one for long fibers; while fibers were weighed and volume percentages were calculated for short and hybrid fibers for the sake of time. If dynamic segregation resistance of a mix is high, the number of fibers in different regions (1^{st}, 2^{nd}, 3^{rd} and 4^{th}) of the specimen should be similar, indicating good fiber driving ability of SCC.

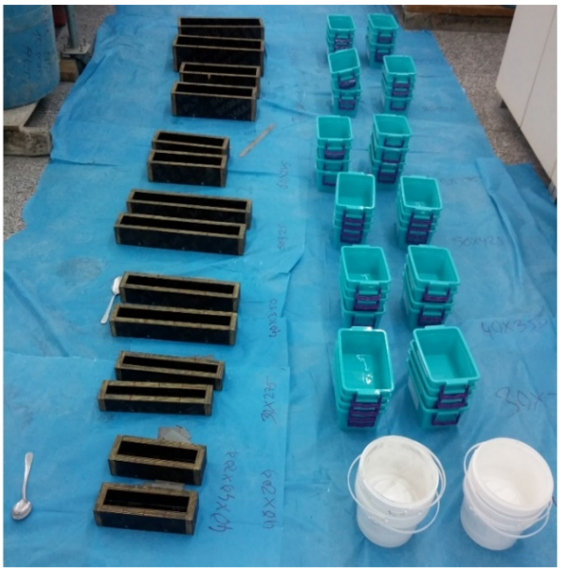

Figure 3.10. Preparations for dynamic segregation analysis test.

Figure 3.11. Specimens including short fibers were left to drying at laboratory.

3.3.3. Static Segregation Resistance Analysis

Static segregation resistance analyses were realized on the SF-SCC on hardened concrete specimens. Static segregation resistance represents concrete's ability to hold fibers as well as aggregates while it is still plastic. Fibers tend to settle down due to the gravity effect; previous research shows that the number of fibers at the bottom parts of the specimens can be higher and the top section (couple of millimeters) may

be left unreinforced which results in non-homogenous and weak section. To control the stability and static segregation resistance of concrete experiments were conducted on 56 specimens (4 SF-SCC mixes x 7 different mould sizes x 2 specimens for each). In the experiment, beam specimens were cut into 4 equal pieces as shown in Figure 3.12 and the 3 of the cut sections were divided into three as top, middle and bottom parts as is seen in Figure 3.13. Steel fiber amounts were counted for each parts and compared to each other to understand static segregation resistance of the mixes. Similar numbers of fibers per unit area on each of the top, middle and bottom sections represent high static segregation resistance.

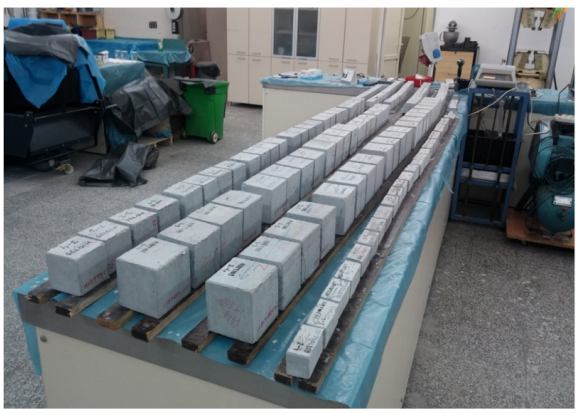

Figure 3.12. Specimens prepared for static segregation analysis.

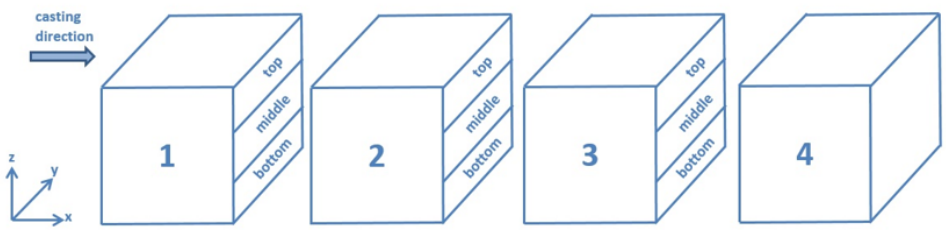

Figure 3.13. Sections of the specimens for static segregation analysis.

3.3.4. Rheology Test

Rheology tests were also conducted on the fresh state of SF-SCCs by using a concrete rheometer in order to measure rheological properties of the mixes (Figure 3.14). First of all, stress growth test was applied to the mixes and maximum torque

measured during the rotation of the vane at a steady slow speed of 0.025 rev/s. Static yield stress was calculated using maximum torque value of the test. Then, the vane was rotated at maximum speed and after breakdown period, vane speed was slowly decreased at six steps. At the same time, average speed and torque values were recorded as a function of constant vane speeds. Bingham parameters were calculated using the plot of torque versus vane rotations speed [72].

Figure 3.14. Rheology tests using a rheometer on SCC mixes.

3.4. Hardened State Tests

3.4.1. Force - Controlled Compressive Strength Test

Force controlled compressive strength tests were carried out on 150 x 150 x 150 mm cube specimens according to TS EN 12390-3 standard [66] at the ages of 1, 7 and 28 days to observe strength evaluation of SCCs. Specimens were axially loaded at a rate of 13.5 kN/s (0.6 MPa/s) as is seen in Figure 3.15. The compressive strength of the cube specimen is calculated by dividing the maximum load reached during the compressive strength test by the cross-sectional area of the specimens. For all of the 5

different series, three cube specimens were tested for average values. Specimens were tested under force-controlled test.

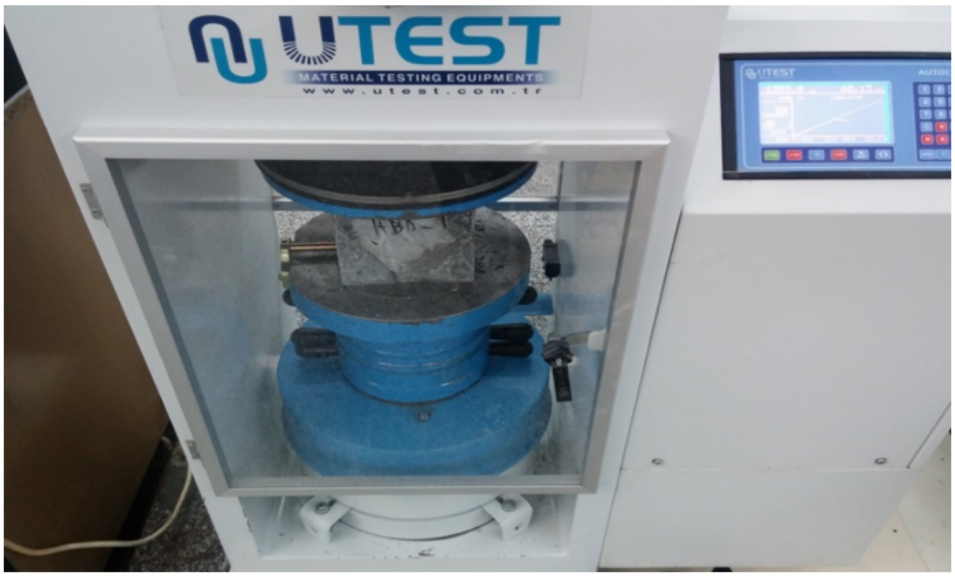

Figure 3.15. Compressive Strength Test.

3.4.2. Displacement Controlled Compressive Strength Test

Displacement controlled compressive strength tests were conducted on SCC specimens at the age of 28 day in order to obtain the parameters required for modelling such as maximum compressive strength ($f_{c,max}$), linear elastic strain limit (ε_{c0}), and ultimate strain limit (ε_{cmax}) and elastic modulus (E) values. Three cylinder specimens with a diameter of 100 mm and a length of 200 mm were cast for each series and tested under displacement-control. Two Linear Variable Displacement Transducers (LVDT) were attached to the cylinder specimens to measure deformations in the specimens. Specimens were loaded using MTS closed-loop displacement controlled test machine with a 500 kN capacity. Stress and strain data were obtained for all specimens.

3.4.3. Splitting Tensile Strength Test

Splitting tensile strength tests were carried out on cylinder specimens with a diameter of 100 mm and a length of 200 mm at the 28 day in accordance with ASTM

C496 / C496 M-11 standard [65]. Specimens were transversely loaded at a rate of 0.5 kN/s (1 MPa / min) as is seen in Figure 3.16. Three cylinder specimens were cast for all of the 5 series of concretes for splitting tensile strength tests. The results were also used for modelling phase of the study.

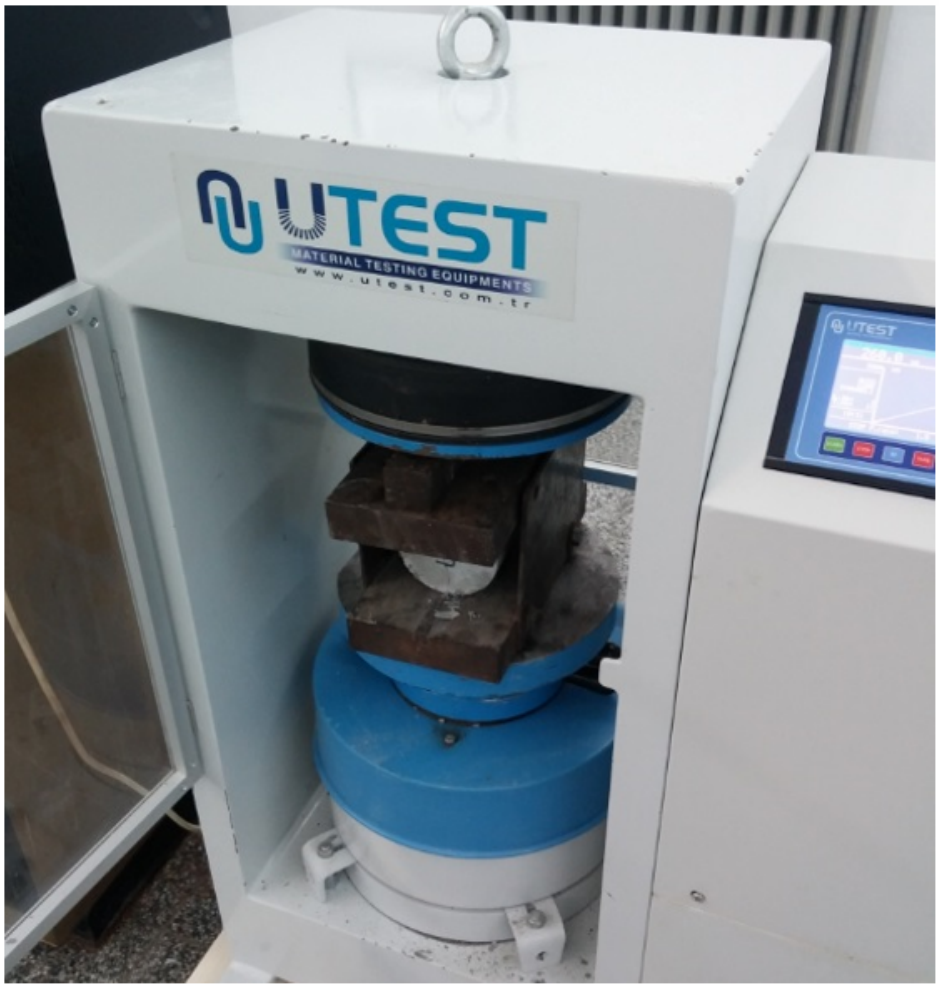

Figure 3.16. Splitting Tensile Strength Test.

3.4.4. Four Point Bending Test on Specimens

Four point bending tests on SCC specimens were realized on prismatic specimens, which was mentioned before on Table 3.9 using MTS closed-loop displacement controlled test machine with a 100 kN capacity. Three specimens were tested for all of the 5 different SCC concrete types and 7 different specimen sizes under flexure. As a total, 105 specimens were tested under four point bending in accordance with ASTM

C1609/C1609M-12 standard [64]. Based on the standard, flexural loading was applied in displacement control at two different rates; loading rate was of 0.05 mm/min from zero deflection to L'/900 deflection, then loading rate was increased to 0.1 mm/min from L'/900 deflection until the termination value of L'/150. Loading rates of four point bending test for different span lengths were given in Table 3.10.

Table 3.10. Loading rates under four point loading.

Dimension types	b (mm)	d (mm)	L (mm)	L' (mm)	L'/900 (mm)	L'/150 (mm)
1	50	50	425	375	0.42	2.5
2	40	40	350	300	0.33	2
3	30	30	275	225	0.25	1.5
4	100	100	425	375	0.42	2.5
5	80	80	350	300	0.33	2
6	60	60	275	225	0.25	1.5
7	40	40	200	150	0.17	1

Specimens were loaded at their one - thirds of the span lengths, which is also equal to shear span (a) as is seen in Figure 3.17. To determine crack opening displacement (COD) of specimens, ends of the maximum moment regions were marked and length change between these markers were monitored via a horizontally located LVDT. Similarly one more LVDT collected data on the other face of the beam and average values of the two LVDTs were used to draw Force or Stress versus COD or strain curves. In addition, two LVDTs were also placed vertically to monitor midpoint deflection of beam.

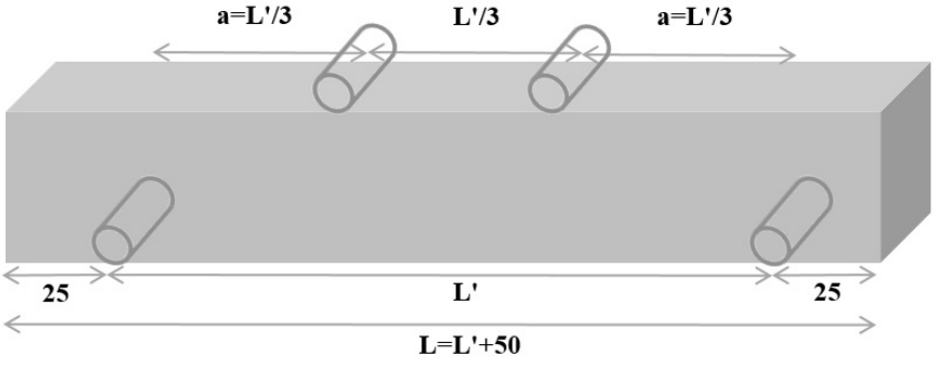

Figure 3.17. Four point flexure loading scheme.

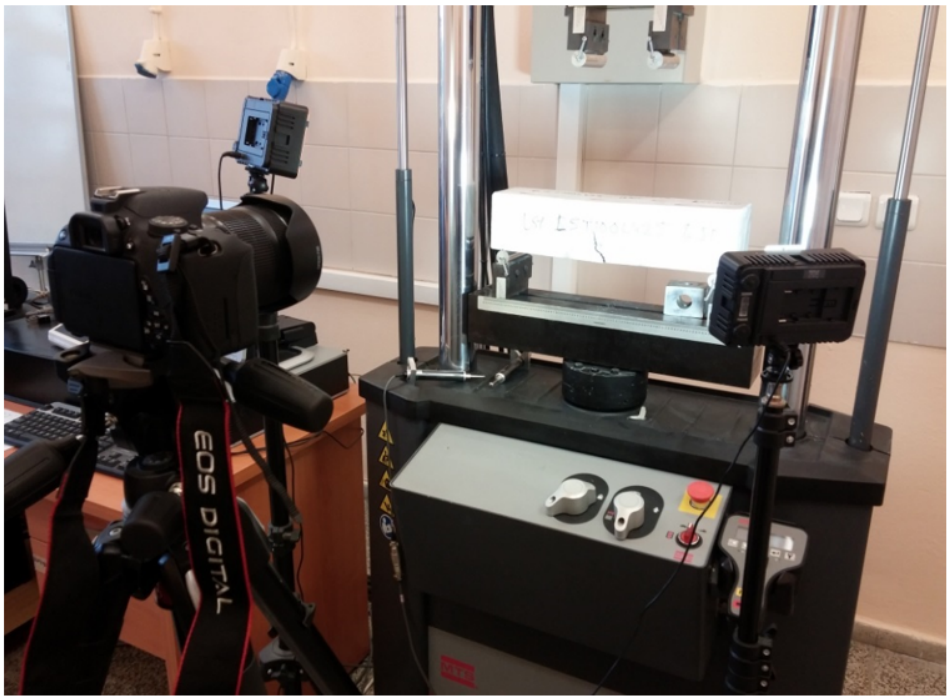

Figure 3.18. Crack monitoring using a camera.

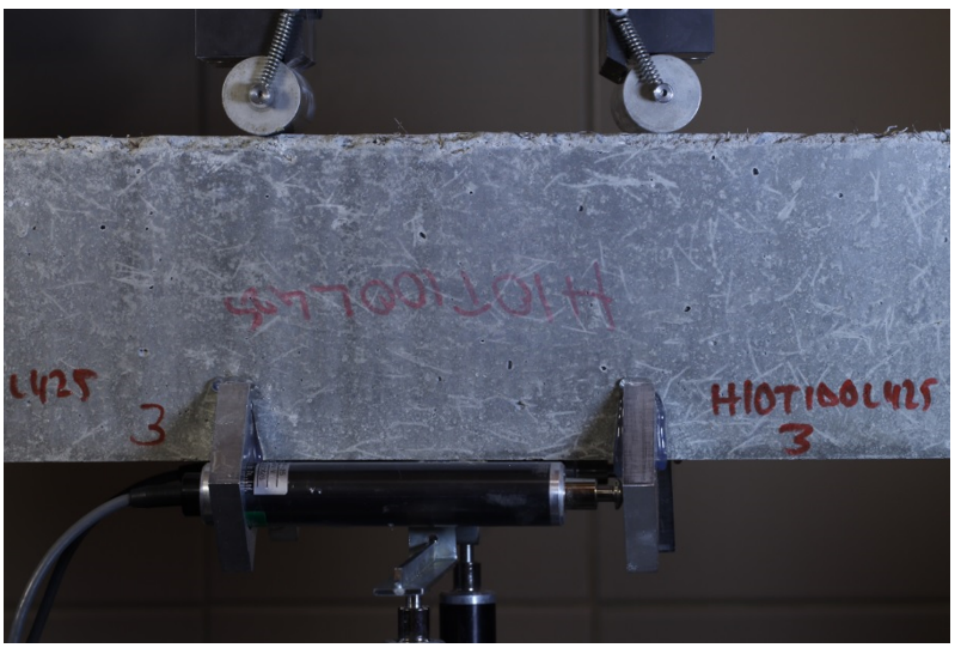

Figure 3.19. LVDT arrangement on a specimen.

3.4.5. Three Point Bending Test on Notched Specimens for Modelling

Three point bending tests were employed on notched specimens for inverse analysis during modelling of bending behavior. Two specimens were poured for each groups, and as a total 10 specimens were produced in accordance with EN 14651 standard [50]. All specimens having widths and depths of 150 mm and lengths of 600 mm and notches were composed on the bottom of the specimens with a 4 mm width and 25 mm height as is seen in Figure 3.20. Specimens had a 125 mm effective height after notch and were tested under three point bending using MTS testing machine.

Based on the standard, three point flexural loading was applied in crack mouth opening displacement (CMOD) control at two different rates; CMOD rate was of 0.05 mm/min from zero to 0.1 mm CMOD, and was increased to 0.2 mm/min from 0.1 mm CMOD to 4 mm CMOD. Experimental procedure was terminated when a CMOD value of 4 mm was reached.

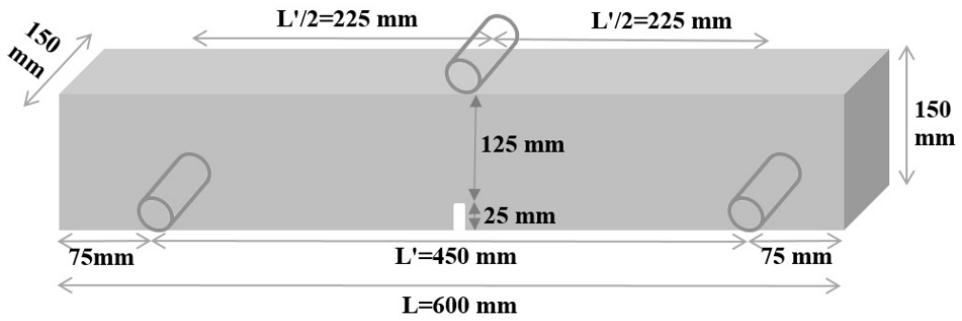

Figure 3.20. Three point bending loading scheme.

Similar with the four point loading test procedure, 4 LVDTs were used (2 lateral and 2 vertical) to measure crack mouth opening displacement and vertical deflections during the overall test procedure together with CMOD gauge. CMOD apparatus positioned on the bottom of the specimen at the notch tip as shown in Figure 3.21. The reason for using horizontal LVDTs together with CMOD gauge for crack opening measurements was to control the results obtained by using the CMOD gauge.

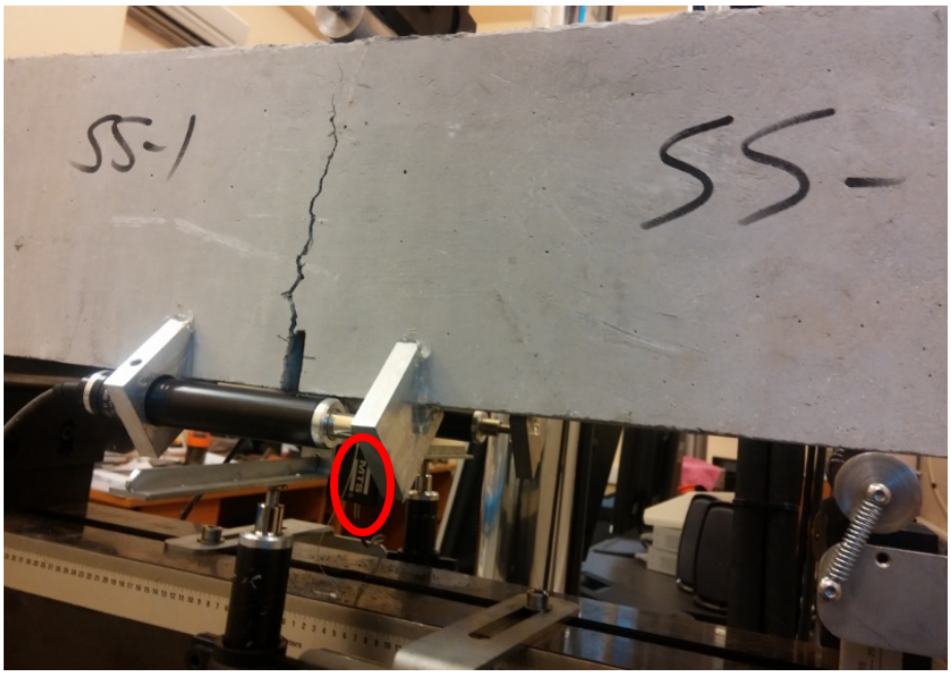

Figure 3.21. LVDT and CMOD arrangement on a specimen.

3.4.6. Flexural (Bending) Strength Calculations

Flexural strength (σ_f) was calculated by using the general equation:

$$\sigma_{\mathrm{f}} = \frac{\mathrm{N}}{\mathrm{A}} \pm \frac{\mathrm{M}}{\mathrm{W}} \tag{3.2}$$

In this formula, N is the normal force with a unit of Newton, A is the area of the specimen with a unit of mm^2, M is the moment with a unit of Nmm, W is the section modulus with a unit of mm^3, sf is the flexural strength with a unit of N/mm^2 (MPa). By using this stress equation, three or four point flexural strength can be calculated. For this purpose, moment and section modulus should be calculated.

For four point bending loading set-up, shear force and bending moment of the specimens are P/2 (N) and PL'/6 (MPa) as indicated in the Figure 3.22. Section modulus of the rectangular cross-section specimen is equal to $bd^2/6$. L' is the distance between supports (mm), b is the width of the specimen (mm) and d is the depth of

the specimen (mm).

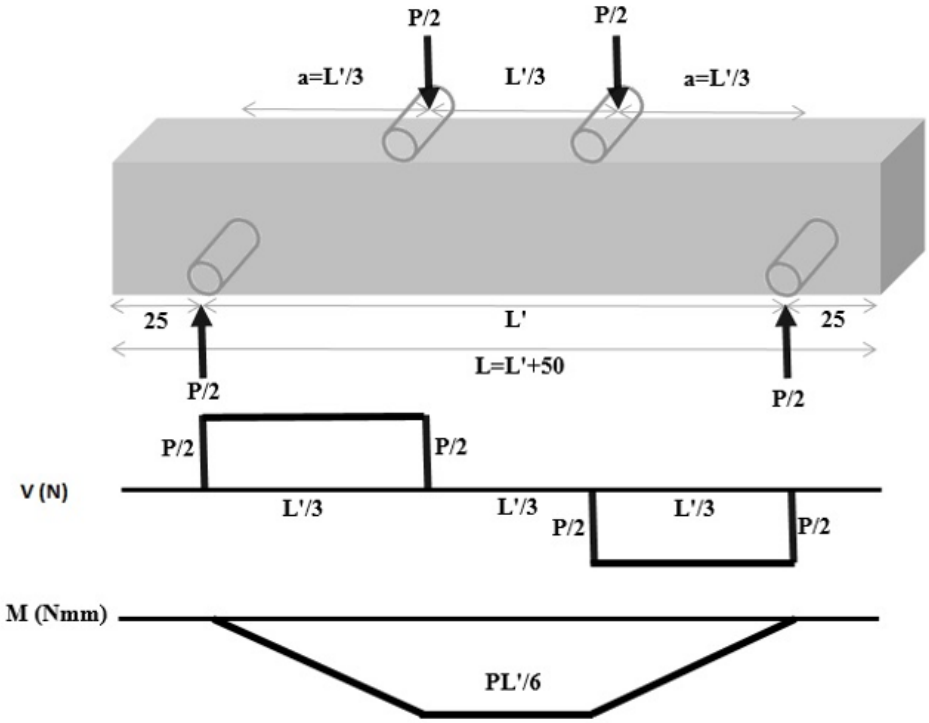

Figure 3.22. Shear Force and Moment diagram on specimens under four point bending.

There was no normal force on the specimen; therefore, first part of the equation (N/A) is equal to zero. The second part of the equation (M/W) for four point bending is equal to:

$$\sigma f = \frac{PL'}{bd^2} \tag{3.3}$$

Shear force and bending moment diagrams of the specimens subjected to three point bending test were given in Figure 3.23.

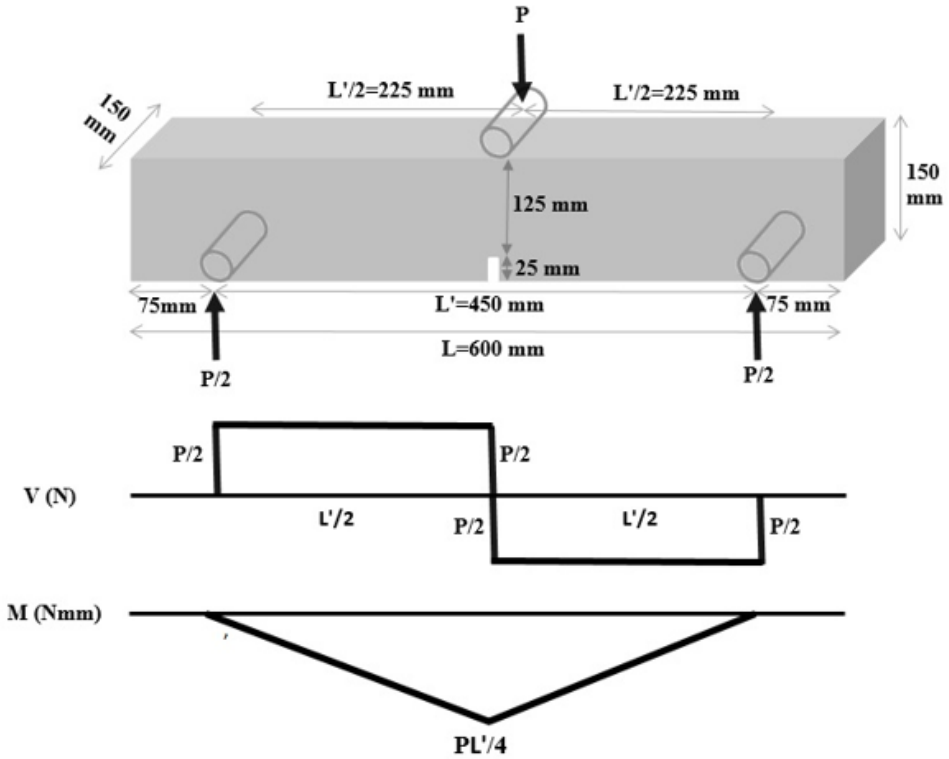

Figure 3.23. Shear Force and Moment diagram on specimens under three point bending.

Similar with four point loading, there was no normal force on the specimen; therefore, first part of the equation (N/A) is equal to zero. The second part of the equation (M/W) for three point bending is equal to:

$$\sigma f = \frac{3}{2}\frac{PL'}{bd^2} \tag{3.4}$$

Flexural bending strengths of the different specimens were calculated and compared to each other.

3.4.7. Flexural Toughness Calculations

After bending (three and four point) tests, flexural toughness values were also calculated for SCC specimens by using load - deflection values recorded during flexural

tests. Two separate toughness values were calculated from 3 and 4 point bending test results, respectively since the toughness value calculated by using the results of 3 point bending tests were required for modelling purposes. Toughness values calculated by using the results of 4 point bending tests were required for comparing the results of specimens cast by using different concrete mixtures with different sizes.

Japan Society of Civil Engineers (JSCE-SF4) standard [49] was used for calculating toughness values. In the JSCE-SF4 standard, flexural toughness factor shall be calculated as following:

$$\mathrm{ft} = \frac{T_b}{L'/150}\frac{\mathrm{L}'}{\mathrm{bd}^2} \tag{3.5}$$

In the formula, FT is the flexural toughness in MPa, Tb is the area under the load-deflection curve in Nmm, L' is the span length in mm, b is the width of the specimen in mm, d is the depth of the specimen in mm.

Flexural toughness values can be calculated in other standards or research up to total deflection or particular deflection value instead of L'/150. However, L'/150 value can be considered as the maximum permissible deflection value for reinforced concrete structures. If deflections exceeds this particular value, an increase in the structural element size would be needed.

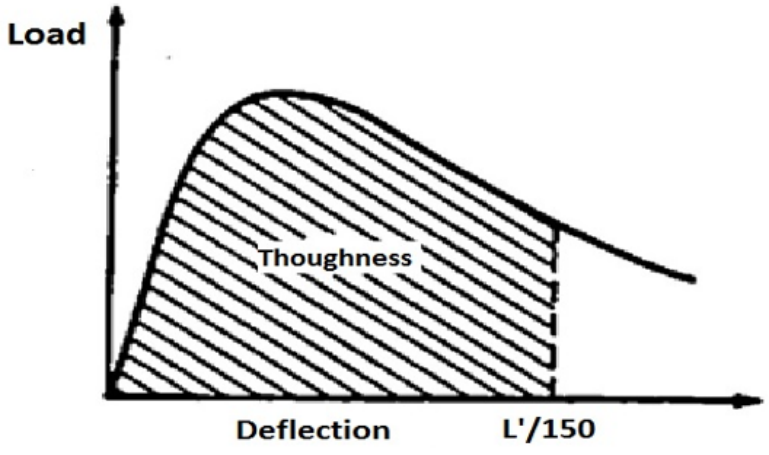

Figure 3.24. Flexural Toughness according to JSCE-SF4 standard [49].

3.4.8. Fiber Orientation

Fiber orientation analyses were performed by using a tensor description method. The objective is to find fiber orientation densities in the x, y and z directions for the specimens with different types of fibers and fiber volumes. This method was applied to the fiber reinforced composite materials by Ozyurt *et al.*, [73]. Details of the tensor description method were described in Mlekusch (1999) [75].

Beam specimens which were cast for 4 point bending tests were used for fiber orientation density analyses. One out of the 3 beam specimens was selected for each series and the selected specimen was cut in the middle (Figure 3.25) since fiber orientation state in the middle section of beams is important by means of flexural performance.

Fiber orientation densities in the x, y and z directions were calculated for all fiber reinforced groups at three different mould sizes (T30L275, T50L425 and T80L350). Casting direction is defined as x direction and selected specimens were cut parallel to yz plane at the midpoint of the specimen as mentioned above. Then 12 concrete slices for the selected specimen types and sizes were obtained and specimen surfaces were prepared by grinding and polishing methods to obtain shiny surfaces and cross sections were divided into small parts (3 mm x 3 mm) as is seen in Figure 3.26. Then, digital images of the small sections were obtained by using an optical microscope. It should be noted that all the fibers on the sections of long fiber reinforced specimens were analyzed one by one. However, the fibers on the selected representative sections were analyzed for the sake of time in case of short and hybrid fiber reinforced specimens since these specimens had hundreds of fibers on a small section. Representative sections were selected such that to reflect the whole fiber orientation situation on the section. Figure 3.27 shows how representative sections were selected for short and hybrid fibrous specimens. White parts show the analyzed sections of these specimens. After obtaining digital images of the pre-determined cross sections, steel fibers were analyzed one by one (Figure 3.28 (a) and (b)). Each fiber section seems as an elliptical on the image and elliptical parameters can be obtained by using a program (Image J) which is available on the web.

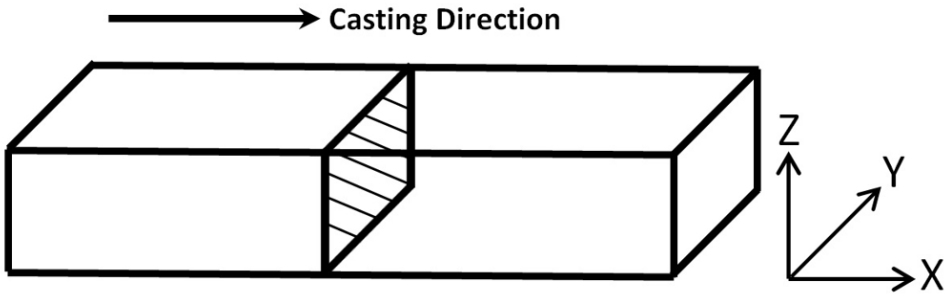

Figure 3.25. Shaded area (ZY section) examined for fiber orientation analysis.

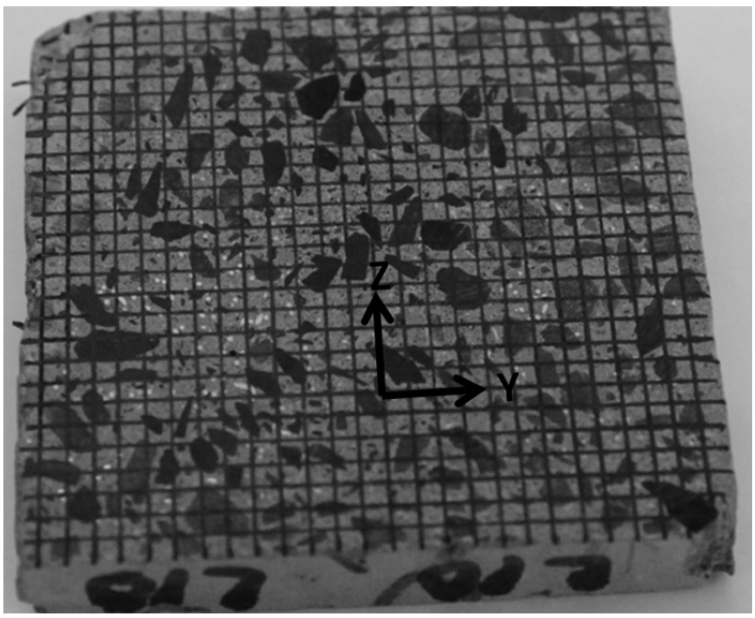

Figure 3.26. Preparation of slices for digital images.

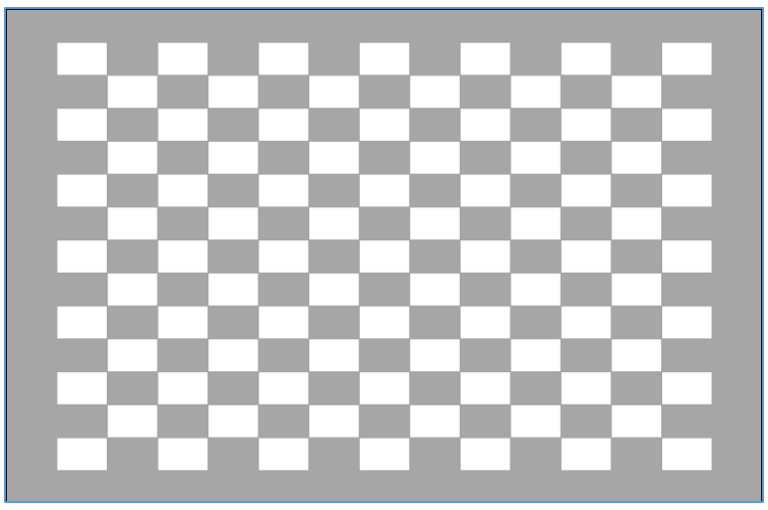

Figure 3.27. Representative section selection for short and hybrid fibrous specimens.

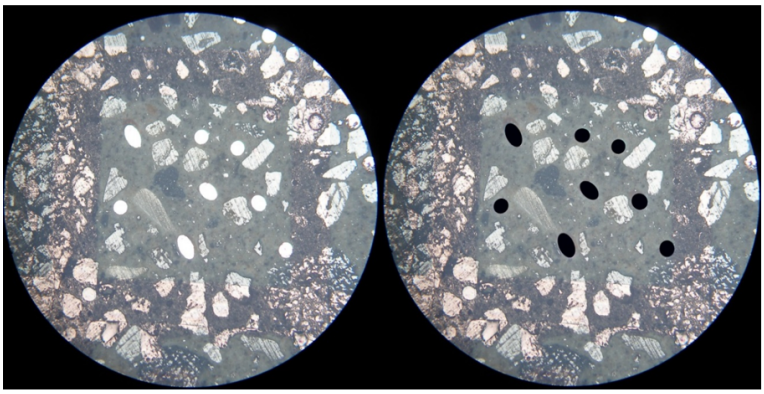

a) Original Photo b) After processed by using Photoshop

Figure 3.28. Selection of fibers using Photoshop program.

Major and minor axis lengths (a, b) and in plane angle (ϕ) of a fiber were determined using Image J program as indicated in Figure 3.29. Fiber orientation state of a single fiber can be determined using in plane (ϕ) and out of plane (Θ) angles as can be seen in Figure 3.30 and vector p shows the fiber orientation state for each fiber. Fiber orientation density for the section can be calculated by using tensor given in Equation 3.6. In the equation, pi, pj represent the fiber orientation state for each fiber and can be calculated by using Equation 3.7. F_n is the weighing function and implies the probability of a fiber being intercepted by the existent surface, and n is the number of fibers on a section. To determine fiber orientation, F_n should be calculated by using Equation 3.8.

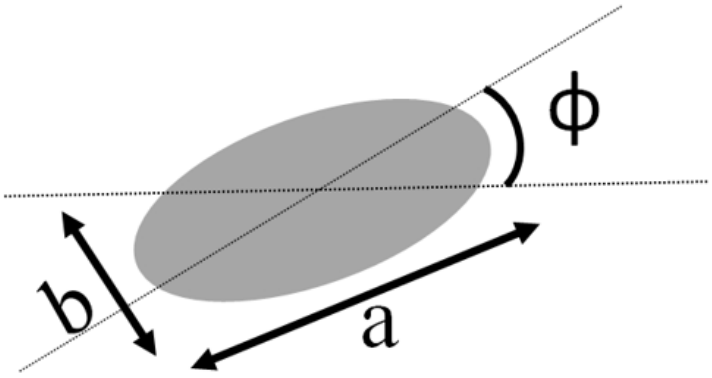

Figure 3.29. Major (a) and minor (b) axis lengths and in plane angle (ϕ) of a fiber.

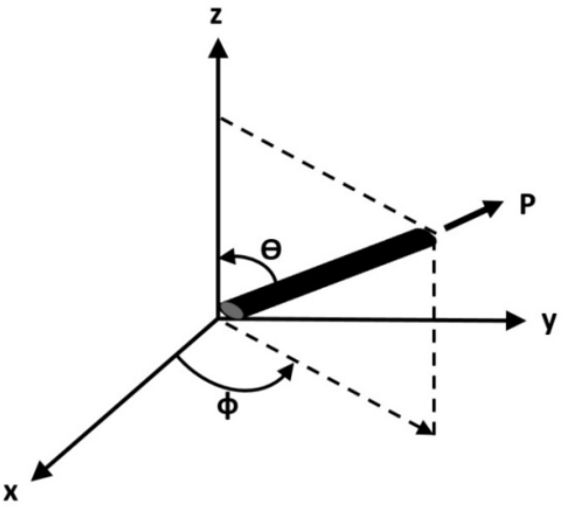

Figure 3.30. Fiber orientation state of a single fiber with in plane (ϕ) and out of plane (Θ) angles.

$$a_{ij} = \frac{\sum^{(p_i p_j)_n} F_n}{\sum^{F_n}} = \left\{ \begin{array}{ccc} a_{xx} & a_{xy} & a_{xz} \\ a_{yx} & a_{yy} & a_{yz} \\ a_{zx} & a_{zy} & a_{zz} \end{array} \right\} i, j = x, y, z \tag{3.6}$$

$$p_X = \sin\theta\cos\phi, p_y = \sin\theta\sin\phi, p_z = \cos\theta \tag{3.7}$$

$$\theta_c = arccos\frac{d}{L}, IF\theta < \theta_c \Rightarrow F_n = \frac{1}{Lcos\Theta_n}, IF\theta > \theta_c \Rightarrow F_n = \frac{L}{D} \tag{3.8}$$

In Equation 3.8, Θ is the out of plane angle, L is the fiber length, and Θ_c is the cutoff angle which is defined as the angle above which a fiber has a useful projected height of fiber diameter d[74]. a_{ij} stands for the components of the orientation tensor as mentioned above. In this study the orientation densities in the X, Y and Z directions were needed and therefore, only main diagonal components (axx, ayy, azz) were calculated.

4. RESULTS AND DISCUSSIONS

Results and discussions parts were divided into two main categories as fresh and hardened state performance. In the fresh state properties part, flowability, passing ability and rheological properties of SFR-SCCs were given. In addition to this, fiber orientation analysis, static and dynamic segregation analysis test results were also given. In the hardened state part, compressive and splitting tensile test results and four point bending test results on different specimen sizes were given. Furthermore, an inverse modeling-multi layer model was adopted and results were compared experimentally with three point bending test results on notched specimens.

4.1. Fresh State Performance

4.1.1. Fresh State Tests

Fresh state tests were conducted in order to find out flowability and passing ability of SCC mixes. The flowability properties of SCCs were measured via slump flow and V-funnel tests; passing ability was measured using J Ring, L - Box and U-Box tests. In the slump flow test, spread of concrete was measured as is seen in Figure 4.1 and t_{500} and tfinal durations were recorded and compared with TS EN 12350-8 standard [58] limits.

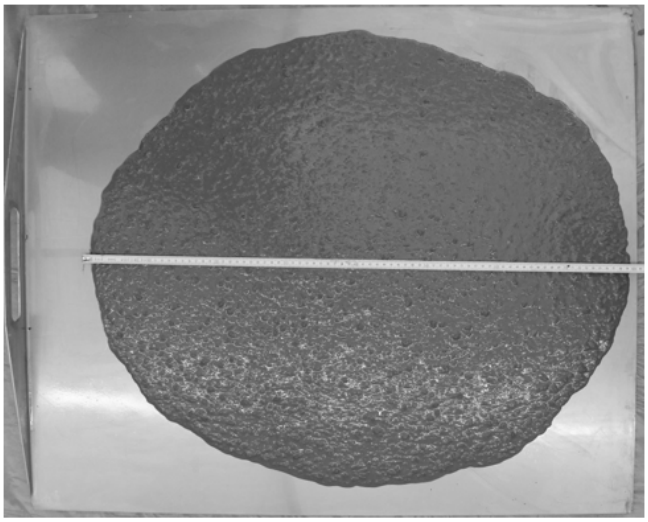

Figure 4.1. Slump flow test - flowability of SCC mixes.

In the J-ring tests, spread and passing ability of the material through the openings of the apparatus were measured as is seen in Figure 4.2 and t_{500J} and tfinalJ durations were recorded and results were compared with TS EN 12350-12 standard [61] limits.

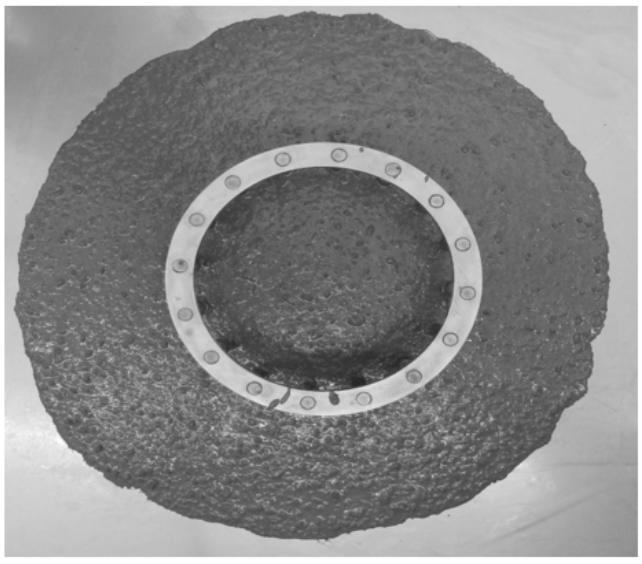

Figure 4.2. J-Ring test - passing ability of SCC mixes.

In the L-Box test, passing ability of the materials was calculated by dividing the concrete height of the lateral section to the concrete height of the vertical section (PL value) and results were compared to TS EN 12350-10 standard [60]. L-Box test set-up

and concrete heights at vertical and lateral section can be seen in Figure 4.3.

Similar to the L-Box tests, U-Box tests were also conducted according to UNI 11044 standard [62]. In the U-Box tests, concrete height difference between two vertical sections was measured as is seen in Figure 4.4.

In the V-funnel tests, discharge duration of the SCC mixes were recorded as is seen in Figure 4.5 and results were checked with TS EN 12350-9 standard [59].

Figure 4.3. L-Box test - passing ability of SCC specimens.

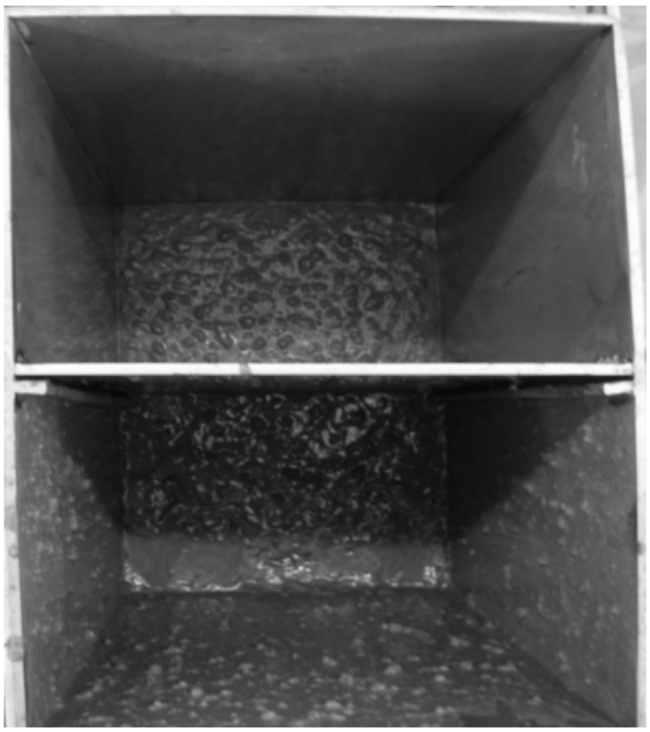

Figure 4.4. U-Box test - passing ability of SCC specimens.

Figure 4.5. V-Funnel test - flowability of SCC specimens.

Table 4.1. Flowability and passing ability test results of the SCC mixes.

Flowability & Passing Ability Tests		**Control**	**0.50% Long FRC Mix**	**1 % long FRC Mix**	**0.50% short FRC Mix**	**Hybrid FRC Mix**	**Standard Limits**
Slump Flow	t_{500} s	2	3	4	4	5	TS EN 12350-8
	t_{final}s	13	15	19	17	19	t_{500}: 0-6 s;
	flow cm	79	79	80	79	75	flow > 60 cm
J-Ring	t_{500} s	3	4	5	5	7	TS EN 12350-12
	t_{final}s	19	19	21	21	23	PJ≤2
	flow cm	73	69	68	69	60	
	PJ cm	0.1	1.8	2.1	2.0	3.4	
L-Box	PL (H2/H1)	1,00	0,96	BLOCKING	0,94	BLOCKING	TS EN 12350-10 PL≥0.8
U-Box	H1-H2	0.6	1.4	BLOCKING	1	BLOCKING	UNI 11044 H1-H2 < 3 cm
V-Funnel	tv s	5	6	BLOCKING	6,5	BLOCKING	TS EN 12350-9; tv ¡ 15 s

Flowability and passing ability test results of the SCC mixes were given in Table 4.1. According to the slump flow test results, flow diameters of SCC mixes were found to be higher than the standard minimum flow diameter of 600 mm. In addition to high flowability, t_{500} values were smaller than the limit value of 6 second for all the mixes. It was observed during the flow test, fibers dispersed better for the mixes with high flowability. Short fiber reinforced mixes required more superplasticizer to show similar flowability due to their high aspect ratios and the higher number of fibers compared to long fibers. J-Ring test results indicated that PJ value of the mixes were equal or under the limit value (2 cm) defined by the related standard except for the hybrid fiber reinforced mix. PJ value was found to be 3.4 for this mix representing low passing ability/blocking for the related mix. This represents that the hybrid mix used in this study may not be suitable for the applications which require congested reinforcement (openings of $\leq 41\pm1$ mm) as stated in the related standard.

PL value measured by using L-box test equipment should be higher than 0.8 according to the related standard. PL values for control specimens and 0.5% fiber-reinforced mixes were above the minimum required value; however, blocking was ob-

served during the tests done on 1% fiber-reinforced mixes. It should be noted that the width between the rods for the L-Box test equipment used for this study was 40 mm, and long steel fibers had a length of 35 mm; therefore accumulation of fibers around the steel rods was expected when high volumes of fibers were used.

The same result can be seen when U box test data is examined. Results of L box and U box tests represent that passing ability of the mix highly decrease when high volumes of fibers are used. Therefore 1 % fiber-reinforced mixes designed in this study may not be suitable for the applications which require congested reinforcement as blocking was observed as can be seen in Figure 4.6a.

Discharge time of the V-Funnel should be smaller than 15 seconds to have filling ability. Discharge time of the control and 0.5% fiber-reinforced mixes was below the limit value; however, blocking was observed for 1% fiber-reinforced mixes as is seen in Figure 4.6b. The related standard states that the test is not suitable for the mixes including aggregates with dimensions greater than 22.4 mm. Flowing of the material seems to be prevented when increased amount of fibers were used.

(a) U-Box (b) V-Funnel

Figure 4.6. Blocking of the (a) U- Box and (b) V-Funnel.

Following conclusions can be driven if the results of the tests given above are evaluated together. Filling and passing ability of the 1% fiber-reinforced mixes were found to be limited and care should be taken when using them for applications which require high amounts of reinforcement with narrow openings. It should be noted that

this result is valid for the materials used in this study.

4.1.2. Dynamic Segregation Analyses

After determining the fresh state properties of the SCC mixes, dynamic segregation analyses were conducted. Dynamic segregation resistance represents the ability of a mixture to drive the fibers with itself in the fresh state. If dynamic segregation resistance of a mix is high, the number of fibers in different regions of the specimen should be similar, indicating good fiber driving ability of SCC. For dynamic segregation analyses, the volume of long fibrous specimens were calculated by counting and the volume of short and hybrid FRC specimens were calculated by weighing the fibers as stated earlier. Table 4.2 represent dynamic segregation analyses results.

For high dynamic segregation resistance, fiber percentages should be around 25% (one-fourth of the total volume) in each region. The difference in the fiber volumes of 1st and 4th regions could be considered as a good measure of fiber driving ability of the mixture. When the results given in Table 4.2 is examined it can be stated that no dynamic segregation is observed (fiber volumes in different regions were found to be very similar) in the specimens except for the smallest specimen of SCC 2 mix. This was expected since the fiber length (35 mm) is longer than the smallest dimension (30 mm) of this specimen.

Table 4.2. Dynamic segregation analyses results (Fiber amounts at each region, in volume %).

SFR-SCC	REGION	Fiber amounts (in volume %)						
		30x30 x275	40x40 x200	40x40 x350	50x50 x425	60x60 x275	80x80 x350	100x100 x425
SCC2 0.5 % Long FRC Mix	1	44	24	25	25	25	24	28
	2	21	30	30	31	23	25	26
	3	18	24	24	22	28	27	24
	4	16	22	21	23	24	24	23
SCC3 1 % Long FRC Mix	1	20	21	27	27	23	22	24
	2	35	29	26	26	25	25	26
	3	28	27	24	26	25	27	25
	4	18	24	23	22	27	27	25
SCC4 0.5 % Short FRC Mix	1	25	28	27	26	26	27	30
	2	27	23	24	26	25	24	24
	3	25	24	26	26	25	26	24
	4	23	25	23	22	24	24	22
SCC5 1 % Hybrid FRC Mix	1	24	30	24	25	26	24	23
	2	28	22	24	27	24	24	26
	3	27	23	26	26	25	26	26
	4	21	25	25	22	25	25	25

4.1.3. Static Segregation Analyses

Static segregation resistance represents concrete's ability to hold fibers as well as aggregates while it is still plastic. For static segregation analyses, fiber percentages at the top, middle and bottom regions were found for all the specimens as is seen in Figure 4.3. It should be remembered that three sections were analyzed for each specimen. The average of the fiber percentages on these 3 sections were calculated and given. Results show that the volume of fibers in the top layer is lower when compared to the middle and bottom layers for almost all the specimens. However the difference is negligible for the short and hybrid fiber-reinforced specimens. On the other hand, the volume of fibers in the top layer of long fiber-reinforced specimens is significantly lower when compared to the middle and bottom layers representing higher tendency for long fibers to settle down.

Table 4.3. Static segregation analyses results (Fiber percentages at each regions (%))

SFR-SCC	REGION	Fiber percentages at each regions (%)						
		30x30 x275	40x40 x200	40x40 x350	50x50 x425	60x60 x275	80x80 x350	100x100 x425
SCC2 Mix 0.5 % Long FRC	Top	20	15	20	24	19	20	23
	Middle	39	37	34	35	38	39	37
	Bottom	41	47	45	41	44	41	40
SCC3 Mix 1 % Long FRC	Top	29	22	29	22	24	24	17
	Middle	34	40	34	39	38	39	38
	Bottom	37	38	37	39	38	36	46
SCC4 Mix 0.5 % Short FRC	Top	30	32	34	30	31	31	32
	Middle	33	35	32	33	32	32	33
	Bottom	37	33	34	37	37	37	35
SCC5 Mix 1% Hybrid FRC	Top	32	30	35	30	27	30	31
	Middle	34	35	37	33	35	33	33
	Bottom	34	35	28	37	38	37	37

4.1.4. Rheological Properties of SCC Mixes

Yield stress and plastic viscosity values were obtained using a concrete rheometer as a result of the rheology test. Yield stress represents the stress required to initiate the flow and plastic viscosity is defined as the resistance to flow. As a result of the stress growth tests, torque versus vane speed relationship of the mixes was obtained as is seen in Figure 4.7.

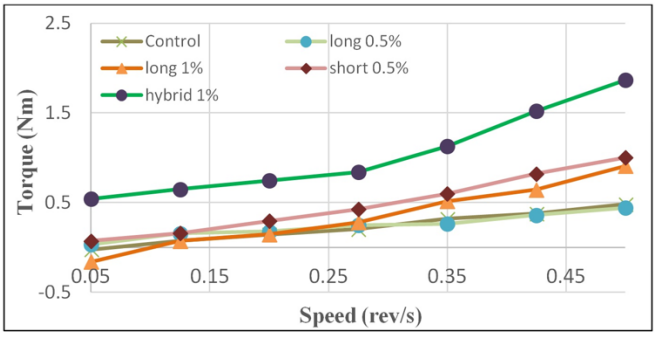

Figure 4.7. Rheological behavior of SCC mixes.

In accordance with the rheology results, the energy required to rotate the SCC mixes at various steady speeds were decreased respectively for hybrid, short, long (1%), and long (0.5%) fiber reinforced and control mixes.

Based on the concrete rheometer test geometry, Bingham parameters were calcu-

lated by using software and results were given in Table 4.4. Bingham parameters were found to be in a good range for the SCC mixes except for the hybrid mix. Hybrid mix represented relatively high yield stress and plastic viscosity value for a SCC design.

Table 4.4. Bingham parameters of the SCC mixes.

SCC CONCRETE	**Bingham Parameters**	
	Yield Stress (Pa)	**Plastic Viscosity (Pa.s)**
Control Mix	0.1	17.9
0.5 % Long FRC Mix	1.2	16.9
1 % Long FRC Mix	0.1	32
0.5 % Short FRC Mix	0.1	36.9
1 % Hybrid FRC Mix	26.4	62.9

4.1.5. Fiber Orientation Analyses

Fiber orientation densities were calculated using a tensor description method. The objective is to find fiber orientation densities in the x, y and z directions for the specimens with different types of fibers and fiber volumes as described earlier. Fiber orientation results were given in Table 4.5. Owing to superior fresh state properties of SCC material, fiber alignments in the X direction (casting direction) is higher for all specimens. The orientation density in the x direction (a_{xx}) is important because it

contributes most to the bending strength. The sum of the orientation densities (a_{zz} + a_{yy} + a_{xx}) must be equal to 1.

Table 4.5. Fiber orientation densities of SCC specimens.

#	**Specimen**	$\mathbf{a}_{zz}$	$\mathbf{a}_{yy}$	$\mathbf{a}_{xx}$
1	L580X80	0.135	0.163	0.702
2	L1080X80	0.087	0.202	0.711
3	H1080X80	0.206	0.15	0.644
4	S580X80	0.205	0.166	0.629
5	L1050X50	0.217	0.105	0.678
6	S550X50	0.169	0.174	0.657
7	H1050X50	0.095	0.28	0.625
8	L550X50	0.09	0.183	0.727
9	L530X30	0.205	0.172	0.623
10	L1030X30	0.171	0.11	0.719
11	H1030X30	0.122	0.238	0.64
12	S530X30	0.221	0.118	0.661

4.2. Hardened State Performance

4.2.1. Force - Controlled Compressive Strength Test Results

Compressive strength test results of the cube SCC specimens were determined at the ages of 1, 7 and 28 days as is given in Table 4.6 and Table 4.8. Results indicated the average of the three specimens for each mixes. Compressive strength values ranged from 19 MPa to 24.5 MPa, 44.5 MPa to 50 MPa and 57.5 MPa to 62 MPa at the ages of 1, 7 and 28 days, respectively. It can be concluded that steel fiber inclusions have little contribution on compressive strength values. Compressive strength and strength variations at different ages of SCC specimens were given in Table 4.6. Increase in compressive strength values was found when fibers were added. The extent of increase was around 2-3 % when 0.5 % short and long fibers were added, while 6-7 % increase

was observed for 1.0 % long and hybrid fiber added specimens.

Table 4.6. Compressive strength values at different ages.

SCC specimens	**Compressive Strength (MPa)**		
	1^{st} day	**7^{th} day**	**28^{th} day**
Control (Non-Fibrous)	20.72	44.47	57.75
0,5 % Long FRC	19.01	48.06	59.23
0,5 % Short FRC	20.44	47.79	58.92
1 % Long FRC	23.46	47.53	61.98
Hybrid FRC 0,5%S+0,5%L	24.53	50.05	61.18

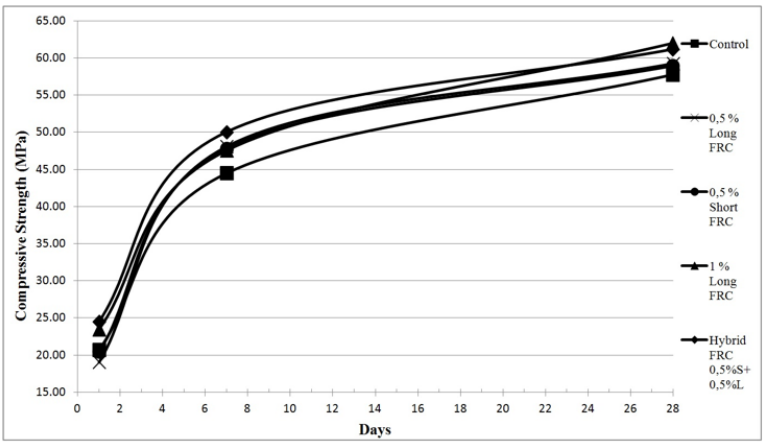

Figure 4.8. Compressive strength test results of SFR-SCC specimens at different ages.

4.2.2. Splitting Tensile Strength Results

Splitting tensile strength tests were performed on cylinder specimens with a diameter of 100 mm and length of 200 mm and results were given in Table 4.7.

Table 4.7. Splitting tensile strength results of SFR-SCC specimens at 28^{th} day

Specimens	**Splitting Tensile Strength (28 day) (MPa)**
Control (Non-fibrous)	4.14
0.5 % Long FRC	4.35
0.5 % Short FRC	4.67
1 % Long FRC	7.57
Hybrid FRC 0.5%S+0.5%L	6.39

Results showed that steel fibers have a significant influence on splitting tensile strength of concrete especially for high steel fiber fractions (≥1%). For 0.5% long and short fiber reinforced SCC specimens, splitting tensile strengths increased up to 5% and 13 %, respectively, whereas for 1% long and hybrid fiber reinforced SCC specimens, splitting tensile strength increased up to 83% and 55%, respectively.

4.2.3. Displacement Controlled Compressive Strength Results

In this study, force-controlled compressive strength test results were conducted on cube specimens to obtain cube compressive strength values required for the modelling phase of the study. In addition to this, displacement controlled compressive strength tests were performed in order to find out elastic modulus of SFR-SCC specimens and to observe post-peak behavior of fiber reinforced SCC specimens and the results were used in the inverse modeling. It can be seen from the Figure 4.10-Figure 4.15 that elastic modulus of fiber reinforced concrete increased with an increase in steel fiber

volume. Similar results were also reported in literature [77, 78].

Average elastic modulus of fiber reinforced concretes with 0.5% short and long fiber volume increased 5% and 8%, respectively when compared to plain concrete. For 1% long and hybrid fiber reinforced specimens, elastic modulus increased up to 26% and 28%, respectively, when compared to plain concrete as is seen in Table 4.8.

Table 4.8. Elastic modulus of SFR-SCC specimens.

Concrete	**Elastic Modulus (MPa)**
Control (Non-Fibrous)	28823
Long (0.5 %) FRC	31217
Short 0.5 % FRC	30323
Long (1%) FRC	36319
Hybrid (1%) FRC	36817

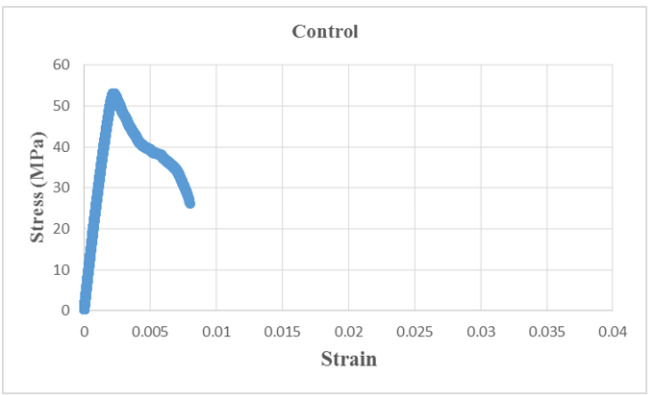

Figure 4.9. Compressive strength test results of SFR-SCC specimens at different ages.

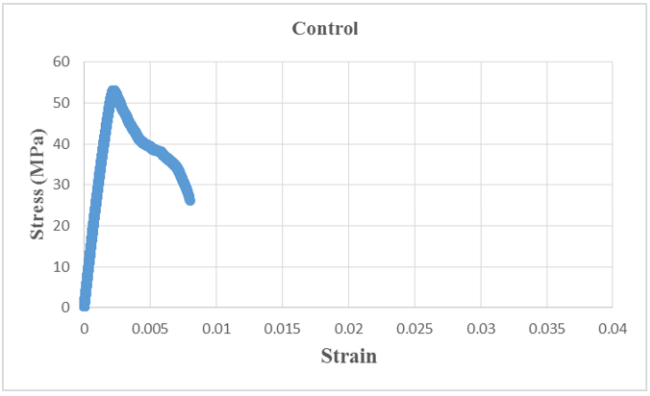

Figure 4.10. Stress-strain diagram of plain SCC under compression .

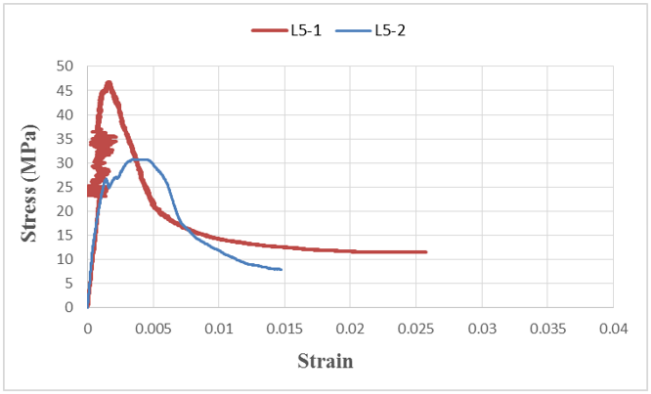

Figure 4.11. Stress-strain diagram of 0.5% long fiber reinforced SCC under compression.

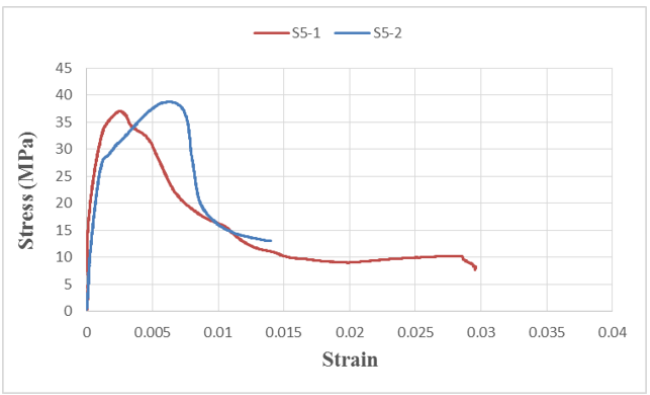

Figure 4.12. Stress-strain diagram of 0.5% short fiber reinforced SCC under compression.

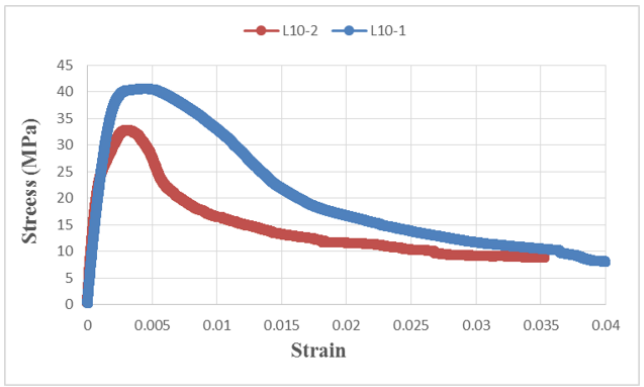

Figure 4.13. Stress-strain diagram of 1% long fiber reinforced SCC under compression.

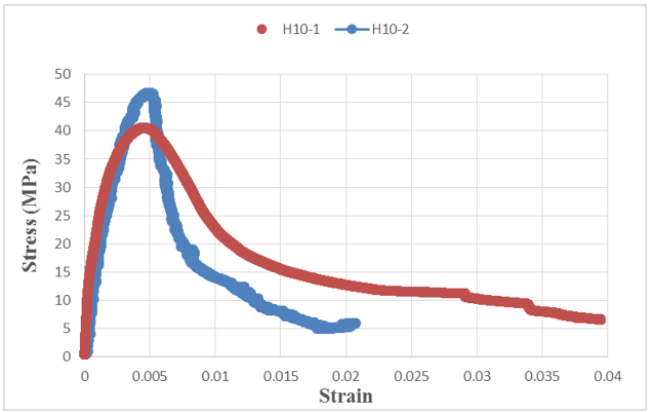

Figure 4.14. Stress-strain diagram of 1% hybrid fiber reinforced SCC under compression.

4.2.4. Four Point Bending Tests on Unnotched Specimens

Four point flexural tests were conducted in order to evaluate bending behavior of different SFR-SCC specimens. For this purpose the effects of several parameters such as specimen thickness / fiber length ratio (t/f_L), shear span-to-depth ratio (a/d), different fiber types (hooked end-short) and amounts (V_f) were investigated. Four point bending tests were performed in stroke displacement control up to the displacement value of L' (span length)/150 was reached as described in Section 3.4.4. Average force versus deflection and average force versus crack opening displacement (COD) diagrams of the SFR-SCC were obtained at the end of the tests as can be seen in Figure 4.15 to Figure 4.28. Results indicated that maximum flexural load increased with an increase in steel fiber volumes of SCC specimens. Long and hybrid fibrous specimens with a fiber volume of 1% attained the highest flexural load during the bending tests. In addition to this, deflection hardening behavior was observed for almost all specimens including 1% steel fiber reinforced specimens, while deflection softening behavior was observed when 0.5% short and long fibrous SCC specimens were tested. Maximum flexural loads also decreased with a decreasing steel fiber volume ($\leq 0.5\%$) as indicated in the Figure 4.15 - Figure 4.28. However, lower amounts of steel fiber addition into SCC improved ductility of SCC specimens significantly as compared to plain SCC specimens.

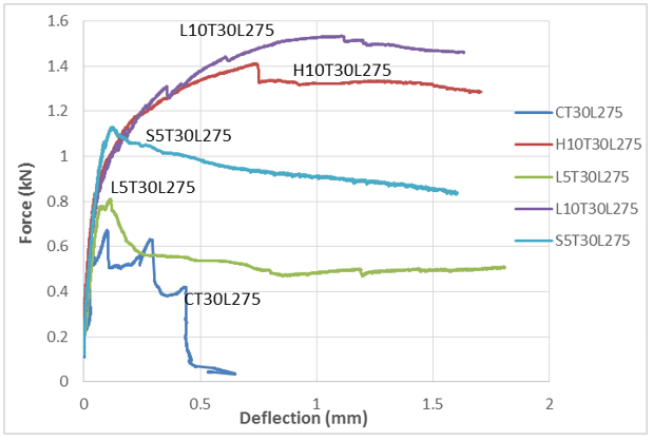

Figure 4.15. Force - deflection diagram of T30L275 specimens (a/d: 2.5).

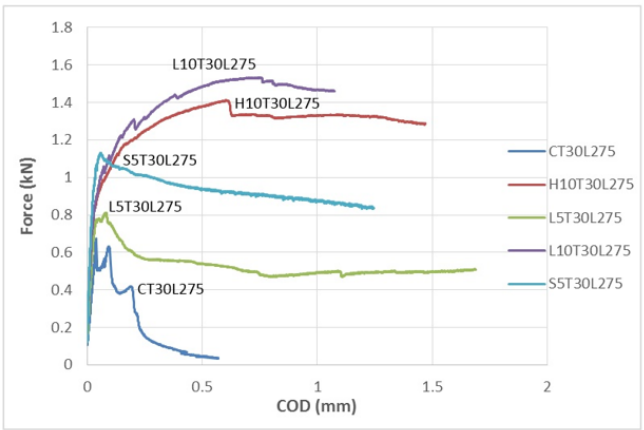

Figure 4.16. Force - COD diagram of T30L275 specimens (a/d: 2.5).

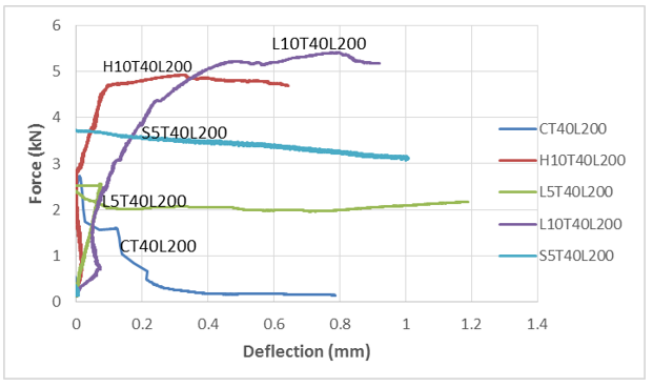

Figure 4.17. Force - deflection diagram of T40L200 specimens (a/d: 1.25).

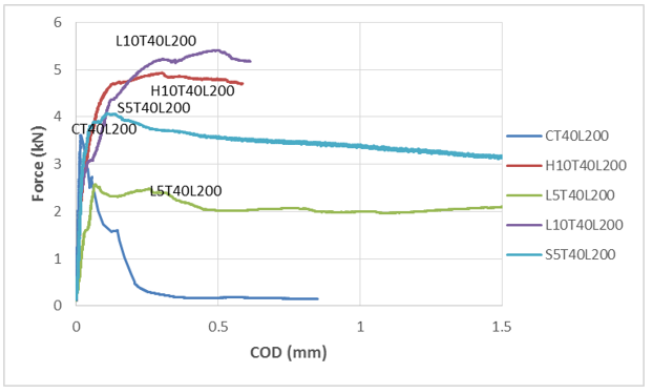

Figure 4.18. Force - COD diagram of T40L200 specimens (a/d: 1.25).

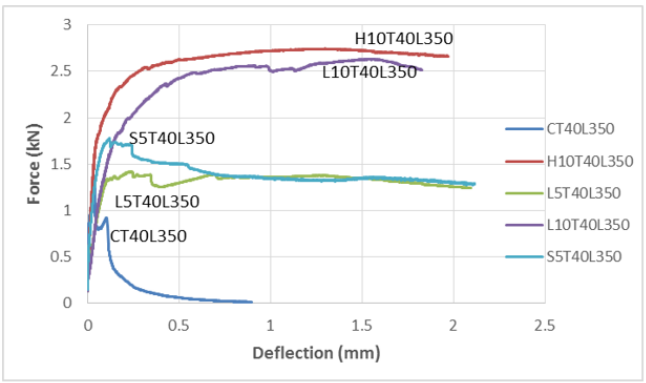

Figure 4.19. Force - deflection diagram of T40L350 specimens (a/d: 2.5).

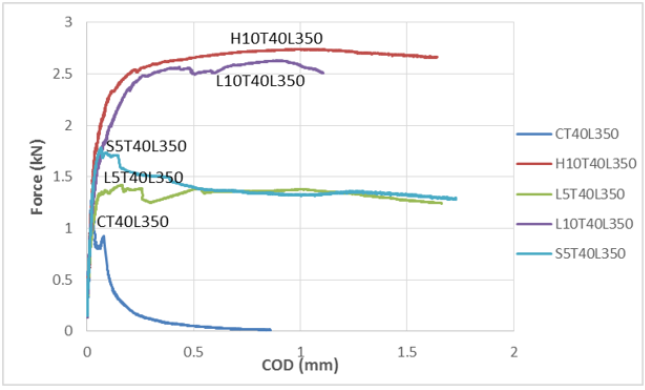

Figure 4.20. Force - COD diagram of T40L350 specimens (a/d: 2.5).

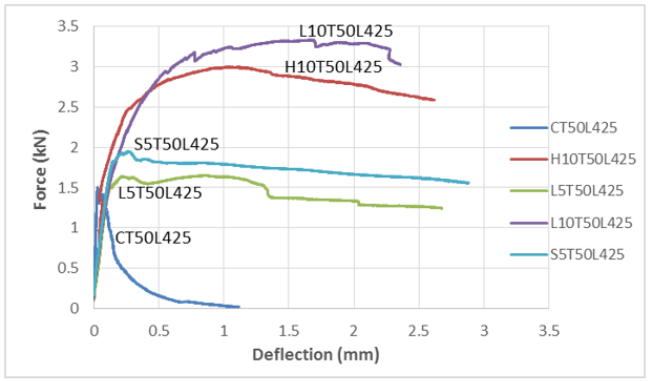

Figure 4.21. Force - deflection diagram of T50L425 specimens (a/d: 2.5).

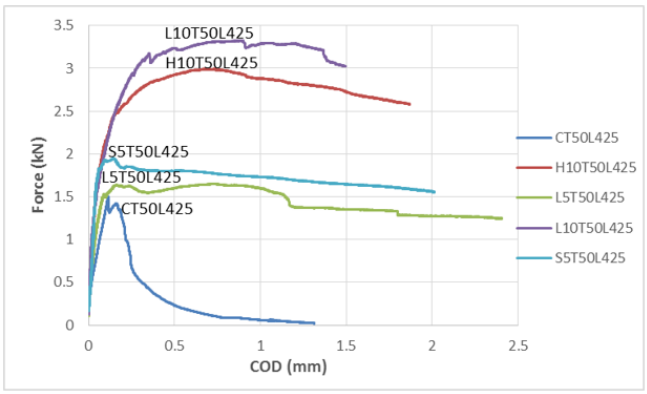

Figure 4.22. Force - COD diagram of T50L425 specimens (a/d: 2.5).

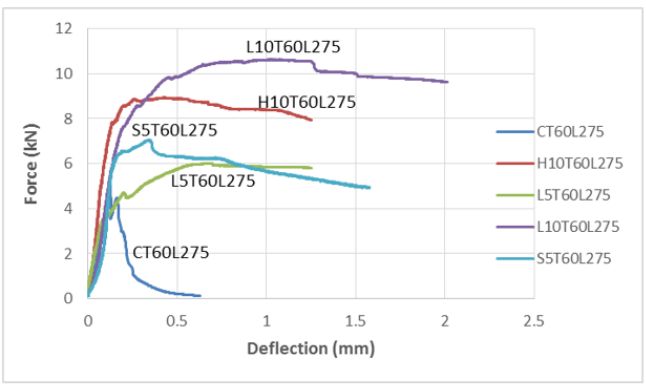

Figure 4.23. Force - deflection diagram of T60L275 specimens (a/d: 1.25).

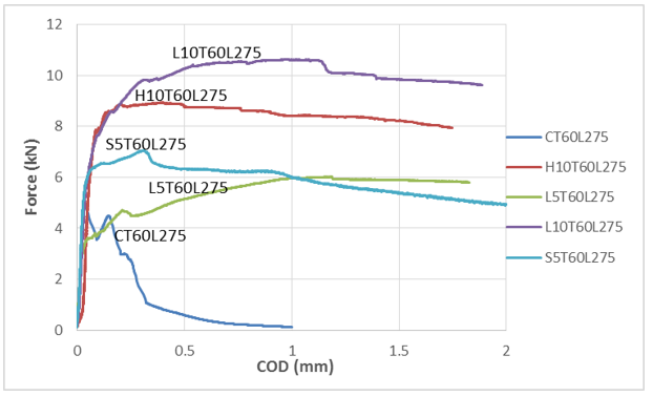

Figure 4.24. Force - COD diagram of T60L275 specimens (a/d: 1.25).

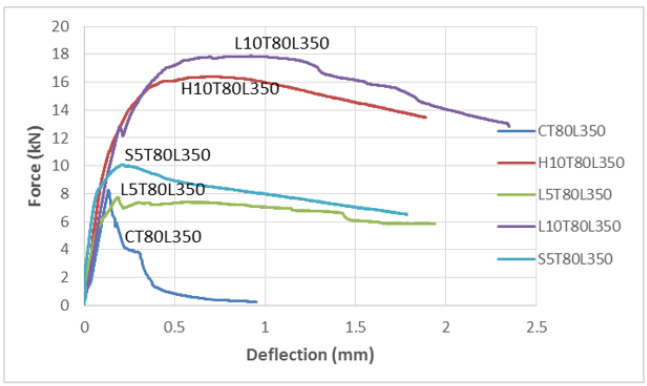

Figure 4.25. Force - deflection diagram of T80L350 specimens (a/d: 1.25).

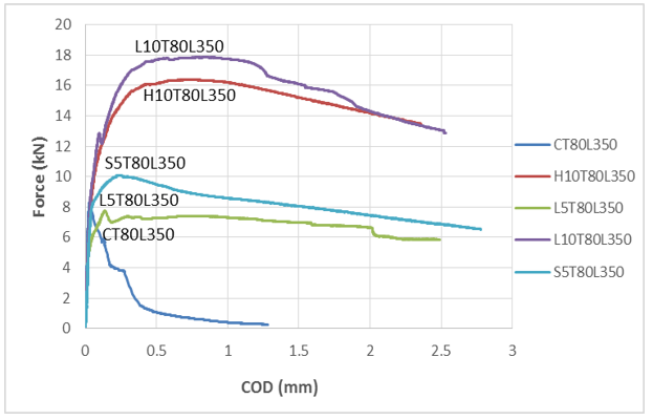

Figure 4.26. Force - COD diagram of T80L350 specimens (a/d: 1.25).

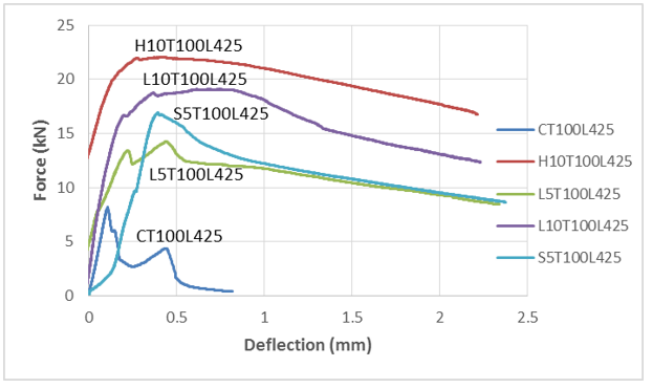

Figure 4.27. Force - deflection diagram of T100L425 specimens (a/d: 1.25).

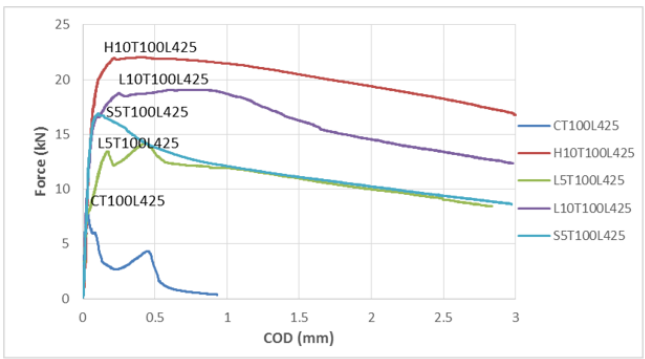

Figure 4.28. Force - COD diagram of T100L425 specimens (a/d: 1.25).

4.2.5. Effect of Varying Shear Span to Depth Ratio (A/D) on Bending Performance

Equivalent bending strength (EBS), flexural toughness factor (FTF) and lateral flexural toughness factor (FTF_{COD}) versus shear span to depth (a/d) relations were investigated considering two shear span-to-depth ratios (1.25 and 2.5). Stress, ultimate deflection and COD values at the maximum moment region were given in Table 4.9 and Table 4.10.

Table 4.9. Stress, deflection and COD values resulting from 4 point bending tests (a/d: 1.25).

Specimen	**a/d**	t/f_L	σ_{max} **(MPa)**	P_{max} **(kN)**	**Deflection (mm)**	**COD (mm)**	**COD /DEF**
CT40L200	1.25	-	9.55	4.08	1	1.19	1.32
L5T40L200	1.25	1.1	7.3	3.12	0.81	1.51	
S5T40L200	1.25	3.1	8.99	3.84	0.73	1.46	
L10T40L200	1.25	1.1	13.1	5.59	1.35	1.14	
H10T40L200	1.25	1.1	11.86	5.06	0.54	0.53	
T40L200	1.25	1.63	10.16	4.34	0.89	1.17	
CT60L275	1.25	-	6.85	6.57	0.68	1.18	1.38
L5T60L275	1.25	1.7	6.39	6.13	1.26	1.83	
S5T60L275	1.25	4.6	7.88	7.57	1.72	2.16	
L10T60L275	1.25	1.7	11.2	10.76	1.48	1.89	
H10T60L275	1.25	1.7	9.58	9.2	1.26	1.76	
T60L275	1.25	2.44	8.38	8.05	1.28	1.76	
CT80L350	1.25	-	5.3	9.04	1.23	1.72	1.3
L5T80L350	1.25	2.3	4.97	8.49	1.87	2.44	
S5T80L350	1.25	6.2	6.28	10.72	1.79	2.78	
L10T80L350	1.25	2.3	10.05	17.16	2.66	2.78	
H10T80L350	1.25	2.3	10.05	17.16	1.98	2.63	
T80L350	1.25	3.25	7.33	12.51	1.91	2.47	
CT100L425	1.25	-	4.43	11.81	1.12	1.31	1.25
L5T100L425	1.25	2.9	5.89	15.71	2.34	2.84	
S5T100L425	1.25	7.7	6.68	17.81	2.38	2.98	
L10T100L425	1.25	2.9	7.27	19.39	2.24	2.99	
H10T100L425	1.25	2.9	8.67	23.12	2.22	2.74	
T100L425	1.25	4.07	6.59	17.57	2.06	2.57	

Table 4.10. Stress, deflection and COD values resulting from 4 point bending tests (a/d: 2.5).

Specimen	**a/d**	**t/f$_L$**	σ_{max} **(MPa)**	P$_{max}$ **(kN)**	**Deflection (mm)**	**COD (mm)**	**COD /DEF**
CT30L275	2.5	-	8.58	1.03	0.57	0.55	0.93
L5T30L275	2.5	0.9	7.25	0.87	1.75	1.69	
S5T30L275	2.5	2.3	10.33	1.24	1.6	1.67	
L10T30L275	2.5	0.9	12.97	1.56	1.64	1.08	
H10T30L275	2.5	0.9	11.89	1.43	1.4	1.46	
T30L275	2.5	1.22	10.61	1.27	1.6	1.47	
CT40L350	2.5	-	7.38	1.58	1.12	1.08	0.88
L5T40L350	2.5	1.1	7.22	1.54	2.21	2.02	
S5T40L350	2.5	3.1	9.05	1.93	2.12	1.73	
L10T40L350	2.5	1.1	14.79	3.16	1.76	1.64	
H10T40L350	2.5	1.1	12.98	2.77	1.98	1.65	
T40L350	2.5	1.63	10.28	2.19	1.84	1.62	
CT50L425	2.5	-	5.38	1.79	0.88	1.03	0.81
L5T50L425	2.5	1.4	5.19	1.73	2.68	2.57	
S5T50L425	2.5	3.8	5.69	1.9	2.94	2.26	
L10T50L425	2.5	1.4	10.5	3.5	2.45	1.59	
H10T50L425	2.5	1.4	9.07	3.02	2.62	1.87	
T50L425	2.5	2.03	7.61	2.39	2.31	1.86	

4.2.5.1. Effects of varying shear span to depth ratio on EBS. When EBS (maximum flexural strength) values were compared, specimens with high a/d ratio (2.5) were found to yield slightly higher EBS results than specimens with low a/d ratio (1.25) as can be seen in Figure 4.29. The average EBS values were calculated as 9.74 MPa and 8.51 MPa for the specimens with a/d ratios of 2.5 and 1.25 without considering different steel fiber volume effect. It was observed that steel fiber volume also influenced the EBS results. EBS versus a/d relations for 0.5 and 1% FRC specimens were indicated

in Figure 4.30 and Figure 4.31. Average EBS values of the 0.5% FRC specimens were found as 7.45 MPa (for a/d: 2.5) and 6.80 MPa (for a/d: 1.25), and average EBS values of 1% FRC specimens were found to be 12.03 MPa (for a/d: 2.5) and 10.22 MPa (for a/d: 1.25). Results showed that EBS values were observed to yield higher results with an increase in a/d ratios of the specimens. This result can be attributed to decreasing tendency of specimens to fail under bending with a decrease in a/d ratio. It should be noted that all the specimens given below are observed to fail under bending.

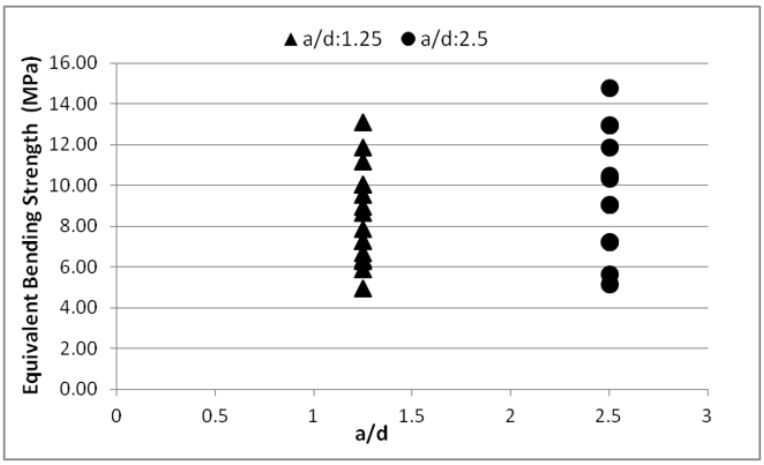

Figure 4.29. EBS versus a/d relation for all FRC specimens.

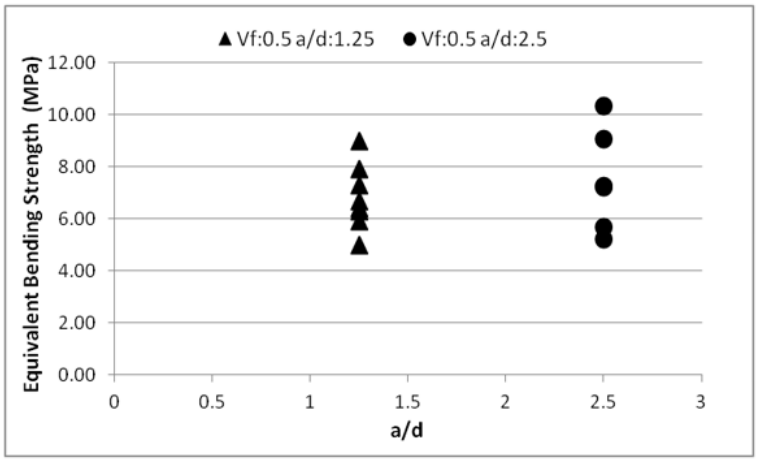

Figure 4.30. EBS versus a/d relation for 0.5% FRC specimens.

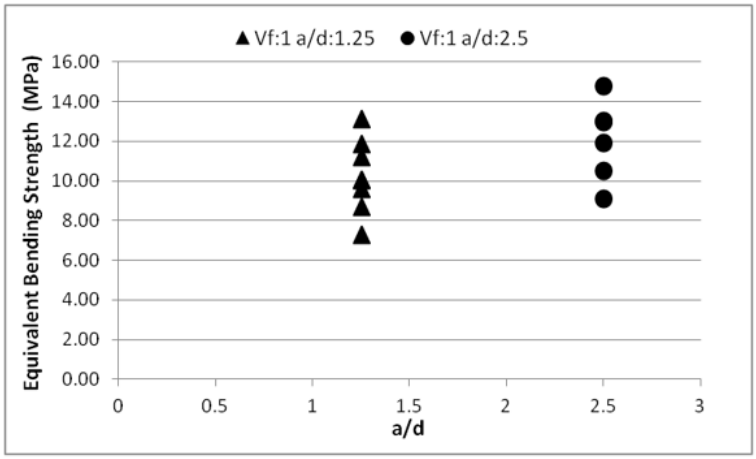

Figure 4.31. EBS versus a/d relation for 1% FRC specimens.

4.2.5.2. Effect of varying shear span to depth ratio on FTF. Toughness is defined as the area under the load-deflection curve. Flexural toughness factor is a dimensionless value of the toughness. In JSCE standard, flexural toughness factor values were calculated by using the area under the load-deflection curve up to a deflection level of L'/150.

FTF versus a/d relations on SFR-SCC specimens were investigated in Figure 4.32 to Figure 4.34. The average FTF values were found as 8.56 MPa and 6.57 MPa for the specimens with a/d ratios of 2.5 and 1.25 without considering the effect of different steel fiber volume, respectively. When steel fiber volume effect was taken into account, average FTF values of the 0.5% FRC specimens were found as 6.37 MPa (for a/d:2.5) and 4.67 MPa (for a/d:1.25) and average FTF values of 1% FRC specimens were found to be 10.75 MPa (for a/d:2.5) and 8.47 MPa (for a/d:1.25). Similar with EBS versus a/d relationships, FTF values were also found to increase with an increase in a/d ratio. As stated above, this result is also attributed to decreasing tendency of having bending failure with a decreasing a/d ratio. Crack evaluations which will be given in Section 4.2.7 also support this finding.

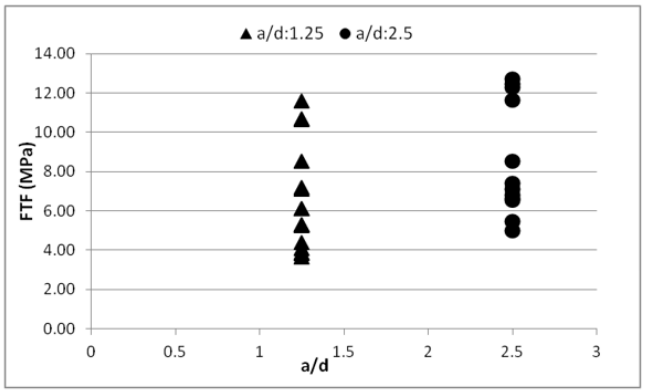

Figure 4.32. FTF versus a/d relation for all FRC specimens.

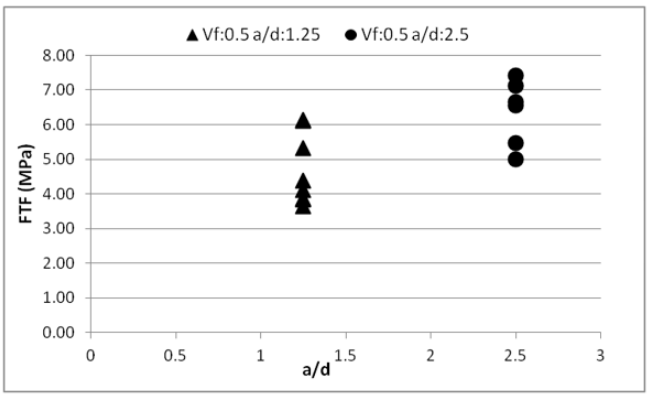

Figure 4.33. FTF versus a/d relation for 0.5% FRC specimens.

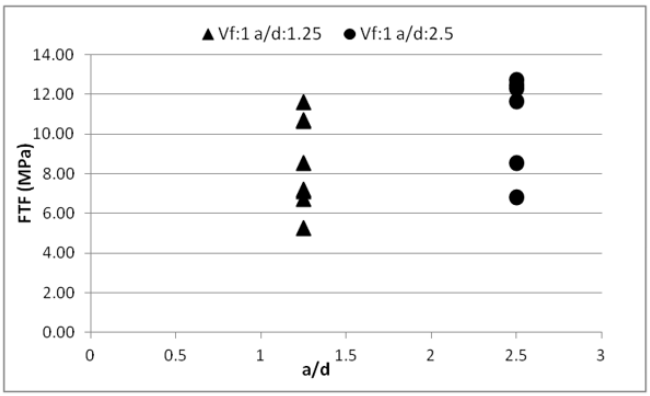

Figure 4.34. FTF versus a/d relation for 1% FRC specimens.

4.2.5.3. Effect of varying shear span to depth ratio on FTF_{COD}. Gopalaratnam *et al.*, (1995) stated that area under the load - CMOD curve was more sensitive to crack propagation than the area under the load - deflection curve, and efficiency of steel fibers

was better represented by load - CMOD curve [79]. In this study, area under the load - COD curve for SFR-SCC was also investigated in order to observe fiber efficiency.

FTF_{COD} versus a/d relations were also given in Figure 4.35 to Figure 4.37. Different from the EBS - a/d and FTF - a/d relationships, which showed higher FTF or EBS results with an increasing a/d ratios, FTF_{COD} values were found to decrease with an increase in a/d ratio. The average FTF_{COD} values were found as 6.70 MPa and 8.60 MPa for the specimens with a/d ratios of 2.5 and 1.25 without considering the effect of steel fiber volumes, respectively. Average FTF_{COD} values of the 0.5% FRC specimens were found as 5.18 MPa (for a/d: 2.5) and 6.85 MPa (for a/d: 1.25), and average FTF_{COD} values of 1% FRC specimens were found to be 8.22 MPa (for a/d: 2.5) and 10.34 MPa (for a/d: 1.25).

It can be concluded that specimens showed higher deflection values when a/d ratio was high (2.5), while specimens exhibited more COD when a/d ratio was low (1.25). It may also be concluded that when a/d ratio is low, failure mechanism of the specimens changes from bending to shear - bending behavior. The total number of cracks decreases with an increase in crack opening.

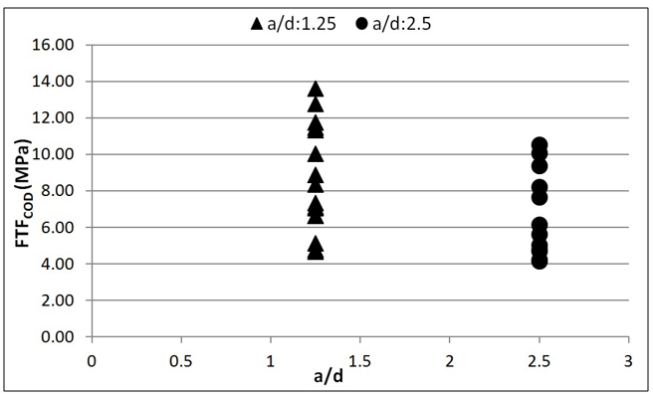

Figure 4.35. FTF_{COD} versus a/d relation for all FRC.

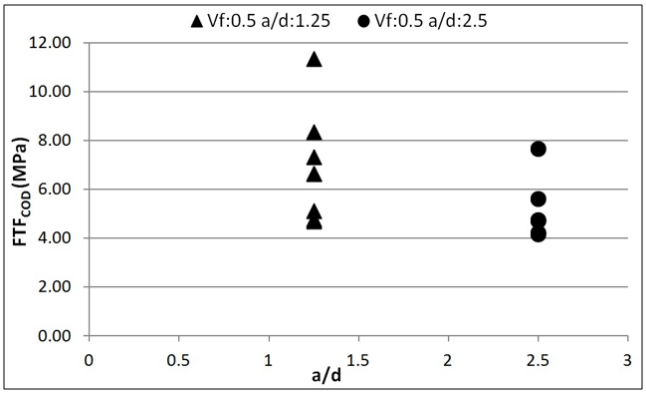

Figure 4.36. FTF$_{COD}$ versus a/d relation for 0.5% FRC.

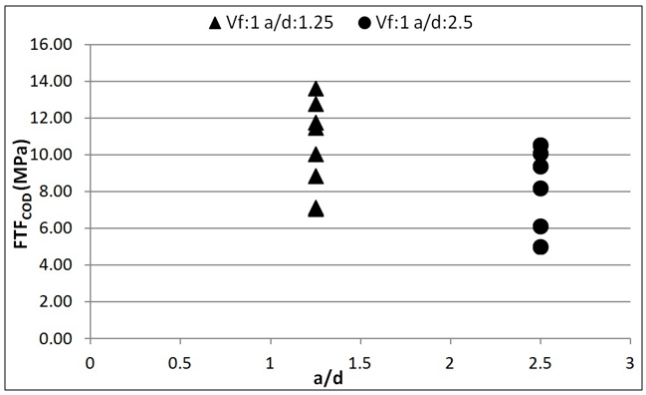

Figure 4.37. FTF$_{COD}$ versus a/d relation for 1% FRC.

4.2.5.4. COD - deflection relationship. In Table 4.9 and Table 4.10, ultimate deflection and COD values at the maximum moment region were given. Results showed that when a/d ratio was low (1.25), ultimate COD values were 31 % higher than the ultimate deflections, when a/d was high (2.5), COD values were 13% smaller than the ultimate deflections (Figure 4.38).

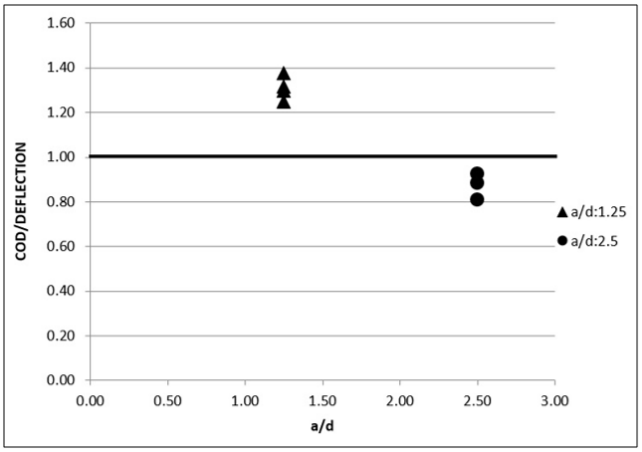

Figure 4.38. COD / Deflection versus a/d relationship on the SFR-SCC specimens.

Shear span to depth ratio effect was also observed on COD - deflection relationship. When the curve plotted neglecting the a/d effect, the relationship was found to be poor (R^2: 0.57); however, when a/d ratio was taken into account, better relationships were observed for specimens with a/d ratios of 1.25 (R^2: 0.86) and 2.5 (R^2: 0.8) as indicated in Figure 4.39 to Figure 4.41.

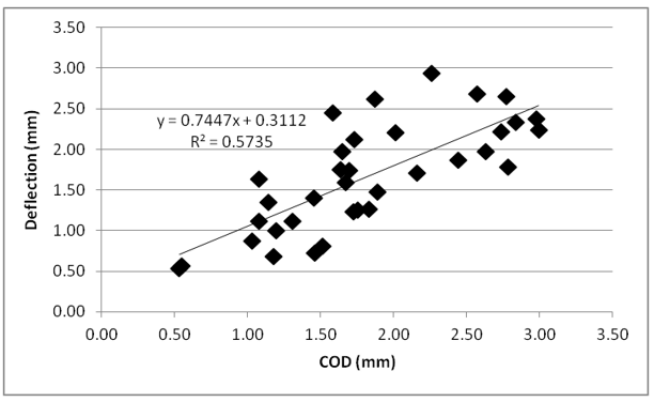

Figure 4.39. Deflection - COD relationship on SFR-SCC specimens without a/d ratio.

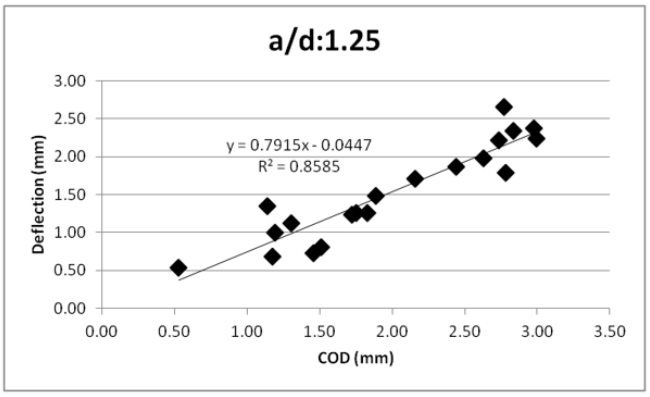

Figure 4.40. Deflection - COD relationship on SFR-SCC specimens with a/d ratio of 1.25.

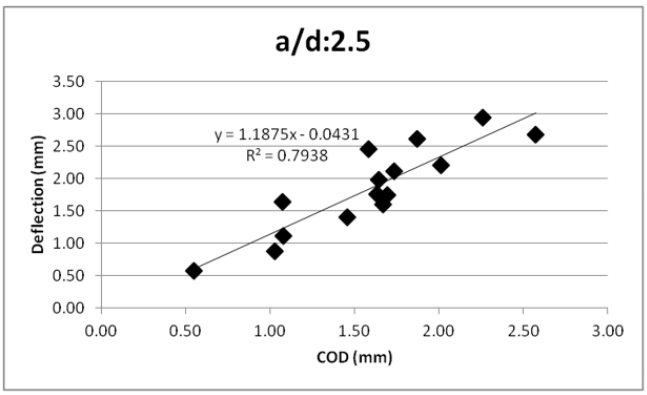

Figure 4.41. Deflection - COD relationship on SFR-SCC specimens with a/d ratio of 2.5.

4.2.6. Specimen Thickness to Fiber Length (t/f_L) effect on Equivalent Bending Strength and Flexural Toughness Factor

Previous studies show that, t/f_L ratio affects flexural behavior of fiber reinforced cement based composite materials [80]. This parameter may be considered as a representation for crack arresting/reinforcing ability of fibers. Reinforcing efficiency of fibers was reported to increase with a decreasing t/f_L ratio. In the scope of the current study, this parameter was further studied when a/d ratio was constant and results were given below.

4.2.6.1. Effects of varying specimen thickness to fiber length ratio on EBS. EBS versus t/f_L relationship was studied on SFR-SCC specimens as can be seen in Figure 4.42 - Figure 4.44. It was observed that EBS decreased with an increase in t/f_L ratio.

Steel fiber amount also influenced the EBS results. EBS values were found to increase with an increase in steel fiber volume as can be seen in Figure 4.43. EBS versus t/f_L relationship for 1% and 0.5% fiber reinforced SCC specimens were given separately in Figure 4.43 and Figure 4.44, respectively. EBS values were ranged from 7 to 15 MPa for 1% FRC specimens and 5 to 10 MPa for 0.5% FRC specimens The decline in the EBS values with an increasing t/f_L ratios was clearly observed for 1% FRC specimens (R^2: 0.66); however, a similar behavior was not observed for 0.5% FRC specimens (R^2: 0.0001). This result is hypothesized to occur due to decreased efficiency of fibers for low volumes of fibers.

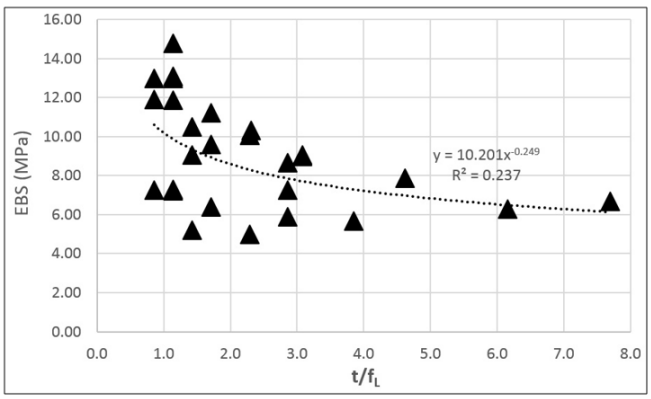

Figure 4.42. EBS versus t/f_L relationship for SFR-SCC specimens.

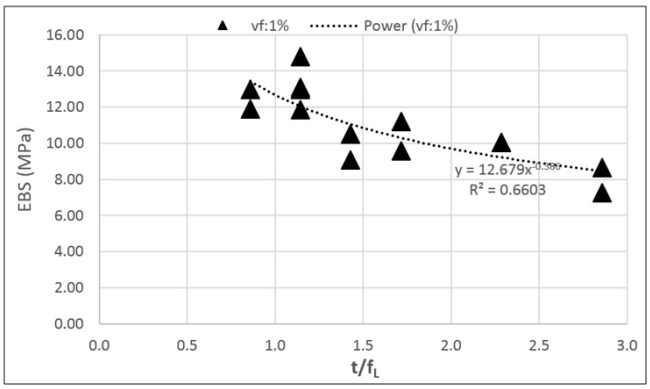

Figure 4.43. EBS versus t/f_L relationship for 1% SFR-SCC specimens.

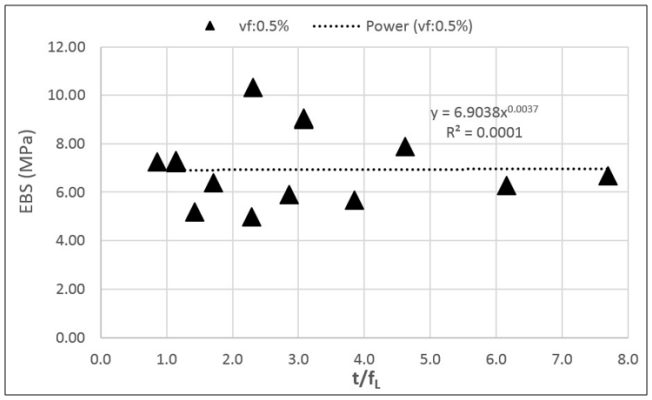

Figure 4.44. EBS versus t/f_L relationship for 0.5% SFR-SCC specimens.

4.2.6.2. Effects of varying specimen thickness to fiber length ratio on FTF. In addition to EBS, t/f_L ratio has a great influence on FTF results as indicated in Figure 4.45 to Figure 4.47. Results showed that FTF values also decreased with an increase in t/f_L ratio as can be seen in Figure 4.45.

FTF values were found to increase with an increase in steel fiber volumes. FTF versus t/f_L relationship for 1% and 0.5% FRC specimens were given in Figure 4.46 and Figure 4.47, respectively. Results indicated that FTF values were ranged from 5 to 12 MPa and 4 to 7 MPa, for 1% and 0.5% FRC specimens, respectively. The decline in FTF values with an increasing t/f_L ratios was observed more for 1% FRC specimens (R^2: 0.43) than 0.5% FRC specimens (R^2: 0.15). It can be concluded that with higher percentage steel fiber amounts, specimens showed better performance when compared to specimens having low amounts of steel fiber as expected.

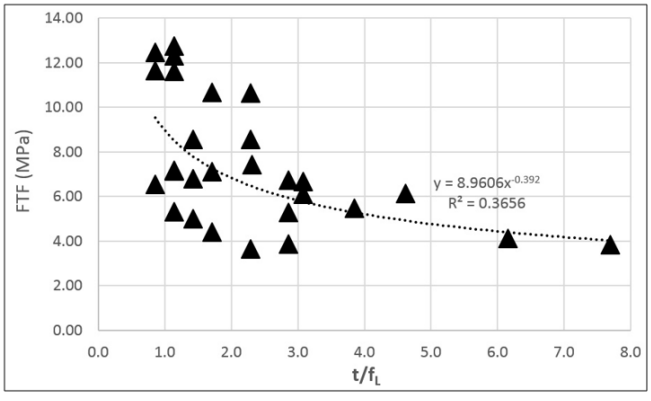

Figure 4.45. FTF versus t/f_L relationship for SFR-SCC specimens.

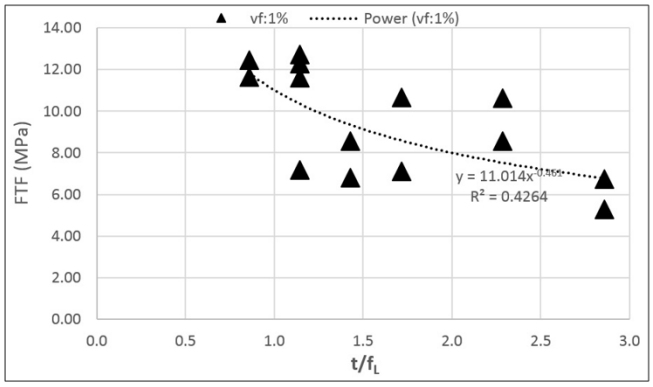

Figure 4.46. FTF versus t/f_L relationship for 1 % SFR-SCC specimens.

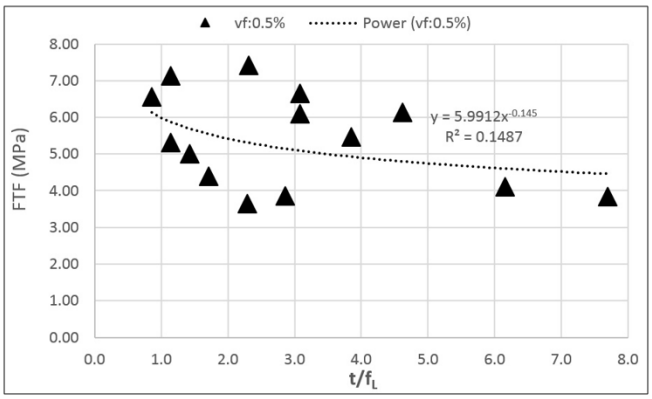

Figure 4.47. FTF versus t/f_L relationship for 0.5 % SFR-SCC specimens.

4.2.6.3. Combined effects of a/d and t/f_L ratios on bending performance. Combined effects of a/d and t/f_L ratios on EBS values of the specimens were also examined and given in Figure 4.48 and Figure 4.49. It was observed that steel fiber volume affected the results significantly. When steel fiber volume was kept constant as 1%, specimens with high a/d ratios (2.5) yielded higher EBS results than specimens having low a/d ratios (1.5). EBS values were found to decrease with an increase in t/f_L and decrease in a/d ratio.

When the results of specimens reinforced with a fiber volume of 0.5 % were examined (Figure 4.49), effect of t/f_L is seen, however; the effect of a/d is not clear.

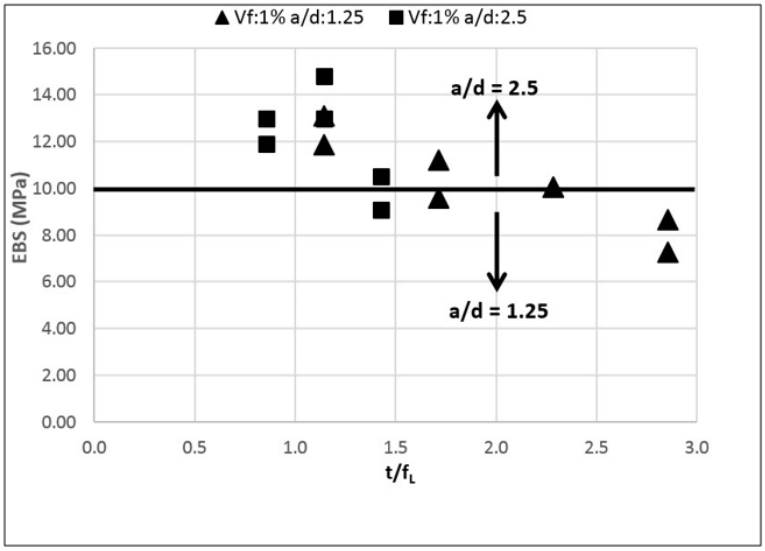

Figure 4.48. EBS versus a/d-t/f_L relationship for 1% SFR-SCC specimens.

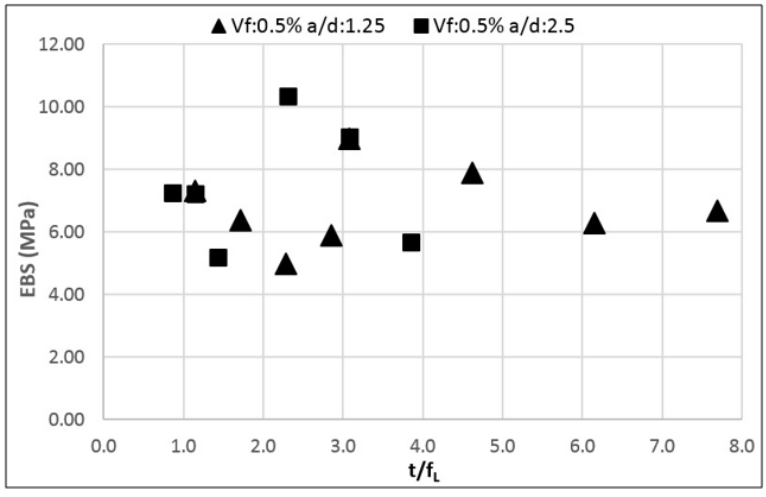

Figure 4.49. EBS versus a/d-t/f_L relationship for 0.5% SFR-SCC specimens.

FTF versus a/d-t/f_L combined relationship for SFR-SCC specimens were examined and given in Figure 4.50 to Figure 4.51. Results showed that steel fibers also have a great influence on FTF results. Specimens with high a/d ratios showed better performance than specimens with low a/d ratios for both 1% and 0.5% fiber volumes. The effect of t/f_L is seen for both fiber volumes and a/d ratios. It can be concluded that low amount of steel fibers also improve toughness.

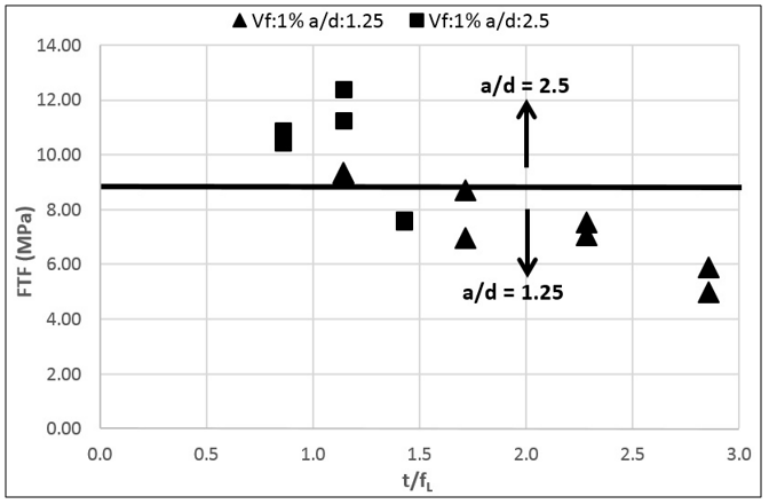

Figure 4.50. FTF versus a/d-t/f_L relationship for 1% SFR-SCC specimens.

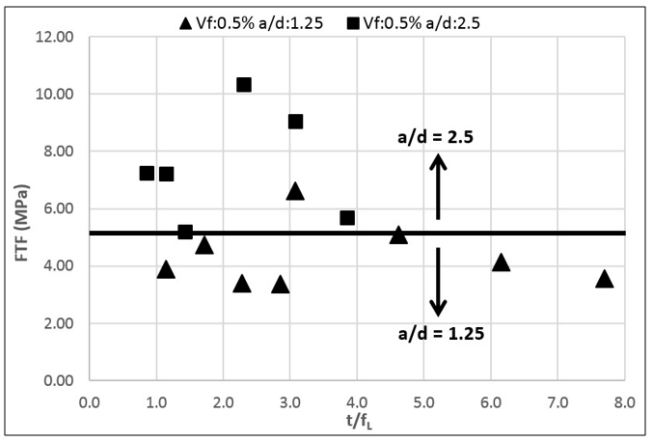

Figure 4.51. FTF versus a/d-t/f_L relationship for 0.5% SFR-SCC specimens.

Table 4.11. EBS, FTF, FTF_{COD} values of SFR-SCC specimens considering a/d effect.

Specimen	t/f_L	a/d	EBS (MPa)	Avg.EBS (MPa)	FTF_{COD} (MPa)	Avg. FTF_{COD} (MPa)	FTF (MPa)	Avg. FTF (MPa)	FTF_{COD}/ FTF
CT40L200	-	1.25	9.55	6.53	1.52	0.88	1.49	0.78	1.12
CT60L275	-		6.85		0.92		0.68		
CT80L350	-		5.3		0.71		0.6		
CT100L425	-		4.43		0.36		0.36		
CT30L275	-	2.5	8.58	7.11	0.7	0.49	1.02	0.65	0.75
CT40L350	-		7.38		0.38		0.42		
CT50L425	-		5.38		0.39		0.51		
L5T40L200	1.1	1.25	7.3	6.14	7.32	5.53	5.31	4.3	1.28
L5T60L275	1.7		6.39		6.63		4.39		
L5T80L350	2.3		4.97		4.78		3.65		
L5T100L425	2.9		5.89		3.38		3.86		
L5T30L275	0.9	2.5	7.25	6.55	4.74	4.53	6.55	6.23	0.73
L5T40L350	1.1		7.22		4.71		7.13		
L5T50L425	1.4		5.19		4.15		5.01		
S5T40L200	3.1	1.25	8.99	7.46	11.33	7.85	9.14	5.81	1.35
S5T60L275	4.6		7.88		8.33		6.14		
S5T80L350	6.2		6.28		6.63		4.11		
S5T100L425	7.7		6.68		5.11		3.83		
S5T30L275	2.3	2.5	10.33	8.36	7.64	5.82	7.41	6.51	0.89
S5T40L350	3.1		9.05		5.61		6.65		
S5T50L425	3.8		5.69		4.21		5.46		
L10T40L200	1.1	1.25	13.1	10.41	13.61	11.25	13.89	10.12	1.11
L10T60L275	1.7		11.2		12.78		10.68		
L10T80L350	2.3		10.05		11.48		10.64		
L10T100L425	2.9		7.27		7.13		5.27		
L10T30L275	0.9	2.5	12.97	12.75	8.2	7.53	12.47	10.67	0.71
L10T40L350	1.1		14.79		9.38		12.73		
L10T50L425	1.4		10.5		5.01		6.79		
H10T40L200	1.1	1.25	11.86	10.04	5.88	9.14	5.78	7.04	1.3
H10T60L275	1.7		9.58		10.03		7.11		
H10T80L350	2.3		10.05		11.76		8.56		
H10T100L425	2.9		8.67		8.87		6.72		
H10T30L275	0.9	2.5	11.89	11.31	10.52	8.91	11.64	10.83	0.82
H10T40L350	1.1		12.98		10.07		12.3		
H10T50L425	1.4		9.07		6.13		8.56		

Equivalent bending strength, flexural and lateral flexural toughness values for specimens with different steel fiber type and amounts were given in Table 4.11 for summarizing the results. Average results showed that EBS and FTF values of the specimens slightly increased with an increase in a/d ratio from 1.25 to 2.5. This result was attributed to the changing failure behavior of the specimens. When the number and type of cracks examined in detail, it was seen that failure pattern was changed from shear-flexure type to flexure type of failure. This phenomenon was given in detail in Section 4.2.7. FTF_{COD} values of the specimens with low a/d ratios (1.25) were found to be higher representing higher crack opening values. When the specimens were examined in detail, it was seen that the specimens with low a/d ratios showed

lower number of cracks with higher crack openings, while the specimens with higher a/d ratios showed more cracks with lower crack opening values. This result is also discussed further in the Section 4.2.7.

Steel fiber length and volume were found to be the most effective parameters as expected. With an increase in steel fiber volume and length EBS, FTF and FTF_{COD} values increased.

4.2.6.4. Comparison with A Previous Study. Sanal performed four point bending tests in order to observe t/f_L effect on high strength (100 MPa) fiber reinforced composite specimens. She selected four t/f_L ratios (1.92, 3.84, 4.17 and 8.33) and two different fiber length (6, 13 mm) and reported that FTF values decreased with an increase in t/f_L ratio [28]. In another study, Sanal used different t/f_L ratios ranging from 2 to 8 and four different steel fiber length (6, 13, 35, 50 mm) in order to observe t/f_L effect further. She found out that FTF values decreased further when higher values of t/f_L ratios (especially higher than 4) were under consideration [81]. The results of the current study were evaluated together with Sanal's study to better understand the effects of changing material properties on the results and given in Figure 4.52 to Figure 4.55.

As is seen from the figures, similar tendencies were observed with an increasing t/f_L and a/d ratios. FTF and EBS values were found to increase with an increase in concrete strength as expected.

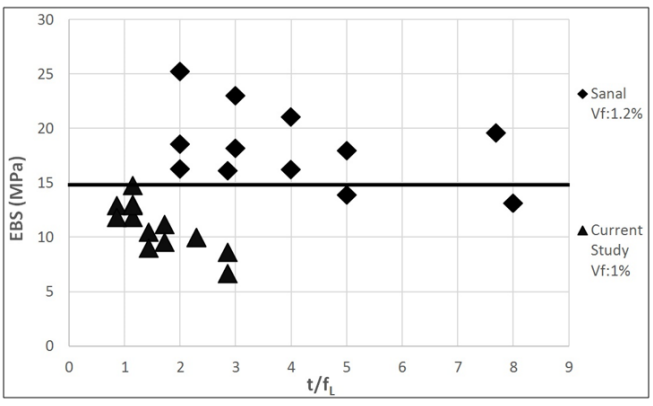

Figure 4.52. EBS versus t/f_L relationship for normal (50 MPa) and high strength (100 MPa) concrete.

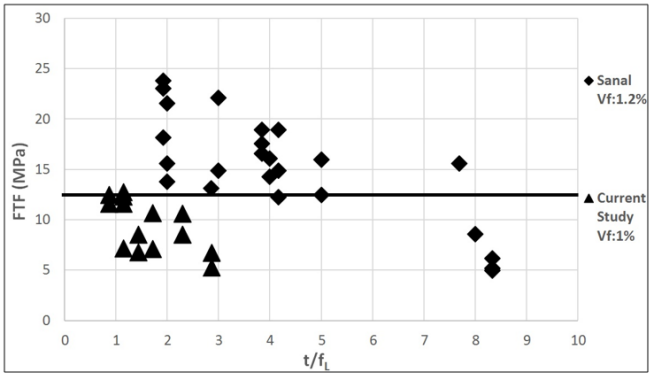

Figure 4.53. FTF versus t/f_L relationship for normal (50 MPa) and high strength (100 MPa) concrete.

Sanal reported a threshold value for t/f_L and mentioned that the effect of t/f_L becomes severe with values higher than 5. When Figure 4.52 is examined it is seen that toughness values severely decrease even for high concrete strengths for increased values of t/f_L representing highly decreased efficiency of fibers for reinforcing the section.

EBS vs. a/d and FTF vs. a/d relationships were given in the following figures for comparison of the effect of changing material properties on the tendencies. Both EBS and FTF increase with an increase in a/d ratio for normal strength and high strength concretes representing importance of a/d ratio on the failure patterns.

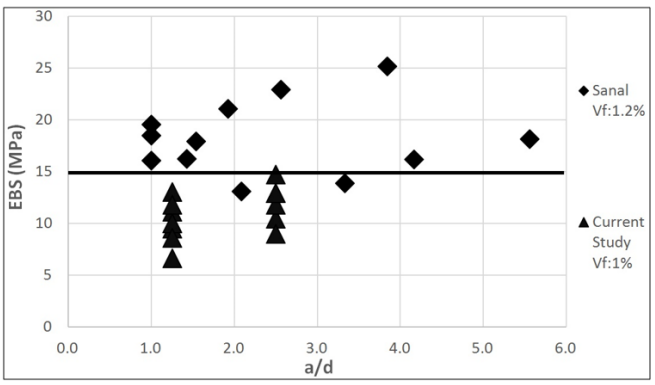

Figure 4.54. EBS versus a/d relationship for normal (50 MPa) and high strength (100 MPa) concrete.

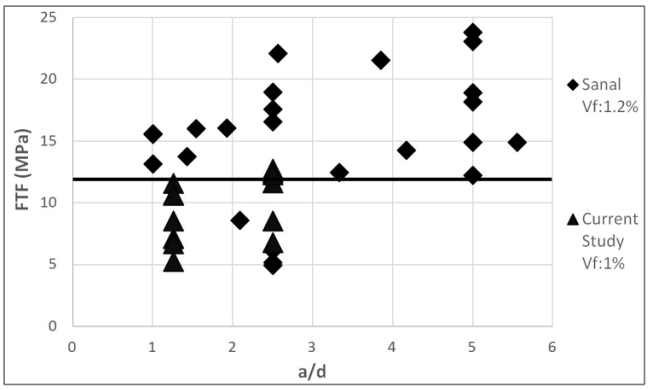

Figure 4.55. FTF versus a/d relationship for normal (50 MPa) and high strength (100 MPa) concrete.

4.2.7. Crack Analyses on Four Point Bending Specimens

In the study, crack pattern/crack development was monitored using a DSLR camera placed in front of the specimens and location of a crack or cracks were monitored during flexural tests as described in Section 3.4.4. The purpose of the crack monitoring was to understand different cracking/failure mechanisms which may occur due to varying parameters such as a/d ratio, t/f_L ratio and fiber volume. It is known that one crack is formed under bending at the maximum moment region when plain specimens are used. If steel fibers are added to the specimens in order to improve flexural behavior, multiple cracking can be observed depending on steel fiber types and amounts. As shear span to depth ratio (a/d) decreases in structural reinforced specimens, cracks can be observed outside the maximum moment region and even shear-flexural type of failure can be observed depending on structural rebar size/amounts (flexural reinforcement) and stirrup size/amounts (shear reinforcement). In literature, there is no study about the effects of varying a/d ratios on the mechanical performance of only fiber reinforced structural components (when no conventional reinforcement was used). Therefore, possible effects of varying a/d ratio on mechanical performance of only fiber reinforced concretes are not known. The use of only fiber reinforced structural components is increasing with an increasing understanding of the material behavior. Material characterization is needed for design of fiber reinforced composite materials. Bending tests are commonly used for material characterization and therefore, it is important

to understand different mechanisms which may affect the material behavior for fiber reinforced materials.

Cracking behavior of the fiber reinforced concrete beams were analyzed and evaluated for different volumes of steel fibers and two shear span to depth ratios (a/d: 1.25 and 2.5) and results were given in Table 4.12 and Table 4.13. Numbers of cracks at the maximum moment region of the specimens were given in Table 4.12. It was observed that number of cracks was increased with an increase in steel fiber volume and maximum number of cracks was observed at 1% long fiber reinforced specimens. Cracks were found to be aligned parallel to the loading direction in the tension zone which indicates flexural type of failure. Effect of shear span to depth ratio (a/d) on the types of cracks occurred was also examined. Higher numbers of cracks were observed for specimens with a/d ratio of 2.5, indicating flexure type of failure.

Number of cracks occurred out of the maximum moment region was also studied and the results are given in Table 4.13. No cracks were observed out of the moment region when fiber volume was low (0.5%) and a/d ratio was high (2.5). However, cracks were found to form in and out of the maximum moment region for higher volumes of fiber (1.0%) and low a/d ratio (1.25). This results represents that probability of having shear type of failure increases for low a/d ratio and higher volumes of steel fibers when steel fiber reinforced specimens were used without conventional reinforcement. This result is attributed to the increased crack arresting capacity of the fibers in the bending region (with an increased fiber volume). Shear region becomes relatively weaker and cracking of specimen occur in that region.

When all specimens were compared, percentage of specimens having cracks out of the maximum moment region decreased with an increase in shear span to depth ratio as shown in Table 4.14. Specimens with high a/d ratios (2.5) yielded less number of outside cracks than specimens with low a/d ratios (1.25). It can be concluded that, when a/d ratio is low, the probability of having shear cracks increase and failure becomes shear-bending failure instead of bending failure.

Table 4.12. Number of cracks at the maximum moment region of the SFR-SCC specimens.

Specimen	**# of cracks / # of specimens**	
	a/d:1.25	**a/d:2.5**
Control	1	1
0.5% Long FRC	1.08	1.44
0.5% Short FRC	1.17	1.33
1% Long FRC	2.08	2.56
1% Hybrid FRC	1.33	2.11

Table 4.13. Number of cracks out of the maximum moment region of the SFR-SCC specimens.

Specimen	**# of cracks / # of specimens**	
	a/d:1.25	**a/d:2.5**
Control	0	0
0.5% Long FRC	0.25	0
0.5% Short FRC	0	0
1% Long FRC	0.58	0.78
1% Hybrid FRC	0.67	0

Table 4.14. Number of cracked specimens in which cracks formed out of the maximum moment zone.

Specimen	**a/d**	**# of cracked specimen out of 12 specimen**	**Crack Percentage (%)**
T30L275	2.5	1	8
T40L350	2.5	2	16
T50L425	2.5	2	16
T40L200	1.25	6	50
T60L275	1.25	4	33
T80L350	1.25	4	33
T100L425	1.25	3	25

4.2.8. Three Point Bending Test Results on Notched Specimens for Modeling

Three point bending tests were performed under CMOD control on notched specimens for obtaining required parameters for modelling of bending behavior. Specimens were loaded up to a CMOD level of 4 mm. The dimensions of the specimens were 150 (b) x 150 (d) x 600 (L) mm. The flexural loading arrangement and CMOD loading rates were described in Section 3.4.5.

Table 4.15. Multi-Layer Model input parameters for the different SFR-SCC specimens.

General Model *Parameters*		**SFR-SCC specimens**			
		0.50% Long	**0.50% Short**	**1% Long**	**1% Hybrid**
Number of layers		500	500	500	500
Influence length, 0.5*hlig (mm)		62.5	62.5	62.5	62.5
Bilinear compressive relation		Input parameters for compression			
Compressive Strength (MPa) (1)	f_c	59.23	58.92	61.98	61.18
Linear elastic strain limit (strain) (2)	ε_{c0}	0.0017	0.0026	0.003	0.004
E-Modulus (MPa) (3)	E	31160	30853	36319	36817
Ultimate limit strain (millistrain) (4)	ε_{cmax}	0.01	0.015	0.015	0.015
Bilinear stress-crack width relation		Input parameters for tension			
Splitting tensile strength (MPa) (5)	$f_{fctm,splt}$	4.35	4.67	7.57	6.39
Uniaxial elastic tensile strength (MPa)	$f_{fctm,ax}$	3.26 ($f_{fctm,splt}$*0.75)	3.5 ($f_{fctm,splt}$*0.75)	56.775 ($f_{fctm,splt}$*0.75)	5.112 ($f_{fctm,splt}$*0.75)
Uniaxial elastic tensile strain (strain)	ε_{ct}	0.0001047 ($f_{fctm,ax}$/E)	0.0001047 ($f_{fctm,ax}$/E)	0.0001563 ($f_{fctm,ax}$/E)	0.0001389 ($f_{fctm,ax}$/E)
Equivalent post cracking tensile strength (MPa)	$f_{fctm,eq,bil}$	0.9787 ($f_{fctm,ax}$*0.3)	15.761 ($f_{fctm,ax}$*0.45)	17.032 ($f_{fctm,ax}$*0.3)	20.448 ($f_{fctm,ax}$*0.4)
Critical crack width (mm)	w0	11.55 (0.33*F_L)	6.5 (0.5*F_L)	11.55 (0.33*F_L)	11.55 (0.33*F_L)
Characteristic crack width (mm)	wc	28.875 (w_0/4)	1.3 (w_0/5)	28.875 (w_0/4)	28.875 (w_0/4)

1) f_c values were obtained from compressive strength tests results of the cube specimens
2,3 and 4) ε_{c0}, ε_{cmax} and E values taken from displacement controlled compressive strength results on the cylinder specimens
5) $ff_{ctm}, splt$ values were taken from splitting tensile test results on cylinder specimens

4.2.8.1. Modelling of the bending behavior of SFR- SCCs. Bending behavior of SFR-SCCs were modelled by using the obtained input parameters. Spreadsheets were formed for different SFR-SCC specimens as described in Section 2.7. Model simulations were repeated until the deviation amount between experimental result and model result became lower than 5% as explained below.

The following data points were used as reference points to check deviation amount between the experimentally and theoretically obtained curves.

- Maximum flexural load (P_{max}).
- 75 % of the maximum experimental flexural load (in the post peak region).

- Toughness values calculated for a CMOD value corresponding to 75% of the maximum experimental flexural load (in the post peak region).
- Toughness values calculated for a CMOD value of 4 mm.

Good results were obtained as can be seen in Figure 4.56 to Figure 4.59. The input parameters was found satisfactory after the deviation checks between experimentally and theoretically obtained curves. 3 point bending test results on notched specimens showed similar findings with the 4 point bending test results. SFR-SCC specimens showed higher load bearing and lateral displacement capacity when compared to plain concretes.

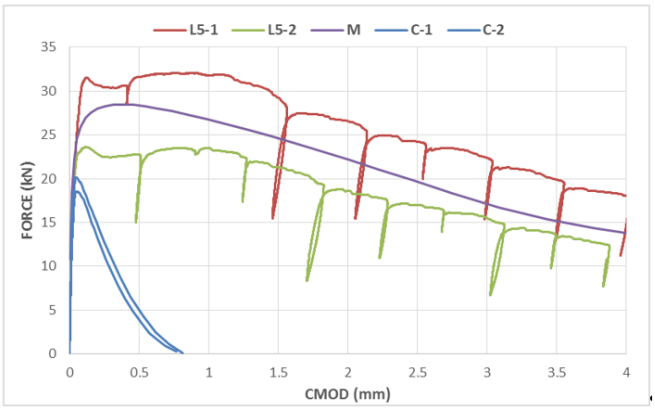

Figure 4.56. Model and experimental results of 0.5% long fibrous specimens.

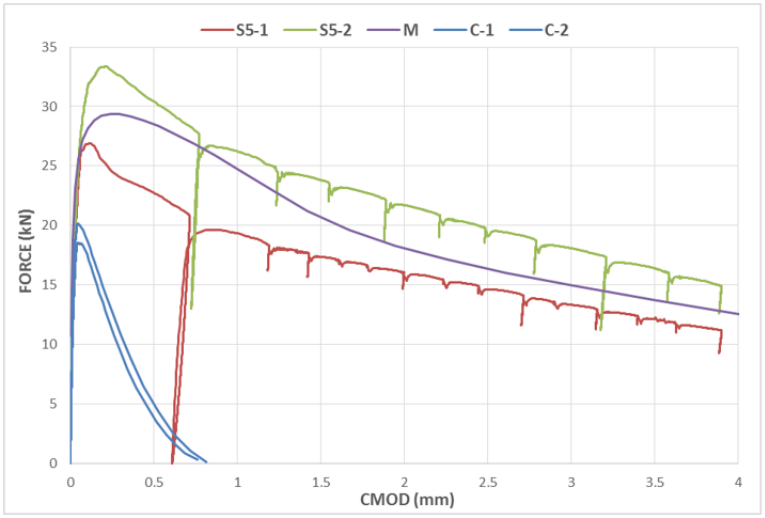

Figure 4.57. Model and experimental results of 0.5% short fibrous specimens.

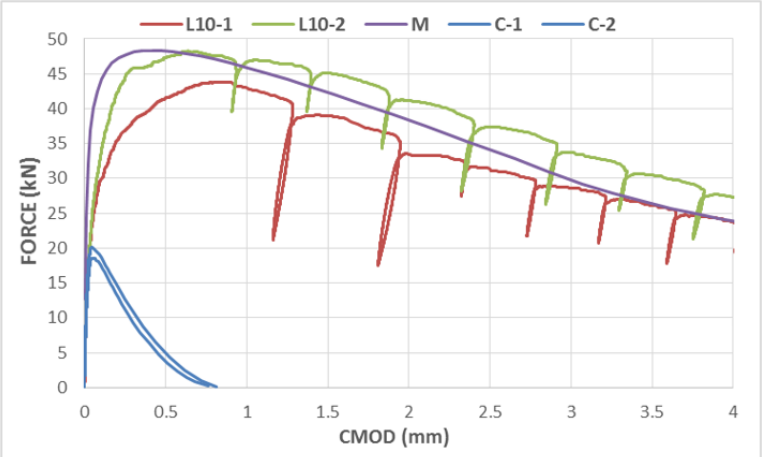

Figure 4.58. Model and experimental results of 1% long fibrous specimens.

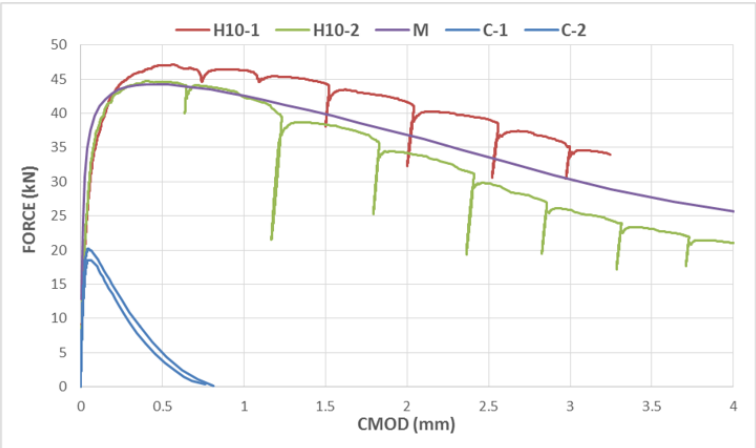

Figure 4.59. Model and experimental results of 1% hybrid fibrous specimens.

4.2.8.2. Contribution Done to Multi-Layer Model in the Scope of this Study. Model input parameters and their effects were explained in detail in the Section 2.7.1. Kooiman [7] modified the multilayer model for only long FRC specimens and Grünewald [23] also adopted and modified the model for SFR-SCC specimens. He used different steel fibers (short and long) and stated that straight short steel fiber results were excluded in his models due to the significantly different deviation between model and experimental results. Lappa [57] also added that short fibers had a different effect on the structural behavior of fiber reinforced concrete specimens and short fibers increased the ultimate tensile capacity of the FRC specimens rather than the ductility in the post peak region. Lappa carried out direct tension test to find $f_{fctm,ax}$, $f_{fctm,eq,bil}$ and w_0, w_c values.

In this study, similar approach as reported by Kooiman [7] and Grünewald [23] were used to obtain the input parameters for modelling of the long fibrous specimens (Table 4.16). However, for the short and hybrid fibrous specimens, new input parameters were successfully defined and used as can be seen in Table 4.16. It was found that short FRC specimens required slightly higher $f_{fctm,eq,bil}$ and w_0 values than the long FRC specimens. By using the above modifications, each models was composed and good results were obtained.

Table 4.16. Tensile input parameters for the modelling.

Input parameters	**Current study**	**Kooiman [7]**	**Grünewald [23]**
$f_{fctm,ax}$	$f_{fctm,splt}$*0.75	0.7-0.8*$f_{fctm,splt}$	0.45-0.68*$f_{fctm,splt}$
$f_{fctm,eq,bil}$	0.3*$f_{fctm,ax}$ (L5,L10) 0.4* $f_{fctm,ax}$ (H10) 0.45* $f_{fctm,ax}$ (S5)	0.2-0.3* $f_{fctm,ax}$	0.2-0.35* $f_{fctm,ax}$
w_0	0.33*F_L (L5,L10,H10) 0.5* F_L (S5)	0.33-0.425* F_L	0.26-0.42* F_L
w_c	0.25*w_0 (L5,L10,H10) 0.2* w_0 (S5)	0.17-0.2* w_0	0.22-0.36* w_0

5. CONCLUSIONS AND RECOMMENDATIONS

Main objective of the study was to investigate the several parameters; steel fiber types and amounts, specimen thickness to fiber length ratio (t/f_L) and shear span to depth ratio (a/d) on different specimen sizes for better understanding of the material behavior and characterization of the SFR-SCC.

Similar to the results and discussions parts, conclusion part was also divided into two main categories as fresh and hardened state. In the fresh state part, the conclusions of flowability, passing ability and rheological properties, fiber orientation analysis, static and dynamic segregation analysis of SFR-SCCs were given. In the hardened state part, results of the compressive and splitting tensile strength tests, four point bending test on different specimen sizes, and inverse modeling-multi layer model conclusions were given.

5.1. Fresh State Performance

The main goal of the fresh state tests was to evaluate the fresh state properties of different SCC mixes. 5 different SCC mixes were composed with varied steel types and 7 different specimen sizes in order to observe flowability, rheological properties, segregation resistance, and fiber orientation characteristics.

5.1.1. Fresh State Test Performance

Fresh state tests were conducted in order to find out flowability and passing ability of mixes. Following conclusions were drawn from the fresh state tests performance;

- Flowability of the SFR - SCC mixes were found satisfactory and meet the specific requirements,
- Flowability of the mixes were found to decrease with an increasing fiber volume,
- It was observed during the flow tests that, steel fibers dispersed better in the

mixes with high flowability,

- Short fiber reinforced mixes required more superplasticizer to show similar flowability due to their high aspect ratios and the higher number of fibers compared to long fibers.
- Filling and passing ability of the 1% (long and hybrid) SFR-SCC mixes were found to be limited and care should be taken when using them for applications which require high amounts of reinforcement with narrow openings,
- Rheological test results were found to be in a good range with the flowability tests results of the SCC mixes except for the hybrid fiber reinforced mix. Hybrid fiber reinforced mix represented relatively high yield stress and plastic viscosity value for a SCC design.

5.1.2. Static and Dynamic Segregation Resistance

Dynamic segregation resistance represents the ability of a mixture to drive the fibers with itself in the fresh state, whereas static segregation resistance represents concrete's ability to hold fibers as well as aggregates while it is still plastic. Dynamic and static segregation resistance must be ensured to be able to make a precise evaluation of mechanical performance. The objective of this part was to observe dynamic and static segregation resistance of mixes. The following results were obtained for SFR-SCC mixes;

- Dynamic segregation resistances of the mixes were found satisfactory.
- Some static segregation was observed for almost all of the specimens; however, it was negligible for the short and hybrid fibrous specimens. On the other hand, the volume of fibers in the top layer of long fiber-reinforced specimens was found significantly lower when compared to the middle and bottom layers representing higher tendency for long fibers to settle down. However, this could be considered as an advantage for the specimens, which will be tested under bending loading, since the increased amount of fibers in the bottom layer of the specimens means increased crack arresting capacity at the tensile zone.

5.1.3. Fiber Orientation Analysis

The objective of the fiber orientation analysis was to find fiber orientation densities in the x, y and z directions for the SFR-SCC specimens with different types of fibers and amounts. Fiber orientation highly affects mechanical performance especially bending strength. Therefore, a thorough analysis of fiber orientation was carried out by using a tensor description method. The following conclusion was drawn;

- Results showed that, maximum fiber alignments were obtained in the casting direction (X direction) for all specimens. This result also confirms that fibers can be aligned in the casting direction to a certain extent (FOD values around 0.6-0.7) when using SCC which as a result ensures similar fiber alignments in the specimens while evaluating mechanical performance of the specimens.

5.2. Hardened State Performance

5.2.1. Compressive Strength Tests

In this study, compressive strength tests were performed in order to understand compressive behavior of the materials as well as to obtain the parameters required for the modeling. Tests were conducted both on cube specimens to obtain compressive strength values and on cylinder specimens to find out elastic modulus and to observe post-peak behavior (ε_{c0}, e_{cmax}) of SFR-SCC specimens. The main findings can be summarized as follows;

- Steel fiber addition to the SCC mixes slightly increased the compressive strength compared to plain mix. The extent of the increase was higher for 1% fiber - reinforced mixes.
- Similar to compressive strength, elastic modulus of SFR-SCC was found to increase with an increase in steel fiber volume and this increase remains limited.

5.2.2. Splitting Tensile Strength Tests

Splitting tensile strength tests were carried out to obtain tensile parameters required for the inverse modeling and results indicated that;

- Steel fibers were found to have a significant influence on splitting tensile strength of concrete, especially for high steel fiber fractions ($\geq$1%). Low amount of steel fibers (0.5%) had no or little contribution to splitting tensile strength results.

5.2.3. Four Point Bending Tests

In this part of the study, several parameters; steel fiber types and amounts, specimen thickness to fiber length ratio (t/f_L) and shear span to depth ratio (a/d) were investigated on different specimen sizes for better understanding of the material behavior of the SFR-SCC. Crack pattern/monitoring was also done. Findings can be summarized as following;

5.2.3.1. Plain Specimens versus Steel Fibrous Specimens. Performance of plain specimens were compared with the steel fibrous specimens. Results indicated that;

- The use of steel fibers enhances the pre/post peak behavior and crack pattern of the specimens.
- Deflection hardening behavior was observed for almost all specimens including 1% steel FRC specimens, while deflection softening behavior was observed when 0.5% FRC specimens and plain specimens used. However, lower amounts of steel fiber addition into SCC improved ductility of specimens significantly as compared to plain SCC specimens as expected.
- Equivalent bending strength (EBS), flexural toughness factor (FTF) and lateral flexural toughness factor (FTF_{COD}) results were found to increase with an increase in steel fiber volumes of SCC specimens (plain specimens $<$ 0.5% FRC specimens $<$ 1% FRC specimens).

5.2.3.2. Effect of a/d ratio on SFR-SCC specimens. In this part, the effect of shear span to depth ratio (a/d) on the bending performance of SFR-SCC specimens was investigated. EBS, FTF and FTF_{COD} versus a/d relations were investigated considering two a/d ratios (1.25 and 2.5). It was observed that most of the specimens failed under bending effects while some of the specimens failed by yielding shear - bending type of behavior. Types of failure were given for all the specimens in section 4.2.7 while analyzing crack patterns. However, the results of the specimens which failed under shear - flexure effect were excluded from bending test analysis for consistency of calculations (since it was not possible to use the bending formula for those specimens).

The findings were given as follows;

- Specimens with high a/d ratio (2.5) were found to yield slightly higher EBS results than specimens with low a/d ratio (1.25). This result can be attributed to decreasing tendency of specimens to fail under bending with a decrease in a/d ratio.
- Similar with EBS versus a/d relationships, FTF values were also found to increase with an increase in a/d ratio. As stated above, this result is also attributed to decreasing tendency of having bending failure with a decreasing a/d ratio.
- Different from the EBS - a/d and FTF - a/d relationships, FTF_{COD} values were found to decrease with an increase in a/d ratio. Specimens with low a/d ratio (1.25) showed higher FTF_{COD} values than specimens with high a/d ratio (2.5). Specimens with low a/d ratio (1.25) showed lower number of cracks with large crack openings, while specimens with high a/d ratios showed multiple cracks with smaller openings.
- a/d ratio effect was also observed on COD - deflection relationship. When COD deflection relations were plotted neglecting the a/d effect, correlation was found to be poor (R^2: 0.57); however, when a/d ratio was taken into account, COD and deflection values were found strongly related (for a/d: 1.25 (R^2: 0.86) and for a/d: 2.5 (R^2: 0.8)).

5.2.3.3. Effect of t/f_L ratio on SFR-SCC specimens. t/f_L ratio may be considered as representing crack arresting/reinforcing ability of fibers. Reinforcing efficiency of fibers was reported to increase with a decreasing t/f_L ratio. In the scope of the current study, EBS and FTF versus t/f_L relationships were studied when a/d ratio was constant (1.25 and 2.5) and results were given below.

- Specimens with low t/f_L ratios were found to yield more EBS values than specimens with high t/f_L ratios. The decline in the EBS values with increasing t/f_L ratios was clearly observed for 1% FRC specimens; however, a similar behavior was not observed for 0.5% FRC specimens. This result was hypothesized to occur due to decreased efficiency of fibers when low volumes of fibers were used.
- Similar to EBS results, specimens with low t/f_L ratios showed higher FTF values than the specimens with high t/f_L ratios. The results supported that reinforcing efficiency of fibers increases with a decreasing t/f_L ratios. In addition, specimens with higher percentage steel fiber amounts showed better FTF - t/f_L relationships when compared to specimens having low amounts of steel fiber.

5.2.3.4. Combined effects of a/d and t/f_L ratios on SFR-SCC specimens. One of the objective of the study was to investigate the combined effects of a/d and t/f_L on mechanical performance and cracking behavior of the specimens. In the literature, there is no study investigating the combined effects of a/d and t/f_L. The separate effects of the parameters were clarified above. The main findings of the combined effects can be given as following;

- It was observed that steel fiber amount influenced the EBS results significantly. When steel fiber volume was kept constant as 1%, EBS values were found to decrease with an increase in t/f_L and decrease in a/d ratio. When specimens with a fiber volume of 0.5% were examined, effect of t/f_L is seen, however, the effect of a/d is not clear.
- FTF results were found to decrease with an increase in t/f_L and decrease in a/d ratio for both steel fiber volumes (0.5% and 1%).

5.2.3.5. Effect of Steel Fiber Type and Amount on Bending Performance. Steel fiber type and amount influenced the bending performance of SFR-SCC specimens in terms of EBS, FTF and FTF_{COD}. The results can be summarized as given below.

- Higher (1%) percentage of long steel fibers were found to show the best performance by means of arresting cracks, while low volumes of short fibers (0.5%) were found to show poor performance. The results supported that short steel fibers cannot resist the macro cracks.
- 1% long fibrous specimens yielded higher EBS, FTF and FTF_{COD} results when compared to the remaining of the steel fibrous specimens (1% hybrid, 0.5% short and long).

5.2.3.6. Crack Analyses on Four Point Bending Specimens. Cracking behavior of the FRC beams (without conventional rebar) were observed and evaluated for different steel fiber types and amounts with two shear spans to depth ratios (a/d: 1.25 and 2.5) and findings were summarized as follows.

When cracks were formed in the maximum moment region;

- It was observed that cracks were aligned parallel to the loading direction in the tension zone which indicates flexural type of failure,
- It was observed that number of cracks was increased with an increase in steel fiber volume and maximum number of cracks was observed at 1% long FRC specimens. These specimens showed deflection hardening behavior.
- Higher numbers of cracks were observed for specimens with a/d ratio of 2.5, indicating more flexure type of failure.

When cracks were formed out of the maximum moment region (shear region);

- No cracks were observed out of the maximum moment region when fiber volume was low (0.5%) and a/d ratio was high (2.5),

- Specimens with high a/d ratios (2.5) yielded less number of outside cracks than specimens with low a/d ratios (1.25),
- Cracks were found to form out of the maximum moment region for higher fiber amounts (1.0%) and low a/d ratio (1.25).

Results represent that probability of having shear type of failure increases with low a/d ratio and higher volumes of steel fibers when SFR-SCC were used without conventional reinforcement.

5.2.3.7. Three point Bending Tests for Modeling. Bending tests are commonly used for material characterization and therefore, it is important to understand different mechanisms which may affect the material behavior for fiber reinforced materials. Due to lack of direct tensile stress-strain diagrams and lack of material characterization, FRC has not been standardized yet. Therefore, an inverse model (multi-layer model) was adopted from previous studies and modified for different steel fiber types and amounts in order to predict tensile stress-strain behavior of SFR-SCCs. The multi-layer model is checked with the experimental results with accuracy checks and results were given as follows.

- Successful model results for each fiber reinforced specimens were obtained,
- The input parameters was found satisfactory after the deviation checks between experimentally and theoretically obtained curves.
- Input parameters selected for long fibrous specimens were similar to the ones reported by Kooiman [7] and Grünewald [23].
- No information was found regarding the input values for the short and hybrid fibrous specimens in the literature. Grünewald [7] reported significant deviation between experimental and model results when short fibers were used. In the current study, new input parameters for short and hybrid fibers were successfully introduced and used. Good results were obtained.

5.3. Recommendations for Further Study

In this study, SFR-SCC specimens were examined by considering the effects of different parameters on the material performance to understand and to promote the use of fiber materials in building industry. For this purpose, the effects of different parameters on SFR-SCC specimens were investigated, an existing tensile stress - strain model was successfully used and some additions were proposed for the modelling of the behavior of short fiber reinforced specimens.

Based on the experimental study carried out here following further studies can be proposed:

- Different standards suggest use of different testing set up for material characterization for structural design of fiber reinforced composites. Especially when unnotched specimens with small thickness is under consideration many parameters such as a/d and t/f_L can be effective (as observed in this study) and varying results can be obtained from the characterization tests. Material characterization for unnotched specimens should be further investigated and modelling studies should be done for developing mathematical equations which may apply to wide variety of materials (with different fibers, fiber lengths, geometry and etc.).

REFERENCES

1. Li, V. C., "Large Volume, High-Performance Applications of Fibers in Civil Engineering", *Journal of Applied Polymer Science*, Vol. 83, No. 3, pp. 660-686, 2002.

2. Rao B. K., and V. Ravindra, "Steel Fibre Reinforced Self-Compacting Concrete Incorporating Class Fly Ash", *International Journal of Engineering Science and Technology*, Vol. 2, No.9, pp. 4936-4943, 2010.

3. Mondo E., *Shear Capacity of Steel Fibre Reinforced Concrete Beams without Conventional Shear Reinforcement*, M.S. Thesis, KTH Royal Institute of Technology, 2011.

4. Löfgren I., *Fiber Reinforced Concrete for Industrial Construction*, Ph.D. Thesis, Chalmers University of Technology, 2005.

5. Mpegetis S. O., *Behavior and Design of Steel Fiber Reinforced Concrete Slabs*, Ph.D. Thesis, Imperial College London, 2012.

6. Cunha V. M. C. F., *Steel Fibre Reinforced Self-Compacting Concrete*, Ph.D. Thesis, University of Minho, 2010.

7. Kooiman A. G., *Modelling Steel Fibre Reinforced Concrete for Structural Design*, Ph.D. Thesis, Delft University of Technology, 2000.

8. Niş A., *Investigation of Rebar Corrosion in Plain and Steel Fibre Reinforced Concrete under Static and Dynamic Loading*, M.S. Thesis, Bogaziçi University, 2011.

9. Prisco M.D., R. Felicetti, F. Iorio, and R. Gettu, "On the Identification of SFRC Tensile Constitutive Behaviour", *Fracture Mechanics of Concrete Structures*, Vol. 2, No. 1, pp. 541-548, 2001.

10. Luo J. W., *Behavior and Analysis of Steel Fibre - Reinforced Concrete under Reversed Cyclic Loading*, Ph.D. Thesis, University of Toronto, 2014.

11. EFNARC (European Federation of Producers and Applicators of Specialist Products for Structures), "Specification and Guidelines for Self-Compacting Concrete", *EFNARC*, 2002.

12. Su N, K. C. Hsu, and H.W. Chai, "A Simple Mix Design Method for Self-Compacting Concrete", *Cement and Concrete Research*, Vol. 31, pp. 1799-1807, 2001.

13. Gencel O., W. Brostow, T. Datashvili, and M. Thedford, "Workability and Mechanical Performance of Steel Fibre-Reinforced Self-Compacting Concrete with Fly Ash", *Composite Interfaces*, Vol.18, pp. 169-184, 2011.

14. Bouzoubaa N. and M. Lachemi, "Self-Compacting Concrete Incorporation High Volumes of Class F Fly Ash Preliminary Results", *Cement and Concrete Research*, Vol. 31. pp. 413-420, 2001.

15. Kumar K. S. and M. N. V. P. Bhushan, "Performance of Steel Fibre Reinforced Self Compacting Concrete", *International Journal for Technological Research in Engineering*, Vol.3, No. 10, pp. 2778-2885, 2016.

16. Okamura H. and M. Ouchi, "Self-Compacting Concrete", *Journal of Advanced Concrete Technology*, Vol. 1, No. 1, pp. 5-15, 2003.

17. Liao W.C., S.H. Chao, S.Y. Park, and A.E. Naaman, "Self - consolidating High Performance Fibre Reinforced Concrete: SCHPFRC", *Proceedings: Fifth International RILEM Workshop on High Performance Fibre Reinforced Cement Composites (HPFRCC5)*, No. 053, pp. 293-302, 2006.

18. Xie Y., B. Liu, J. Yin, and S. Zhou, "Optimum Mix Parameters of High Strength Self-Compacting Concrete with Ultrapulverized Fly Ash", *Cement and Concrete*

Research, Vol. 32, pp. 477-480, 2002.

19. Grünewald S. and J. C. Walraven, "Parameters-study on the Influence of Steel Fibres and Coarse Aggregate Content on the Fresh State Properties of Self-compacting Concrete", *Cement and Concrete Research*, Vol. 31, pp. 1793-1798, 2001.

20. Corinaldesi V., and G. Moriconi, "Durable Fibre Reinforced Self-Compacting Concrete", *Cement and Concrete Research*, Vol. 34, pp. 249-254, 2004.

21. Deeb R., *Flow of Self-Compacting Concrete*, Ph.D. Thesis, Cardiff University, 2013.

22. EFNARC (European Federation of Producers and Applicators of Specialist Products for Structures), "The European Guidelines for Self-Compacting Concrete", *EFNARC*, 2005.

23. Grünewald S., *Performance-based Design of Self-Compacting Fibre Reinforced Concrete*, Ph.D. Thesis, Delft University of Technology, 2004.

24. Akkaya Y., P. S. Shah, and B. Ankenman, "Effect of Fibre Dispersion on Multiple Cracking of Cement Composites", *Journal of Engineering Mechanics*, Vol. 127, No. 4, pp. 311-316, 2001.

25. Özyurt N., T. O. Mason, and S. P. Shah, "Correlation of Fibre Dispersion, Rheology and Mechanical Performance of FRCs", *Cement and Concrete Composites*, Vol.29, pp. 70-79, 2007.

26. Sarmiento E.V., "Flowable Fibre-Reinforced Concrete for Structural Applications", PhD Thesis, Norwegian University of Science and Technology, 2015.

27. Spangenberg J., N. Roussel, J. H. Hattel, E. V. Sarmiento, G. Zirgulis, and M. R. Geiker, "Patterns of Gravity Induced Aggregate Migration during Casting of Fluid Concretes", *Cement and Concrete Research*, Vol. 42, pp. 1571-1578, 2012.

28. Şanal I., *Effects of Formwork Dimensions on the Mechanical Performance of Fibre-Reinforced Cement Based Materials*, M.S. Thesis, Bogazici University, 2008.

29. Şanal I., and N. Özyurt, "To What Extent does the Fibre Orientation affect Mechanical Performance?", *Construction and Building Materials*, Vol. 44, pp. 671-681, 2013.

30. Ferrara L., M. Faifer, and S. Toscani, "A Magnetic Method for Non Destructive Monitoring of Fibre Dispersion and Orientation in Steel Fibre Reinforced Cementitious Composites-part 1: Method Calibration", *Materials and Structures*, Vol. 45, pp. 575-589, 2012.

31. Stahli P., R. Custer, and J. G. M. M. Mier, "On Flow Properties, Fibre Distribution, Fibre Orientation and Flexural Behavior of FRC", *Materials and Structures*, Vol. 41, pp. 189-196, 2008.

32. Ferrara L. and A. Meda, "Relationship between Fibre Distribution, Workability and The Mechanical Properties of SFRC applied to Precast Roof Elements", *Materials and Structures*, Vol. 39, pp. 411-420, 2006.

33. Akkaya Y., J. Picka, and S. P. Shah, "Spatial Distribution of Aligned Short Fibres in Cement Composites", *Journal of Materials in Civil Engineering*, Vol. 12., No. 3, pp. 272-279, 2000.

34. Eberhardt C. and A. Clarke, "Fibre-orientation Measurements in Short-glass-fibre Composites. Part I: Automated, High-angular-resolution Measurement by Confocal Microscopy", *Composites Science and Technology*, Vol. 61, pp. 1389-1400, 2001.

35. Duque L. F. M., and B. Graybeal, "Fibre Orientation Distribution and Tensile Mechanical Response in UHPFRC", *Materials and Structures*, Vol. 55, pp. 1-17, 2017.

36. Boulekbache B., M. Hamrat, M. Chemrouk, and S. Amziane, "Flowability of Fibre

Reinforced Concrete and its Effects on the Mechanical Properties of the Material", *Construction and Building Materials*, Vol. 24, pp. 1664-1671, 2010.

37. Zijl V. G. P. A. G., and S. Zerenka, "The Impact of Rheology on the Mechanical Performance of Steel Fibre Reinforced Concrete", *The Sixth International RILEM Conference on High Performance Fibre Reinforced Cement Composites (HPFRCC6)*, No. 1, pp.59-66, 2012.

38. Zhao M., *Study on Effects of Flowability on Steel Fibre Distribution Patterns and Mechanical Properties of SFRC*, M.S. Thesis, RMIT University, 2016.

39. Ou Y.C., M.S. Tsai, K.Y. Liu, and K.C. Chang, "Compressive Behavior of Steel Fibre Reinforced Concrete with a High Reinforcing Index", *Journal of Materials in Civil Engineering*, Vol. 24, No. 2, pp. 207-215, 2012.

40. Schumacher P., *Rotation Capacity of Self-Compacting Steel Fibre Reinforced Concrete*, Ph.D. Thesis, Darmstadt University of Technology, 2006.

41. Rawashdeh O.J.Z., *Shear Behavior of Steel-Fibre Reinforced Ultra-High-Strength Self-Compacted Concrete Beams*, M.S. Thesis, United Arab Emirates University, 2015.

42. Reedy S. L., R. N. V. Ramana, and R. T. D Gunneswara, "Finite Element Analysis of High Strength Beams in Shear-without Web Reinforcement and with Fibre in Shear Predominant Regions", *International Journal of Innovative Research in Science, Engineering and Technolog*, Vol. 4, No. 4, pp. 2475-2484, 2015.

43. Naik U. P., and S. Y. Kute, "Effect of Shear Span to Depth Ratio on Shear Strength of Steel Fibre Reinforced High Strength Concrete Deep Beam using ANN", *International Journal of Engineering Research and Technology*, Vol. 3, Issue 6, pp. 927-930, 2014.

44. Dinhh H. H., *Shear Behavior of Steel Fibre Reinforced Beams without Stirrup Re-*

inforcement, Ph.D. Thesis, University of Michigan, 2009.

45. American Concrete Institute-American Society of Civil Engineering Committee 426, "Shear Strength of Reinforced Concrete Members", *American Concrete Institute Journal Proceedings*, Vol. 70, No. 7, pp. 471-473, 1973.

46. Al-lami K. A., *Experimental Investigation of Fibre Reinforced Concrete Beams*, M.S. Thesis, Portland State University, 2015.

47. Nataraja M. C, N. Dhang, and A. P. Gupta, "Toughness Characterization of Steel Fibre-Reinforced Concrete by JSCE Approach", *Cement and Concrete Research*, Vol.30, pp. 593-597, 2000.

48. Blanco A., *Characterization and Modelling of SFRC Elements*, Ph.D. Thesis, Universitat Politecnica de Catalunya, 2013.

49. Japan Society of Civil Engineers, Tokyo SF-4, "Method of Test for Flexural Strength and Flexural Toughness for Fibre Reinforced Concrete", *Concrete Library of Japan Society of Civil Engineers*, No. 1, Vol.3, pp. 58-61, 1984.

50. EN 14651, "Test Method for Metallic Fibreed Concrete - Measuring the Flexural Tensile Strength Limit of Proportionality LOP, Residual, *European Standard*, 2005.

51. Jatale V. B. and M.N. Mangulkar, "Flexural Behavior of Self Compacting High Strength Fibre Reinforced Concrete (SCHSFRC)", *International Journal of Engineering Research and Applications*, Vol. 3, No. 4, pp. 2503-2505, 2013.

52. Trottier J.F., and N. Banthia, "Toughness Characterization of Steel-Fibre Reinforced Concrete", *Journal of Materials in Civil Engineering*, Vol. 6, No. 2, pp. 264-289, 1994.

53. Frazao C., A. Camoes, J. Barros, and D. Gonçalves, "Durability of Steel Fibre Reinforced Self-Compacting Concrete", *Construction and Building Materials*, Vol.

80, pp. 155-166, 2015.

54. Amin A., S.J. Foster, and A. Muttoni, "Evaluation of the Tensile Strength of SFRC as derived from Inverse Analysis", VIII International Conference on Fracture Mechanics of Concrete and Concrete Structures, *FraMCoS-8*, 2013.

55. CNR-DT 204/2006, *Guidelines for the Design, Construction and Production Control of Fibre Reinforced Concrete Structures*, Italian National Research Council, Rome, 2006.

56. Hordijk D. A., *Local approach to fatigue of concrete*, Ph.D. Thesis, Delft University of Technology, 1991.

57. Lappa E.S., *High Strength Fibre Reinforced Concrete - Static and Fatigue Behaviour in Bending*, Ph.D. Thesis, Darmstadt University of Technology, 2007.

58. TS EN 12350-8, *Testing Fresh Concrete - Part 8: Self-compacting concrete - Slump - flow test*, 2011.

59. TS EN 12350-9, *Testing Fresh Concrete - Part 9: Self-compacting concrete - V funnel test*, 2011.

60. TS EN 12350-10, *Testing Fresh Concrete - Part 10: Self-compacting concrete - L box test*, 2011.

61. TS EN 12350-12, *Testing Fresh Concrete - Part 12: Self-compacting concrete - J ring test*, 2011.

62. UNI 11044, *Testing Fresh Self Compacting Concrete - Determination of Confined Flowability in U - Shape Box, Italian Standards*, 2003.

63. American Society for Testing and Materials C1018, *Standard Test Method for Flexural Toughness and First-Crack Strength of Fibre-Reinforced Concrete Using Beam with Third Point Loading* , 1997.

64. American Society for Testing and Materials C1609/C1609 M-12, *Standard Test Method for Flexural Performance of Fibre-Reinforced Concrete*, Using Beam with Third Point Loading, 2012.

65. ASTM C496/C496 M-11, *Standard Test Method for Splitting Tensile Strength of Cylindrical Concrete Specimens*, 2011.

66. TS EN 12390-3, *Testing Hardened Concrete - Part 3: Compressive Strength of Test Specimens*, 2003.

67. TS 13515, *Complementary Turkish Standard for the implementation of TS EN 206*, 2014.

68. TS EN 196-3, *Methods of Testing Cement - Part 3: Determination of Setting Times and Soundness*, 2017.

69. TS EN 196-6, *Methods of Testing Cement - Part 6: Determination of Fineness*, 2010.

70. TS EN 196-2, *Methods of Testing Cement - Part 2: Chemical Analysis of Cement*, 2014.

71. TS EN 196-1, *Methods of Testing Cement - Part 1: Determination of Strength*, 2016.

72. Koehler E. P. and D. W. Fowler, "ICAR Report 105-3F: Development of a Portable Rheometer for Fresh Portland Cement Concrete", *International Center for Aggregates Research*, The University of Texas at Austin, 2004.

73. Özyurt N., L. Y. Woo, T. O. Mason, and S. P. Shah, "Monitoring Fibre Dispersion in Fibre-Reinforced Cementitious Materials: Comparison of AC-Impedance Spectroscopy and Image Analysis", *American Concrete Institute Materials Journal*, Vol. 103, No. 5, pp. 340-347, 2006.

74. Özyurt N., *Correlating Fibre Dispersion, Rheology, and Mechanical Performance for Fibre Reinforced Cement Based Materials*, Ph.D. Thesis, Istanbul Technical University, 2006.

75. Mlekusch B., "Fibre Orientation in Short-Fibre-Reinforced Thermoplastics II. Quantitative Measurements by Image Analysis", *Composites Science and Technology*, Vol. 59, pp. 547-560, 1999.

76. RILEM TC 162-TDF: "Test and Design Methods for Steel Fiber Reinforced Concrete", *Material and Structures*, Vol.36, pp. 560-567, 2003.

77. Jo B.W., Y.H. Shon, and Y.J. Kim, "The Evaluation of Elastic Modulus for Steel Fiber Reinforced Concrete", *Russian Journal of Nondestructive Testing*, Vol.37, No.2, pp. 152-161, 2001.

78. Gul M., A. Bashir and J.A. Naqash, "Study of Modulus of Elasticity of Steel Fiber Reinforced Concrete", *International Journal of Engineering and Advanced Technology*, Vol.3, Issue 4, pp. 304-309, 2014.

79. Gopalaratnam V.S., R. Gettu, S. Carmona and D. Jamet, "Characterization of the Toughness of Fiber Reinforced Concretes using the Load - CMOD Response", *Fracture Mechanics of Concrete Structures*, Vol. 1, pp. 770-782, 1995.

80. Şanal I., N. Özyurt, and A. Hosseini, "Characterization of Hardened State Behavior of Self Compacting Fiber-Reinforced Cementitious Composites (SC-FRCC's) with Different Beam Sizes and Fiber Types", *Composites Part B: Engineering*, Vol. 105, pp. 30-45, 2016.

81. Şanal I., *Evaluating Effects of Various Factors on Mechanical Performance of SC-FRCs*, PhD Thesis, Bogazici University, 2015.

82. Dubey R. and P. Kumar, "An Empirical Approach for the Optimization of fly ash Content in Self-Consolidating Concrete", *Proceedings of the Fifth North American*

Conference on the Design and Use of Self-Consolidating Concrete, Chicago, May 12-15, Illinois, USA, 2013.

83. Ferrara L., "Fiber Reinforced Self-Compacting Concrete (FR-SCC): a State of the art Perspective", *Proceedings of the Fifth North American Conference on the Design and Use of Self-Consolidating Concrete*, Chicago, May 12-15, Illinois, USA, 2013.

84. Aoude H., *Structural Behaviour of Steel Fiber Reinforced Concrete Beams*, Ph.D. Thesis, McGill University, 2007.

85. Şanal I. and N. Özyurt, "Effects of Formwork Dimensions on the Mechanical Performance of Fiber-Reinforced Cement Based Materials", 9^{th} *International Congress on Advances in Civil Engineering*, September 27-30, Karadeniz Technical University, Trabzon, Turkey, 2010.

APPENDIX A: FOUR POINT BENDING TEST RESULTS

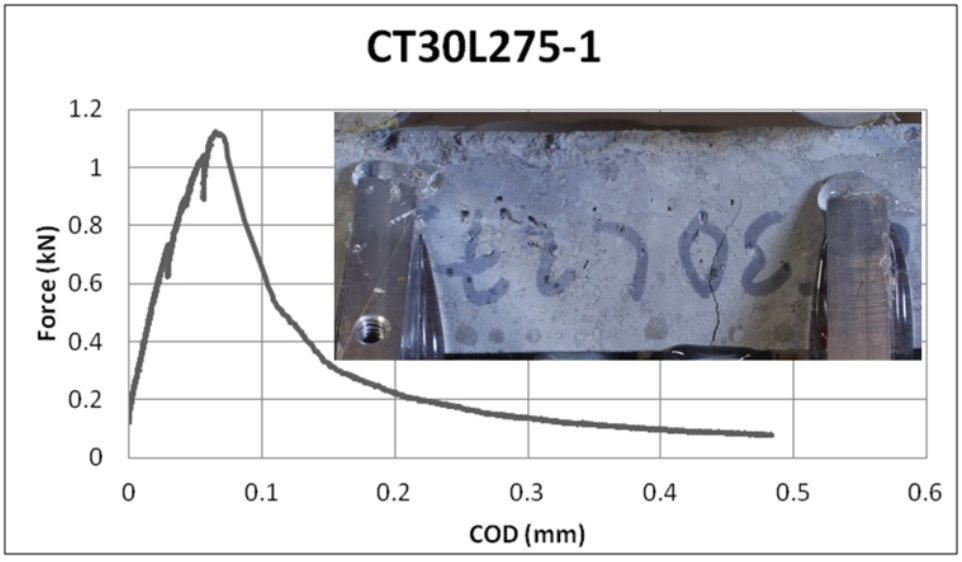

Figure A.1. CT30L275-1.

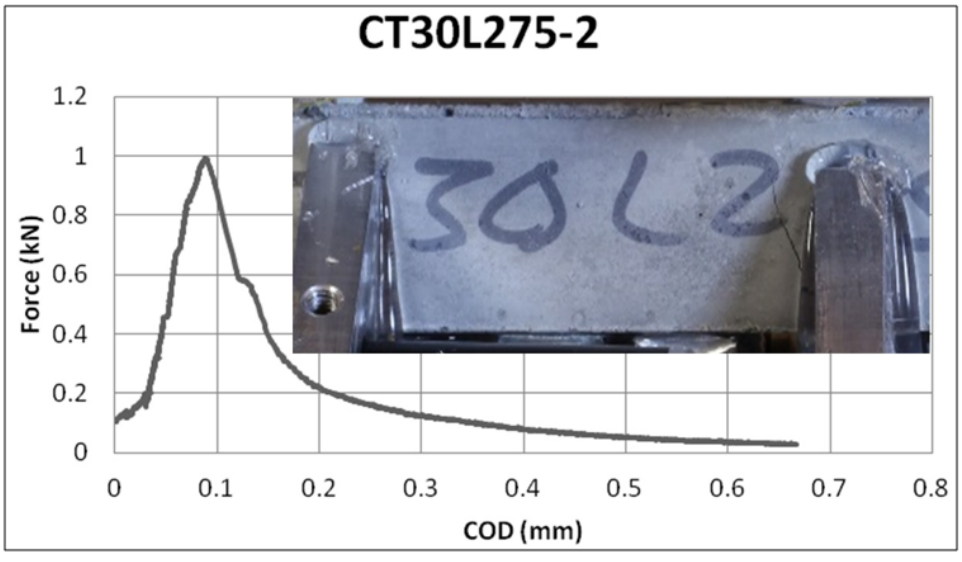

Figure A.2. CT30L275-2.

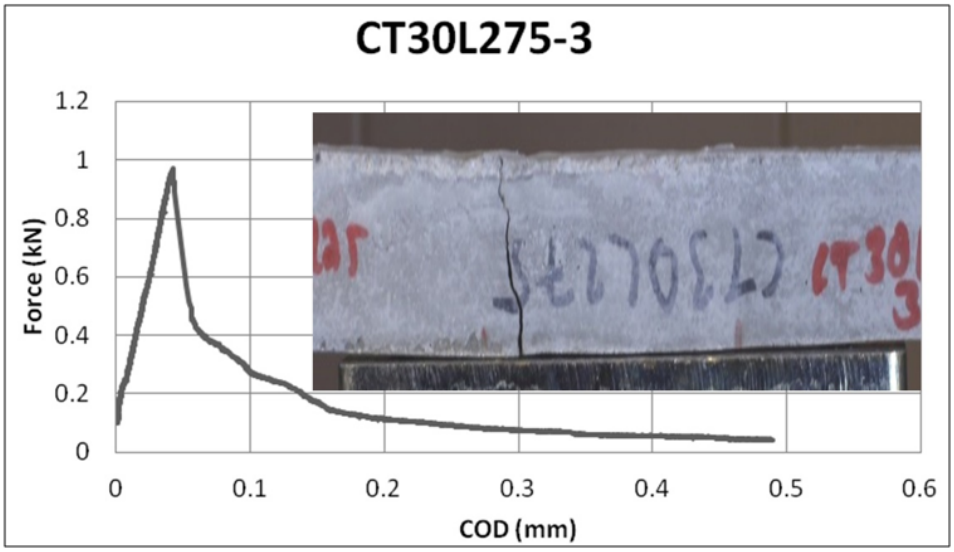

Figure A.3. CT30L275-3.

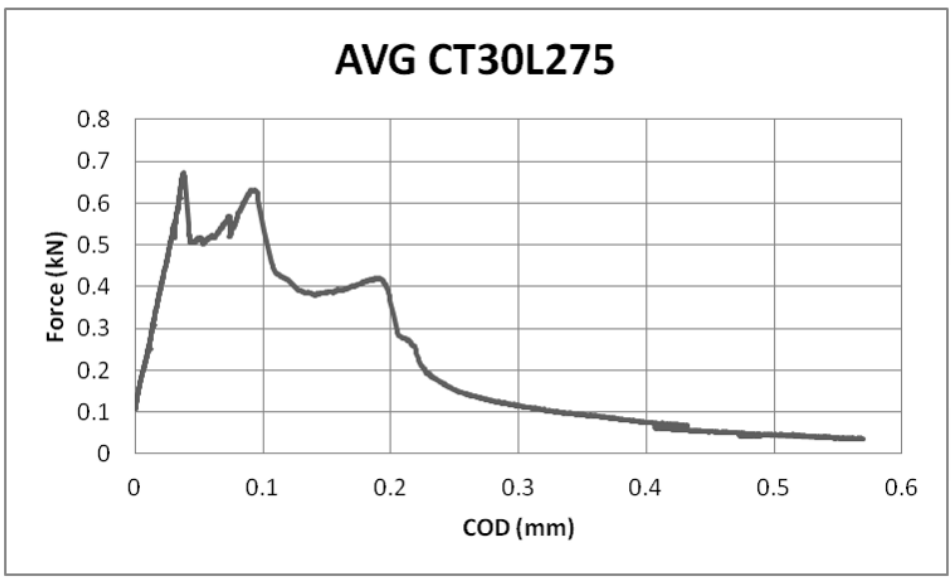

Figure A.4. AVG CT30L275.

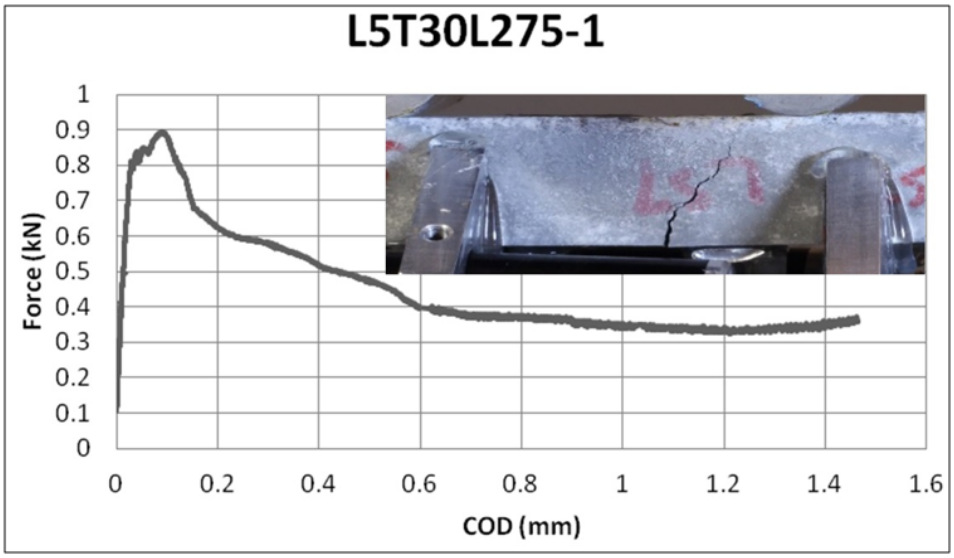

Figure A.5. L5T30L275-1.

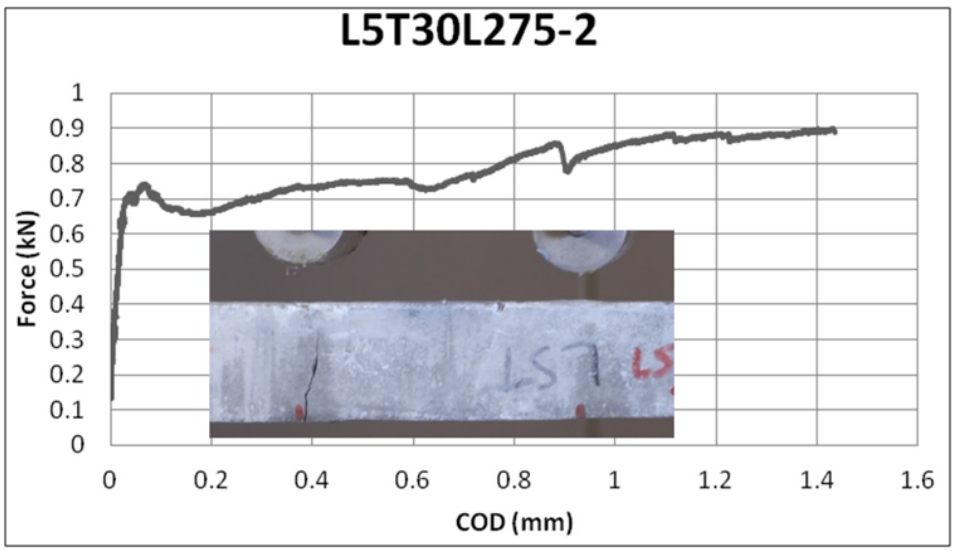

Figure A.6. L5T30L275-2.

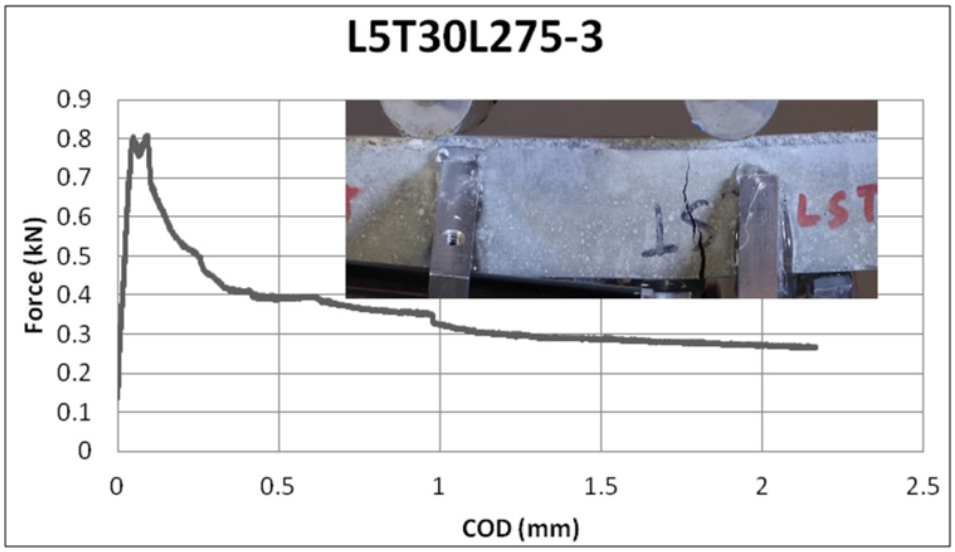

Figure A.7. L5T30L275-3.

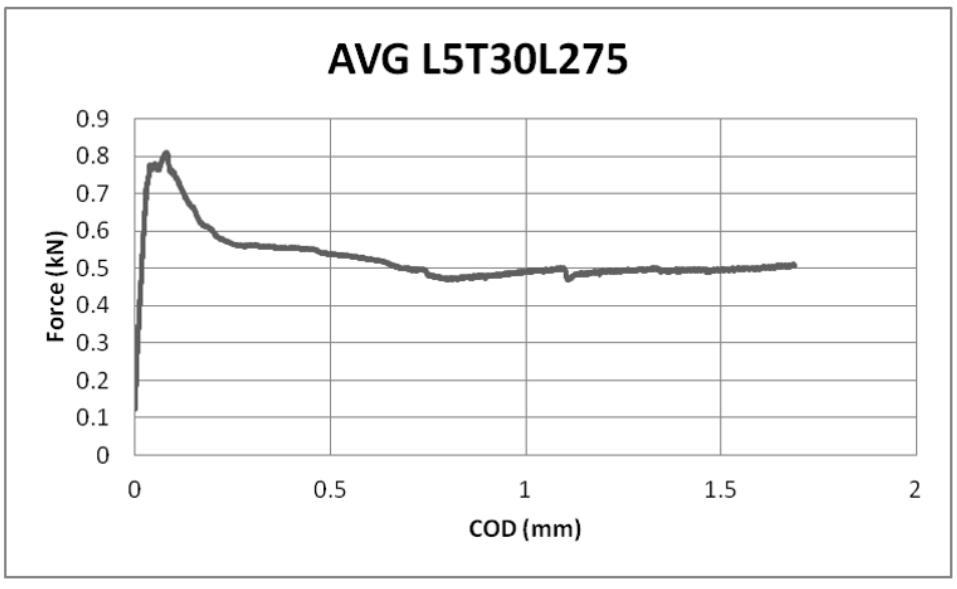

Figure A.8. AVG L5T30L275.

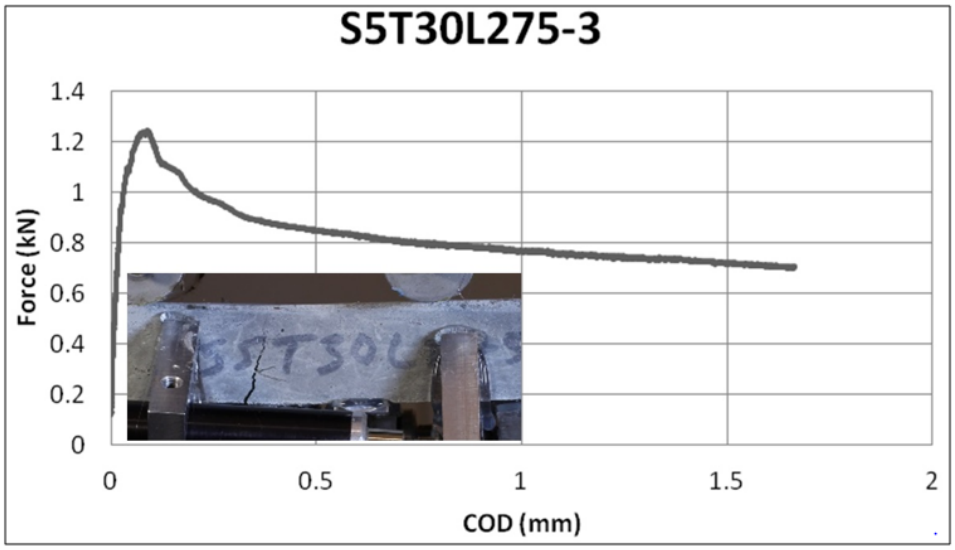

Figure A.9. S5T30L275-3.

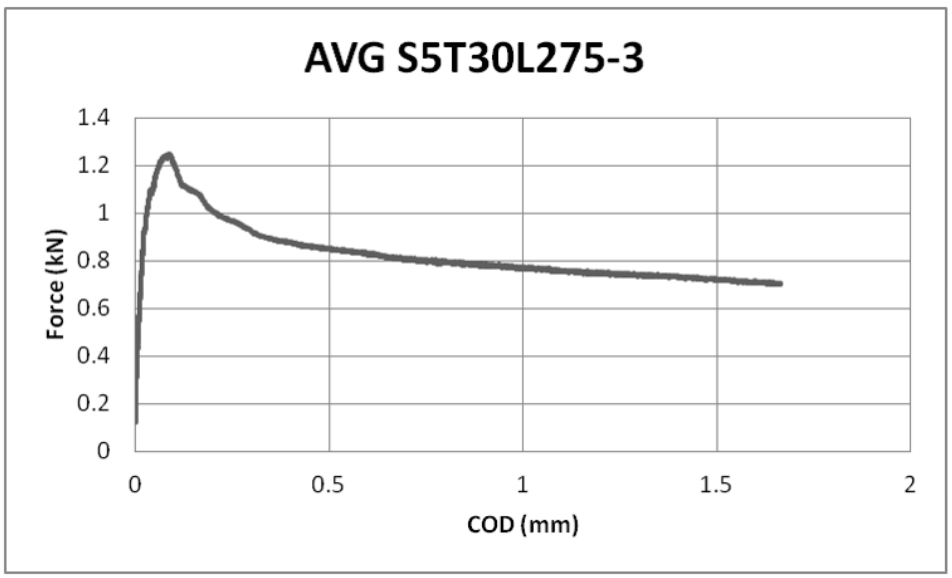

Figure A.10. AVG S5T30L275-3.

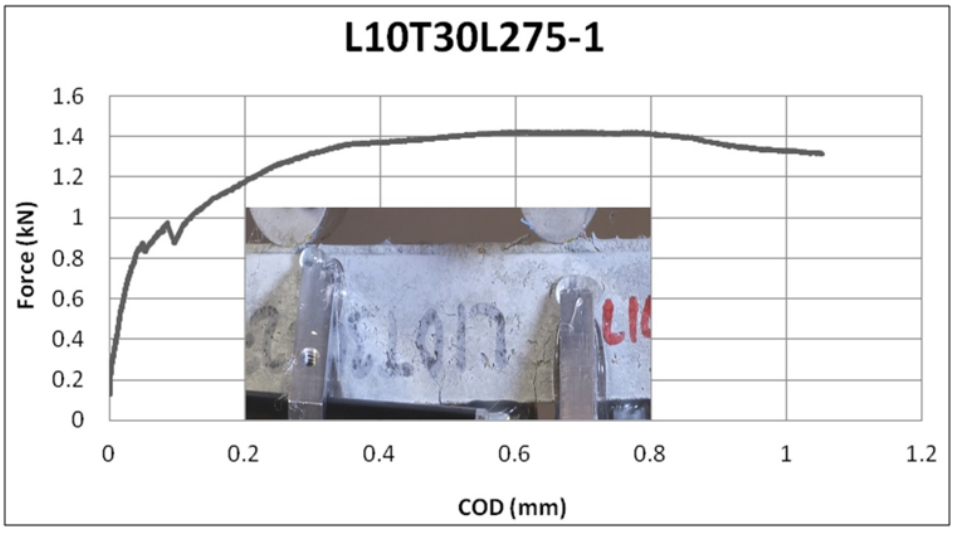

Figure A.11. L10T30L275-1.

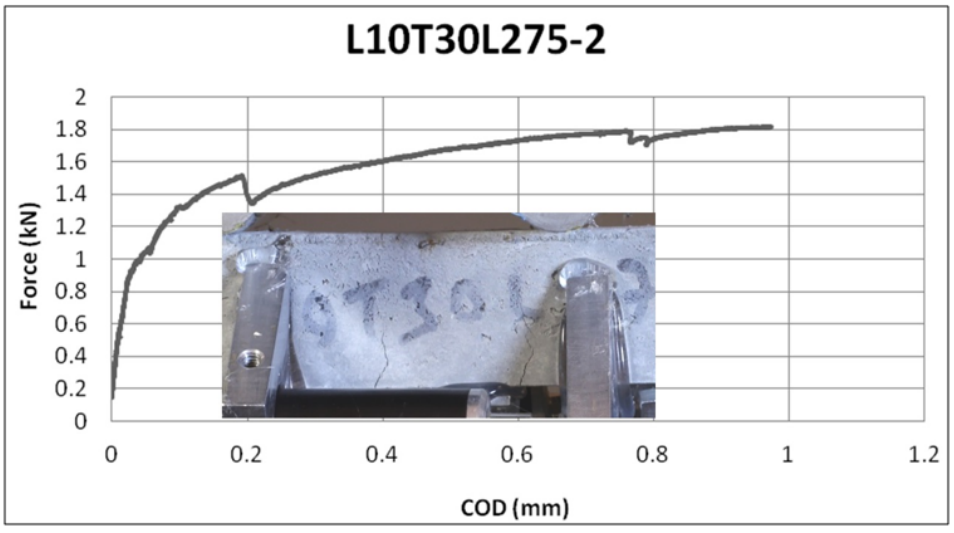

Figure A.12. L10T30L275-2.

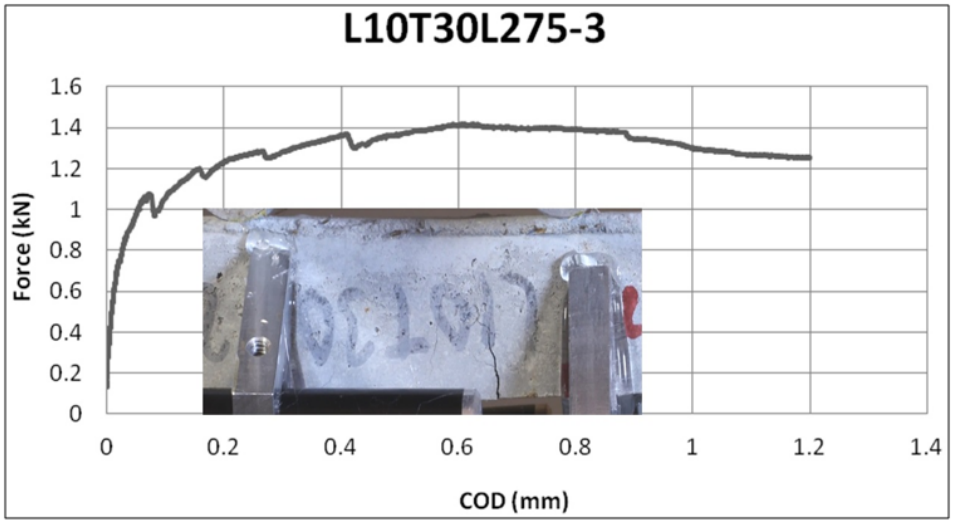

Figure A.13. L10T30L275-3.

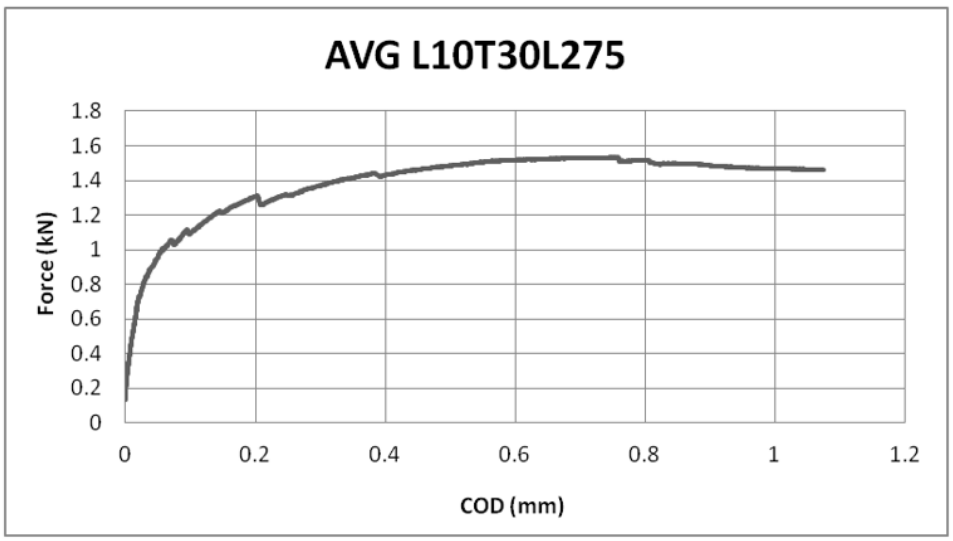

Figure A.14. AVG L10T30L275.

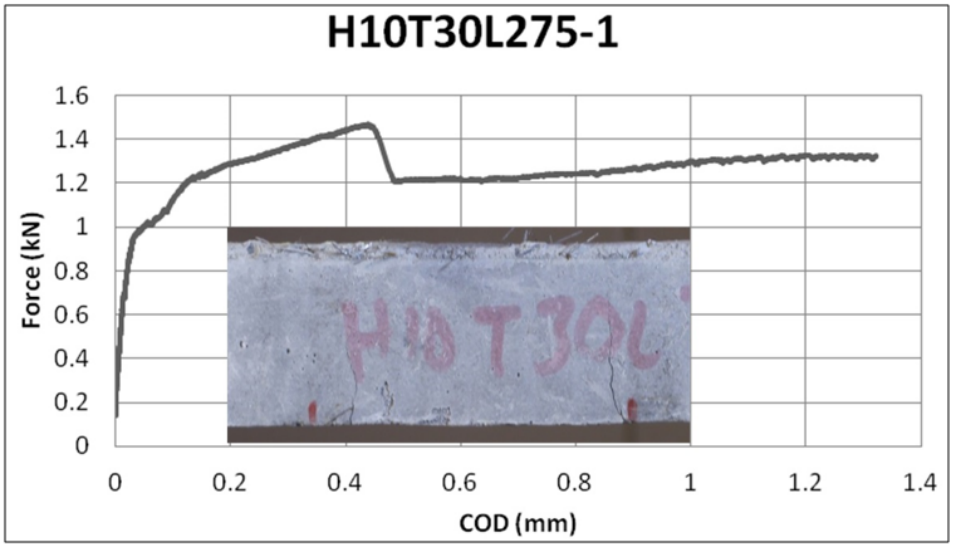

Figure A.15. H10T30L275-1.

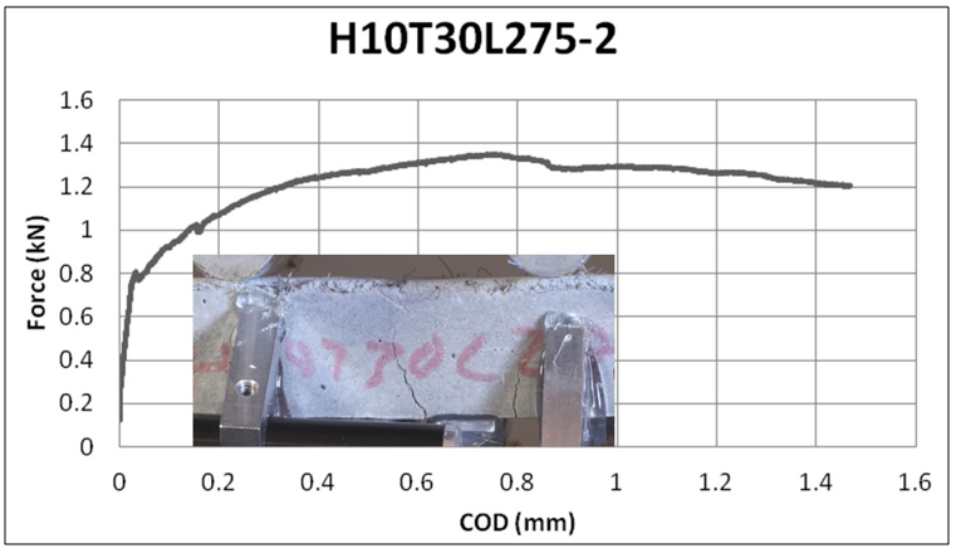

Figure A.16. H10T30L275-2.

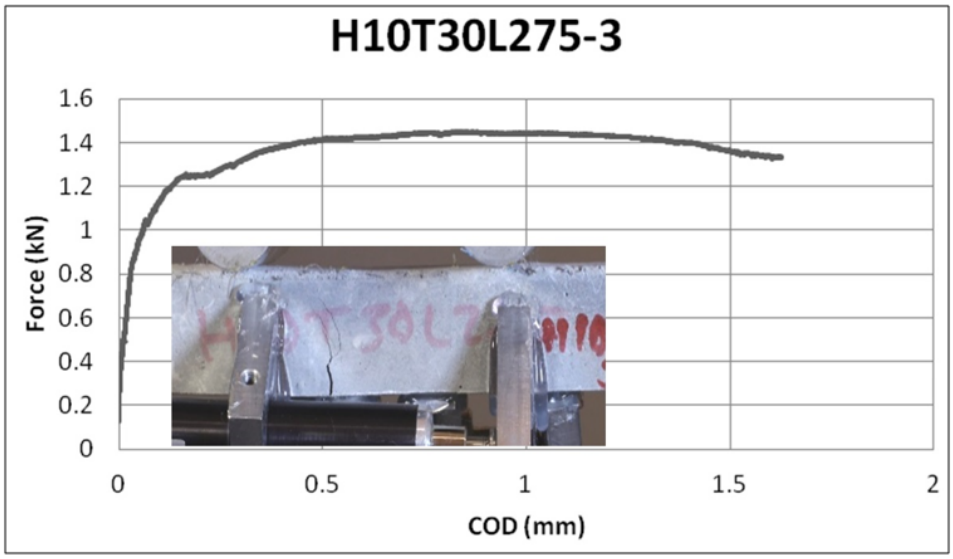

Figure A.17. H10T30L275-3.

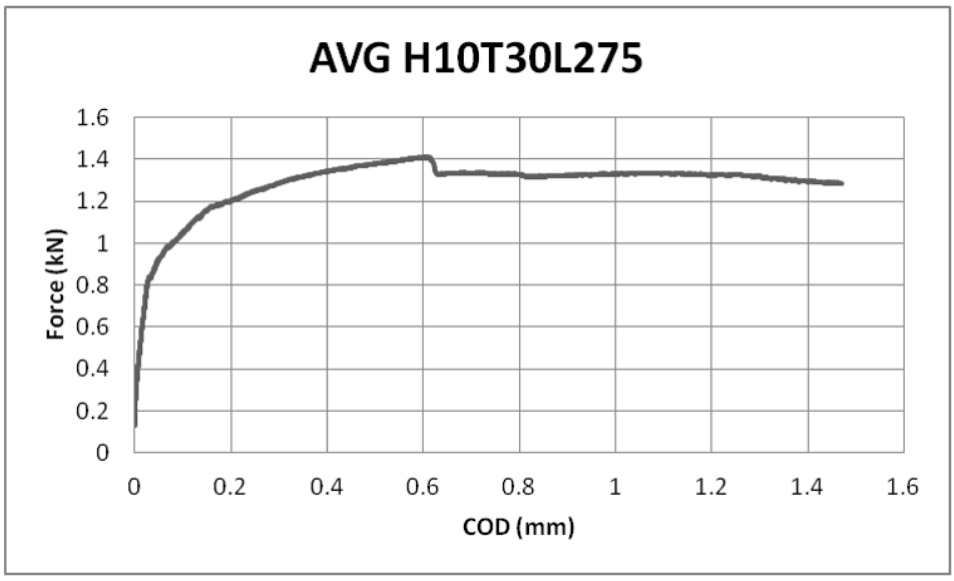

Figure A.18. AVG H10T30L275.

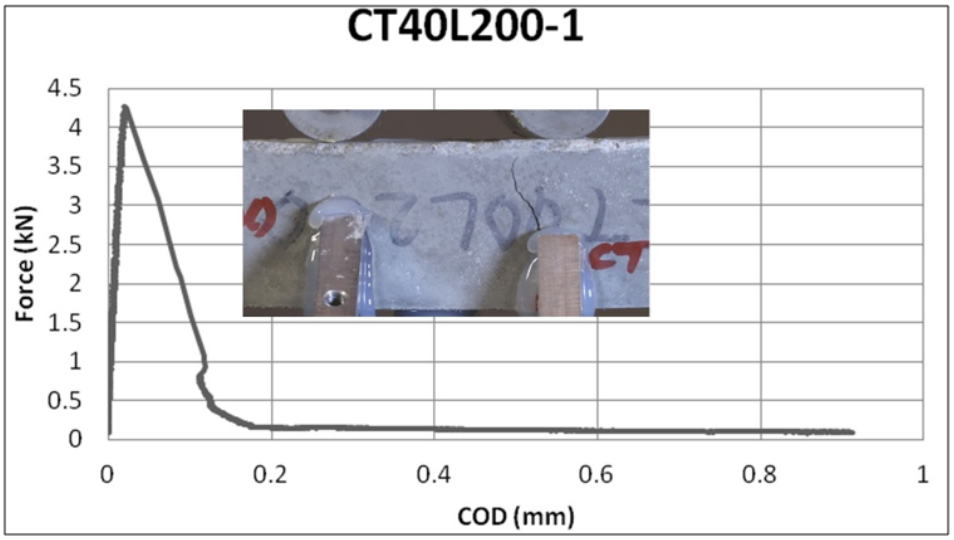

Figure A.19. CT40L200-1.

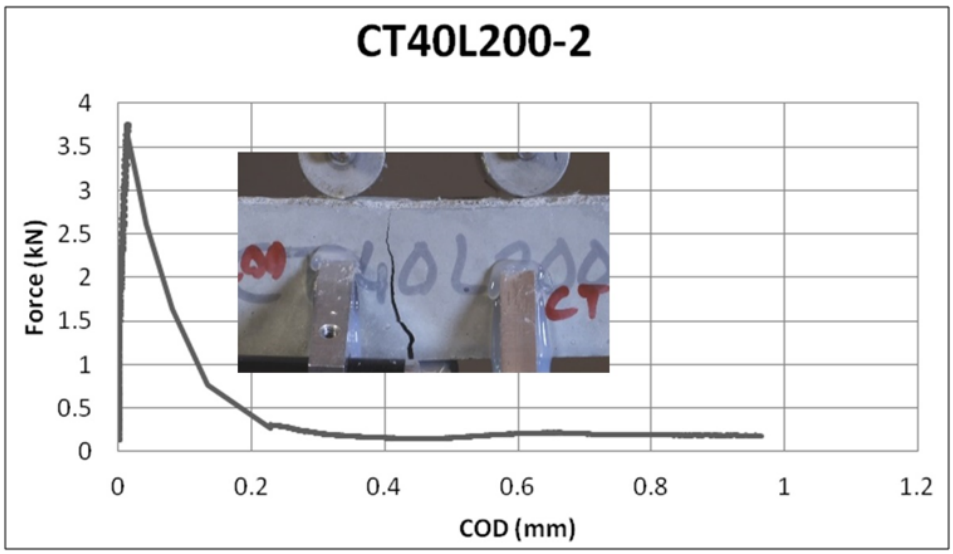

Figure A.20. CT40L200-2.

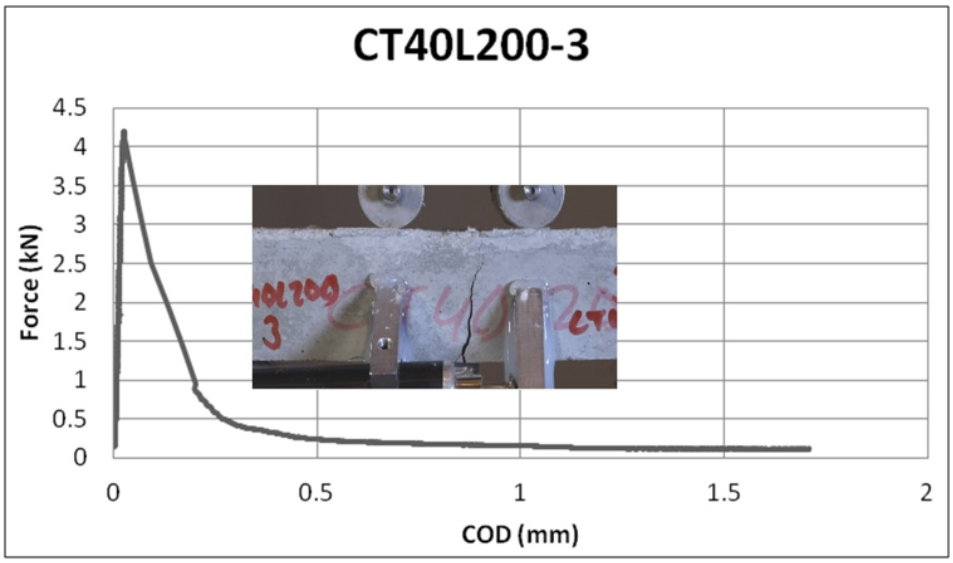

Figure A.21. CT40L200-3.

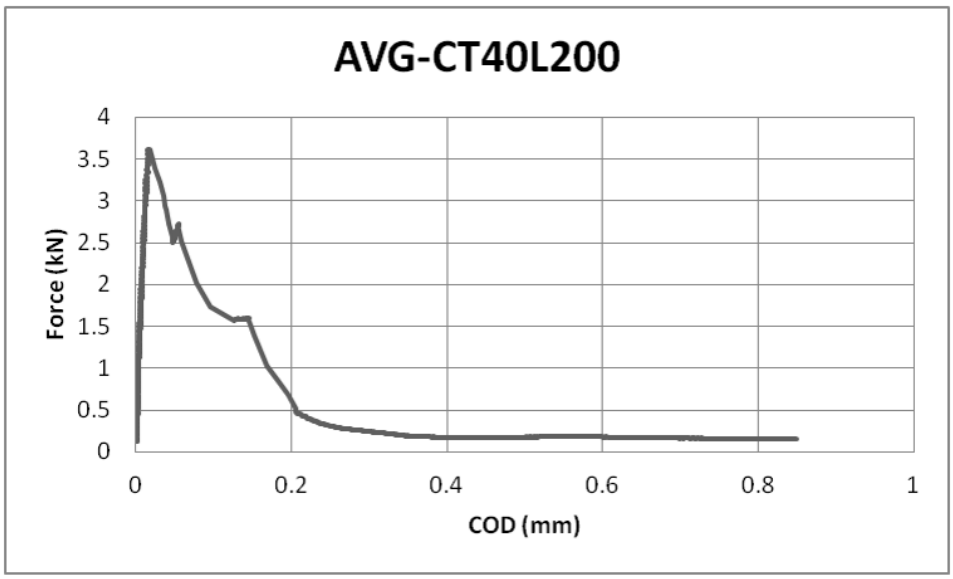

Figure A.22. AVG-CT40L200.

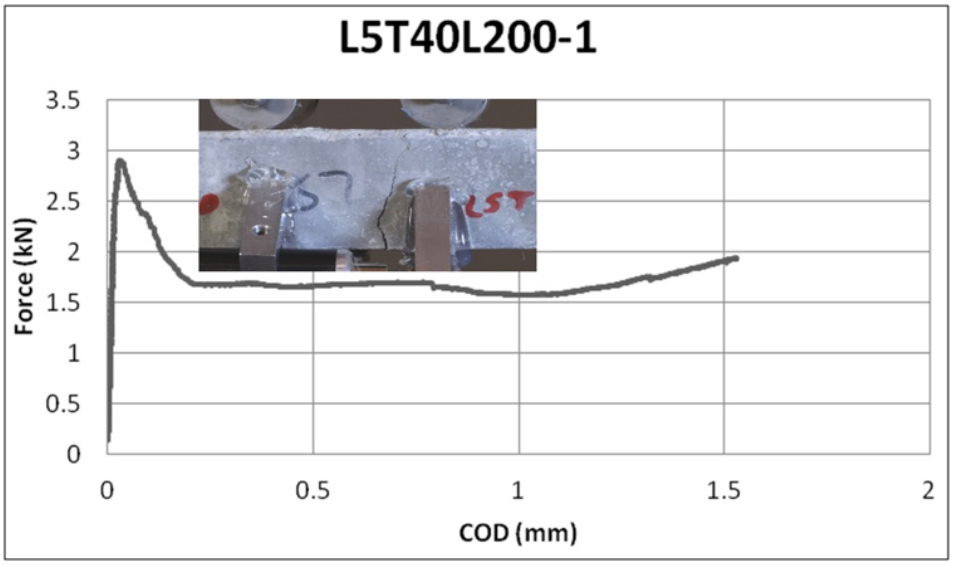

Figure A.23. L5T40L200-1.

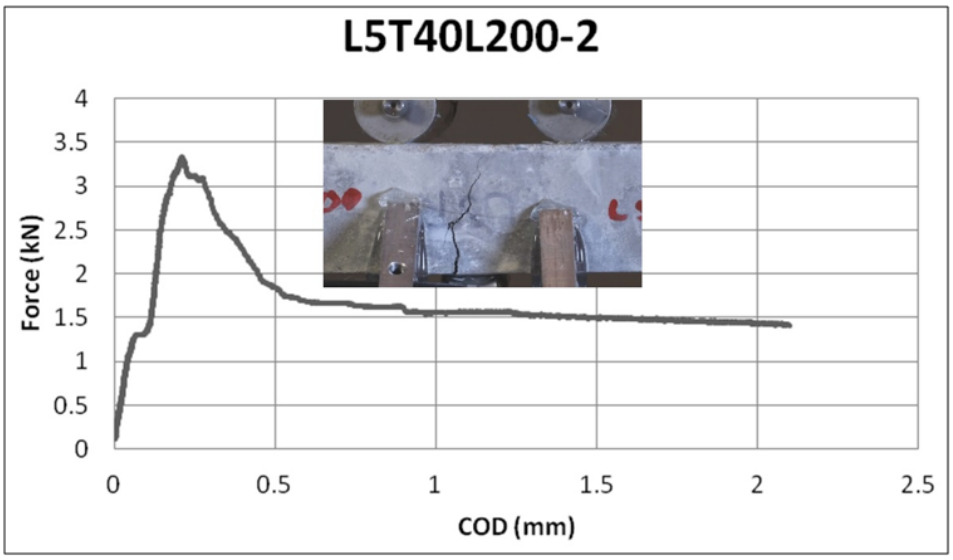

Figure A.24. L5T40L200-2.

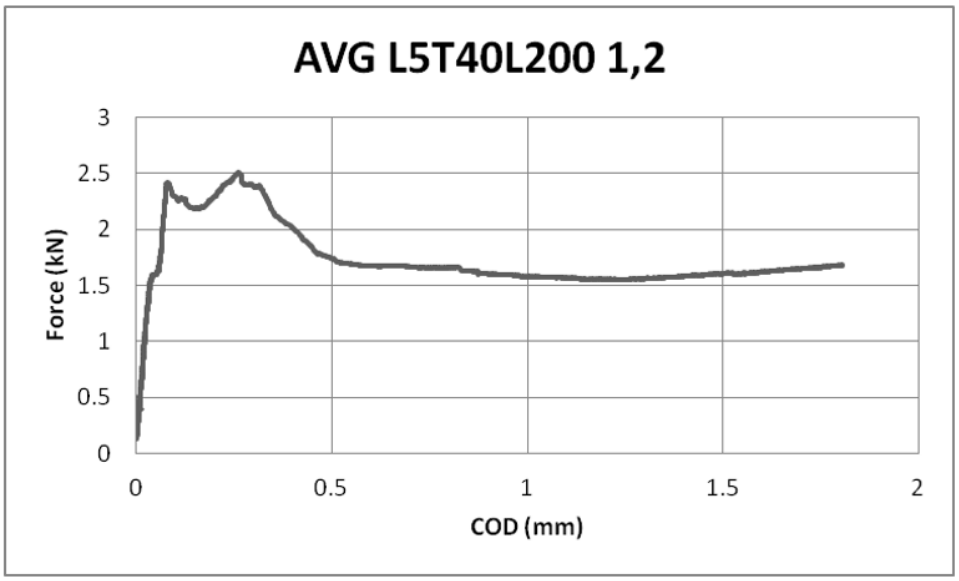

Figure A.25. AVG L5T40L200 1,2.

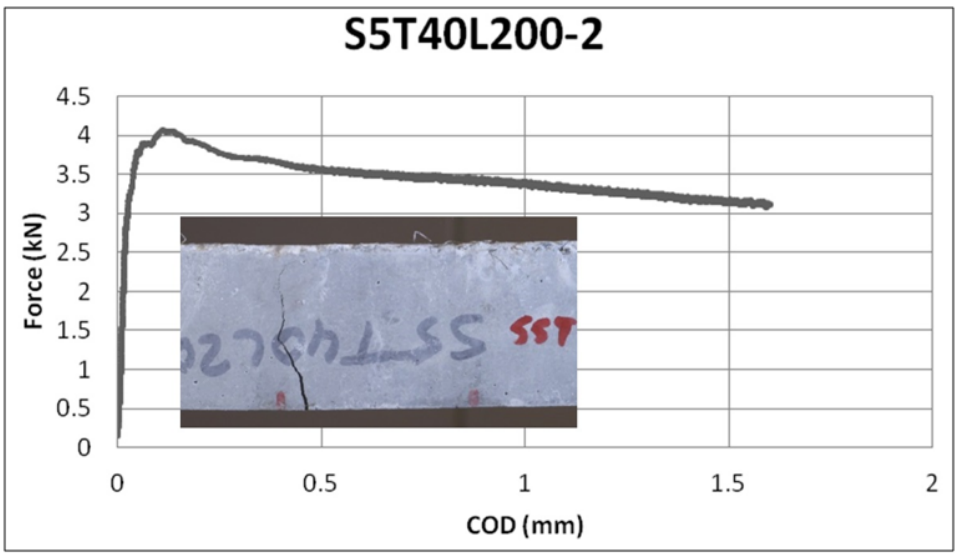

Figure A.26. S5T40L200-2.

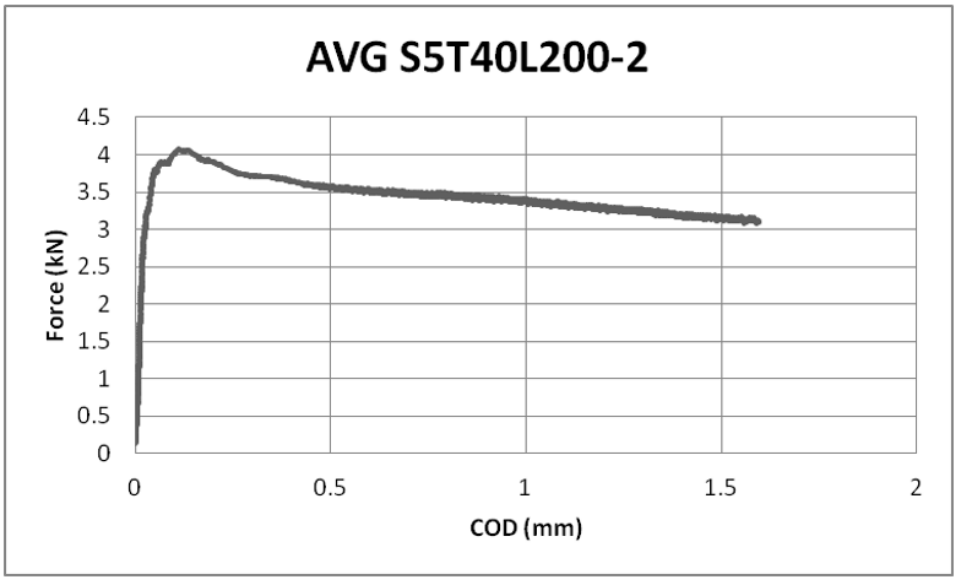

Figure A.27. AVG S5T40L200-2.

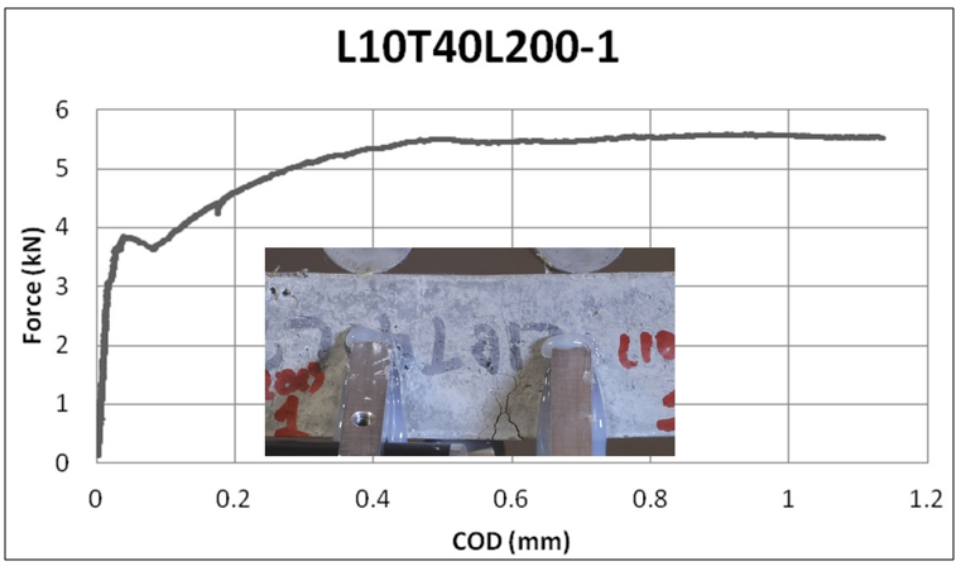

Figure A.28. L10T40L200-1.

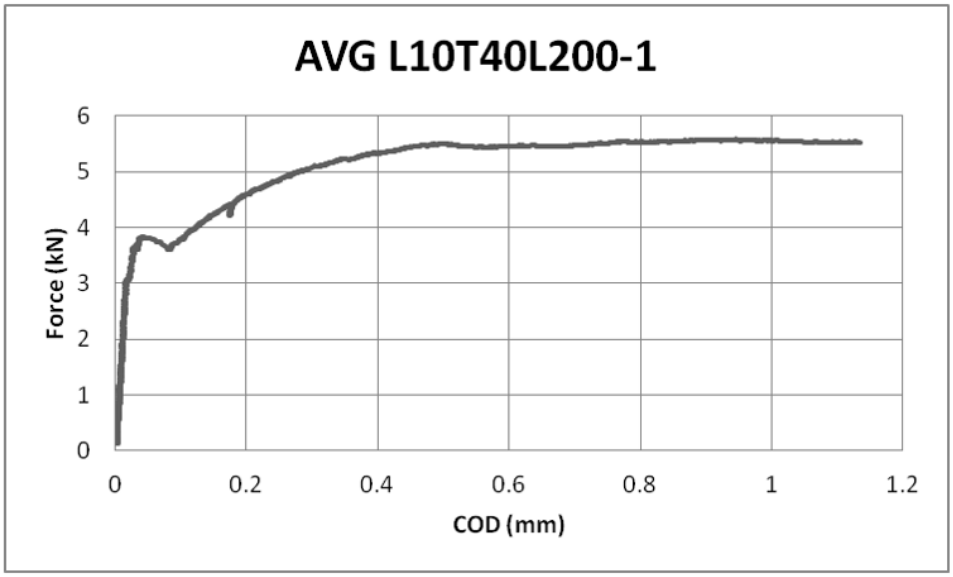

Figure A.29. AVG L10T40L200-1.

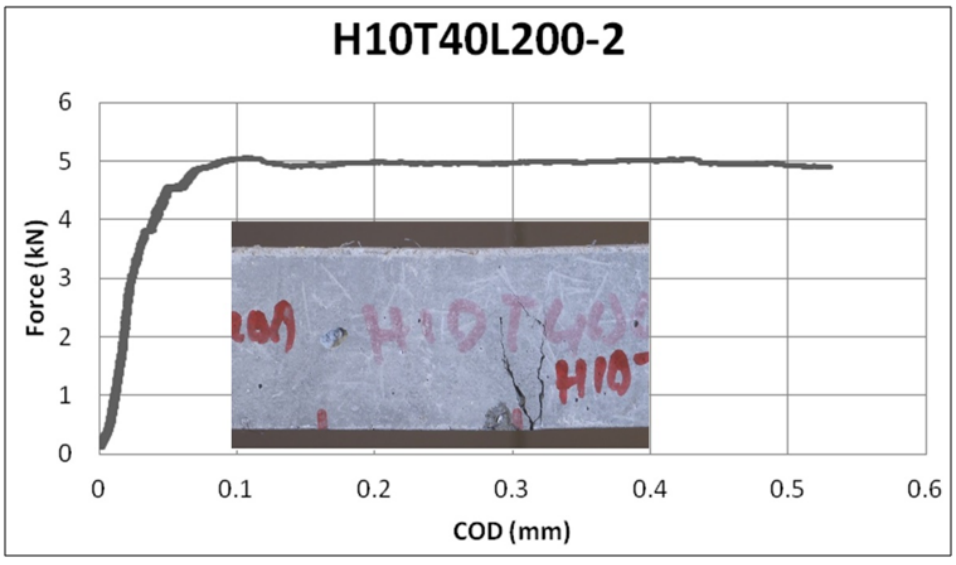

Figure A.30. H10T40L200-2.

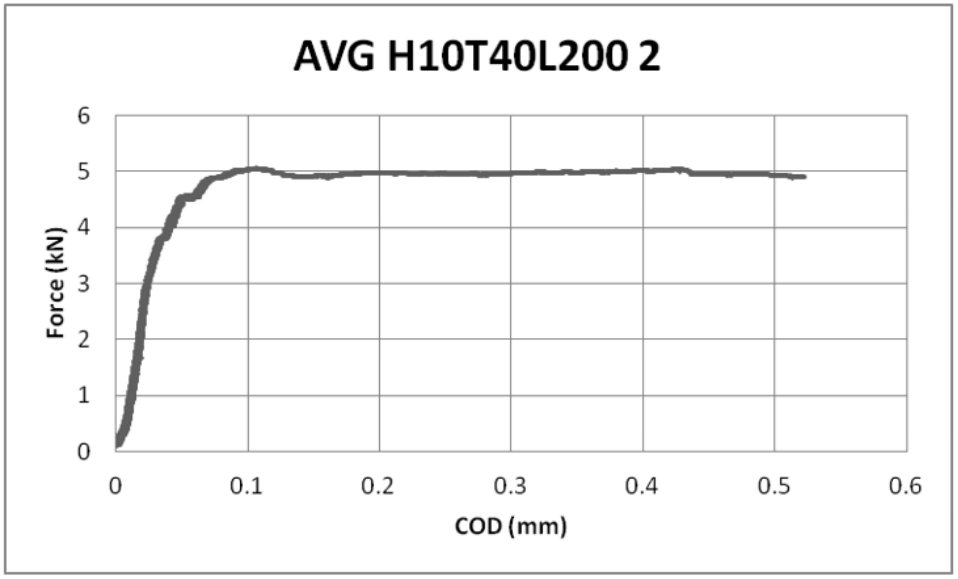

Figure A.31. AVG H10T40L200 2.

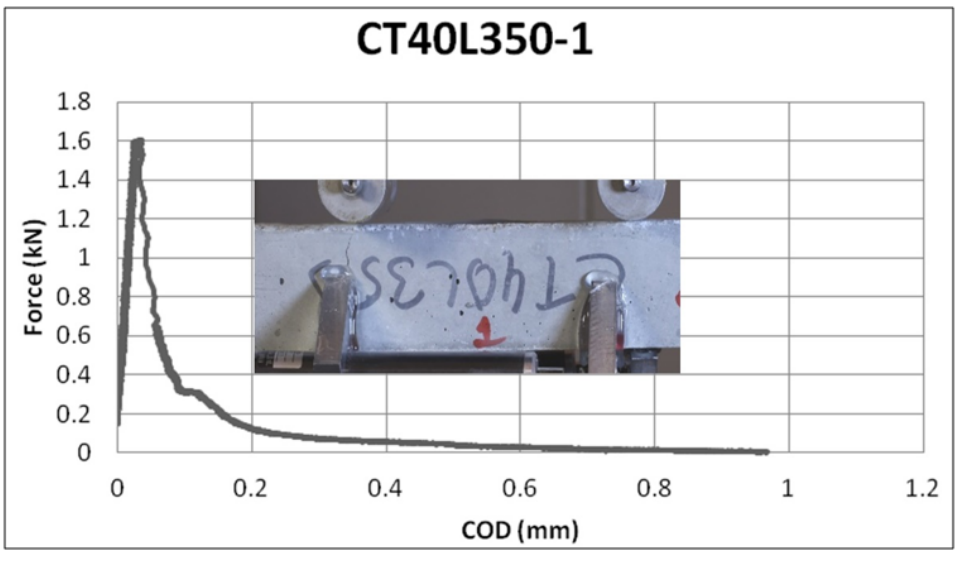

Figure A.32. CT40L350-1.

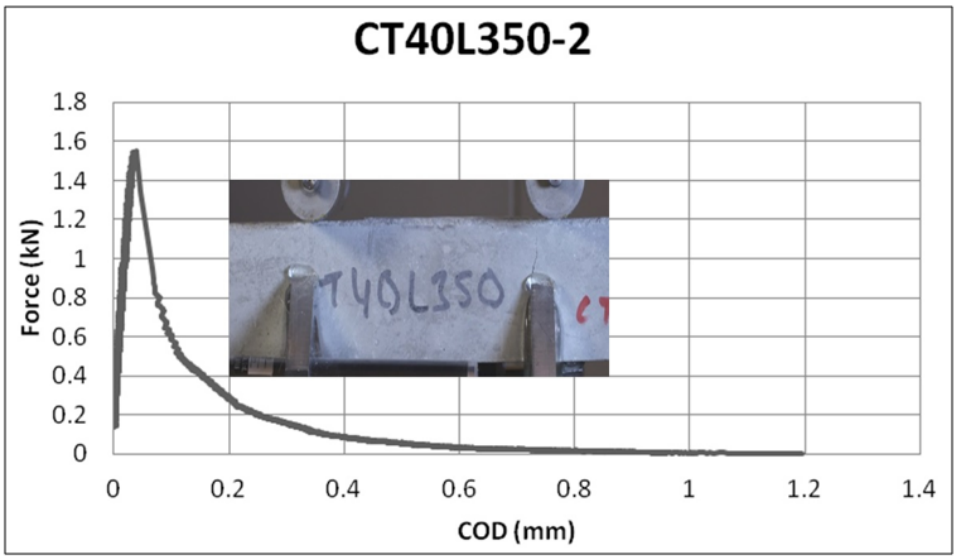

Figure A.33. CT40L350-2.

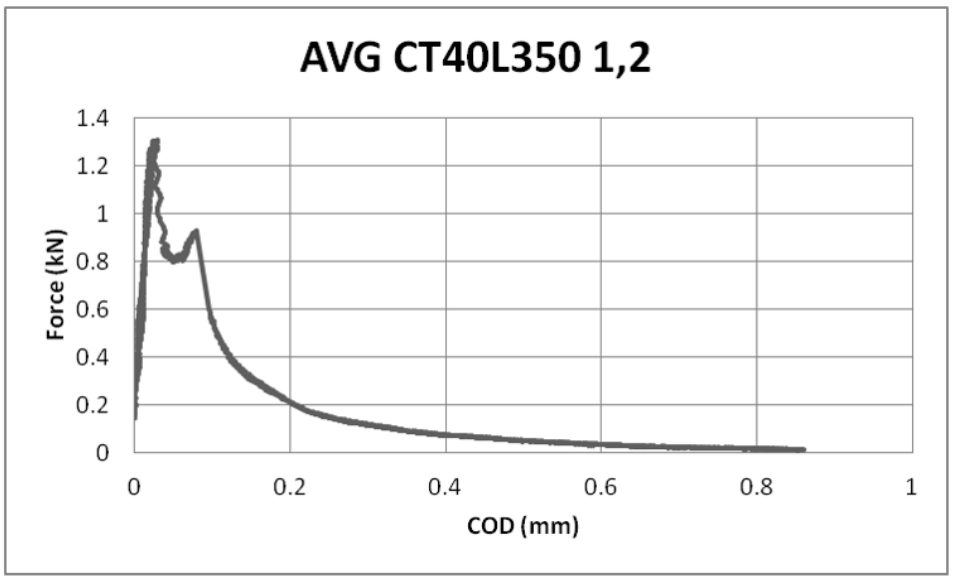

Figure A.34. AVG CT40L350 1,2.

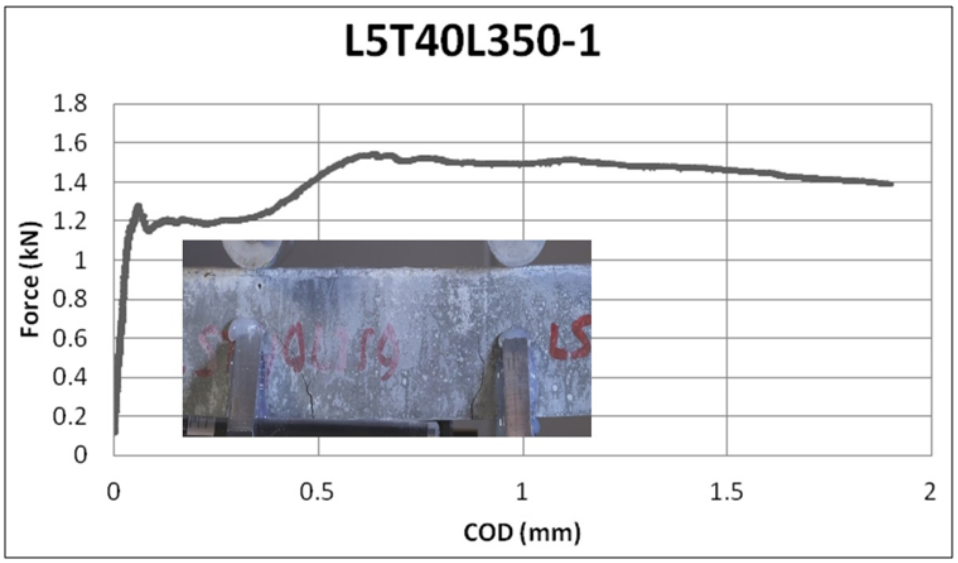

Figure A.35. L5T40L350-1.

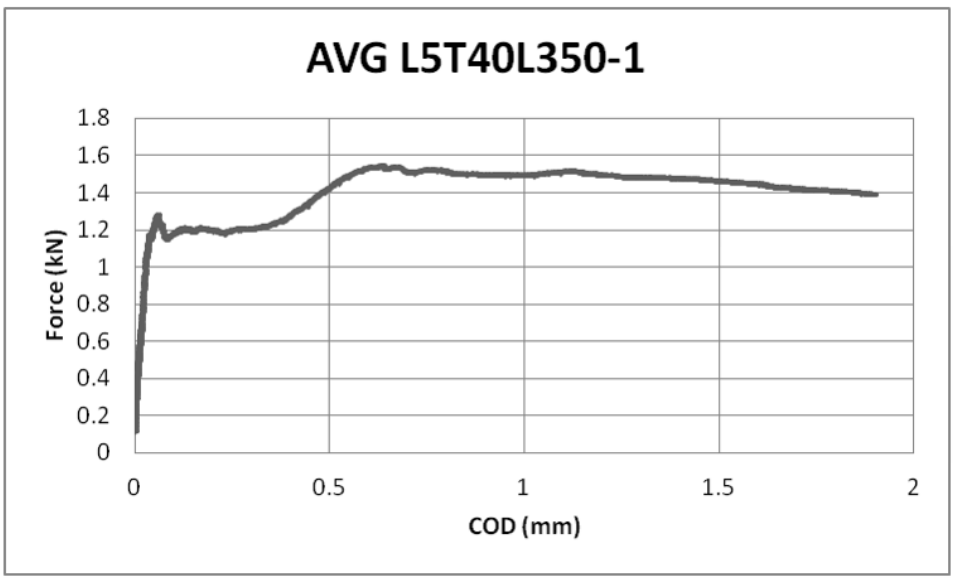

Figure A.36. AVG L5T40L350-1.

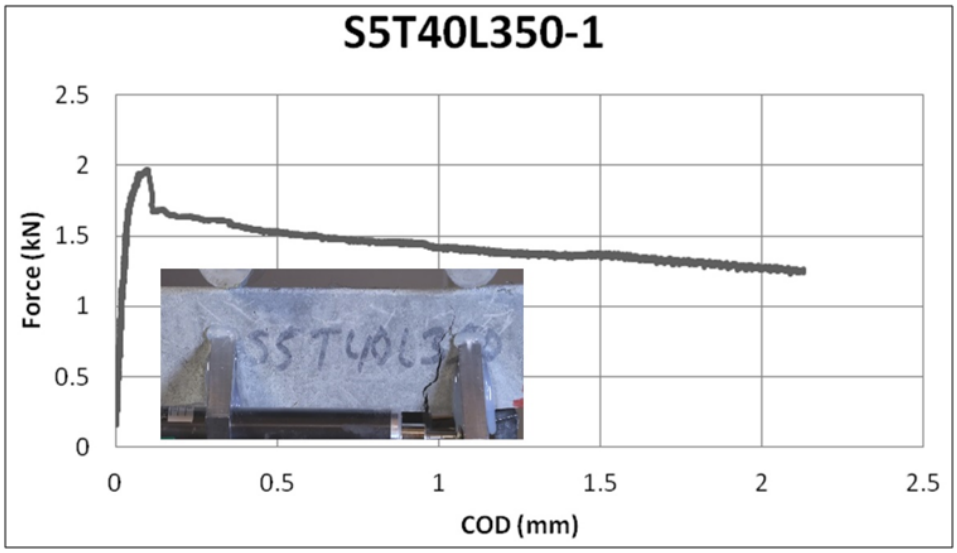

Figure A.37. S5T40L350-1.

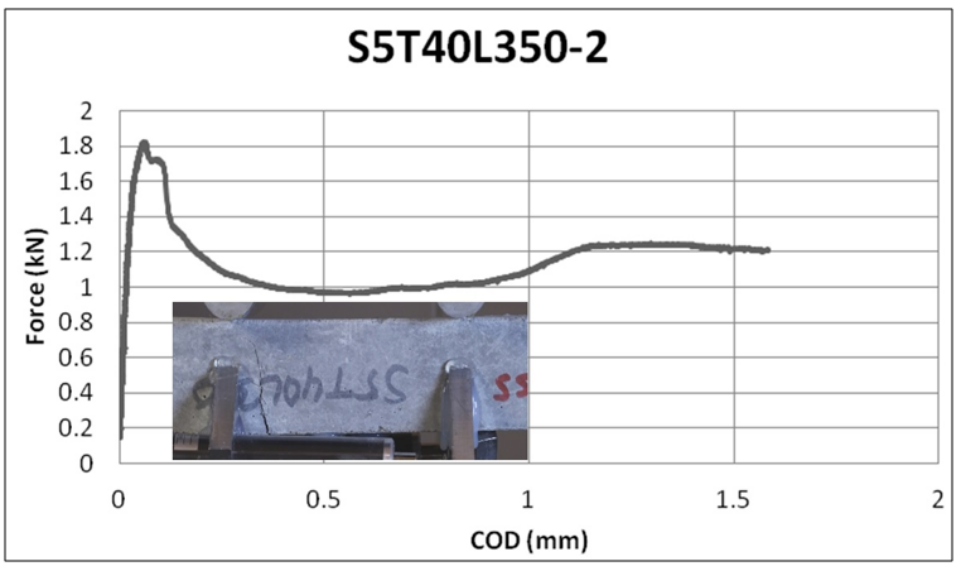

Figure A.38. S5T40L350-2.

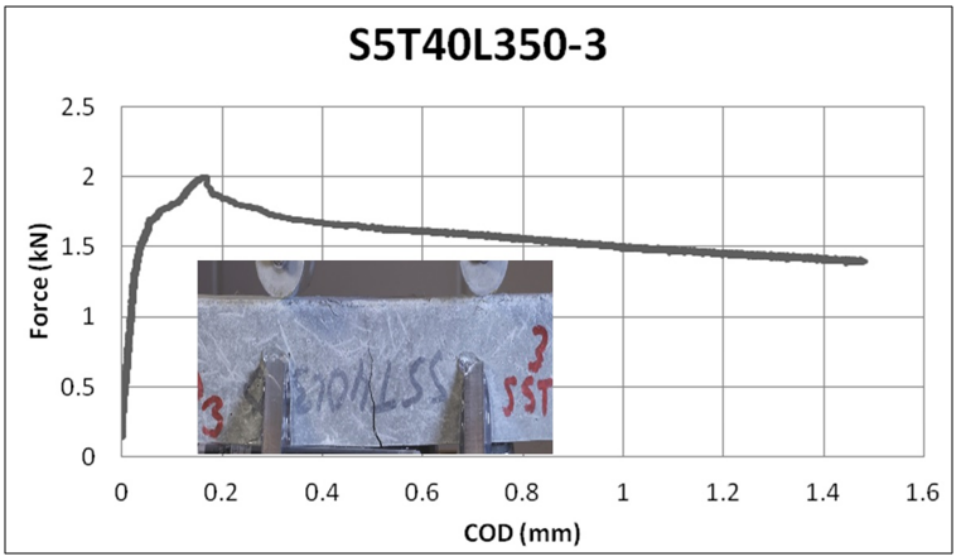

Figure A.39. S5T40L350-3.

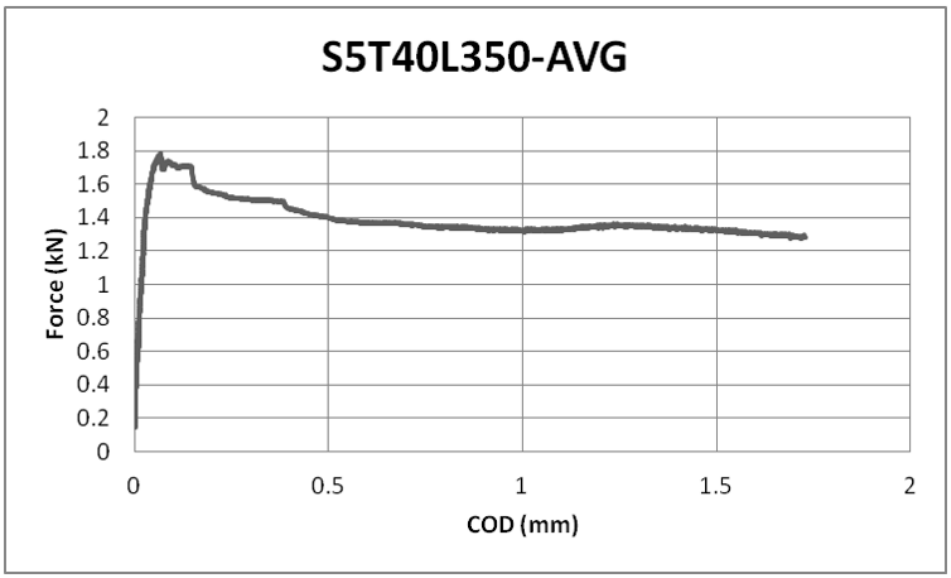

Figure A.40. S5T40L350-AVG.

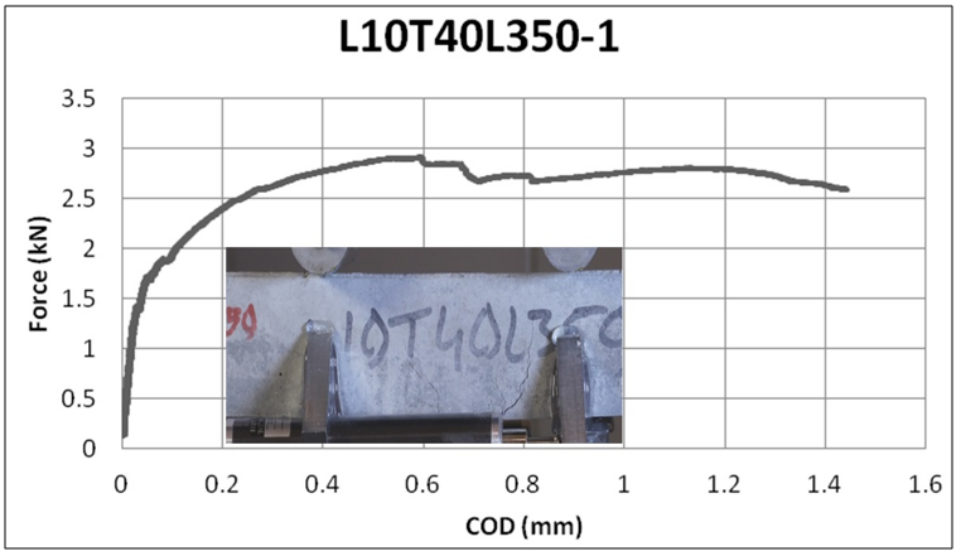

Figure A.41. L10T40L350-1.

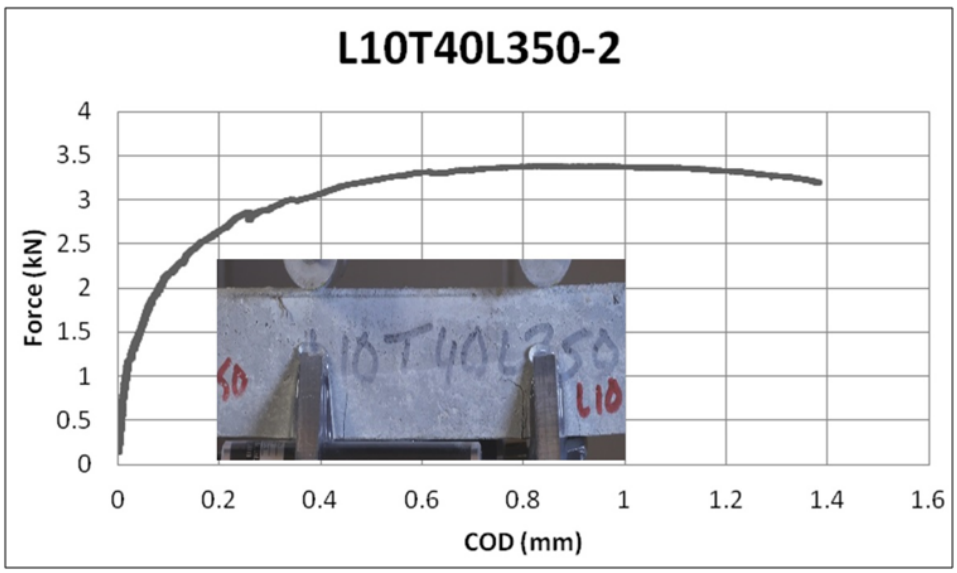

Figure A.42. L10T40L350-2.

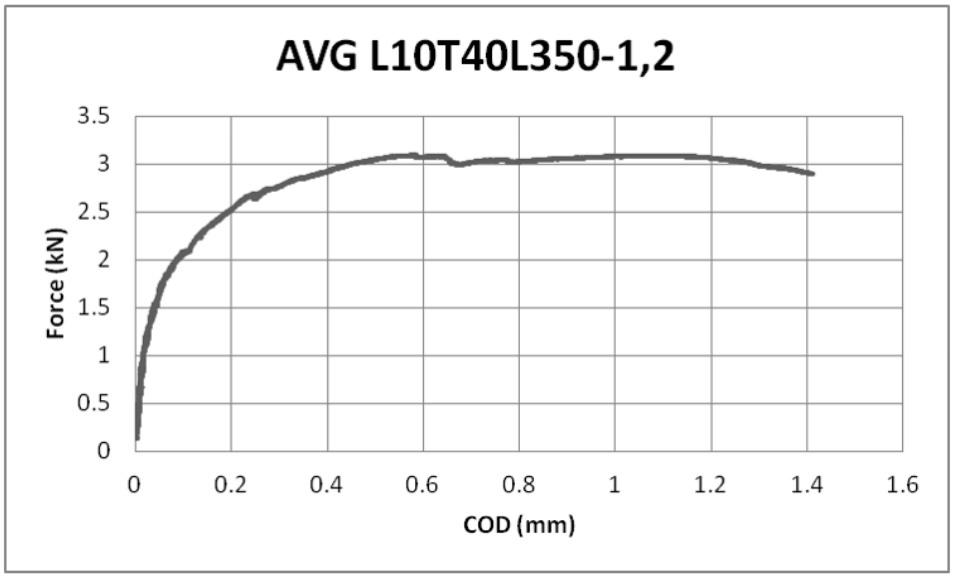

Figure A.43. AVG L10T40L350-1,2.

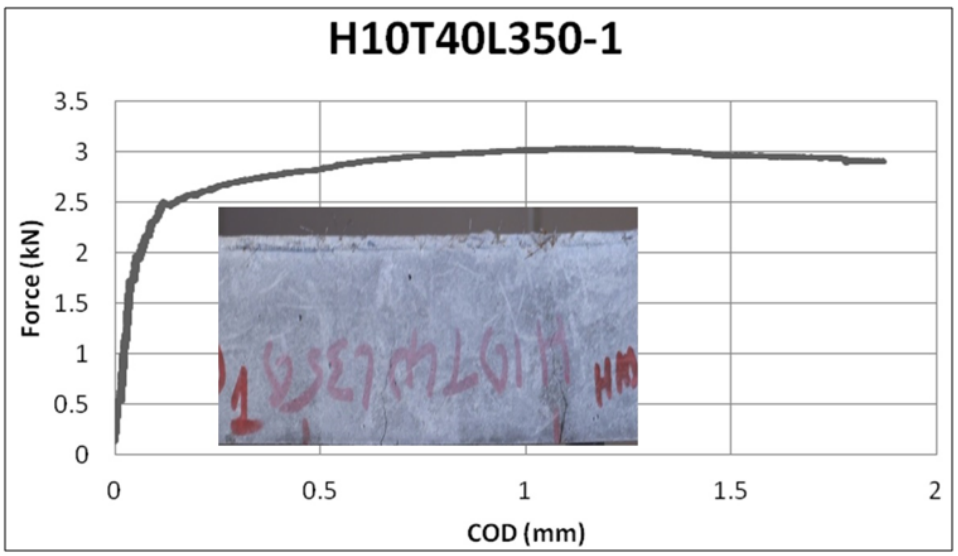

Figure A.44. H10T40L350-1.

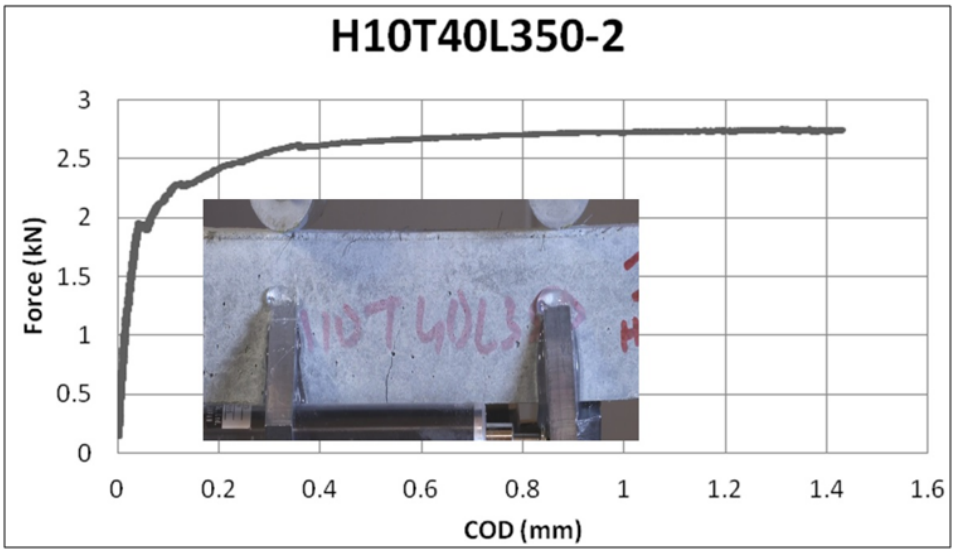

Figure A.45. H10T40L350-2.

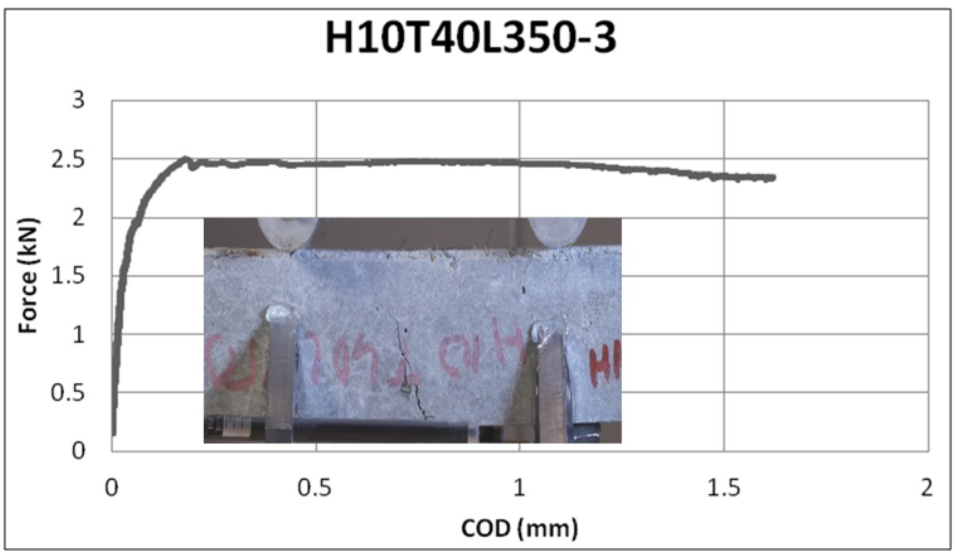

Figure A.46. H10T40L350-3.

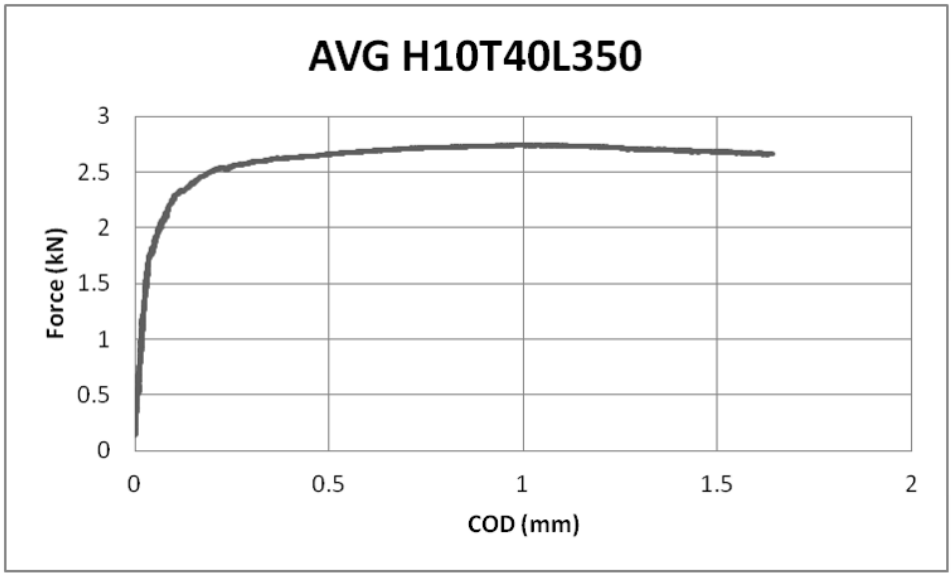

Figure A.47. AVG H10T40L350.

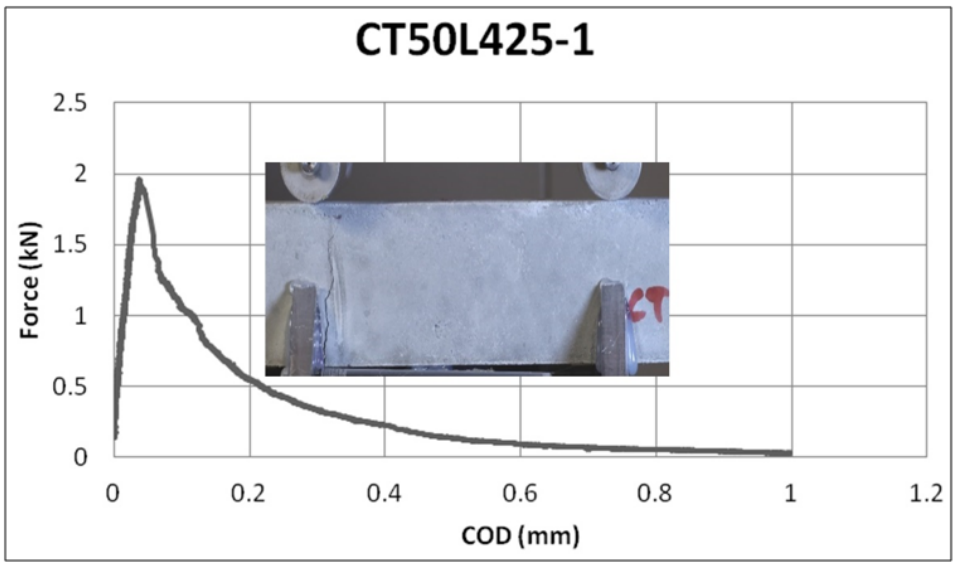

Figure A.48. CT50L425-1.

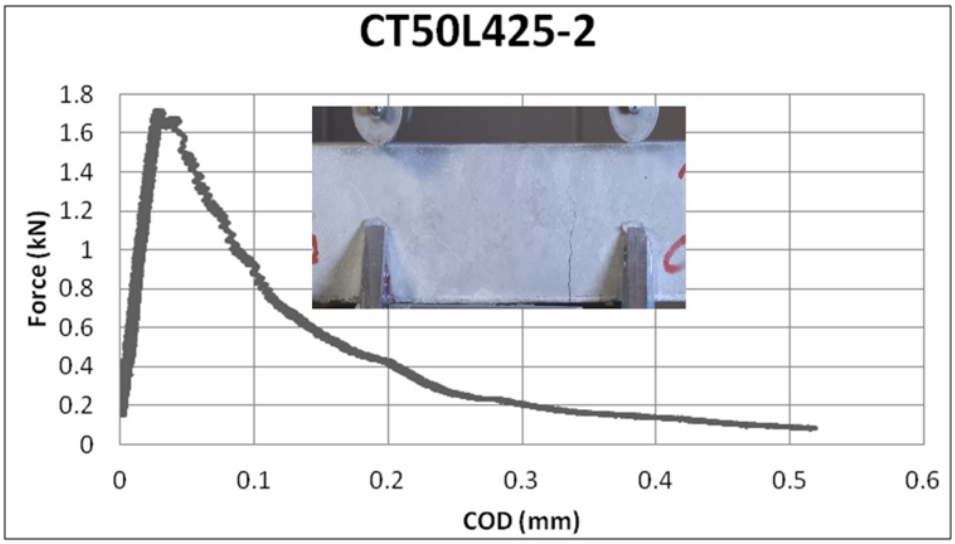

Figure A.49. CT50L425-2.

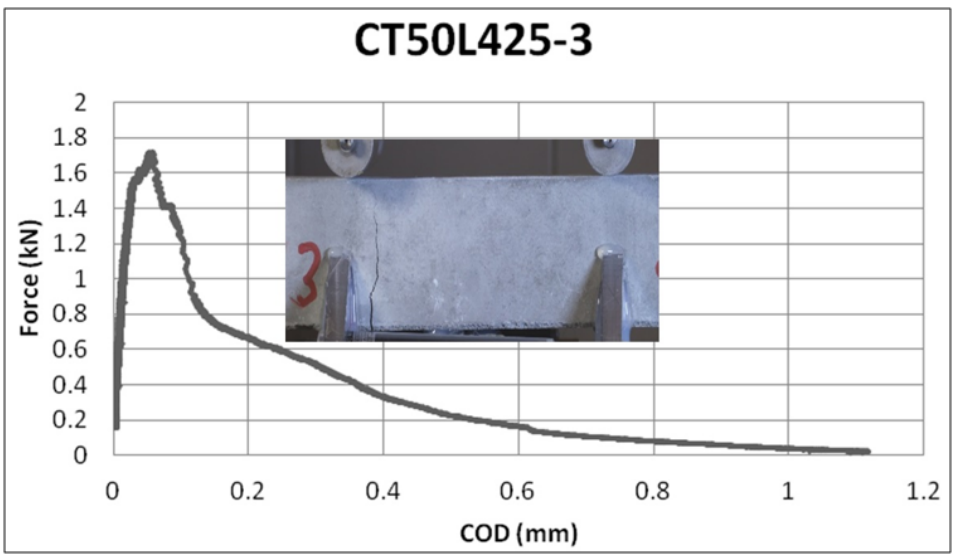

Figure A.50. CT50L425-3.

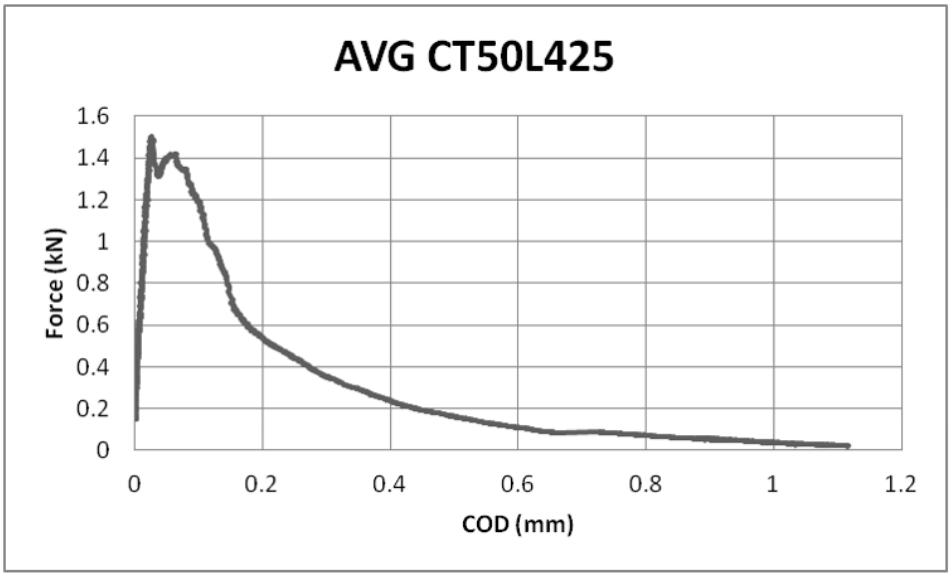

Figure A.51. AVG CT50L425.

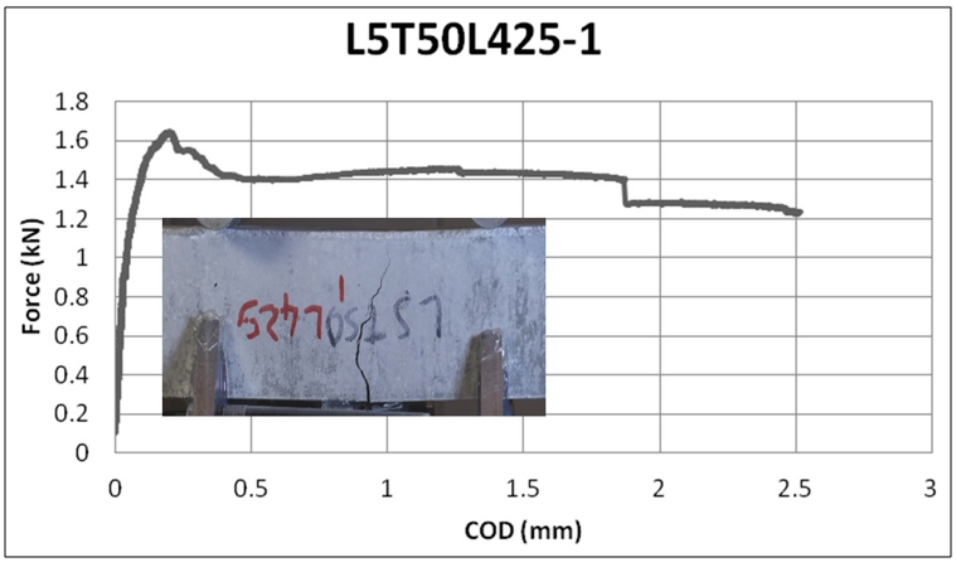

Figure A.52. L5T50L425-1.

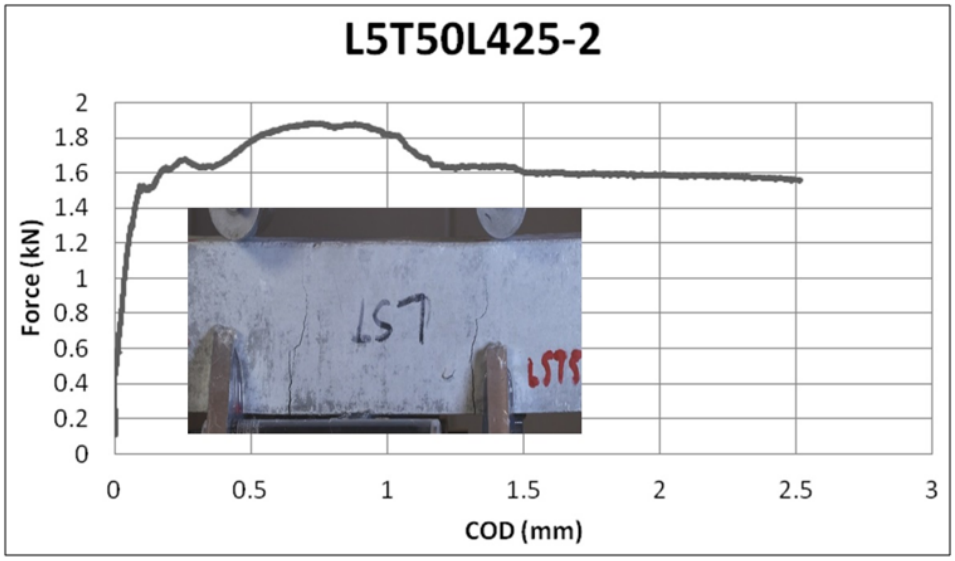

Figure A.53. L5T50L425-2.

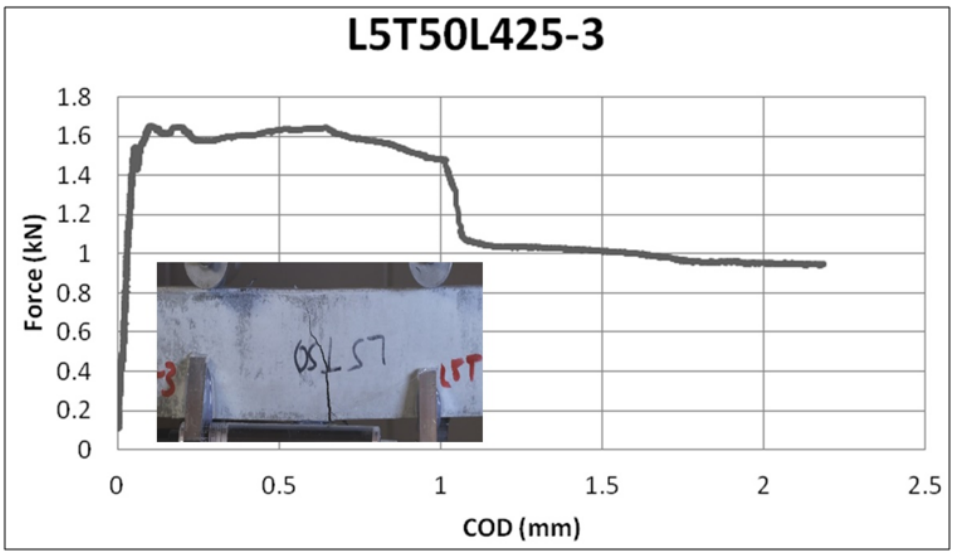

Figure A.54. L5T50L425-3.

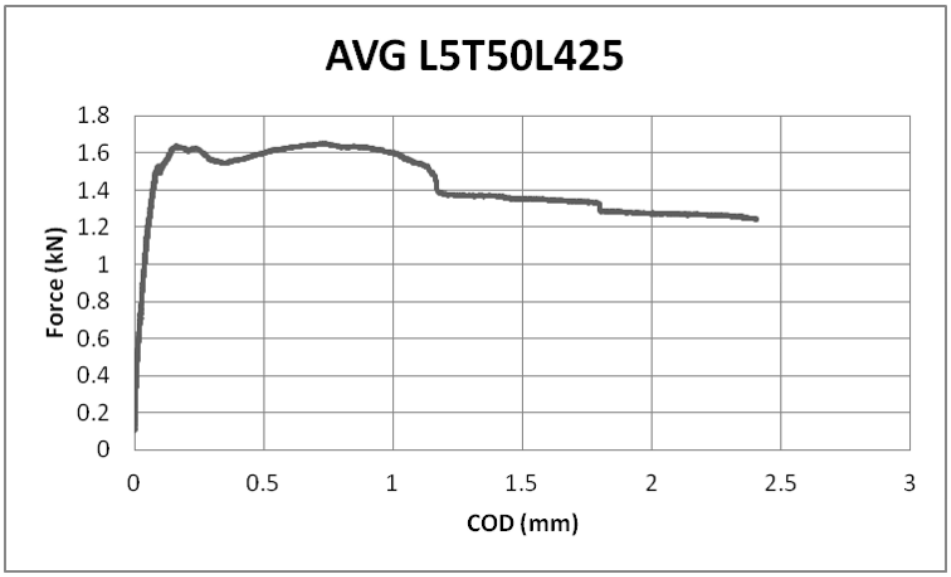

Figure A.55. AVG L5T50L425.

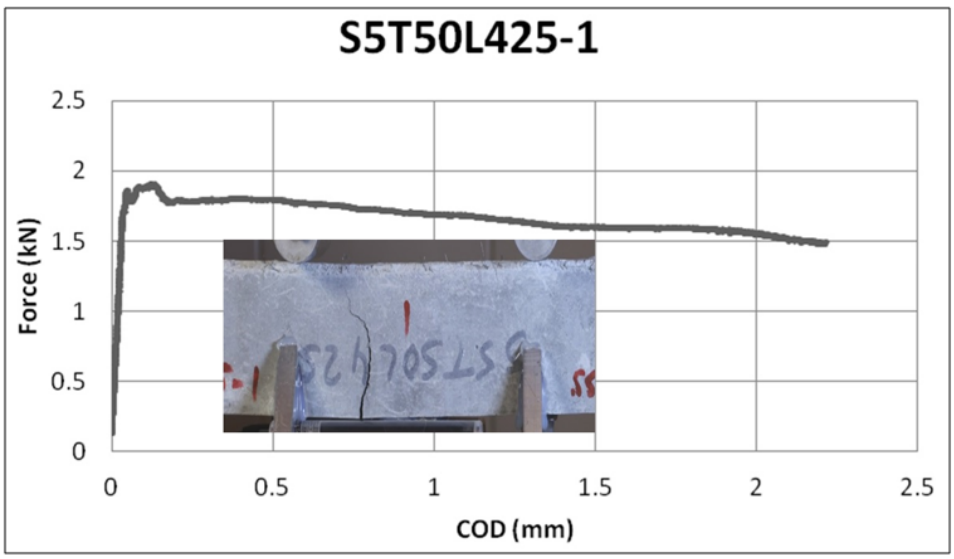

Figure A.56. S5T50L425-1.

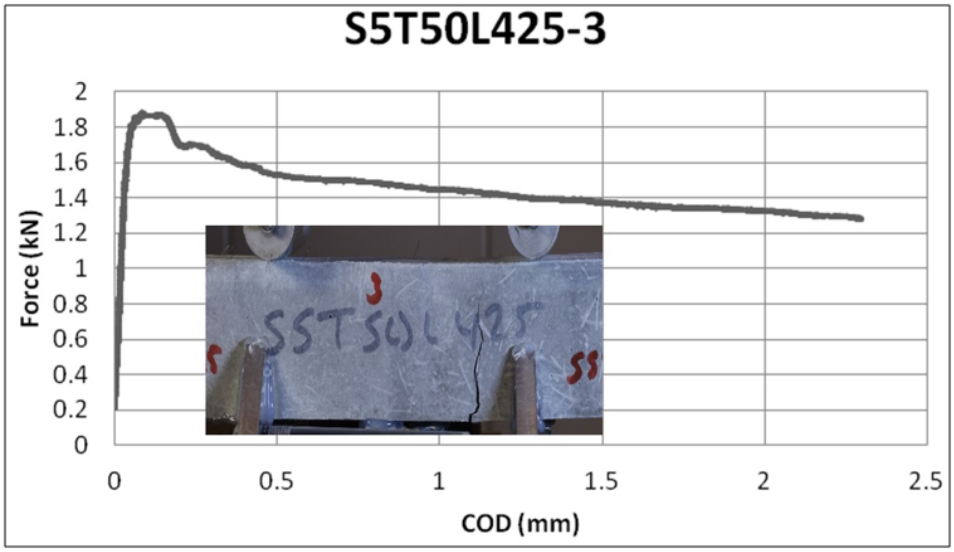

Figure A.57. S5T50L425-3.

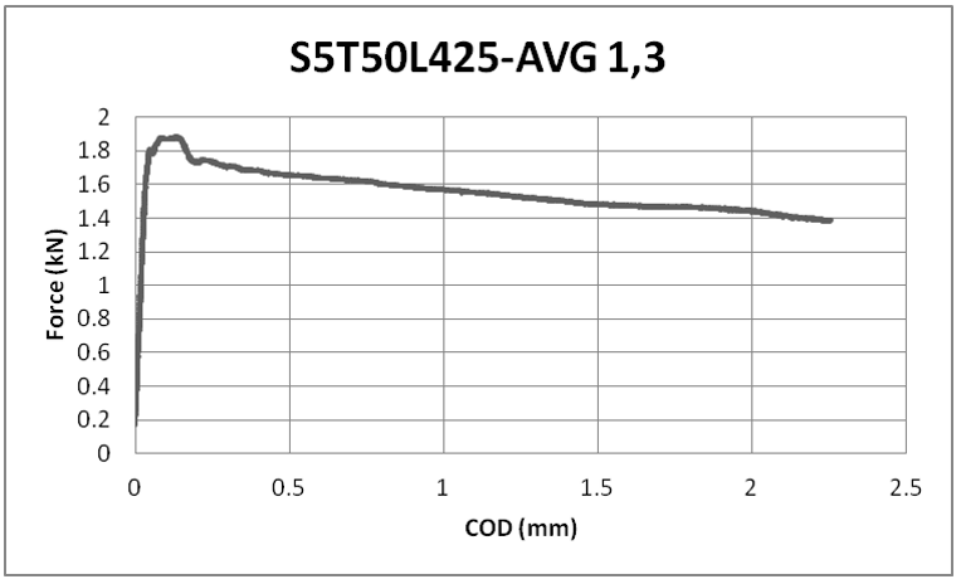

Figure A.58. S5T50L425-AVG 1,3.

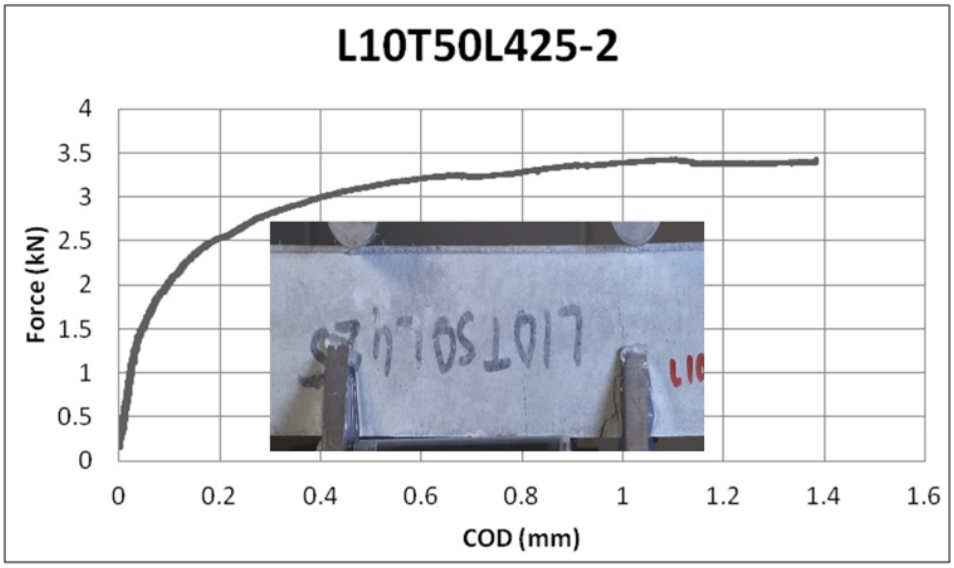

Figure A.59. L10T50L425-2.

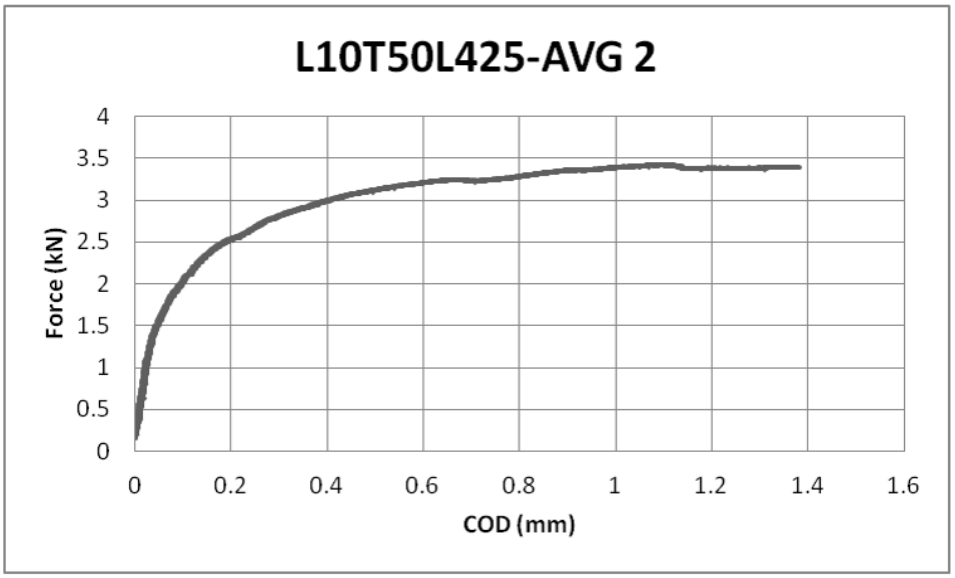

Figure A.60. L10T50L425-AVG 2.

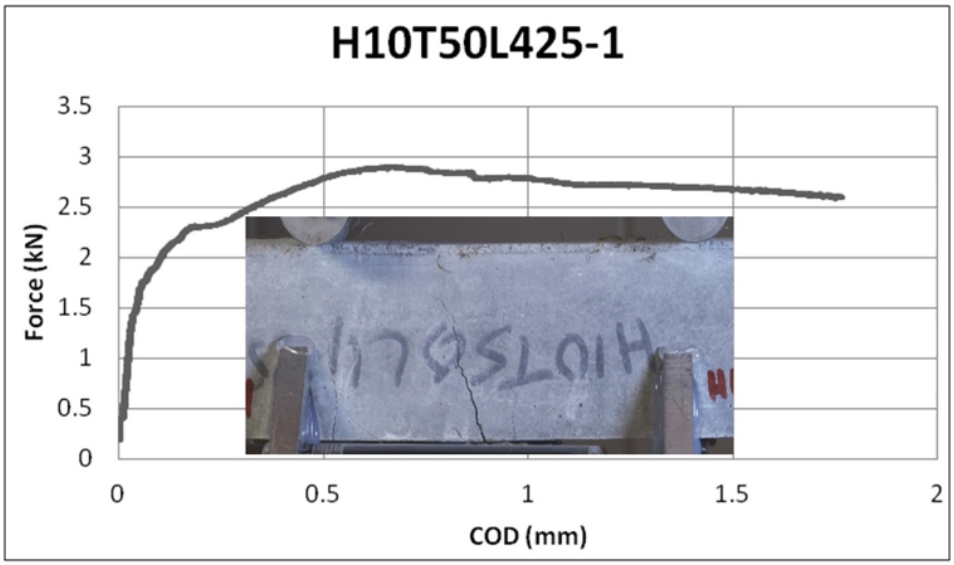

Figure A.61. H10T50L425-1.

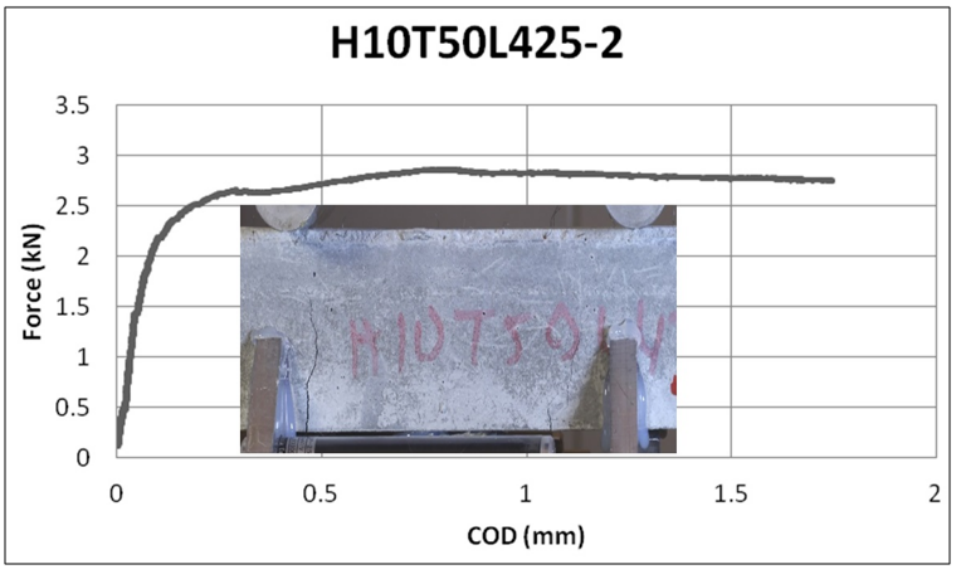

Figure A.62. H10T50L425-2.

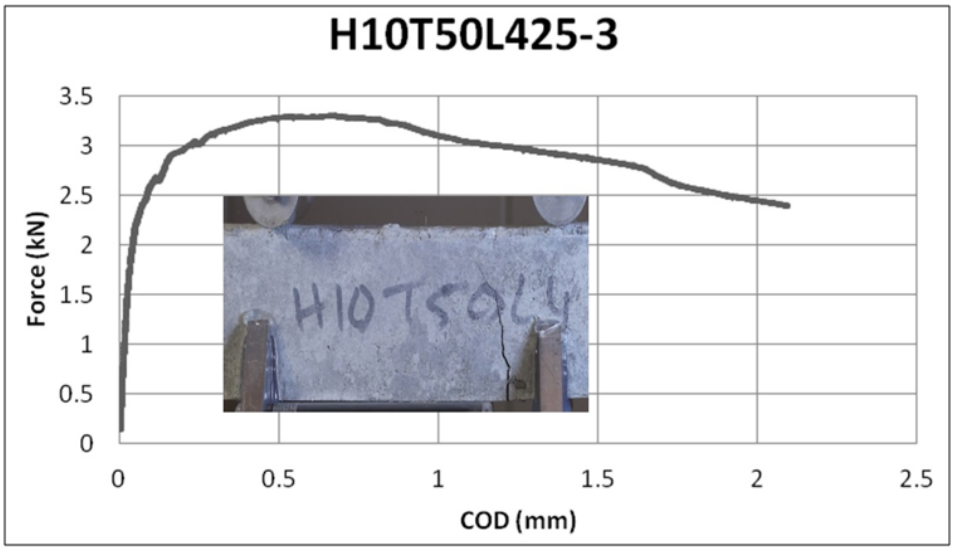

Figure A.63. H10T50L425-3.

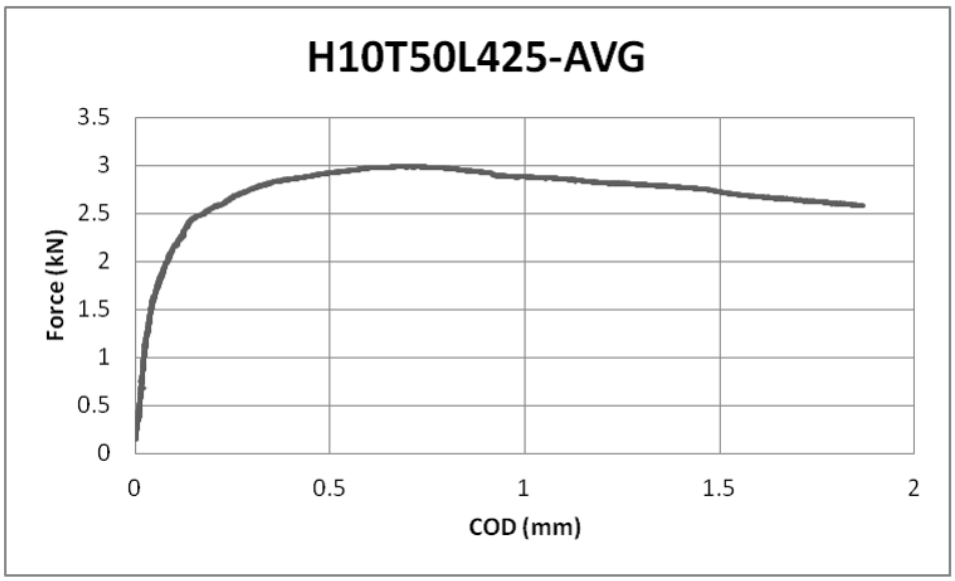

Figure A.64. H10T50L425-AVG.

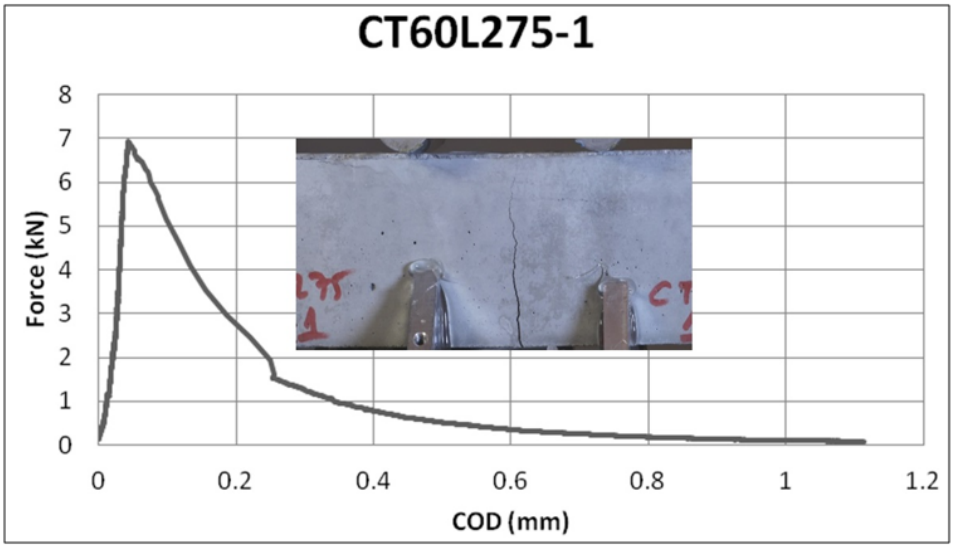

Figure A.65. CT60L275-1.

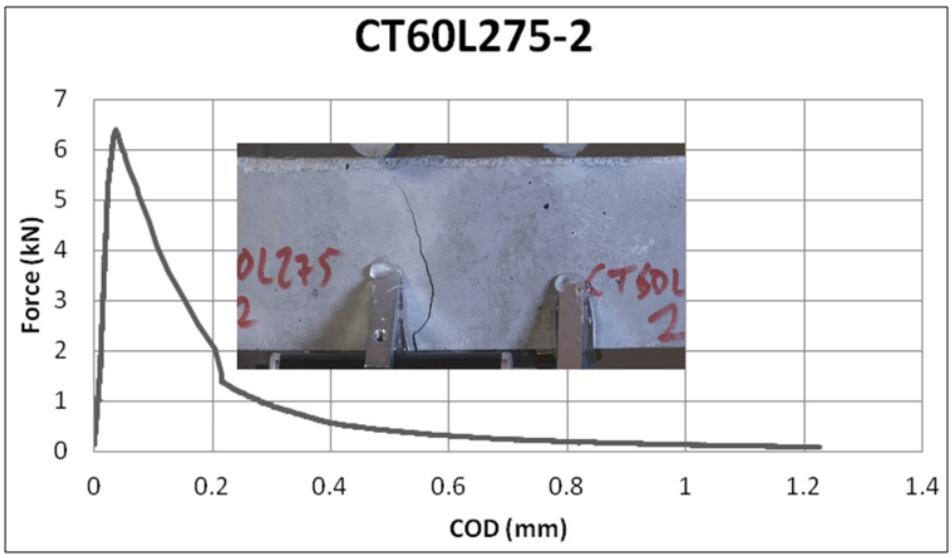

Figure A.66. CT60L275-2.

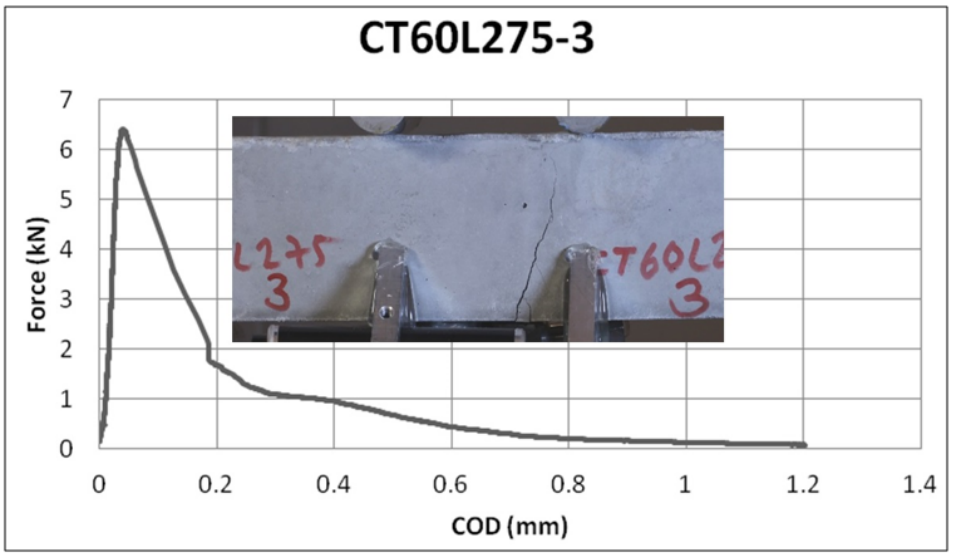

Figure A.67. CT60L275-3.

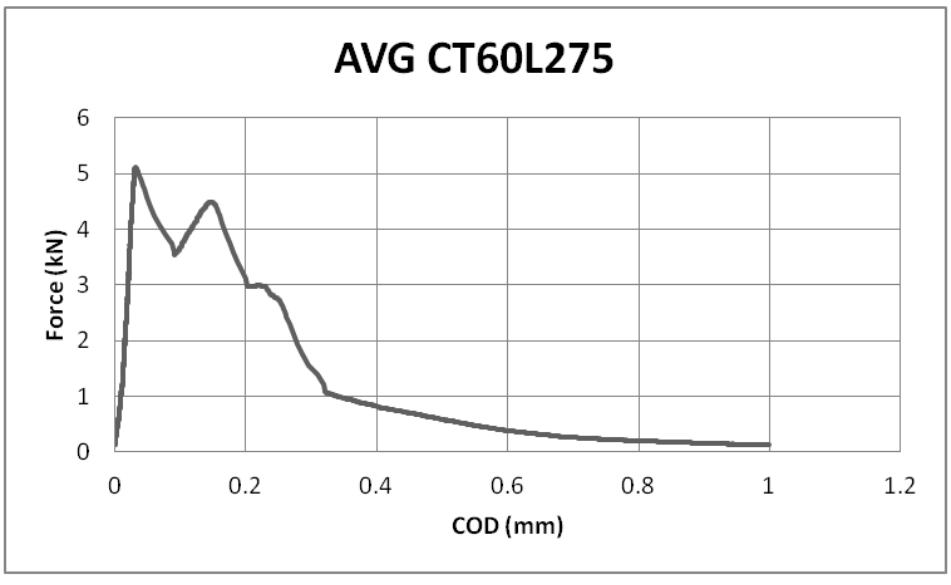

Figure A.68. AVG CT60L275.

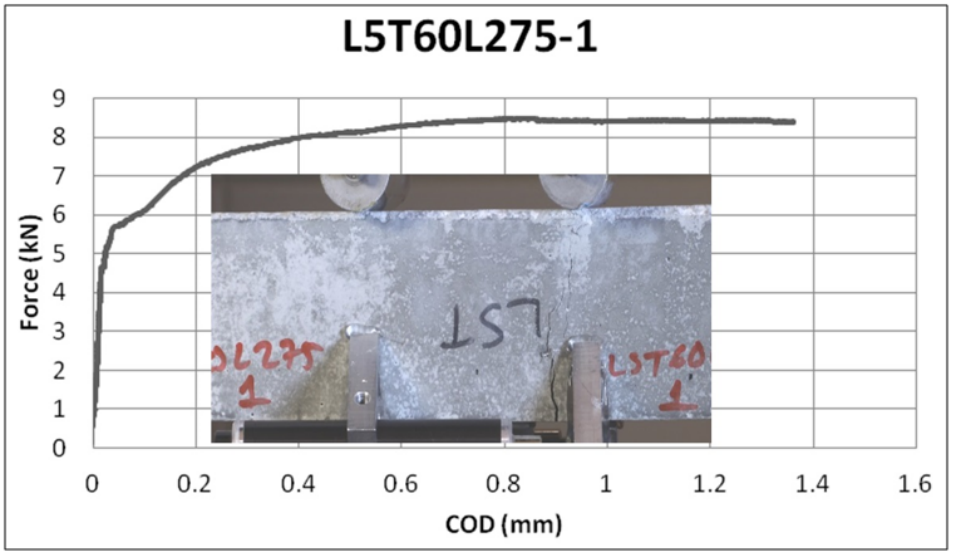

Figure A.69. L5T60L275-1.

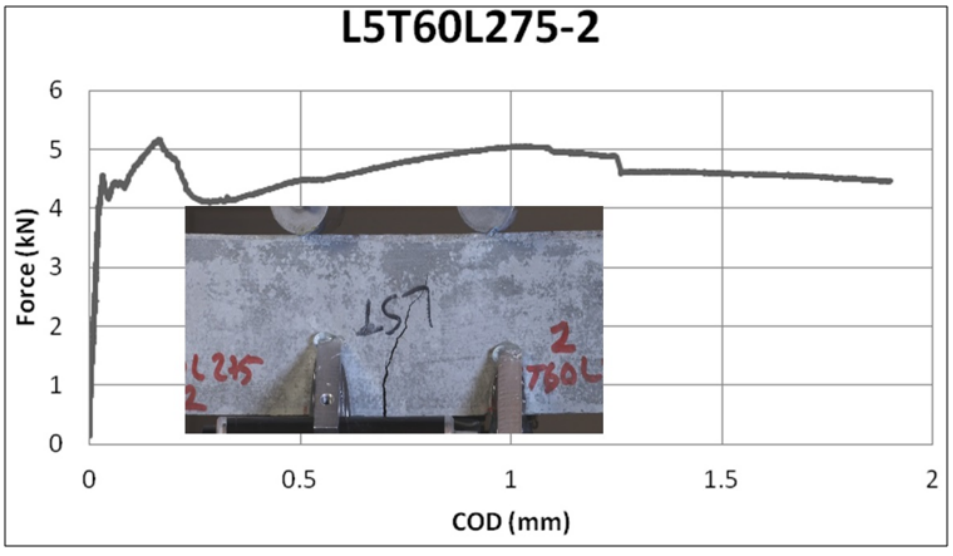

Figure A.70. L5T60L275-2.

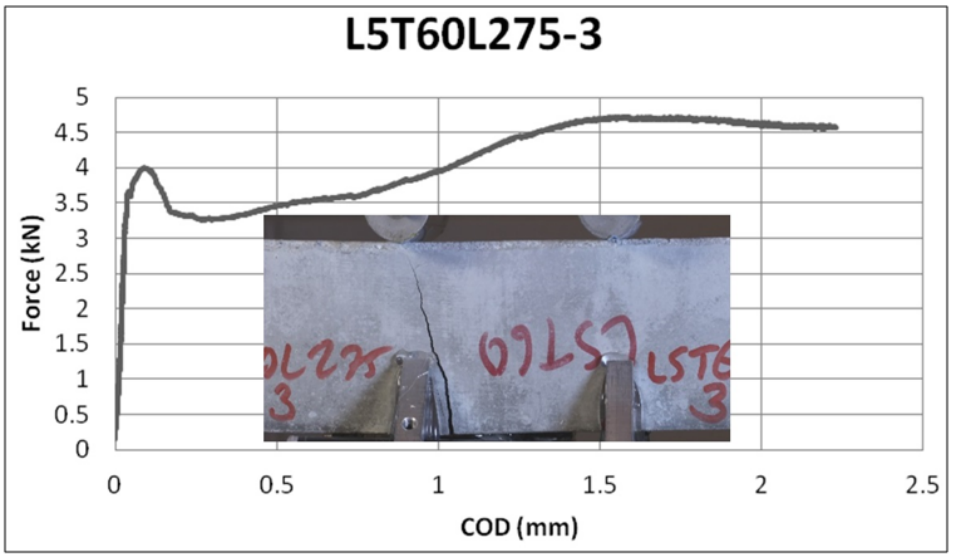

Figure A.71. L5T60L275-3.

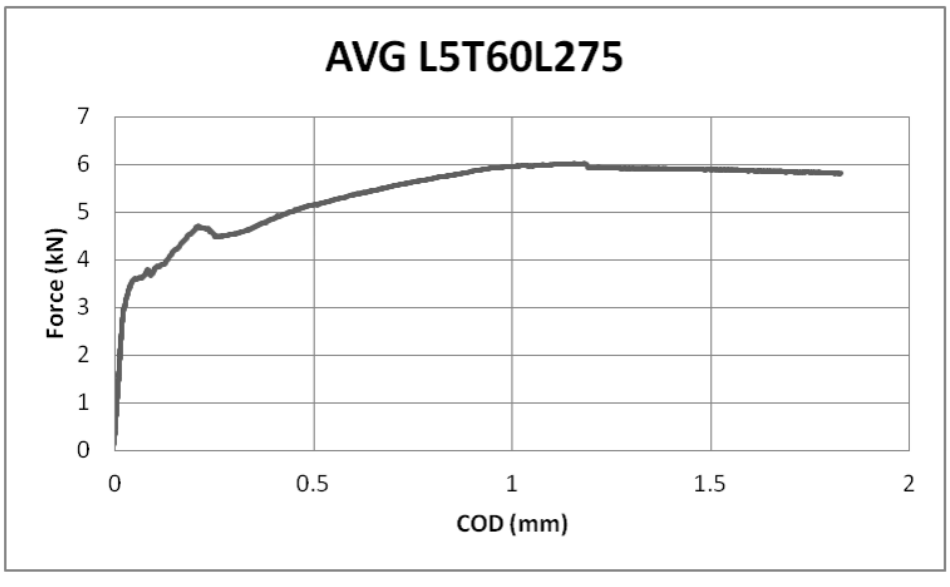

Figure A.72. AVG L5T60L275.

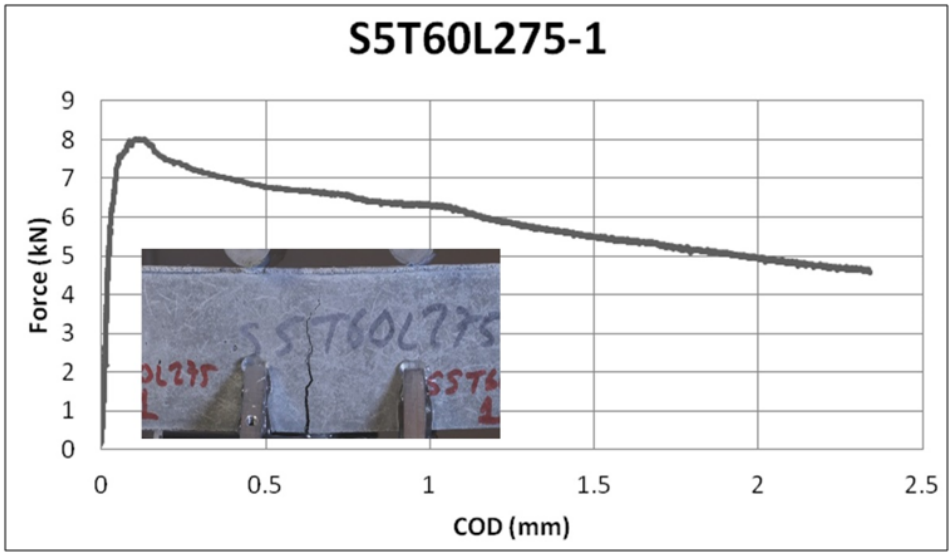

Figure A.73. S5T60L275-1.

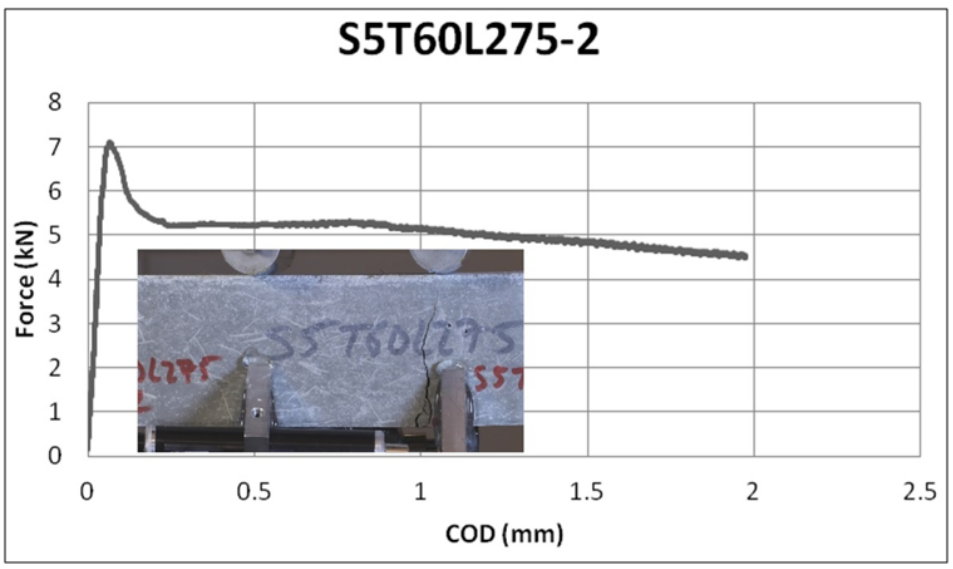

Figure A.74. S5T60L275-2.

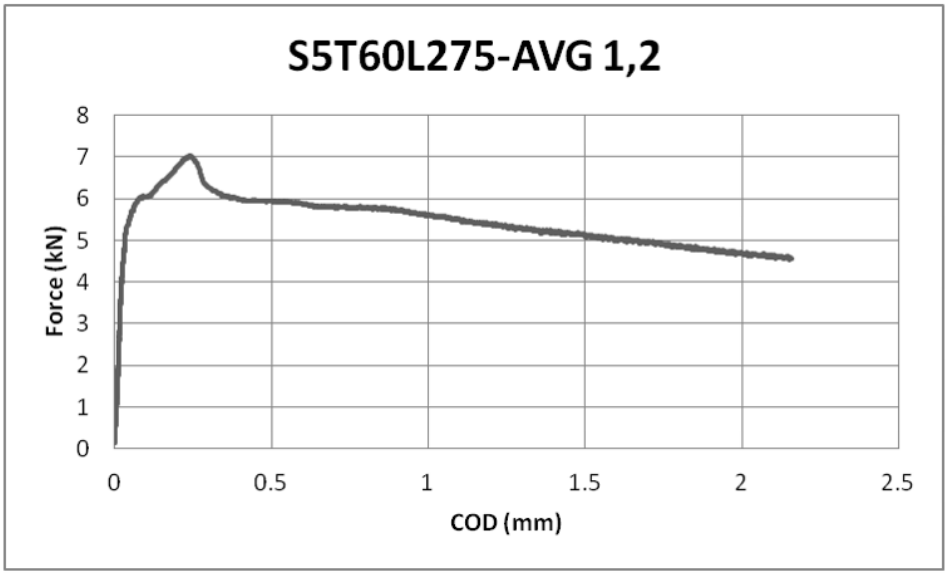

Figure A.75. S5T60L275-AVG 1,2.

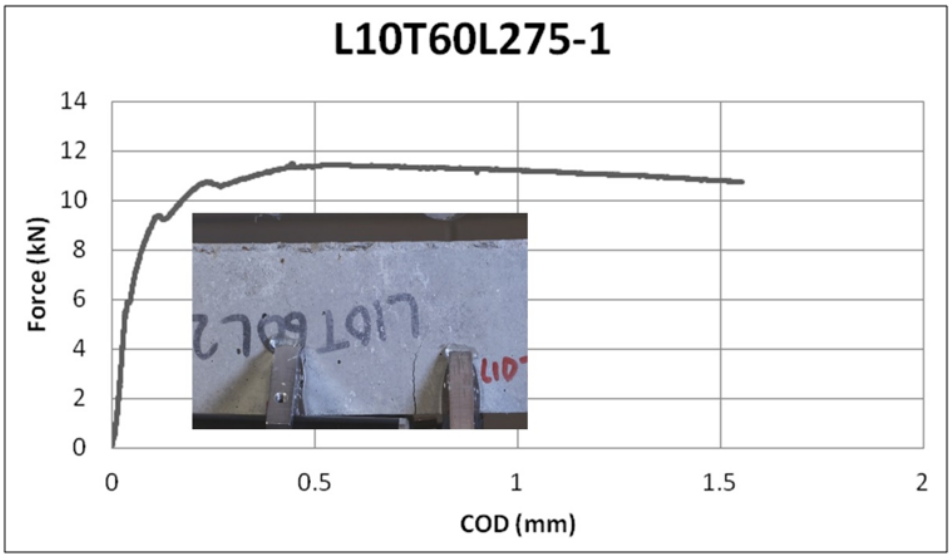

Figure A.76. L10T60L275-1.

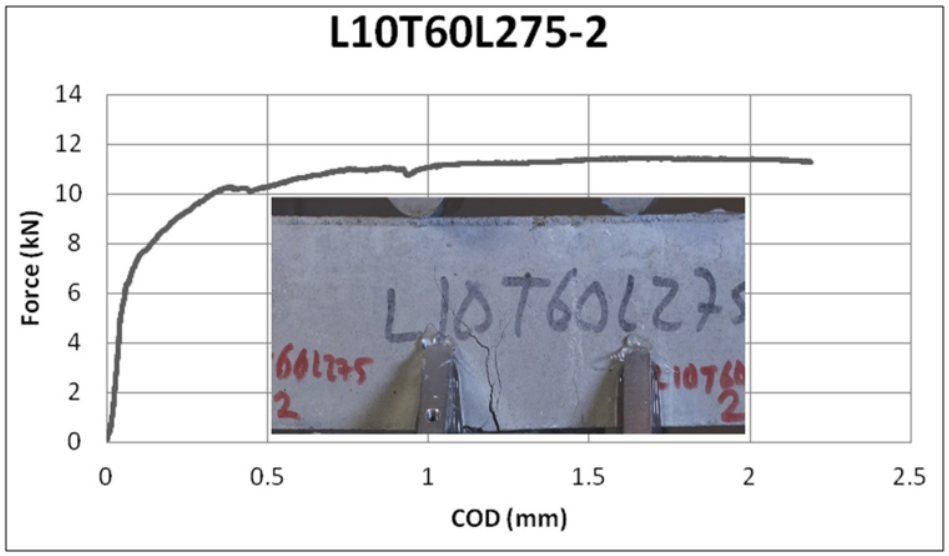

Figure A.77. L10T60L275-2.

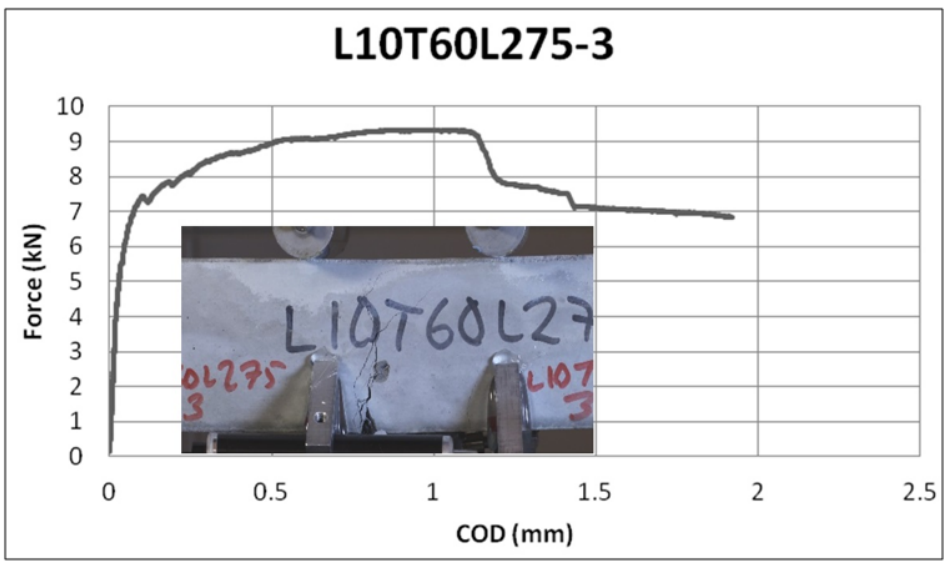

Figure A.78. L10T60L275-3.

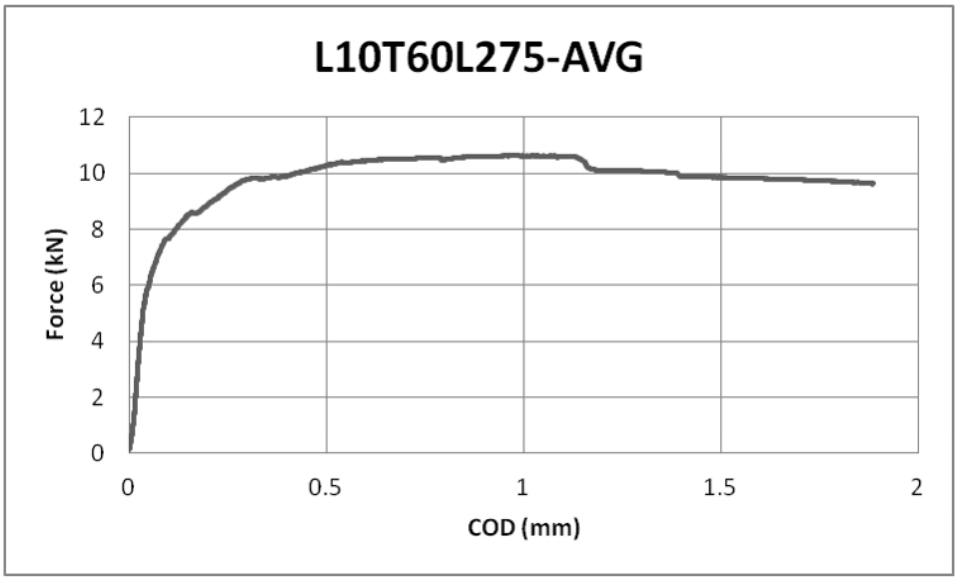

Figure A.79. L10T60L275-AVG.

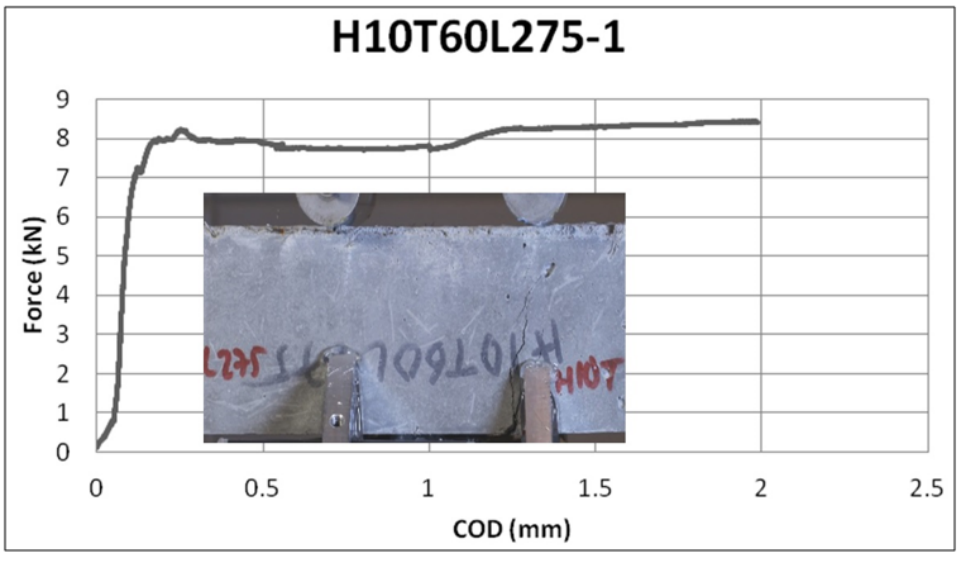

Figure A.80. H10T60L275-1.

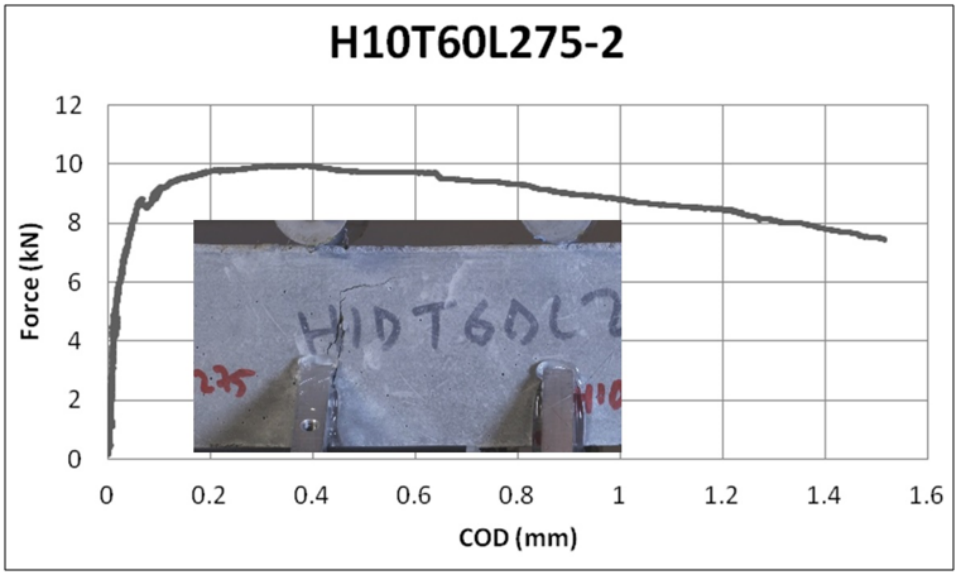

Figure A.81. H10T60L275-2.

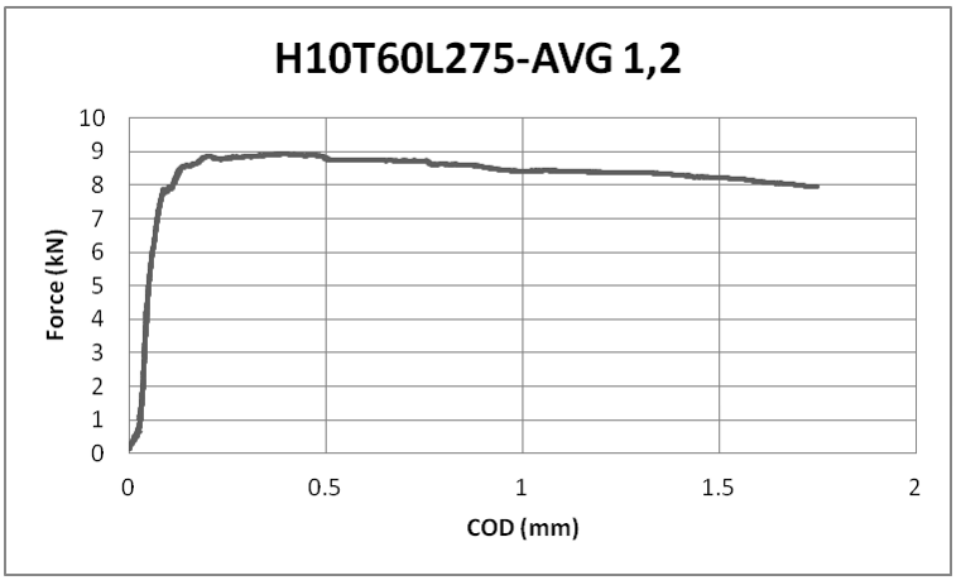

Figure A.82. H10T60L275-AVG 1,2.

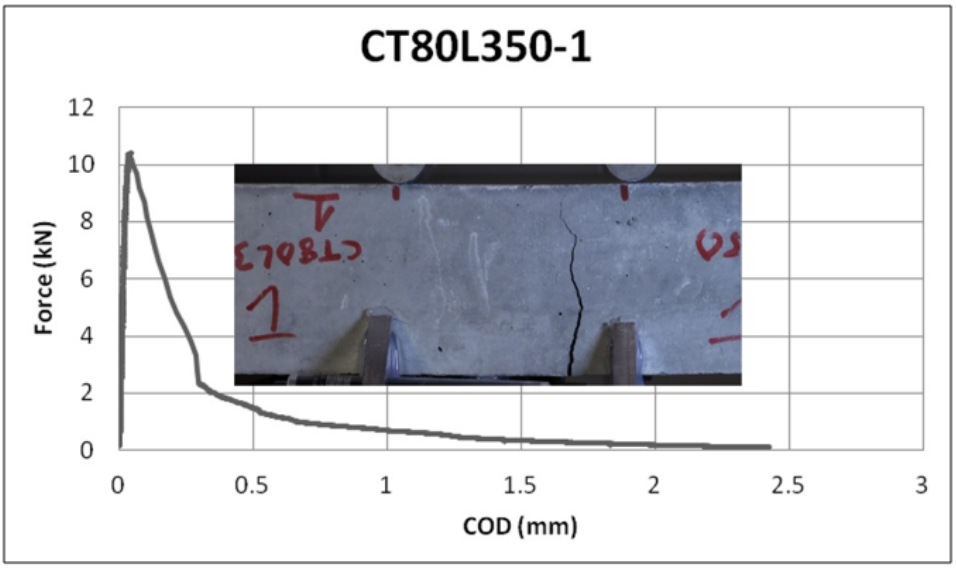

Figure A.83. CT80L350-1.

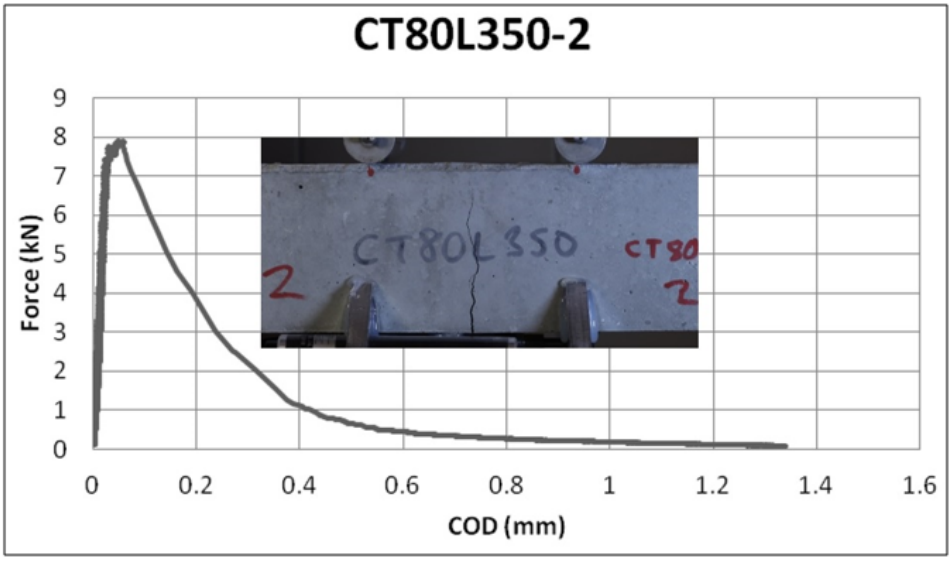

Figure A.84. CT80L350-2.

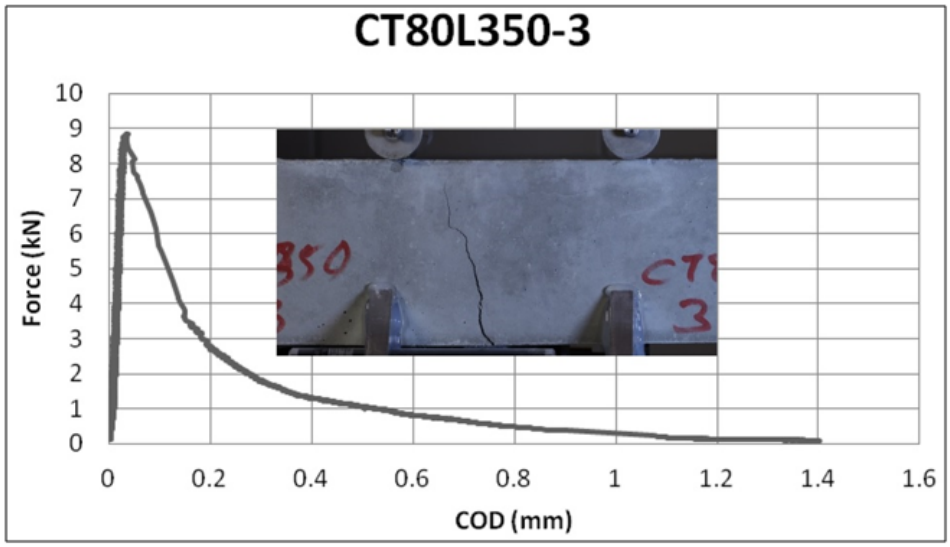

Figure A.85. CT80L350-3.

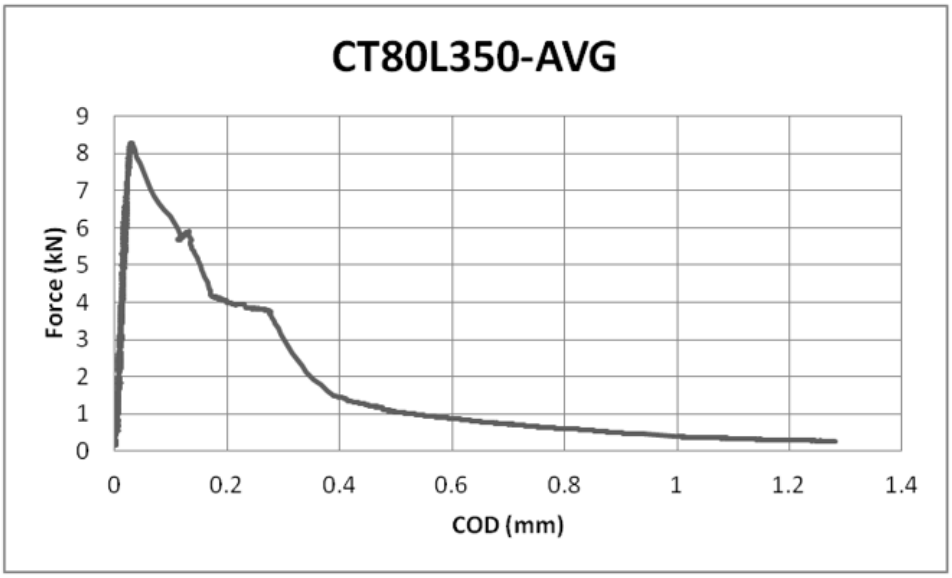

Figure A.86. CT80L350-AVG.

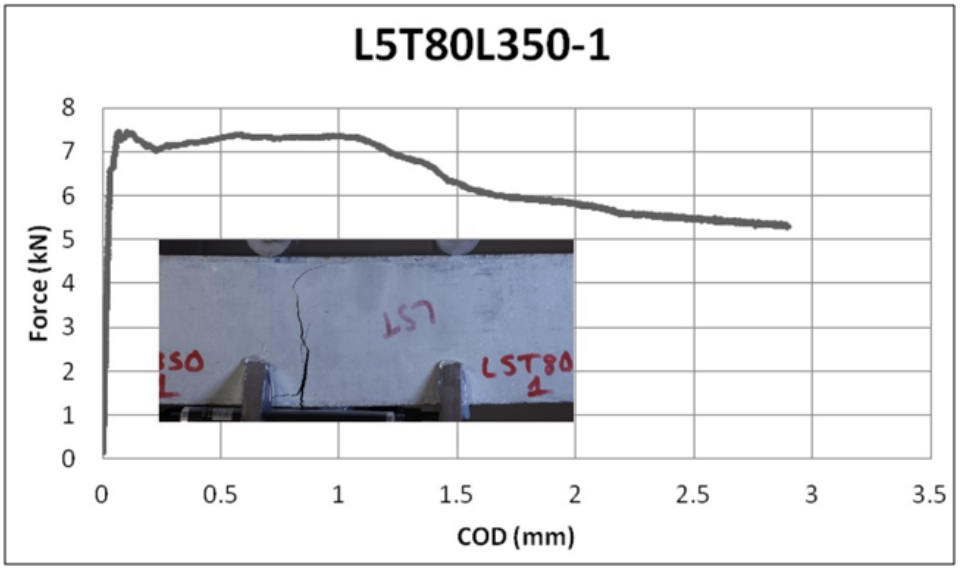

Figure A.87. L5T80L350-1.

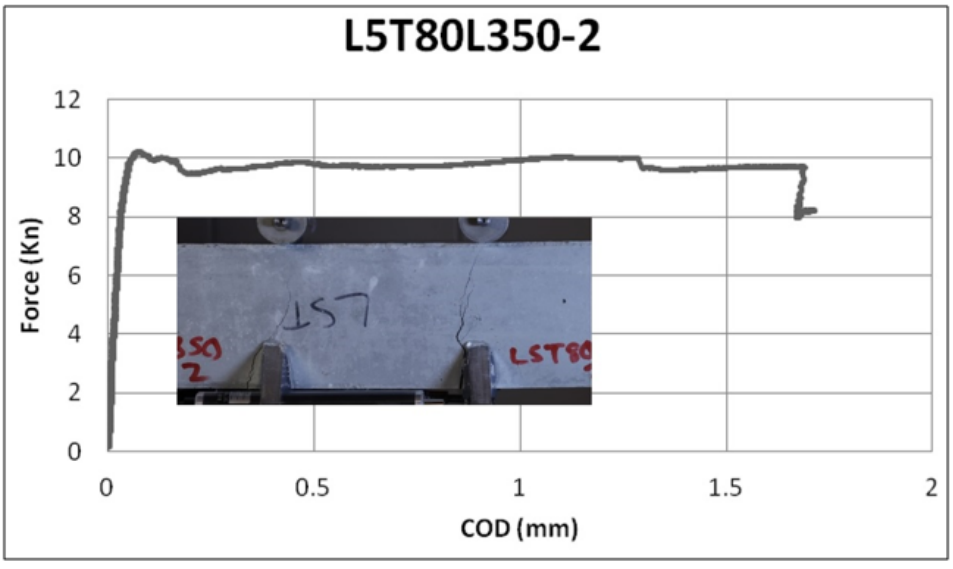

Figure A.88. L5T80L350-2.

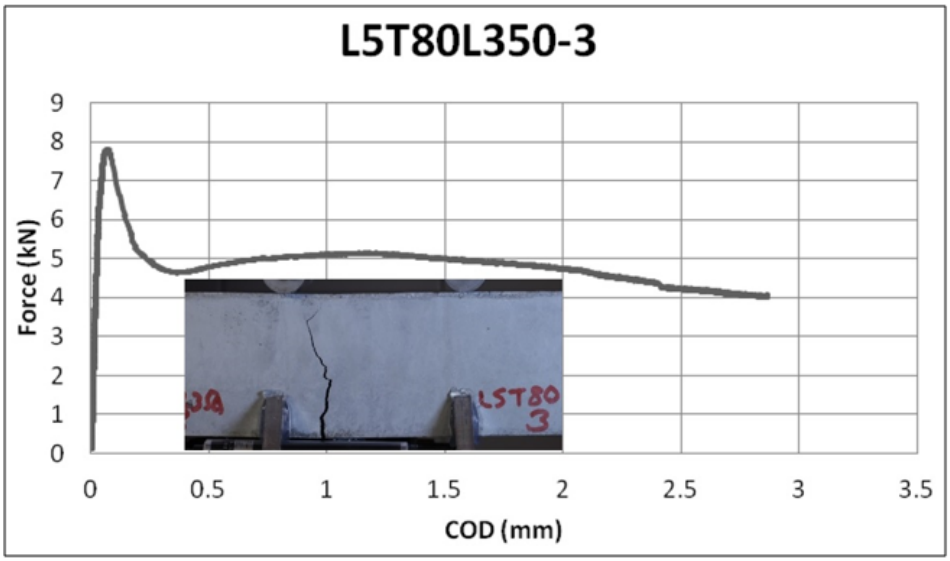

Figure A.89. L5T80L350-3.

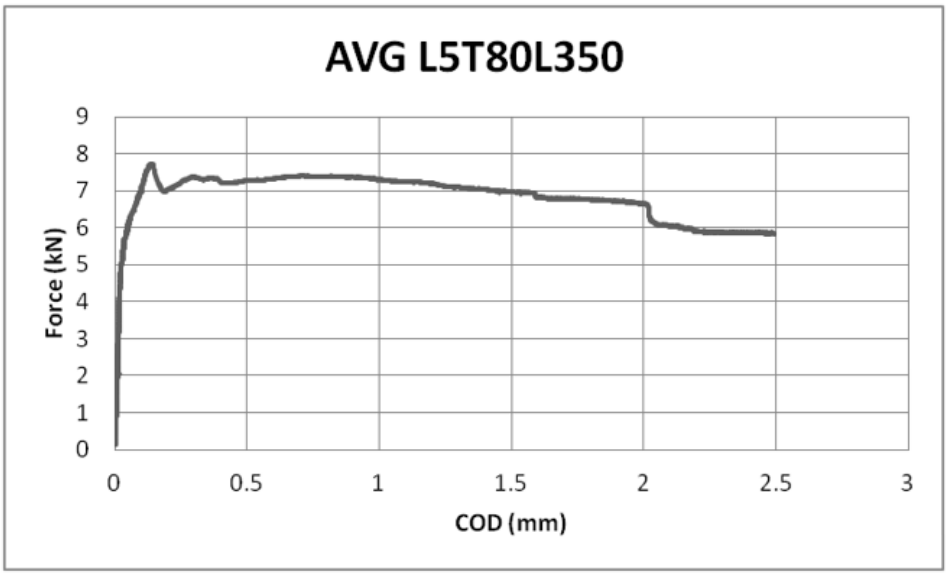

Figure A.90. AVG L5T80L350.

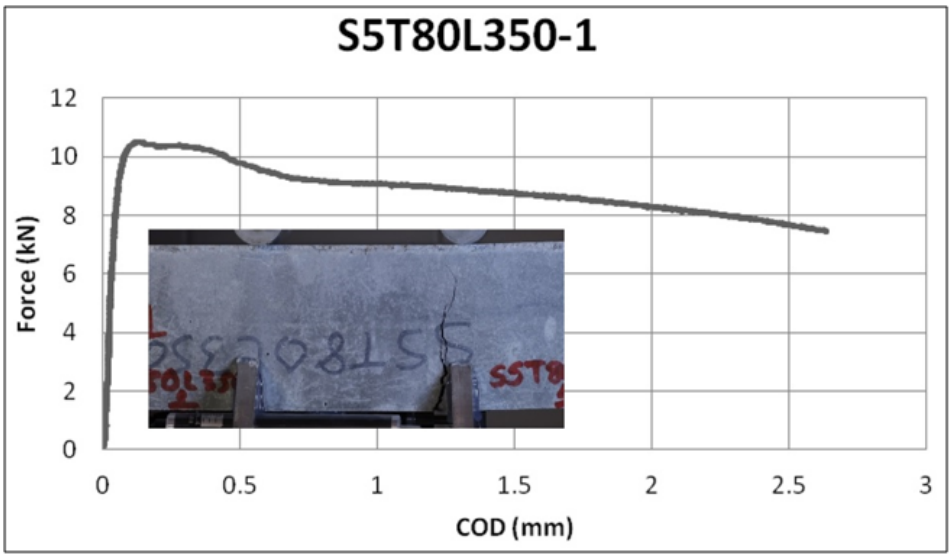

Figure A.91. S5T80L350-1.

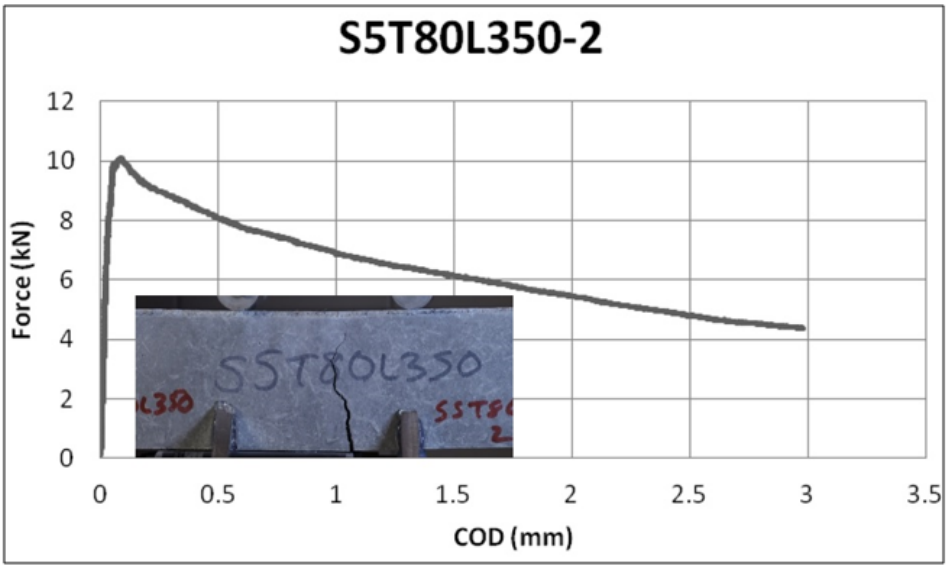

Figure A.92. S5T80L350-2.

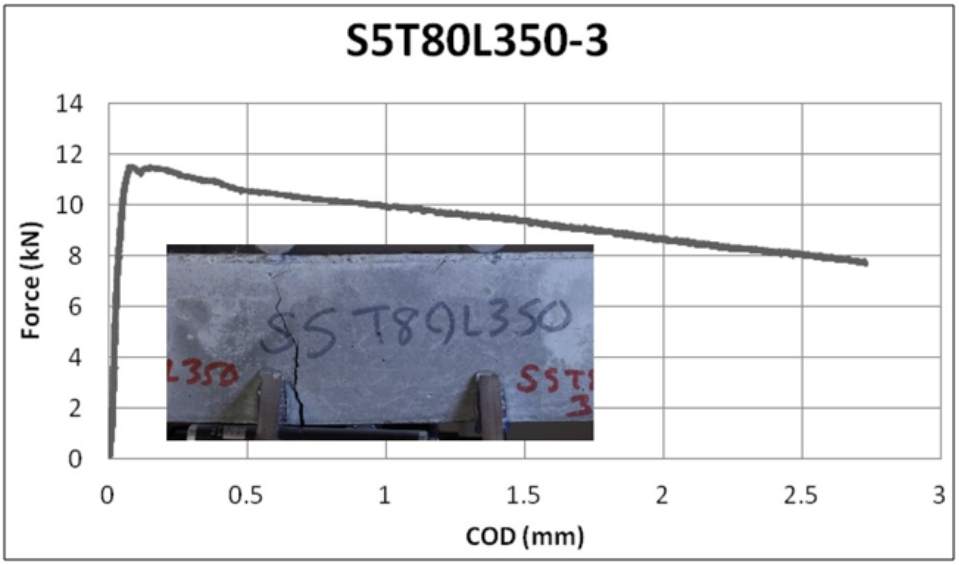

Figure A.93. S5T80L350-3.

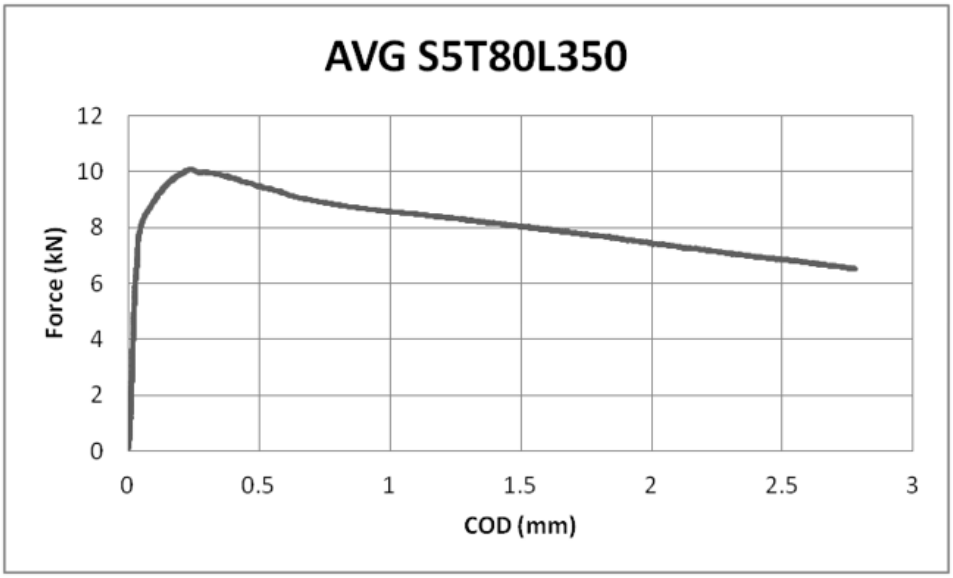

Figure A.94. AVG S5T80L350.

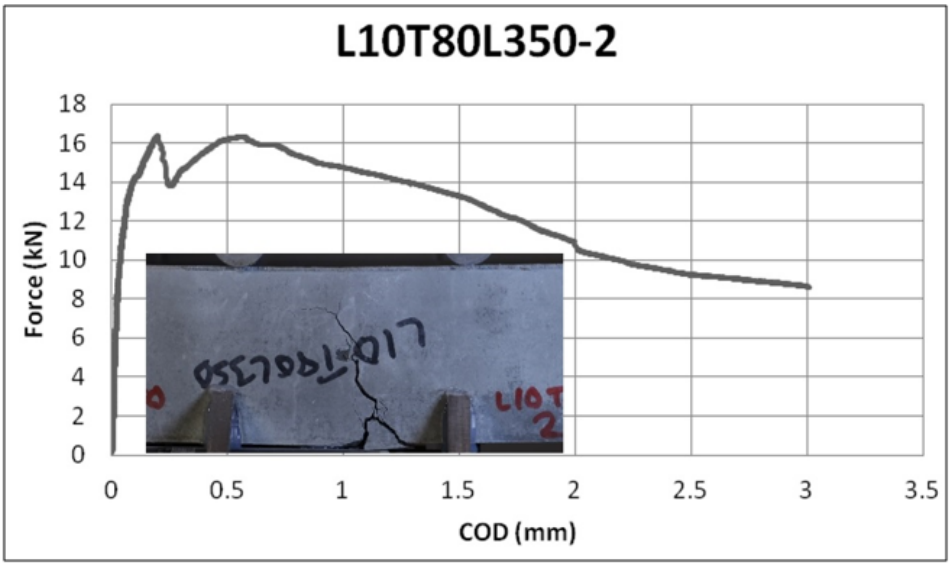

Figure A.95. L10T80L350-2.

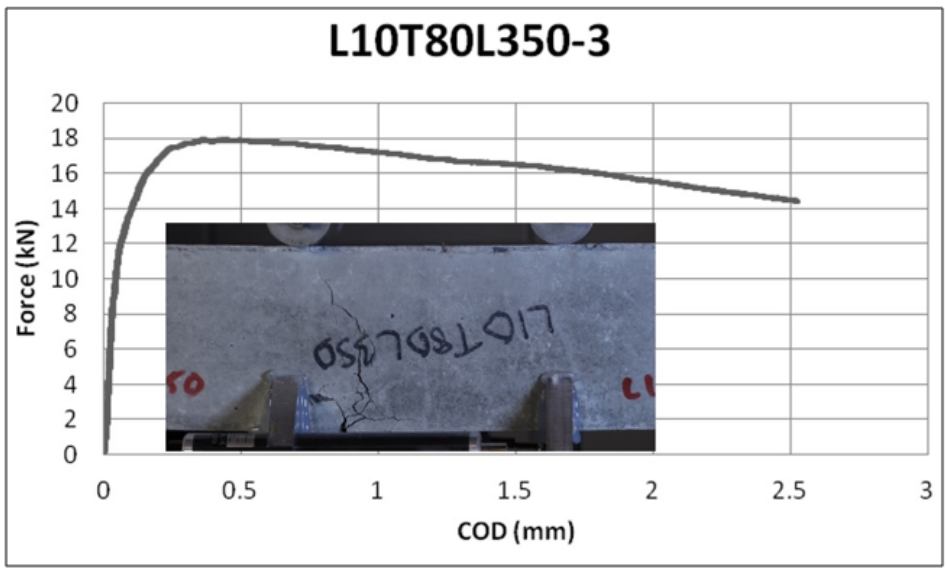

Figure A.96. L10T80L350-3.

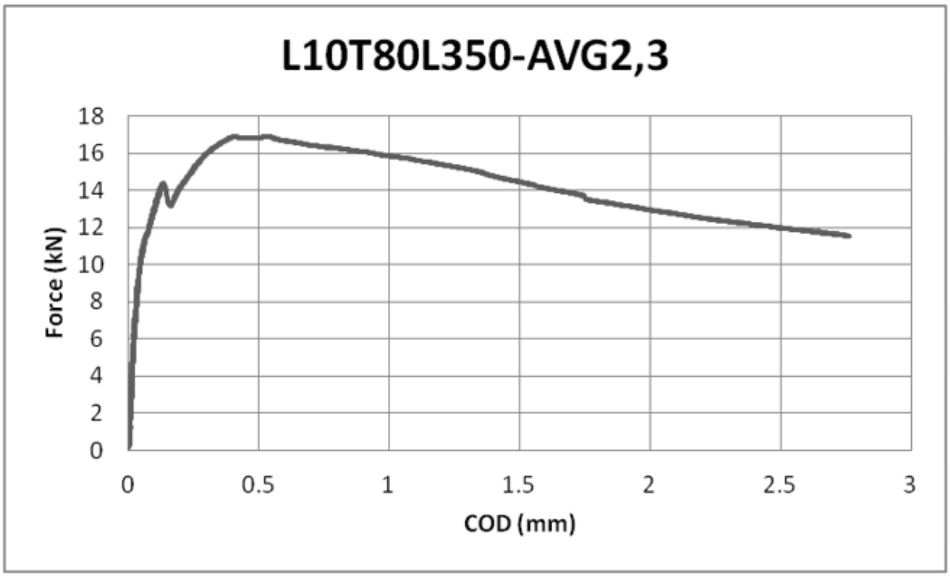

Figure A.97. L10T80L350-AVG2,3.

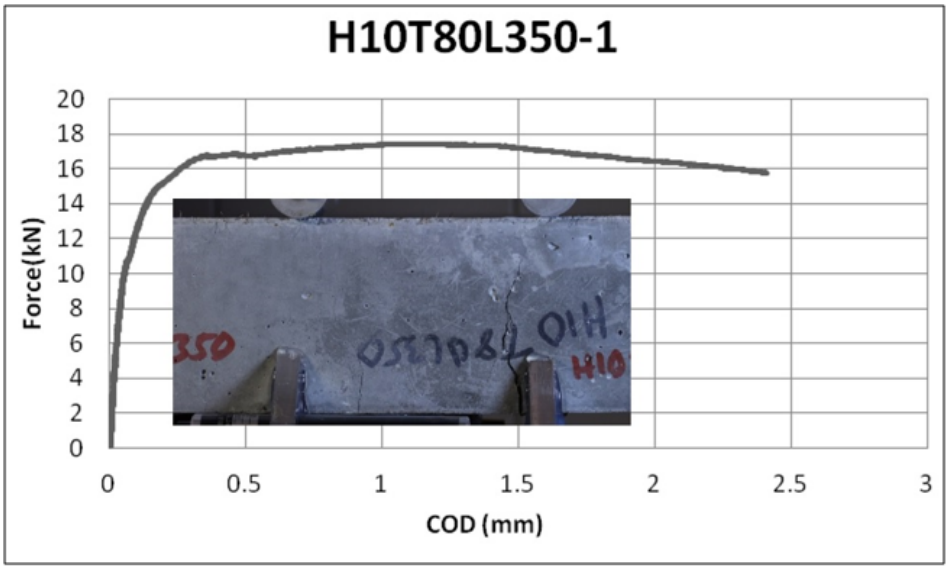

Figure A.98. H10T80L350-1.

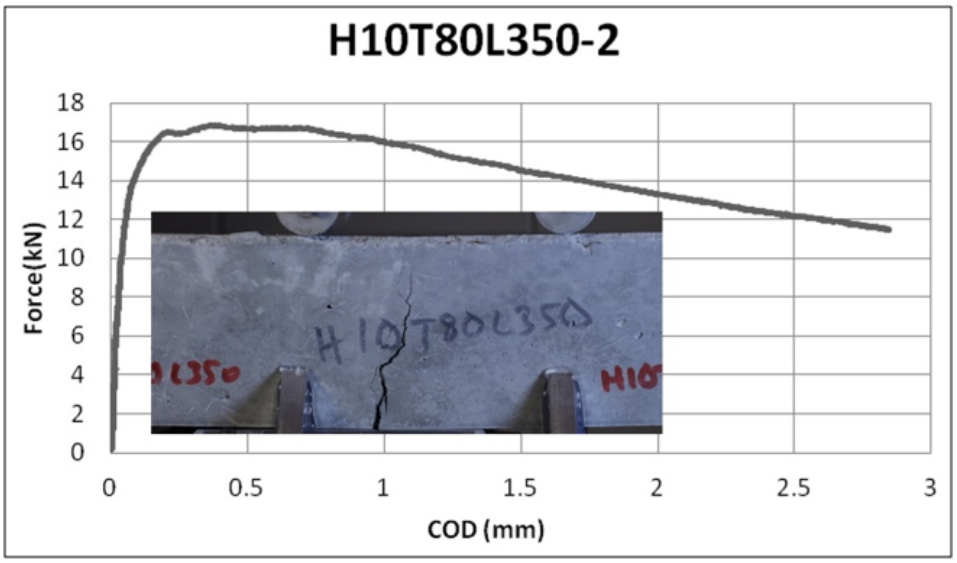

Figure A.99. H10T80L350-2.

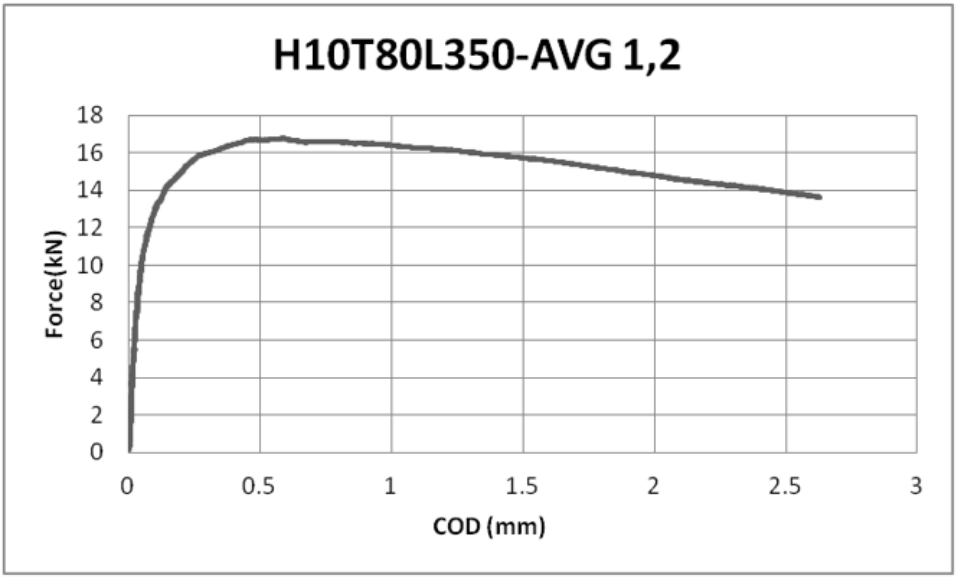

Figure A.100. H10T80L350-AVG 1,2.

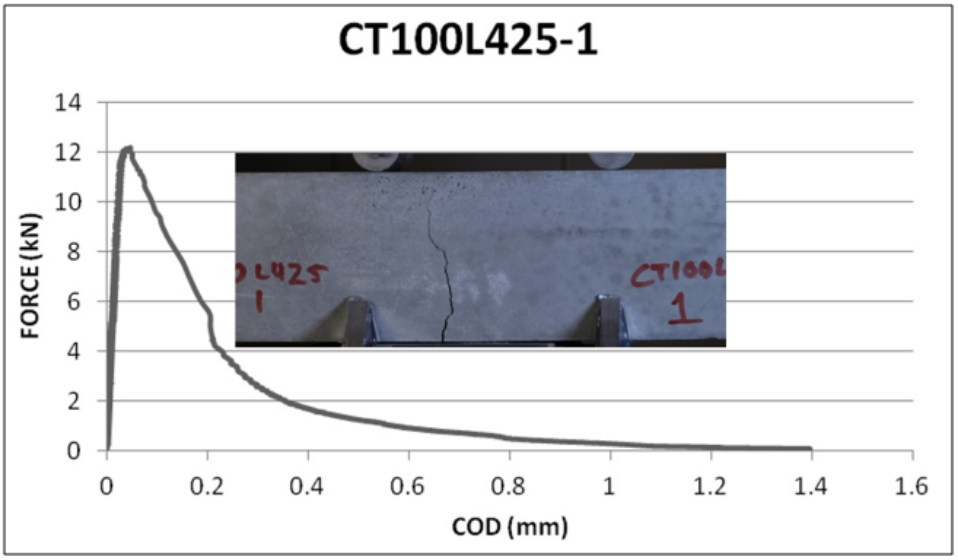

Figure A.101. CT100L425-1.

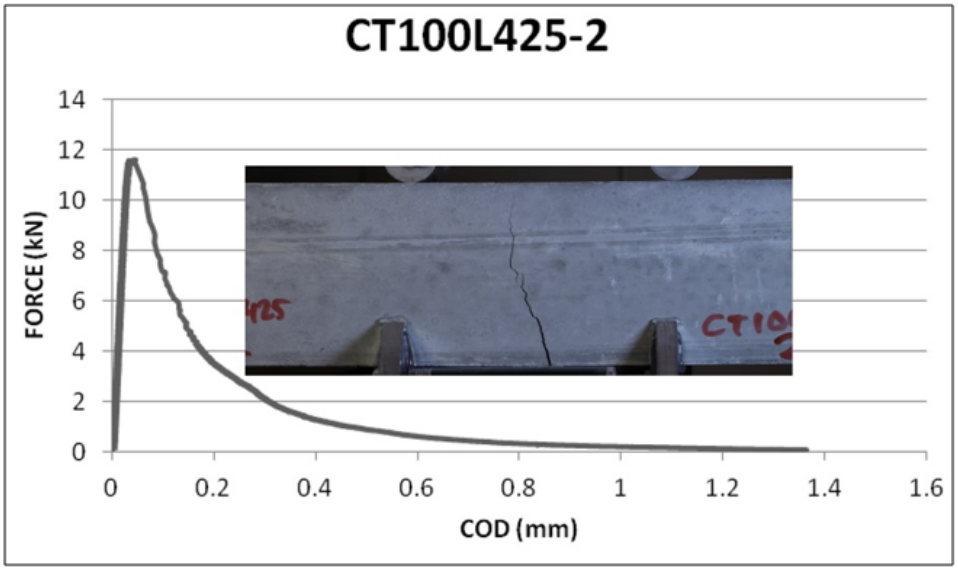

Figure A.102. CT100L425-2.

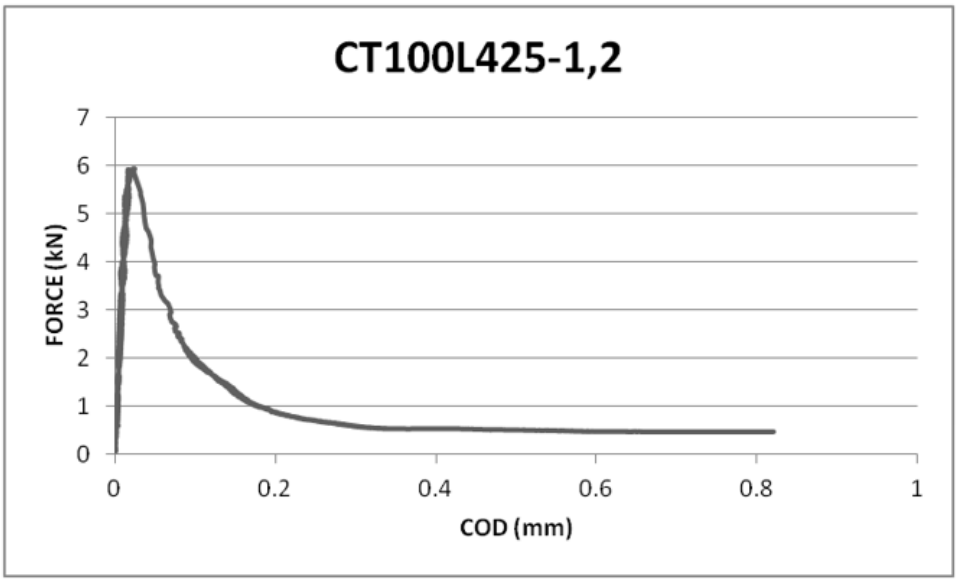

Figure A.103. CT100L425-1,2.

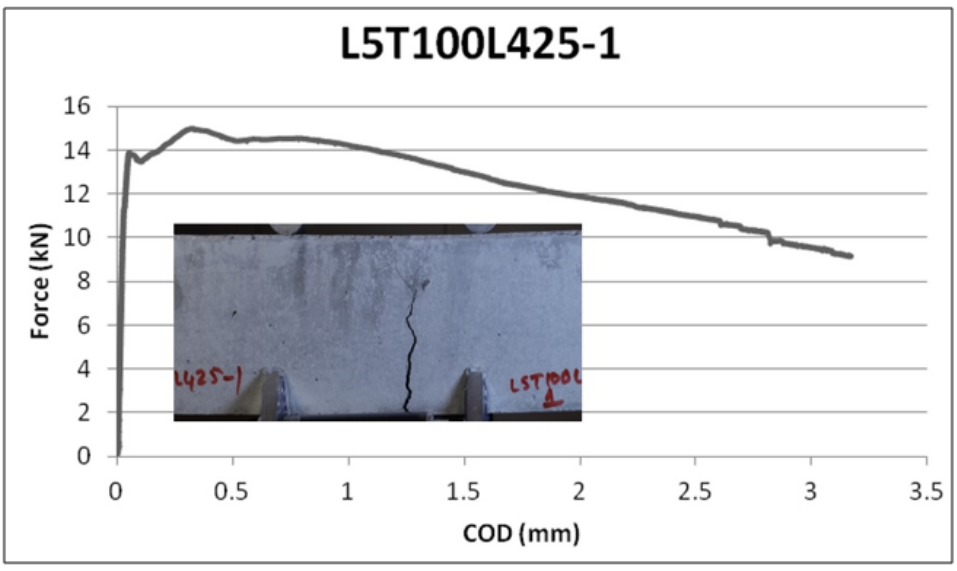

Figure A.104. L5T100L425-1.

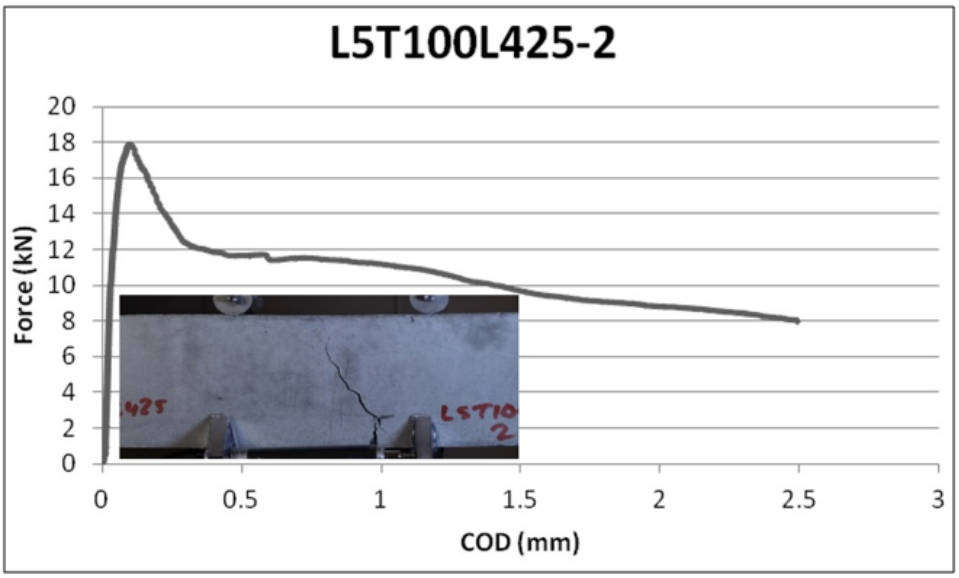

Figure A.105. L5T100L425-2.

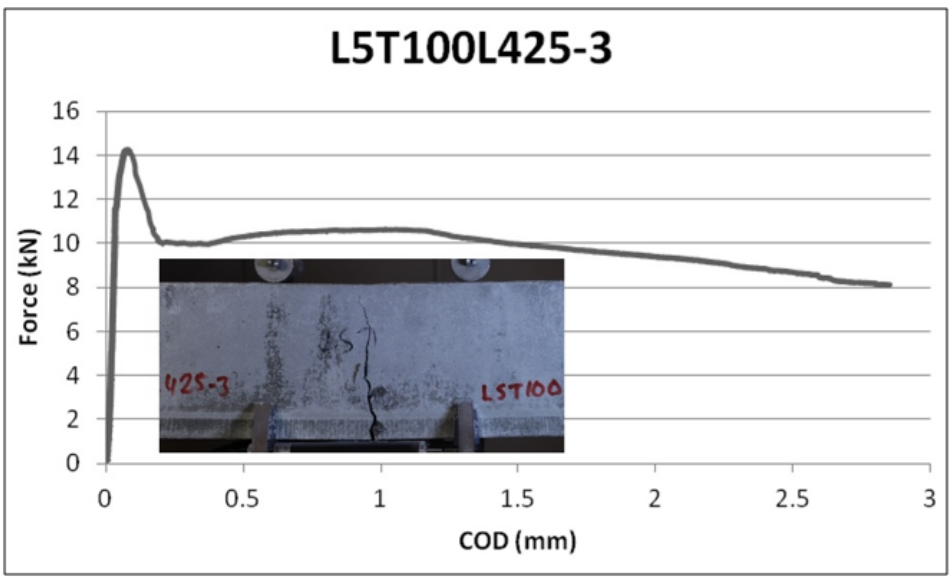

Figure A.106. L5T100L425-3.

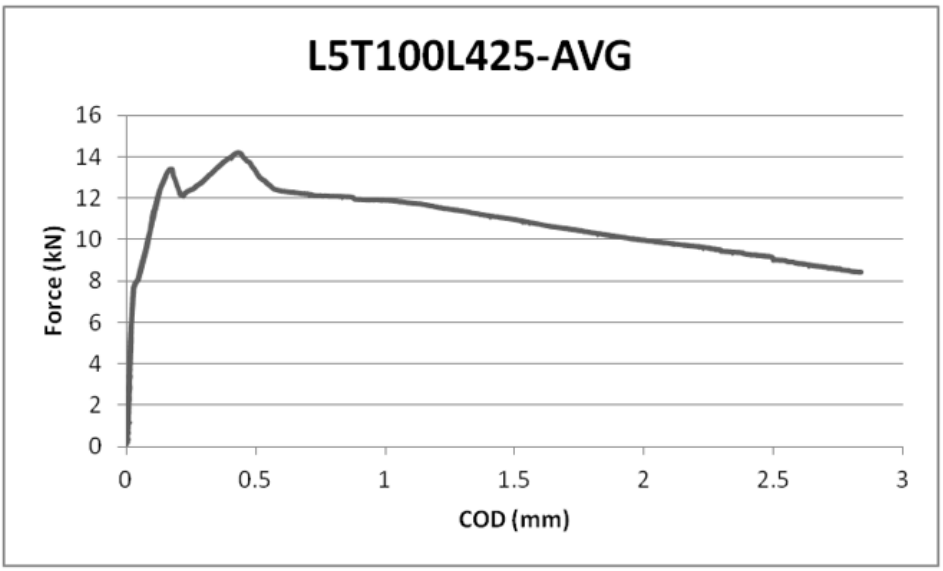

Figure A.107. L5T100L425-AVG.

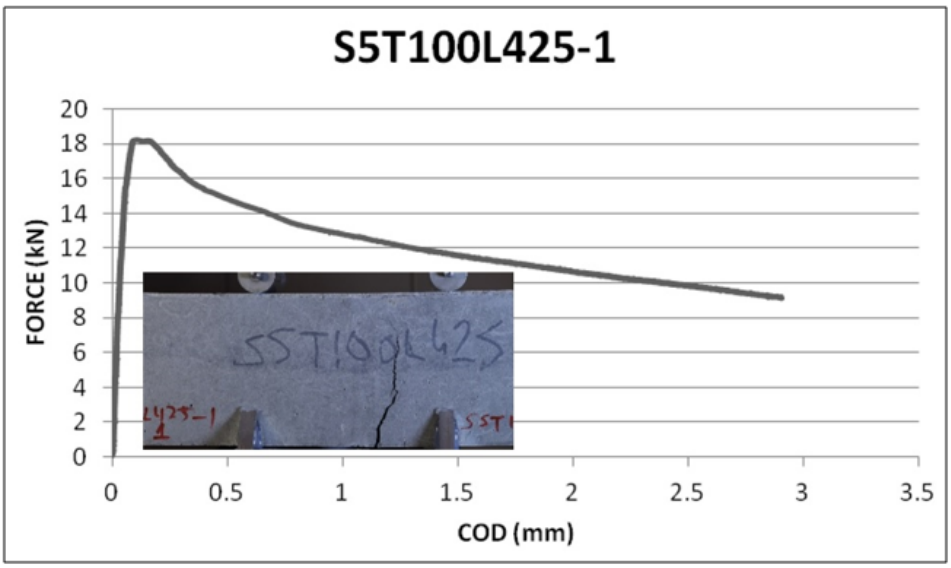

Figure A.108. S5T100L425-1.

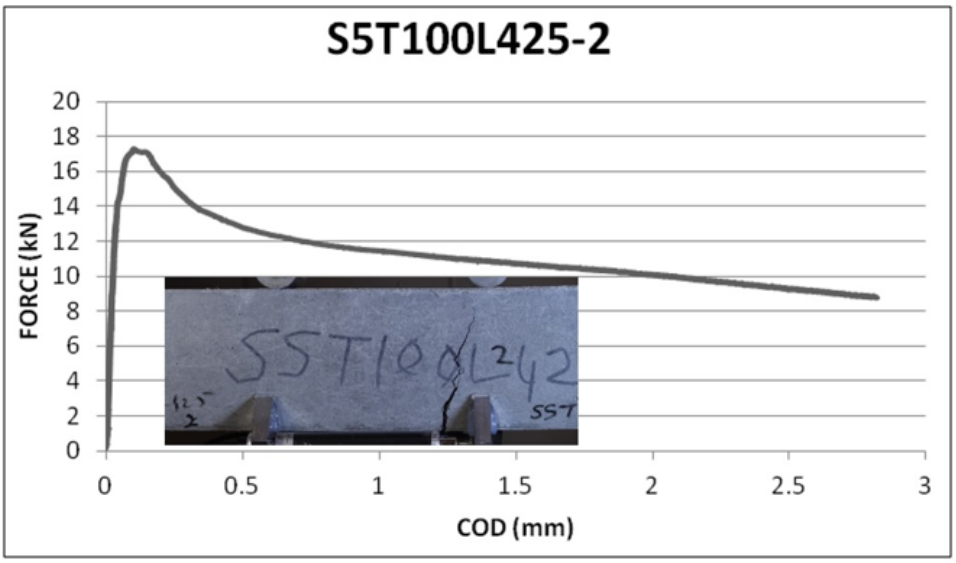

Figure A.109. S5T100L425-2.

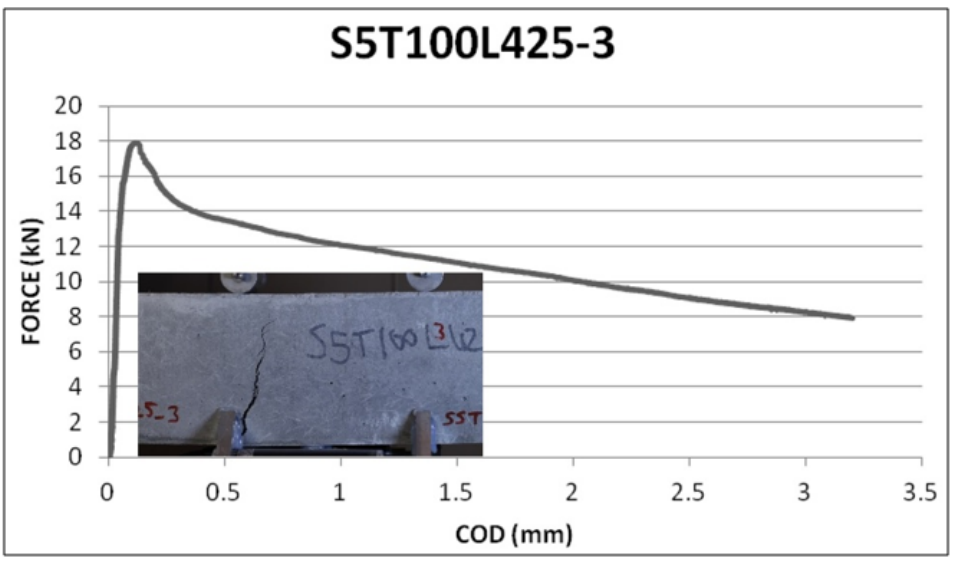

Figure A.110. S5T100L425-3.

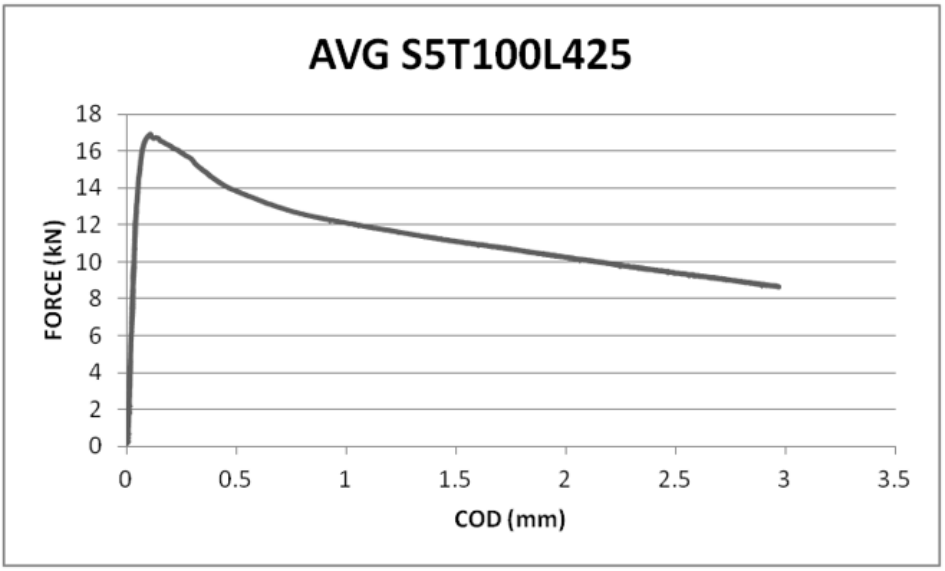

Figure A.111. AVG S5T100L425.

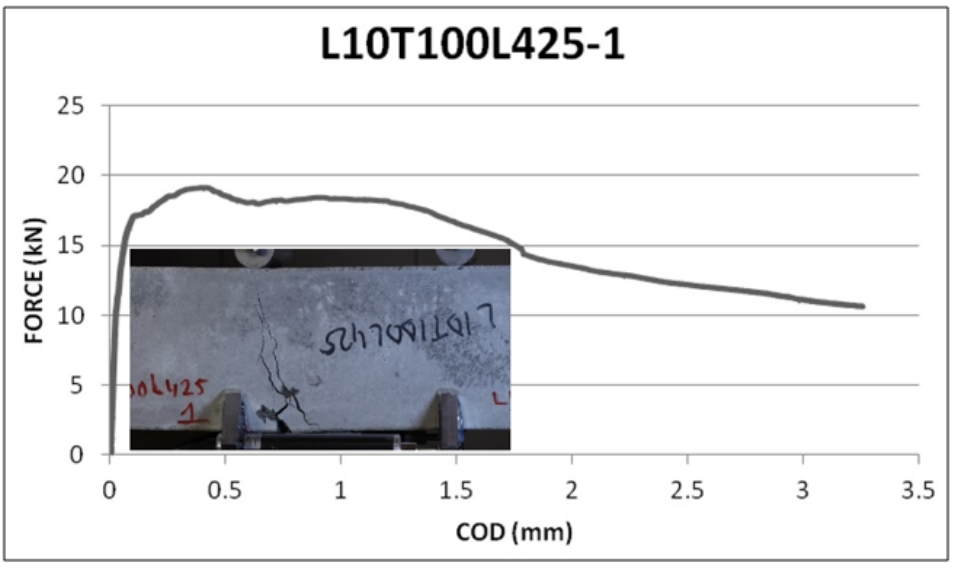

Figure A.112. L10T100L425-1.

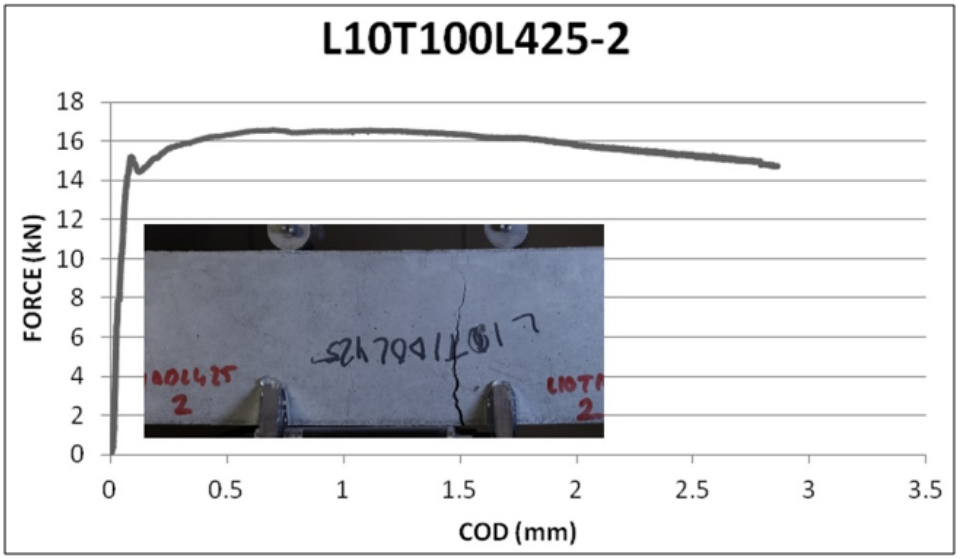

Figure A.113. L10T100L425-2.

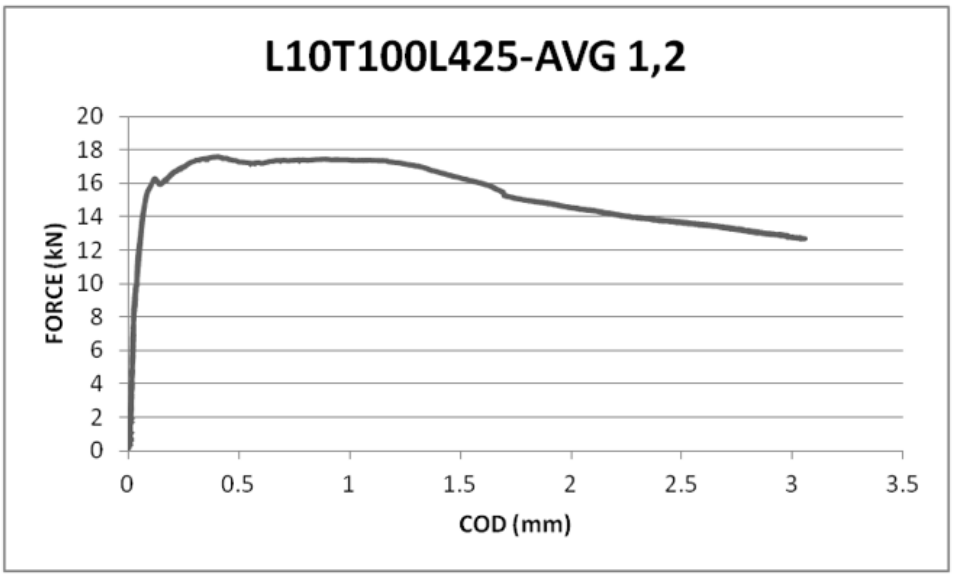

Figure A.114. L10T100L425-AVG 1,2.

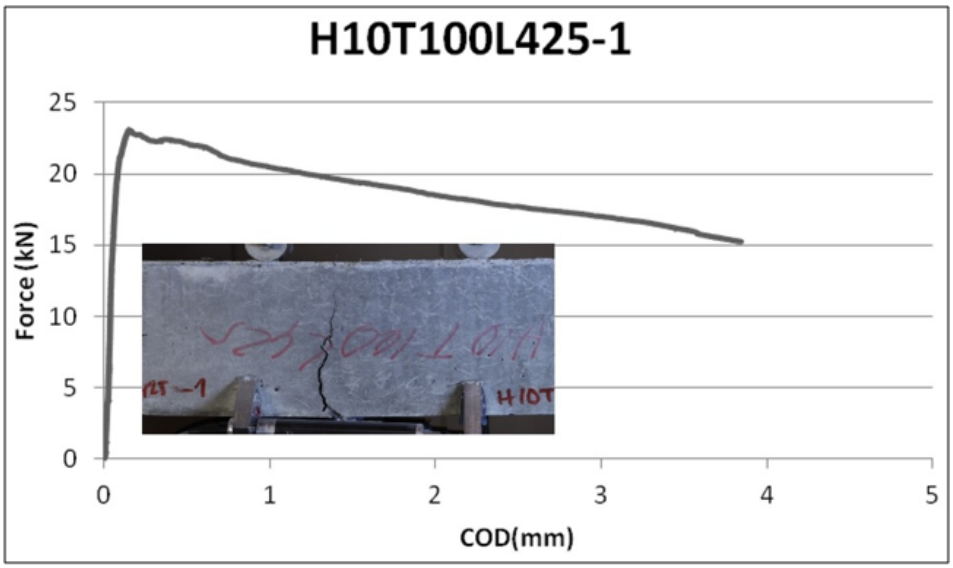

Figure A.115. H10T100L425-1.

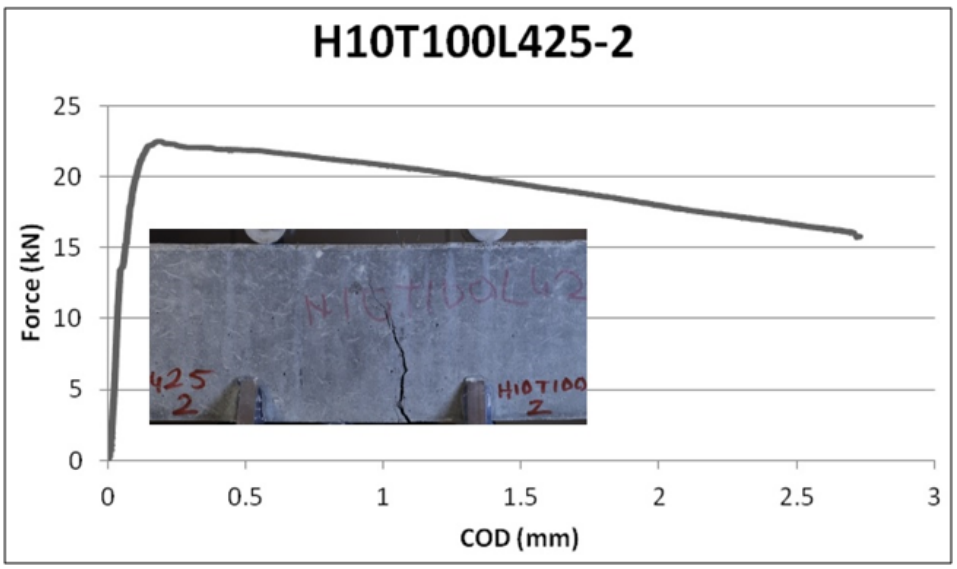

Figure A.116. H10T100L425-2.

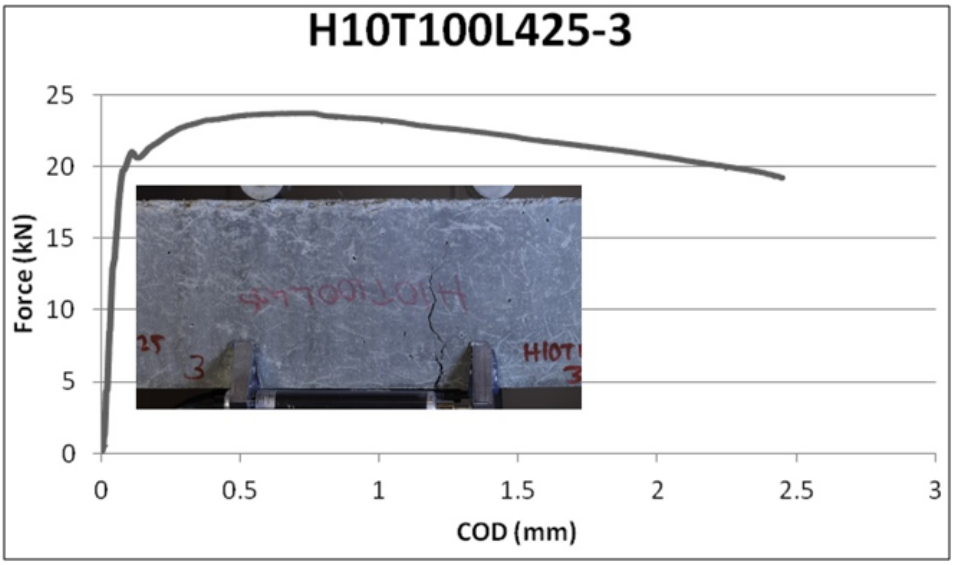

Figure A.117. H10T100L425-3.

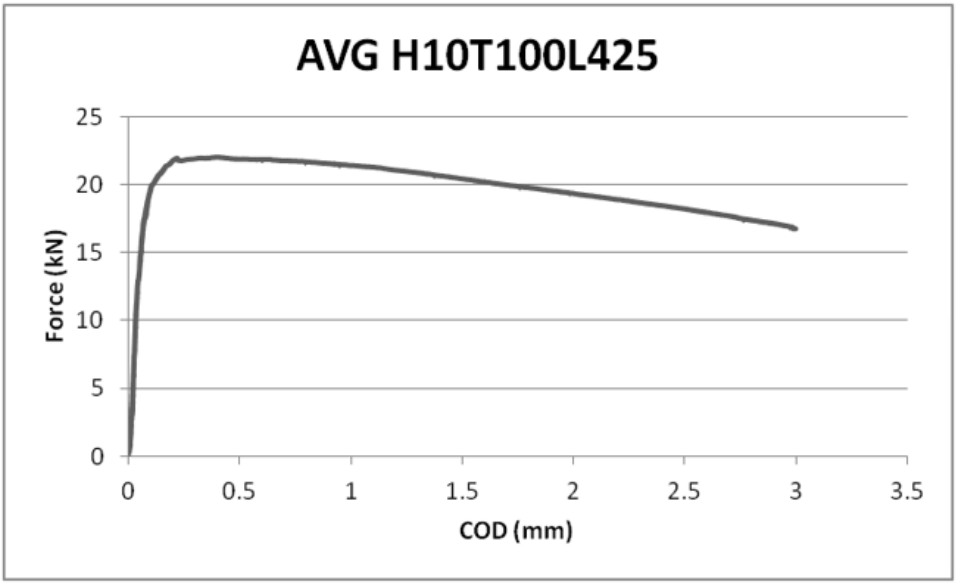

Figure A.118. AVG H10T100L425.

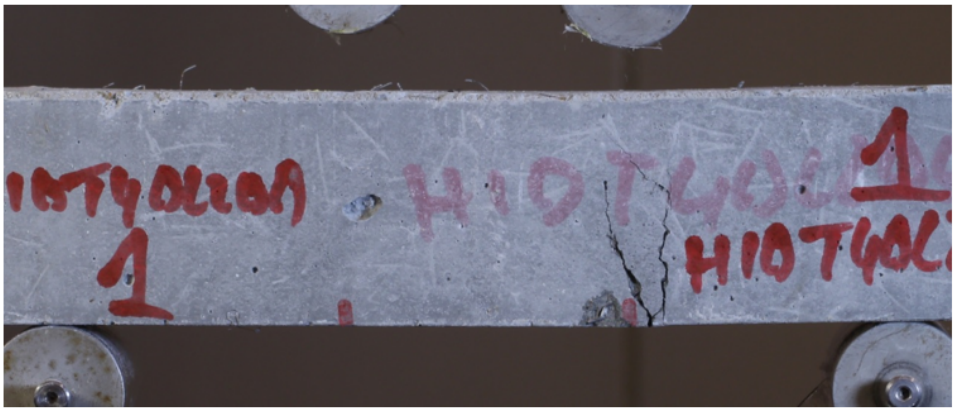

Figure A.119. H10T40L200-1.

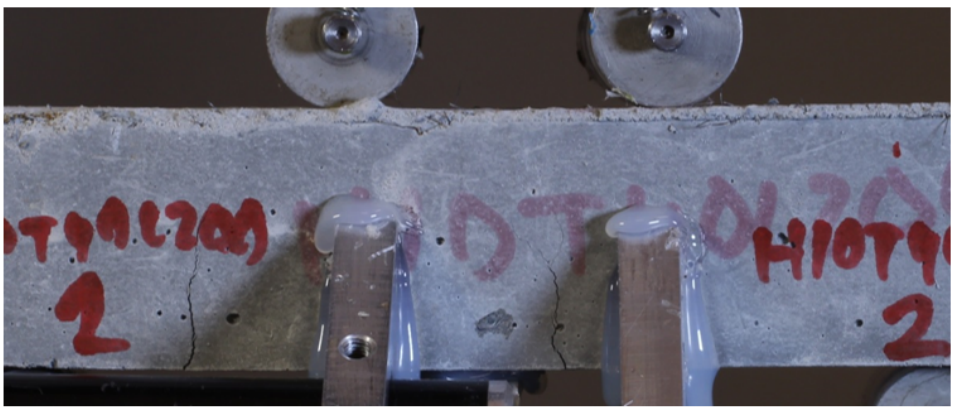

Figure A.120. H10T40L200-2.

Figure A.121. H10T40L200.

Figure A.122. H10T60L275-2.

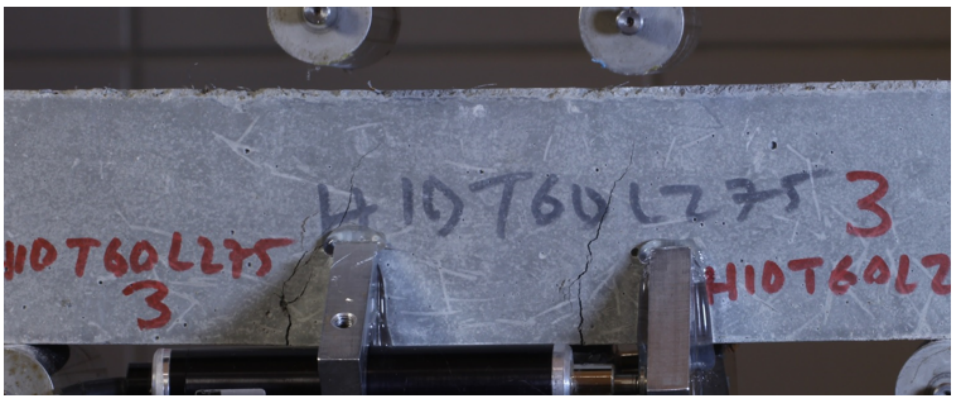

Figure A.123. H10T60L275-3.

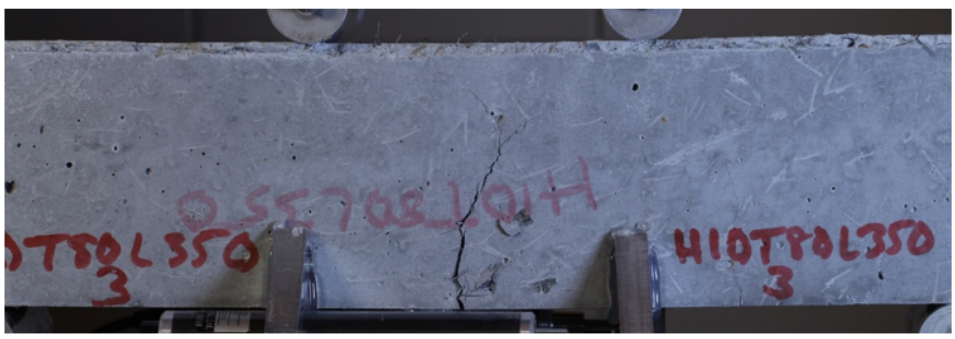

Figure A.124. H10T80L350-3.

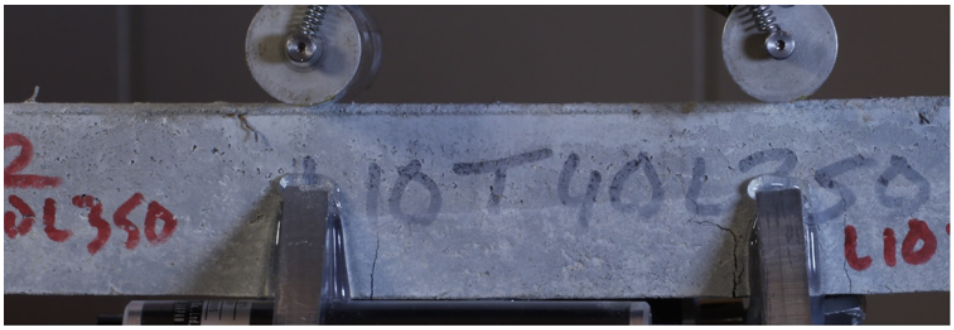

Figure A.125. L10T40L350.

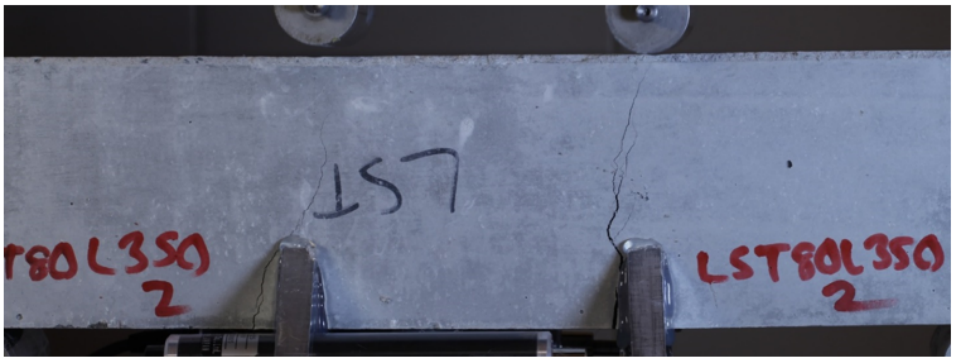

Figure A.126. LST80L350-2.

Figure A.127. L10T30L275.

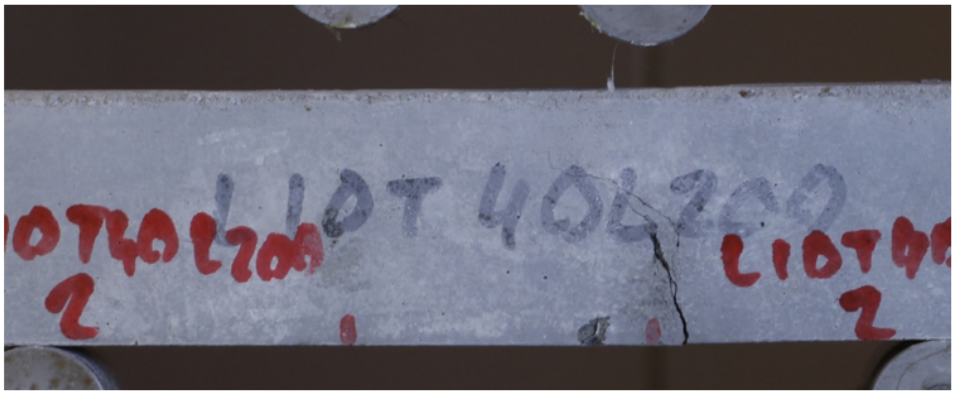

Figure A.128. L10T40L200-2.

Figure A.129. L10T40L200-3.

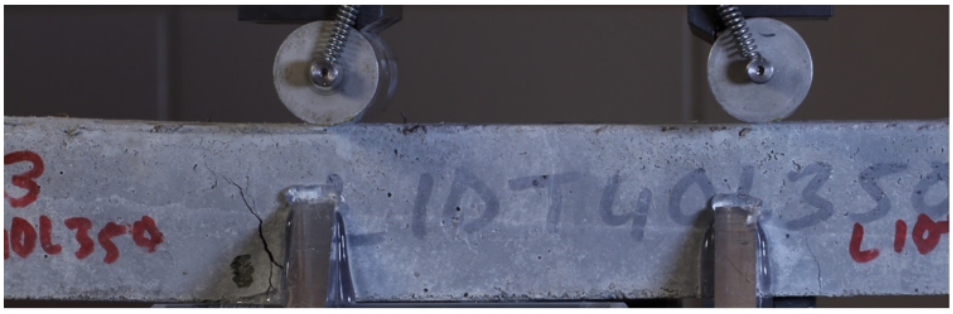

Figure A.130. L10T40L350-3.

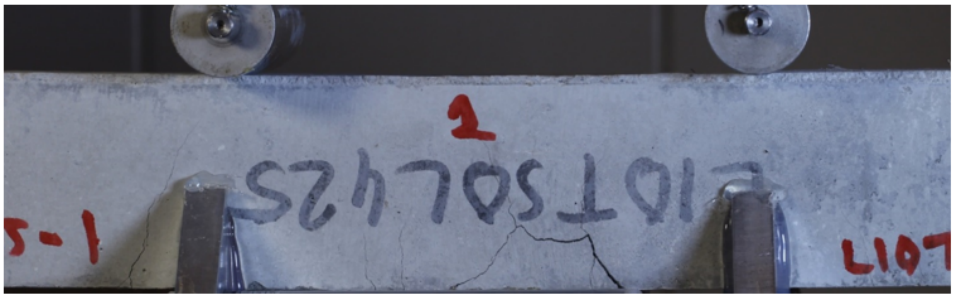

Figure A.131. L10T50L425-1.

Figure A.132. L10T50L425-2.

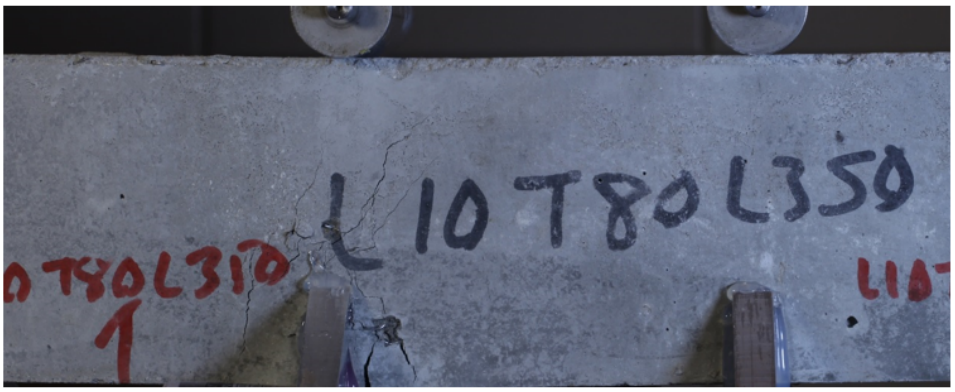

Figure A.133. L10T80L350-1.

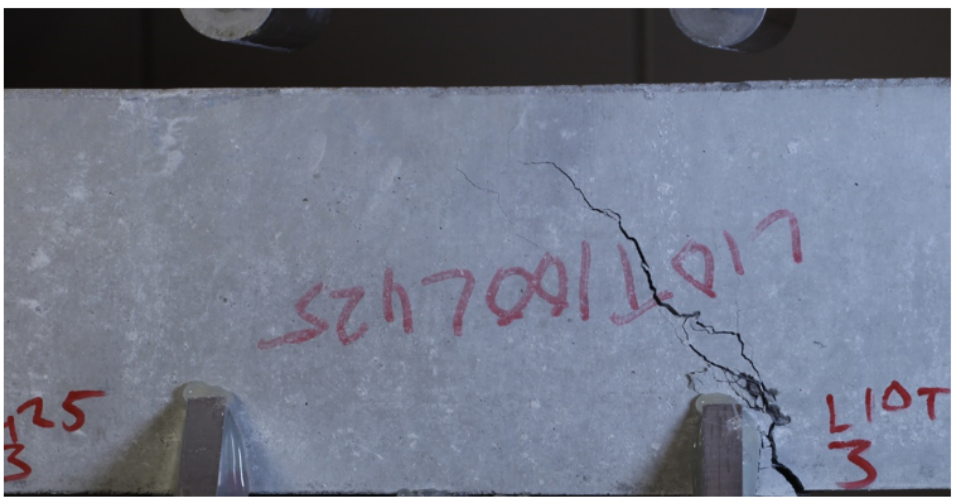

Figure A.134. L10T100L425-3.